

eman ta zabal zazu



Universidad
del País Vasco

Euskal Herriko
Unibertsitatea

Natural Killer (NK) cells and cancer: nanotechnology-based new methods development for the enhancement of antitumor immunotherapy efficacy

PhD thesis

Idoia Mikelez Alonso

Donostia, 2022



Células natural killer (NK) y cáncer: desarrollo de nuevos métodos basados en nanotecnología para incrementar la eficacia de la inmunoterapia antitumoral.

Tesis doctoral

para la optar al grado de Doctor en Investigación
Biomédica por la Universidad del País Vasco-Euskal
Herriko Unibertsitatea (UPV-EHU)

presentada por

IDOIA MIKELEZ ALONSO

Donostia-San Sebastian, 2022

Supervisores de tesis: Prof. Aitziber L. Cortajarena (Biomolecular Nanotechnology, CIC biomaGUNE) y Prof. Francisco Borrego Rabasco (Immunopathology, Biocruces Bizkaia)

Tutor de la universidad: Prof. Ana Isabel Alonso Varona (Departamento de Biología celular e histología, Facultad de Medicina y enfermería, Universidad del País Vasco, UPV-EHU)



Natural Killer (NK) cells and cancer: nanotechnology-based new methods development for the enhancement of antitumor immunotherapy efficacy

Ph.D. Thesis

for the degree of Doctor in Biomedicine Research at
the University of the Basque Country (UPV-EHU)

by

IDOIA MIKELEZ ALONSO

Donostia, 2022

Thesis supervisors: Prof. Aitziber L. Cortajarena (Biomolecular Nanotechnology, CIC biomaGUNE) and Prof. Francisco Borrego Rabasco (Immunopathology, Biocruces Bizkaia Health Research Institute)

University tutor: Prof. Ana Isabel Alonso Varona (Department of Cellular biology and histology, Faculty of Medicine and Nursing, University of Basque Country (UPV/EHU))

*Nire familiarentzako,
baita aukeratu dudan familiarentzako ere,
gaudenak eta ez gaudenak,*

*Eta zuretzako,
hel nazazu eskutik.*

Funding Agencies

This doctoral thesis was carried out between the Biomolecular Nanotechnology Group from CIC biomaGUNE and Immunopathology Group from Biocruces Bizkaia Health Research Institute. During the doctoral thesis, the predoctoral contract of Idoia Mikelez Alonso was funded by project from the Government of the Basque Country “Research and health projects” (2018222038, 2019222027, 2020333024) and a project from the “Fundación Científica AECC”- Spanish Association Against Cancer (PROYE16074BORR).

Table of contents

<i>Abbreviations</i>	v
<i>Figures, tables and appendix index</i>	xi
<i>Laburpena</i>	xv
<i>Summary</i>	xxi
Chapter I <i>Introduction. Harnessing the innate immune system through nanoparticle-based immunotherapy.</i>	3
1.1. Cancer disease in numbers	3
1.2. The immune system against cancer	4
1.2.1. NK cell-based immunotherapies	5
1.2.2. Cytokines as stimulators of the innate immune system	19
1.2.3. Cancer nano-immunotherapy	22
1.3. Anticancer nano-immunotherapy: “The good, the bad and the ugly”	25
1.3.1. Immune-blinding as a consequence of PC formation	26
1.3.2. Immune response or immune reactivity as a consequence of PC formation	28
1.3.3. Gold standard of nano-immunotherapy strategies	31
1.4. Justification and objectives of the research	42
Chapter II <i>Design, synthesis and characterization of the hIL-15HIS coated PEGylated IONP</i>	47
2.1. Introduction	47
2.1.1. Anticancer therapies using IONPs	49
2.1.2. Synthesis of biocompatible IONP	52
2.1.3. Biofunctionalization strategies	54
2.2. Result and discussion	57
2.2.1. Synthesis of IONP-based micelles and magnetic characterization	57
2.2.2. Expression and the biofunctionalization of protein	61
2.2.3. IONP@hIL15HIS characterization	70
2.3. Conclusion	75
Chapter III <i>In vitro assays with IONP@hIL15HIS</i>	79
3.1. Introduction	79
3.1.1. IL-15 application in the clinic	80
3.1.2. Engineering IL-15 to improve its therapeutic effect	81
3.2. Results and discussion	83
3.2.1. IONP toxicity determination by a proliferation assay	84
3.2.2. Determination of hIL-15HIS activity.	88
3.2.3. NK cell activation and polyfunctionality in response to IONP@IL15his pre-stimulation at day 0	90

3.2.4.	NK and T56 cell activation and polyfunctionality in response to IONP@IL15HIS priming at day 4	98
3.2.5.	Phenotype of NK and T56 cells primed with a combination of IL-12, IL-15 and IL-15: role of IONP@hIL15HIS	107
3.2.6.	T56 and NK cells expansion with IL-2 or IL-15 in its soluble or immobilized forms	113
3.3.	Conclusions	120
Chapter IV	<i>In vivo study of IONP@hIL15HIS as antitumoral immunotherapy</i>	125
4.1.	Introduction	125
4.1.1.	State of the art of the nano-immunotherapy <i>in vivo</i>	125
4.2.	Results and discussion	129
4.2.1.	ACTT <i>in vivo</i> model with IONP@hIL15HIS primed PBMCs	129
4.2.2.	Antitumor therapeutic effect of IONP@hIL15HIS	137
4.3.	Conclusions	149
	<i>Summary of results and general conclusions</i>	153
	EXPERIMENTAL SECTION	155
	<i>Appendixes</i>	173
	<i>References</i>	181
	<i>Acknowledgement</i>	I
	<i>Curriculum Vitae</i>	III

Abbreviations

Ab	antibody	CD	Circular Dichroism
ACTT	adoptive cell transfer therapy	cdDNA	complementary DNA
ADCC	antigen dependent cellular cytotoxicity	cdGMP	cyclic diguanylate monophosphate
Ag	antigen	CDS	coding DNA sequence
ALL	acute lymphoblastic leukemia	CEA	carcinoembryonic antigen
AMF	alternative magnetic field	CFSE	Carboxyfluorescein succinimidyl ester
AML	acute myeloid leukemia	CHS	contact hipersensitivity
Amp	ampicillin	CHI3L1	chitinase-3-like protein 1
AmpR	resistance to Amp	CIML	cytotoxic T lymphocyte
ATP	adenosine triphosphate	cIL-15	commercial IL-15
Au/AgNP	gold/silver nanoparticle	CMV	citomegalovirus
BCA	bicinchoninic assay	COOH	carboxylic group
BCG	Bacillus Calmette-Guérin	CRC	colorectal cancer
BiKE	bi-specific killer engagers	CSC	Cancer Stem Cells
BiTE	Bi-specific T-cell engager	CTLA-4	Cytotoxic T-Lymphocyte Antigen
BP	bandpass	CTPR	Consensus tetratricopeptide repeat
BSA	bovine serum albumin	CTPRHIS	His tagged CTPR
C3	complement 3	CTS	cytometer setup and tracking
CAR	chimeric antigen receptor	DAMP	Danger-Associated Molecular Patterns
CAR-NK	CAR on NK cells	DC	Dendritic Cell
CAR-T	CAR on T cell	DCS	Differential Centrifugal Sedimentation
CCL	C-C motif chemokine ligand	Dex	DC derived exosomes
		DINP	Dual Immunotherapy nanoparticle

D.I.T.	digital integration time	FDA	Food and Drug Administration
DLS	Dynamic Light Scattering	FPLC	Fast protein liquid chromatography
DMA	DOTAP and MPEG-PLA	FSC/SSC	forward and side scatter
DMSA	dimercaptosuccinic acid	GBM	glioblastoma
DNA	deoxyribonucleic acid	GD2	disialoganglioside carbohydrate antigen
DNAM	DNAX accessory molecule	GM-CSF	granulocyte-macrophage colony stimulating factor
DOPA	1,2-dioleoyl-sn-glycero-3-phosphate	GvHD	graft versus host disease
DOTAP	1,2-dioleoyl-3-trimethylammonium propane	GvL	graft versus leukemia
Dox	doxorubicin	HA	hyaluronic acid
DSPE-PEG2000	1,2-distearoyl-sn-gycero-3-phosphoethanolamine-N-[methoxy(polyethylene glycol)-2000]	hCMV	human CMV
<i>E. coli</i>	<i>Escherichia Coli</i>	hIL-15HIS	his-tagged human interleukin-15
EDC	1-Ethyl-3-[3-dimethylaminopropyl]carbodiimide hydrochloride	HIV	human immunodeficiency virus
EGFR	epidermal growth factor receptor	HLA	human leucocyte antigen
EpCAM	epithelial cell adhesion molecule	HSCT	hematopoietic stem cell transplantation
EPI	epirubicin	HSP	heat shock protein
ESI-ToF-MS	electrospray ionization time of flight mass spectroscopy	hTERT	human telomerase reverse transcriptase
FAS	first apoptosis signal	hIONP	hydrophobic IONP
FASL	FAS ligand	ICG	indocyanine green
Fc	fragment crystallizable region	ICP-MS	inductively coupled plasma-mass-spectrometry
FCS	fluorescence correlation spectroscopy	IFN	interferon

Ig	immunoglobulin	LPS	lipopolysaccharide
IL	interleukin	mAb	monoclonal antibody
IL-2Rγ_c	IL-2 γ common receptor	Maldi-ToF-MS	Matrix Assited Laser Desorption/Ionization Time Of Flight Mass Spectrometry
IL-2R$\alpha\beta\gamma$_c	IL-2 high affinity receptor	MCMV	murine citomegalovirus
IL-15	interleukin 15	MFI	mean fluorescence intensity
IL-15Rα	interleukin 15 receptor α	MHA	magnetic hydroxyapatite
IL15R$\beta\gamma$_c	IL-2/IL-15 $\beta\gamma$ common receptor	MHC	major histocompatibility complex
IONP	Iron Oxide Nanoparticle	MICA/MICB	MHC class I chain related protein A and B
IONPm	IONP micelle	mPEG	monomethoxy-poly-(ethylene glycol)
IONP-NTA	IONP binded to NTA molecule	MPEG-PLA	methoxy poly(ethylene glycol)-poly(lactide)
IONP@hIL15HIS	IONPm functionalized with hIL-15HIS	MPLA	monophosphoryl lipid A
IPTG	isopropyl- β -D-1-thiogalactopyranoside	MPS	mononuclear phagocytic system
ITC	Isothermal Titration Calorimetry	MRI	Molecular Resonance Imaging
ITIM	immunoreceptor tyrosine-based inhibitory motif	MSN	mesoporous silica nanoparticles
i.v.	intravenously	mTOR	mammalian target of rapamicin
kDa	kiloDalton	MUC-1	mucin-1
KIR	killer Ig-like immunoglobulin receptor	NB	neuroblastoma
LC-MS	liquid chromatography mass spectroscopy	NCA.6S	PEG-COOH and PEG NH ₂ IONP micelle
LP	longpass	NCR	natural cytotoxicity receptor
		NGO	nanoscale graphene oxide

NHS	N-hydroxysuccinimide	PEG	Poly-ethylene glycol
NIR	Near InfraRed	PEG-CH3	PEG phospholipid with methoxy
NK	Natural Killer cell	PEG-COOH	PEG phospholipid with carboxylic
NMA.6S	PEG-CH3 and PEG NH2 IONP micelle	PEG-NH2	PEG phospholipid with amine
NMR	nuclear magnetic resonance	PEG-NTA-PL	NTA functionalized PEG-PL
NMC.6S	PEG-CH3 and PEG-COOH IONP micelle	PEG-PL	PEG phospholipid
NP	Nanoparticle	PEI	polyethyleneimine
NTA	nitrilotriacetic acid	PELG	poly (2-aminoethyl-L-glutamate)
OD	optical density	PI	proliferation index
ON	overnight	PL	phospholipid
ORF	open reading frame	PLA	Poly-Lactic Acid
ori	origin of replication	PLAM	PLA microspheres
OVA	ovalbumin	PLE	poly-L-glutamic acid
PAA	poly(acrylic acid)	PLGA	Poly Lactic-co-Glycolic Acid
PBMC	peripheral blood mononuclear cells	PLM	polymer lipid hybrid
PBS	phosphate buffer saline	PLR	poly-L-arginine
PC	protein corona	PM	plasma membrane
PDA	polydopamine	PMT	photomultiplier tube
PD-1	programmed cell death-1	PRR	pattern recognition receptor
PD-L1	programed death-ligand 1	PS	photosensitizer
PDLLA	poly-(D,L-lactide)	PSMA	prostate specific membrane antigen
PDT	photo-dynamic therapy	PT	phototherapy

PTT	photothermal therapy	TAM	tumor associated macrophages
QCM	quartz crystal microbalance	TCR	T cell receptor
QOD	every two days	T_{CM}	central memory T cell
RBC	red blood cell	T_{EM}	effector memory T cell
RCC	renal cell carcinoma	T_N	naïve T cell
RNA	ribonucleic acid	TE	echo time
ROS	reactive oxygen species	TEM	transmission electron microscopy
RT	room temperature	TEV	tobacco etch virus nuclear-inclusion-a endopeptidase
SDS-PAGE	sodium dodecyl sulphate- poly-acrylamide gel electrophoresis	TFA	trifluoroacetic acid
scIL-15	single chain IL-15	Th	T helper lymphocytes
scFv	single chain variable fragment	TIGIT	T cell receptor with Ig AND ITIM domain
SLE	systemic lupus erythematosus	TIL	tumor infiltrated lymphocytes
SN	supernatant	TLR	toll like receptor
SPDP	succinimidyl 3-(2- pyridyldithiol)propionate	TME	tumor microenvironment
SPION	superparamagnetic iron oxide nanoparticle	TNBC	triple negative breast cancer
SPR	surface plasmon resonance	TNF	tumor necrosis factor
STING	stimulator of IFN genes	TNFR	TNF receptor
SVNP	synthetic vaccine nanoparticle	TRAIL	TNF-related apoptosis-inducing ligand
T56	CD56 expressing T cells	TRAILR	TRAIL receptor
TA	tumor antigen	Treg	regulatory T cell
TAA	tumor associated antigen	TriKE	tri-specific killer engager
		ULBP	UL16 binding protein

UP-LC ultra-performance
chromatography

liquid

VLP virus like particle

VSV vesicular stomatitis virus

UV/Vis ultraviolet visible

VZV varicella-zoster virus

Figures, tables and appendix index

CHAPTER I. INTRODUCTION.

HARNESSING THE INNATE IMMUNE SYSTEM THROUGH NP-BASED IMMUNOTHERAPY

FIGURE 1.1	Cancer statistics in 2020.	3
FIGURE 1.2	Immune response elucidated by tumors.	6
FIGURE 1.3	Activating and inhibitory receptors of human NK cells.	9
FIGURE 1.4	Heterogeneity of memory and memory-like NK cells.	18
TABLE 1.1	Examples of nanocomposites loaded with cytokines for antitumor immunotherapies.	20
TABLE 1.2	Recently studied nanoformulations for immunotherapy.	24
FIGURE 1.5	Nanoparticle-based immunotherapy failure because of protein corona (PC) formation.	28
FIGURE 1.6	NP contribution to antitumoral therapies.	32
FIGURE 1.7	Nanoparticles (NPs) used to modulate NK cells effector function.	34
TABLE 1.3	Examples of nanoplatforms targeting NK cells.	35
FIGURE 1.7	Physiological and NP-mediated IL-15 stimulation of NK cells.	44

CHAPTER II.

DESIGN, SYNTHESIS AND CHARACTERIZATION OF THE hIL-15HIS COATED PEGYLATED IONP

FIGURE 2.1	Current applications of IONP in biomedicine.	49
FIGURE 2.2	Common biofunctionalization strategies.	54
FIGURE 2.3	Synthesis and water transfer of hIONPs scheme.	58
FIGURE 2.4	hIONP and IONP micelles characterization by TEM, Z-sizer, and spectrophotometer.	59
FIGURE 2.5	Magnetic characterization of IONP micelles.	60
FIGURE 2.6	IL-15 sequence and purification.	63
FIGURE 2.7	Lab made IL-15 (hIL-15HIS) characterization.	64
FIGURE 2.8	Comparison of commercial IL-15 and hIL-15HIS.	65
FIGURE 2.9	Conjugation strategy step by step.	67
FIGURE 2.10	PEG-NTA-PL molecule and forming micelles characterization.	68
FIGURE 2.11	Purification of IONP@hIL15HIS with Sepharose 6cLB resin column.	70
FIGURE 2.12	Characterization of IONP@hIL15HIS.	71
TABLE 2.1	Size difference between micelle and IONP@hIL15HIS.	72
FIGURE 2.13	Indirect quantification of hIL-15HIS bound to the IONP.	73
FIGURE 2.14	Size distribution of IONP@hIL15HIS by DLS.	74

CHAPTER III.

IN VITRO ASSAYS WITH IONP@HIL15HIS

TABLE 3.1	Examples of ongoing clinical trials with IL-2 and IL-15 as part of combination therapy of cancer treatment.	79-80
FIGURE 3.1	Schematic representation of pre-activation and expansion phases.	83
FIGURE 3.2	Scheme of different lipid composition of micelles.	85
FIGURE 3.3	IL-2 (1000 IU/ml) cultured PBMCs during 4 days in the presence of IONPm covered with different lipid composition (n=2)	86
FIGURE 3.4	PBMCs subsets (NK, T56 and T cells) proliferation after incubation with IONPm for 4 days (n=1).	87
FIGURE 3.5	Expression, purification and characterization of His-tagged human IL-15 (hIL-15HIS).	89
FIGURE 3.6	Lymphocyte cell subsets frequencies at day 0 (n=14).	92

FIGURE 3.7	CD25 and CD69 activation markers expression in lymphocytes at day 0 after pre-activation phase (n=7).	93
FIGURE 3.8	CD62L and CXCR4 homing markers variation on lymphocytes at day 0 after pre-activation phase (n=7).	94
FIGURE 3.9	Functional profile and polyfunctionality of NK cells at day 0 (n=7).	96
FIGURE 3.10	Functional profile and polyfunctionality of T56 cells at day 0 (n=7).	97
FIGURE 3.11	Cell subpopulation percentage at day 4 (n= 14).	99
FIGURE 3.12	CD25 and CD69 activation markers expression profile at day 4 (n=7).	100
FIGURE 3.13	CD16 expression and perforin at day 4 (n=7).	102
FIGURE 3.14	CXCR4 and CD62L homing receptors expression at day 4 (n=7).	103
FIGURE 3.15	NK and T56 cells proliferation at day 4 (n=7).	104
FIGURE 3.16	NK functional profile after expansion phase at day 4 (n=7).	105
FIGURE 3.17	T56 functional profile after expansion phase at day 4 (n=7).	106
FIGURE 3.18	Schematic representation of pre-activation and expansion phases of CIML-NK cells.	107
FIGURE 3.19	CD25 and homing receptors (CXCR4 and CD62L) expression after PBMCs priming with a cytokine combination at day 0 (n=2).	109
FIGURE 3.20	Degranulation (CD107a) and cytokine production after PBMCs priming with a cytokine combination at day 0 (n=7).	109-110
FIGURE 3.21	Activation markers expression and proliferation after PBMCs priming with a cytokine combination and expanded with IL-2 at day 4 (n=7).	111
FIGURE 3.22	Homing receptors expression after PBMCs priming with a cytokine combination and expanded with IL-2 at day 4 (n=7).	112
FIGURE 3.23	Degranulation (CD107a) and cytokine production after PBMCs priming with cytokine combination at day 4 (n=7).	113
FIGURE 3.24	PBMCs expansion with IL-2 and IL-15 formulations: functional profile and activation markers on NK cells at day 4 (n=7).	115
FIGURE 3.25	PBMCs expansion with IL-2 and IL-15 formulations: functional profile and activation markers on T56 cells at day 4 (n=7).	116
FIGURE 3.26	Effect of IL-2 and IL-15-mediated expansions in NK and T56 cells pre-activated with cytokines combination: Activation and proliferation at day 4 (n=7).	117
FIGURE 3.27	Effect of IL-2 and IL-15-mediated expansion in NK and T56 cells pre-activated with cytokines combination: Effector markers at day 4 (n=7).	118
FIGURE 3.28	Effect of IL-2 and IL-15-mediated expansion in NK and T56 cells pre-activated with cytokines combination: Functional markers at day 4 (n=7).	119

CHAPTER IV.

IN VIVO STUDY OF IONP@HIL15HIS AS ANTITUMORAL IMMUNOTHERAPY

FIGURE 4.1	NPs-based formulations <i>in vivo</i> .	126
FIGURE 4.2	Schematic representation of ACTT protocol.	129
FIGURE 4.3	The ratio between human CD45+ and murine CD45+ cells.	131
FIGURE 4.4	CXCR4 and CD62L homing receptors and CD25 activating receptor expression on human CD45+ cells.	133
FIGURE 4.5	Human T cells in bone marrow and secondary lymphoid organs.	134
FIGURE 4.6	Mean fluorescence intensity (MFI) of homing markers (CXCR4 and CD62L) and activation marker (CD25) on T cells before transfer (day 0) and at day 6.	136
FIGURE 4.7	Schematic representation of antitumor therapy schedule.	138
FIGURE 4.8	Therapeutic effect of systemically administered hIL-15HIS and IONP@hIL15HIS in the mouse B16F10 model.	139
FIGURE 4.9	NK and T cells frequencies in blood.	141

FIGURE 4.10	Expression of CD69 activation marker in circulating cells the day before treatment.	142
FIGURE 4.11	CD8+ T cells subpopulations frequencies in blood the day before treatment.	144
FIGURE 4.12	Percentages of CD4+ T cells subpopulations in blood the day before treatment.	145
FIGURE 4.13	Tumor infiltrating cell quantification.	146
EXPERIMENTAL SECTION		
FIGURE ES.1	DNA and protein sequences of hIL-15 cloned in pUC57 and pProEX-HTa vectors.	158
FIGURE ES.2	Conjugation strategy reaction scheme.	160
FIGURE ES.3	Scheme of cell culture protocol and the studied parameters.	162
TABLE ES.1	Flow cytometry panels for multiparametric cell analysis <i>in vitro</i> .	163-164
TABLE ES.2	Flow cytometry panels for multiparametric cell analysis <i>in vivo</i> .	165-166
TABLE ES.3	Flow cytometer configurations	170
FIGURE ES.4	Flow cytometer optics configuration.	171
APPENDIX I		
FIGURE AI.1	IL-15 in pUC57 vector map and sequence.	175-176
FIGURE AI.2	IL-15 in pProEX-HT vector map and sequence.	177-179
FIGURE AI.3	Sequences of His-tagged IL-15.	179

Laburpena

Minbizia askoren egunerokotasunean presente dagoen gaixotasun bortitza da. Hitzaren etimologiari erreparatzen badiogu, erderaz <<cáncer>> den bitartean, euskaraz bizirik dagoen mina bezala definitzen da, <<minbizia>>. Izan ere, minbizia hutsegite molekular multzo zabal batek osatutako gaixotasuntzat har daiteke, gaixotasun heterogeneo eta dinamikoan bilakatzen duena. Hain zuzen ere, ezaugarri horiek dira minbizia sendatzeko egun dauden terapien oztopo nagusiak.

Gaitz honen aurkako tratamenduen garapenean urteak dihardute ikertzaile, mediku eta espezialista ezberdinek ikuspuntu berriak dituzten terapien bila. Urte askotan zehar, tumore zelulen bikoizteko gaitasuna inhibitzean edo tumore-masa ezabatzean oinarritu dira terapiak, horretarako kimioterapia, erradioterapia edo/eta kirurgia erabiltzen direlarik. Tratamendu hauek kasu askotan eraginkorrak diren arren, eragiten dituzten albo kalteak ugariak dira eta zenbait kasutan erresistentziak ere garatzen dira hauen aurrean.

Erresistentzia hauek saihesteko helburuarekin, terapia berriak garatzen joan dira, eta horien artean aipagarrienetako bat immunoterapia da. Terapia mota honetan, tratamenduaren eraginkortasuna norbanakoaren immunitate sistema indartuz/trebatuz lortzen da. Oro har, immunitate sistemak gorputzari arrotzak zaizkion molekula, mikroorganismo eta tumore-zelulak ezagutzeko gaitasuna du, eta immunoterapiak immunitate sistemak berezkoa duen gaitasun hori areagotuko luke. Alde batetik, tumorearen aurkako terapia espezifikoa izanik eta, beste aldetik, albo ondorioak gutxituz.

Minbiziaren aurka immunoterapia erabiliko bada, berezko eta moldaerazko erantzun immunitarioak izan daitezke jomuga, biek hartzen baitute parte bai tumorearen identifikazioan eta baita ezabatzean ere. Immunitate sistema gai da, nahiz eta tumore-masa osatzen duten zelulak propioak izan (eta printzipioz propioa denaren aurka erantzun immunologikorik ematen ez den arren), hauek arrotzak bezala ezagutzeko. Esaterako, berezko immunitate sistemako zelulek (zelula dendritikoak (ingelesezik “dendritic cells”, DC),

NK zelulak (ingelesezik “natural killers”, “zelula hiltzaileak”), neutrofiloak edota makrofagoak) tumore-zelulak mekanismo inespezifikoaren bidez arrotzak bezala ezagutzen dituzte. Esaterako NK zelulak histokonpatibilitate konplexu nagusiaren (ingelesezik “major histocompatibility complex”, MHC) adierazpen murrizketa sumatzeko gai dira, eta ondorioz, MHC gutxiago adierazten duten zelula horiek (tumore-zelula esaterako) suntsitzen dituzte, perforina eta granzima molekula zitotoxikoen askapenaren bidez batik bat. Moldaerazko immunitate sisteman aldiz, T eta B linfuzitoak dira zelula mota nagusiak eta, normalean, zelula arrotzen aurkako bigarren mailako erantzun immunitarioan hartzen dute parte, baina, oraingoan modu espezifikoan, MHC-ren bidez adierazitako antigenoa identifikatzeko gai baitira. T zelulen kasuan adibidez, MHC molekularen bidez T zelulei tumorearen antigeno espezifikoa adierazten zaie, eta horrela, trebatutako T zelula horiek, tumore zehatz horren aurka egingo dute. Bi erantzun immunitarioen arteko desberdintasun nagusiak erantzun-denbora, memoria eta espezifikotasuna dira, azken hau moldaerazko erantzun immunitarioaren ezaugarri bereizgarria izanik.

Esan bezala, aipatutako bi zelula mota hauen aktibazioa abiarazteko moduetako bat tumore-zelulen identifikazioa da. Baina horretaz gain, badira beste modu batzuk zelula hauen funtzioa nolabait areagotzeko, interleukinen bidez esaterako. Interleukina (IL)-2-ak NK eta T zelulen aktibazioa eta ugartzea sustatzen du eta, ondorioz, zitotoxikotasun zelularren bidez tumore-zelulen aurka egiteko gaitasuna areagotzen da. Izan ere, IL-2-a klinikan erabiltzen da dagoeneko leuzemia mieloide akutuaren (ingelesezik “acute myeloid leukemia”, AML) tratamenduan. Hala ere, zitokina honetan oinarritutako tratamenduen eraginkortasuna baldintzatuta egon daiteke zitokinaren tamaina txikiak bioerabilgarritasunean duen efektuarengatik. Horregatik, IL-2 kontzentrazio altuak erabiltzen dira terapia egiterako orduan eta albo ondorioak azaleratzen dira, kapilare-filtrazio sindromea, hots. Arazo honi erantzun berriak bilatzeko asmoz, hainbat alternatiba proposatu dira, adibidez, beste zitokina estimulatzaile batzuk erabiltzea (IL-15, adibidez) edo bioerabilgarritasuna handituko duten

molekula moldaerak edo nanopartikuletan (NP) oinarritutako nanoformulazioak erabiltzea (ingelesez drug delivery delakoa).

IL-15 proteina IL-2-aren alternatiba bezala proposatu da, alde batetik, estimulazioaren efektua hein batean antzekoa delako (zelulen ugaltzea, zelulen aktibazioa, etab.), eta bestetik, bi zitokinen errezeptoreak komunak direlako errezeptorearen bi katetan. IL-2-a ezagutzen duen errezeptorea hiru katez osatuta dago: α (IL-2R α edo CD25), β (IL-2R β edo CD122) eta γ (IL-2R γ edo CD132). Azken bi kateek heterodimero bat osatzen dute (IL-2R $\beta\gamma$), eta bi kate hauek dira IL-2 eta IL-15 zitokinak ezagutzeko ahalmena dutenak. Nahiz eta errezeptorean antzekotasuna izan, lortzen den erantzuna ez da guztiz berdina, IL-2-ak nolabait zitotoxizitate handiagoa azaltzen duelarik.

Immunoterapiarako nanoteknologia erabiltzearen onurak asko direla jakina da, baina zehazki, NP-en erabilpenaren onurak oso garrantzitsuak dira terapiari dagokionez. Esan bezala, bioerabilgarritasunaren areagotzea izango litzake efektuetako bat, baina horretaz gain, NP bat erabiltzeak beste bi onura nagusi izan ditzake bese askoren artean. Alde batetik, gainazal zabala izateagatik, molekula bat baino gehiago eraman ditzake, “codelivery” delakoa ahalbidetuz. Eta bestalde, modulu bakar batean terapia ezberdinak aplikatzeko aukera ere ahalbidetzen du. Esate baterako, NP magnetikoak erabiltzen badira, terapia fototermikoa edo hipertermia erabili daitezke NP-ren gainazalean jarritako molekularen efektu terapeutikoari gehigarri moduan. Finean, NP-ak oso formulazio moldakorra dira, multiterapia ahalbidetzeko gaitasuna dutenak.

Alternatiba horiek erreferentziatzat hartuta, Doktorego tesi honen helburu orokorra NP batean funtzionalizatutako IL-15-ak NK eta T56 (T linfozito mota bat) zelulen funtzioan duen efektua ikertzea izango da. Horretarako, ondorengo helburu espezifikoak proposatzen dira:

- ◆ Uretan disolbagarria den eta burdin (Fe) oxidoan oinarritzen den mizela (ingelesez iron oxide NP, IONP) garatu eta karakterizatzea.

- ◆ Konjugazio estrategia aproposa aukeratzea laborategian egindako His-tag sekuentziadun IL-15 zitokina IONP mizelaren gainazalean atxikitzeko (IONP@hIL15HIS deitutako nanoformulazioa garatuz).
- ◆ IONP@hIL15HIS nanoformulazioak, gizabanako osasuntsuen NK zelula eta T linfzitoen estimulazioan duen efektua *in vitro* karakterizatzea.
- ◆ IONP@hIL15HIS-rekin *in vitro* estimulatutako eta sagu immunodefizienteetan injektatutako zelulen biodistribuzioa *in vivo* ikertu eta aztertzea.
- ◆ IONP@hIL15HIS-ren efektu terapeutikoa *in vivo* ikertzea eredu murinoak erabiliz.

Horretarako, deskonposizio termiko bidez batzbesteko 6 nm-ko diametroa duten NP hidrofobikoak sintetizatu dira. Fosfolipidoak erabiliz, mizelak eratzen dira NPak hauen barruan antolatuz eta nanoformulazioa uretan disolbagarria bihurtuz, batzbesteko diametroa 50 nm-koa izanik. Mizela hau osatzen duten fosfolipidoek talde karboxilikoak dituzte beraien alde polarrean, ezinbestekoak direnak laborategian adierazitako proteina funtzionalizatzeko. Hauetara NTA (ingelesez “nitrilo tri-acetic acid”) molekula batzen da lehenik eta ondoren, NTA-His-tag nikel bidezko koordinazioari esker, His-tag duten proteinak batzen dira. Emaizta bezala 70 nm-ko diametrodun IONP@hIL15HIS nanoformulazioa lortzen da, 20-40 μM -eko proteina kontzentrazioa eta batezbesteko 0,5 mM Fe kontzentrazioa duena egindako lote guztietan.

IONP@hIL15HIS-aren karakterizazioarako teknika ezberdinak erabili dira, hala nola, dikroismo zirkularra, absorbantzia espektroa eta tamainaren eta kargaren distribuzioa (DLS ingelesetik “dynamic light scattering” bidez) hain zuzen ere. Karakterizazio ikerketek NP eta proteinaren presentzia baieztatu dute eta azken hau NP-ren gainazalean aurkitzen dela frogatu da.

Behin nanoformulazioaren karakterizazioa eginda, *in vitro* eta *in vivo* esperimentuak egin dira IONP@hIL15HIS nanoformulazioak immunitate sistemako NK eta T56 zelulak aktibatzeke duen gaitasuna ikertzeko.

In vitro esperimentuen xedea, odol emaile osasuntsuetatik lortutako odol zelula mononuklearrak (ingelesezik “peripheral blood mononuclear cells”, PBMCs) (bereziki, NK eta T56 zelulak) IONP@hIL15HIS-rekin estimulatzearen efektua zein den ikustea izan da. Horretarako, zelula hauen inkubazio protokoloa bi urrats nagusitan banatu da: 1) aktibazio-fasea, 16-18 orduko iraupena duena eta zelulak IL-15 formulazioekin (disolbagarria edo IONP@hIL15HIS) inkubatzean datzana, eta 2) hedapen-fasea, 4 egun irauten duena eta zelulak IL-2 proteinarekin inkubatzean datzana. Aktibazio-fasearen ondoren, fluxu-zitometroaren bidez, aktibazio (CD25, CD69) eta ehunetara migratzeko errezeptoreen (CXCR4, CD62L) adierazpena aztertu da NK eta T56 zeluletan. Hedapen-fasearen ondoren ere fluxu-zitometrotik pasatu dira zelulak, eta aipatutako molekulen adierazpena aztertzeaz gain, perforina askapena eta CD16 aktibazio errezeptorearen adierazpen maila ere aztertu dira. Horretaz gain, zelulen proliferazioa ere neurtu da, baldintza ezberdinetan zelulen hedapen ahalmena ezagutzeko. Bai aktibazio fasearen ondoren eta baita hedapen-fasearen ondoren ere, hIL15HIS eta IONP@hIL15HIS bidezko estimulazioek NK eta T56 zelulak aktibatze ahalmena dutela ikusi da. Horretaz gain, IONP@hIL15HIS nanoformulazioarekin estimulatu ondoren, migrazio errezeptoreen adierazpena altuago mantentzen da aztertutako bi zelula motetan, adierazpen altuago hauek balizko migrazio-ahalmen handiago batekin lotuta egon daitezkeela ondorioztatzen delarik (CXCR4 adierazten dutenak hezur muhinera migratuz eta CD62L adierazten dutenak ganglio linfatikora). Efektu horretaz gain, IONP@hIL15HIS formulazioak, hein batean, aktibazio ahalmen handiagoa duela esan daiteke. Aztertutako aktibazio errezeptoreen adierazpena areagotu egin da IONP@hIL15HIS-rekin inkubatu diren NK eta T zeluletan, nahiz eta efektu hau ez den beti estatistikoki adierazgarria izan.

Doktorego tesi honen helburuetako bat IONP@hIL15HIS formulazioaren eraginkortasuna *in vivo* neurtzea izan da, eta horretarako bi *in vivo* eredu erabili dira. Erabilitako eredu bat adopziozko zelula-transferentzia terapian (ingelesez “adoptive cell transfer therapy”, ACTT) oinarritu da, non IL-15 formulazioekin (hIL15HIS eta IONP@hIL15HIS) *in vitro* estimulatutako PBMCak (aktibazio-fasea) sagu immunodefizienteetan injektatzen diren (hedapen-fasea),

hauen hedapena *in vivo* aztertzeko. PBMcak 18 orduz estimulatu dira *in vitro* eta hedapen-faseak (*in vivo* gertatzen dena) 6 egun iraun ditu. Lortutako emaitzak ez dira esanguratsuak izan, injektatutako zelulak ez baitira espero bezala ugaltu.

Bigarren eredu aldiz, IONP@hIL15HIS-ren efektu terapeutikoa aztertu nahi izan da eredu prekliniko moduan B16F10 tumorea duten C57BL/6 saguak erabiliz. IONP@hIL15HIS tratamendua jaso duten animalietan tumoreen hazkunde tasa moteltzeko joera ikusi da, nahiz eta ez den diferentzia estatistikorik antzeman ikertutako tratamendu desberdinen artean. Bizirauteko probabilitatea ere aztertu da tratamendu desberdinen eraginkortasuna neurtzeko. Kasu honetan ere, taldeen arteko diferentzia esanguratsurik aurkitu ez den arren, IONP@hIL15HIS tratamendua jaso duen sagu taldeak erakutsi du bizirauteko aukerarik handiena.

In vitro eta *in vivo* esperimentuetan lortutako emaitzak eztabaidagarriak diren arren, tesi honen ekarpena baliotsua da gaur egungo ezagutza immunologikorako, zehazki terapia antitumoraleko agente gisa IL-15 proteinaren erabilerari dagokionez. Gainera, Fe-an oinarritutako nanopartikula-formulazio bat diseinatu, garatu eta probatu da, non IL-15 proteina NP-en gainazalean transirudikatzeko ibilgailu gisa erabili den. Modu honetan, NP-ak fisiologikoki monozitoek eta zelula dendritikoei NK zelulei IL-15 proteina erakusteko modua imitatzen duelarik.

Summary

It is known that the stimulation of natural killer (NK) and T cells with different cytokines, such as interleukins, enhances their effector functions, which is a reliable strategy for cancer elimination. In this thesis, we present the design and generation of a nanoformulation (IONP@hIL15HIS), based on a biocompatible, biodegradable, and traceable nanomaterial, which activates NK and T cells *in vitro*, by the presence of interleukin-15 (IL-15) on the surface of the nanoparticle (NP). Importantly, the immobilization of IL-15 on the NP provided this cytokine with certain properties, highlighting, among others, a capacity to lessen the down-regulation of homing receptors when T and NK cells are stimulated. Furthermore, two *in vivo* studies were carried out for two purposes: 1) to model an adoptive cell transfer therapy where IONP@hIL15HIS pre-stimulated human cells were infused in immunodeficient mice (NOD.Cg-Prkdc^{scid} Il2rg^{tm1Wjl}/SzJ) and 2) to evaluate the antitumoral therapeutic effect of IONP@hIL15HIS compared to soluble administration of IL-15 in a melanoma C56BL/6 bearing mouse model. Results showed that mice treated with IONP@hIL15HIS have a tendency to slow tumor growth. Altogether, the results from this thesis are a first step to consider immobilized IL-15 on NPs, i.e. IONP@hIL15HIS, as a new therapeutic tool for cancer treatment.

Chapter I. Introduction

Harnessing the innate immune system through nanoparticle-based immunotherapy

Parts of this chapter have been published in:

Mikelez-Alonso I, Aires A, Cortajarena AL. Cancer Nano-Immunotherapy from the Injection to the Target: The Role of Protein Corona. *Int J Mol Sci.* 2020 Jan 14;21(2):519. doi: 10.3390/ijms21020519. PMID: 31947622; PMCID: PMC7014289.

Mikelez-Alonso I, Magadán S, González-Fernández Á, Borrego F. Natural killer (NK) cell-based immunotherapies and the many faces of NK cell memory: A look into how nanoparticles enhance NK cell activity. *Adv Drug Deliv Rev.* 2021 Sep;176:113860. doi: 10.1016/j.addr.2021.113860. Epub 2021 Jul 5. PMID: 34237404.

Chapter I Introduction. Harnessing the innate immune system through nanoparticle-based immunotherapy.

1.1. Cancer disease in numbers

The high cancer incidence is socially evident, not only demonstrated by the statistics of people with cancer, but also because a big segment of the population knows somebody with cancer from their close social network. In 2019, cancer was classified as the first cause of death in the first world (i.e. Europe, America). Specifically, Europe represents 22.8% of cases and 19.6% of deaths from the total cancer cases, although Europeans only represent 9.7% of the world population. On the other hand, people with cancer die at earlier age in undeveloped countries (Fig. 1.1). The cancer type that exhibited most new cases in 2020 was female breast cancer followed by lung cancer. Furthermore, lung cancer also showed the highest mortality rates¹.

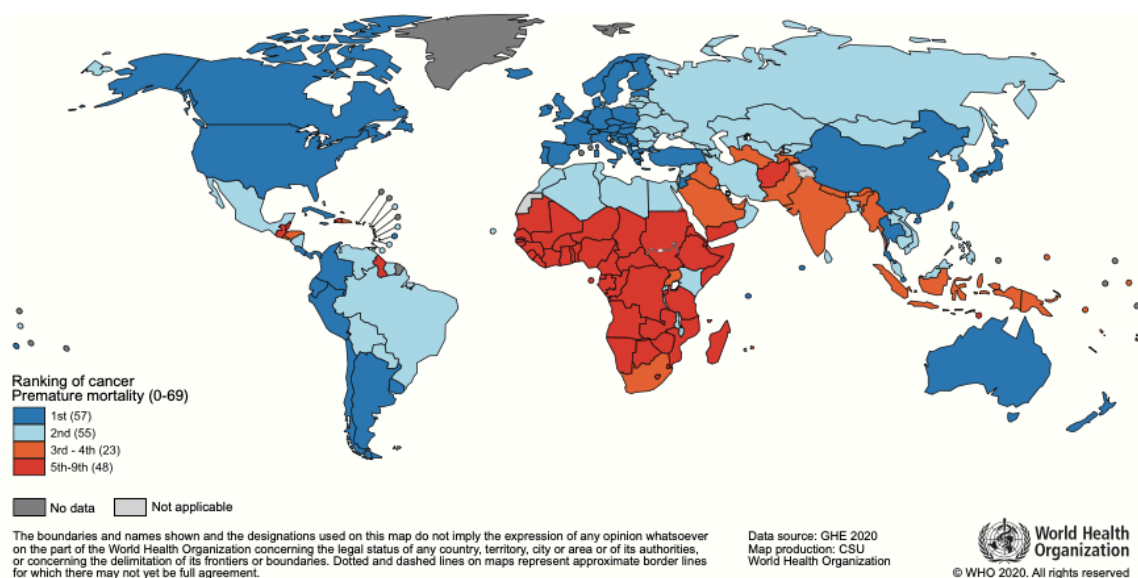


Figure 1.1. Cancer statistics in 2020. Worldwide ranking of cancer premature mortality defined as death before the age of 70¹. Color code is used to classify countries in the ranking of cancer death as 1st (dark blue), 2nd (light blue), 3rd-4th (orange) and 5th-9th (red) reason of death. From Sung et al., *CA Cancer J Clin.* 2021;71(3):209-249. doi:10.3322/caac.21660²

Introduction. Harnessing the innate immune system through NP-based immunotherapy

Cancer is a group of diseases characterized by the uncontrolled growth of cells, which is a consequence of an accumulation of disorders. Those disorders make cancer a heterogeneous disease and is very dynamic. These characteristics are the principal obstacle for reaching an effective cure for cancer³⁻⁵.

The formation of the cancer-initiating cells is still a matter of discussion. There are some postulations which defends genetic disorders, such as reciprocal translocations (for example t(9;22)(q34;q11) that generates what is known as the Philadelphia chromosome), start the tumorigenesis⁶, but others propose that the mutations are the consequence of other disorders such as mitochondrial damage⁷. Nevertheless, the most accepted tumor progression process is the one published by Hanahan and Weinberg in 2000, and reviewed in 2011, where they described acquired capabilities of cancer cells, what they named hallmarks⁸. They affirm that these hallmarks are modulated by two general conditions: the genomic instability of cancer cells and the inflammatory state caused by the altered immune response, although is not completely clear the order in which these processes occur.

Cancer treatment has been based for many years on the inhibition of the proliferative capacity of tumor cells and their elimination using chemotherapy, radiotherapy and/or surgery. Some of these therapies are focused on mechanisms involving molecular interactions such as DNA intercalation (i.e., doxorubicin) or physical elimination by resection of the tumor mass. Nevertheless, the success of these therapies is somehow limited on many occasions. One example of these limitations is the resistance of cancer stem cells (CSC) to chemotherapy. Also, a mathematical model has showed how CSC could proliferate in the meanwhile that cancer cells are dying. This is the so called “tumor growth paradox”, by which immune-mediated killing of tumor cells at the same time select for the CSC, which may show resistance to the action of the immune system⁹. Given these and other kind of limitations, additional therapies are needed. Among those therapies in the clinical practice, immunotherapy is a relatively recent, but also consolidated, established approach that complements other therapies against cancer. There are numerous examples of how immunotherapies alone or in combination with other therapeutic agents are able to induce complete remissions of many cancer types^{10,11}.

1.2. The immune system against cancer

The immune system is the principal line of defense to combat foreign agents such as microorganisms and also cancer cells. Hence, the main objective of anticancer immunotherapies is the induction

and/or the enhancement of an effective immune response, in the same way after encountering a pathogen, and direct this response against the tumor cells.

Dendritic cells (DCs), T lymphocytes and natural killer (NK) cells, among other cell types, are considered as targets for immunotherapies. The rationale for targeting those cells is that they can trigger a cytotoxic function against tumors (T and NK cells), or indirectly by activating other immune cells (DC), leading to the elimination of cancer cells. Its success will depend on the careful and adequate design of each immunotherapeutic strategy for each tumor. For this purpose, it is vital to unravel the immune system function and its interaction with tumor cells.

The immune response is generally classified in two types: the innate and the adaptive immune response. The first involves DC, NK cells, neutrophils and macrophages, among other cells, and it is responsible for the first encounter with pathogens. DCs and macrophages reside in many different tissues and when a foreign agent is recognized by the pattern recognition receptors (PRR), they elicit inflammatory signals which serves as an alert to other immune cells (innate and adaptive cells). Innate immune cells are capable of migrating to the inflammation area enhancing the alert signal, and the adaptive immune cells (such as T lymphocytes) start a specific response. The main differences between the two immune responses are the response-time, memory and the specificity, being the latter an unique feature of the adaptive immune response^{12,13}. In the case of anti-cancer immune response, the innate and the adaptive responses participate in the recognition and also in the elimination of the tumor mass^{14,15} (Fig. 1.2). On the one hand, DCs¹⁶ presenting to T lymphocytes¹⁷ are the principal cells in the recognition and the mediation of the adaptive immune response. And in the case of innate immune response both NK cells¹⁸ and macrophages¹⁹ have a very relevant role.

1.2.1. NK cell-based immunotherapies

NK cells were identified more than four decades ago and they were defined as large granular lymphocytes that could kill target cells without requiring priming or restriction by major histocompatibility complex (MHC) molecules^{20,21}. They are a subset within the innate lymphoid cells (ILC) family, which include ILC1, ILC2, ILC3, NK cells and LTi cells²². There are localized in different anatomical locations, including secondary lymphoid organs, liver, lungs, kidney, decidua, etc²³. They are capable of killing transformed cells through a mechanism of

Introduction. Harnessing the innate immune system through NP-based immunotherapy

exocytosis of granules containing the pore-forming molecule perforin and death-inducing enzymes, such as granzymes. This pathway is triggered by activation signals from cell surface receptors and does not require prior sensitization, which differentiates them from CD8 T cells 24–26.

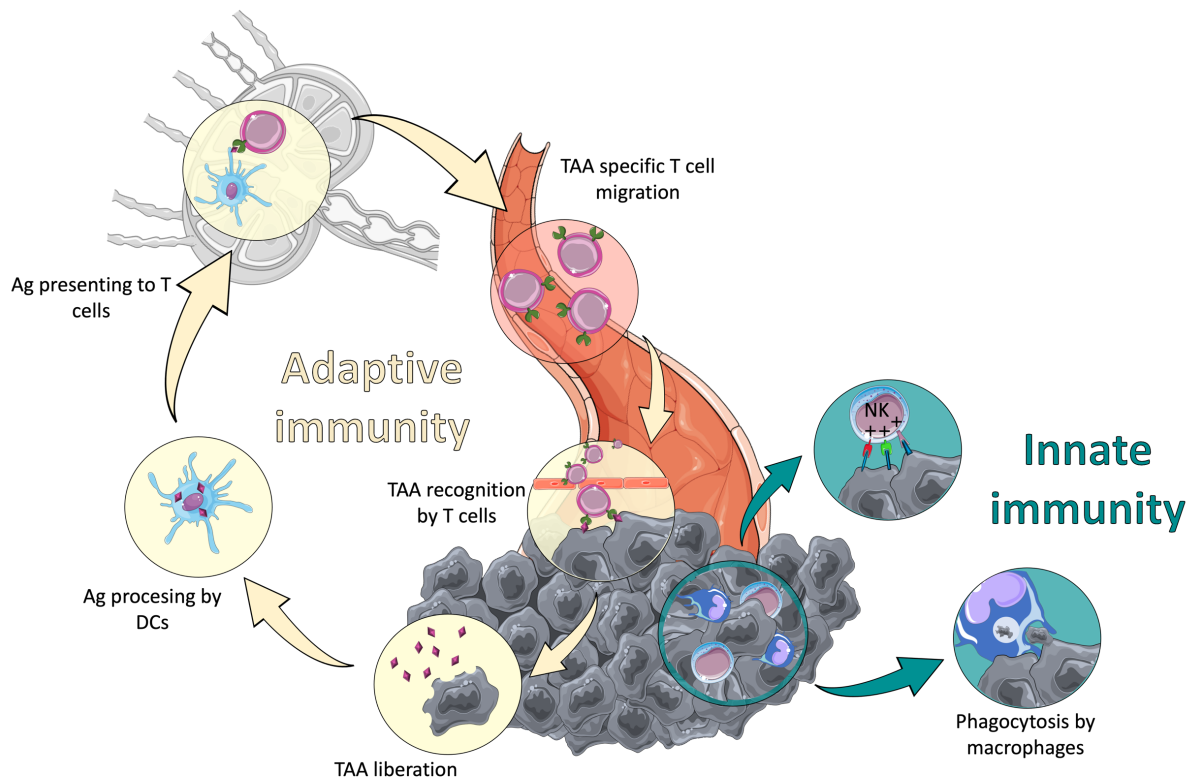


Figure 1.2. Immune response elucidated by tumors. In the figure the two arms of the immune response are represented: innate and adaptive responses. Innate immune cells (DCs, NK cells and macrophages are depicted) recognize tumor cells by different mechanisms. Dendritic cells (DCs) will trigger the adaptive immune response after engulfing tumor-associated antigens (TAA) and presenting them to T cells in the draining lymph node. Effector T cells migrate into the tumor and kill cancer cells releasing more TAA that can be captured by DCs, perpetuating the cancer-immunity cycle. On the other hand, macrophages may be activated by danger-associated molecular patterns (DAMPs) (i.e. heat shock proteins (HSP), adenosin triphosphate (ATP) or calreticulin)²⁷, are able to phagocytose aberrant cells (cancer cells) and also present TAA. There are ligands that may be expressed on the cancer cells membrane and that will engage NK cells activating receptors. Several activating receptor-ligand pairs examples are NKG2D-MICA/MICB, DNAM1-CD155/CD112, OX40-CD134L, NKp30-B7-H6, NKG2C-HLA-E (NK-tumor)¹⁸. Adapted from *Immunity*, (2013), 39(1), doi:10.1016/j.immuni.2013.07.012¹⁵. Ag: antigen, DC: dendritic cell, TAA: tumor-associated antigen, NK: natural killer.

NK cells also eliminate target cells through death receptor pathways, such as the tumor necrosis factor (TNF)-related apoptosis-inducing ligand (TRAIL)-TRAIL receptor (TRAILR), and the first apoptosis signal (FAS)-FAS ligand (FASL), also known as the CD95-CD95L pathway^{28,29}.

Besides eliminating tumor cells, NK cells are able to recognize and kill virus-infected cells^{30–32}, and they also engage in reciprocal interactions with other immune cells such as DCs and T cells^{25,33–35}. In addition to their direct cytotoxic capacity, and in response to stimulation with cytokines and through activating cell surface receptors, NK cells also secrete cytokines such as TNF α and interferon (IFN)- γ , and chemokines such as C-C motif chemokine ligand 3 (CCL3) and CCL4^{24–26,36,37}. Although NK cells are mainly known for their role in the surveillance against tumors and during viral infections, through their cytotoxic activity and secretion of soluble components, they have also been shown to have a great relevance in the generation of a more efficient T helper type 1 (Th1) immunity, in the modulation of autoreactivity and during pregnancy, among others^{38–41}. Therefore, a current view is that NK cells play a fundamental role in the maintenance of homeostasis and in the control of the immune response. Thus, on the one hand they promote inflammation, while on the other they are capable of restricting the adaptive immune response that could lead to excessive inflammation and even autoimmunity.

1.2.1.1. Activating and inhibitory receptors of NK cells

NK cells can discriminate between target cells and healthy “self” cells, and a lot of progress has been made to identify the cellular and molecular mechanisms that NK cells use to distinguish them, and all the accumulated data are involved in the so called “dynamic equilibrium concept”⁴². This concept explains the equilibrium between the activating and inhibitory receptors where the integration of their signaling cascades determine the response (or absence) of NK cells (Fig. 1.3). NK cells will kill and produce cytokines if the sum of the signals from activating receptors is higher than the sum of the signals from the inhibitory receptors. In general, activating receptors will recognize induced ligands expressed in aberrant or infected cells but not (or at very low levels) in healthy cells. By contrast, inhibitory receptors such as killer immunoglobulin (Ig)-like Ig receptors (KIR) and CD94/NKG2A will recognize “self” (i.e. MHC-I) and in consequence NK cells will not kill^{43,44}. This mechanism of action makes NK cells attractive to use them in anti-tumor therapy because in certain

Introduction. Harnessing the innate immune system through NP-based immunotherapy

occasions tumor cells will display more ligands for activating receptors than for inhibitory receptors⁴⁵.

Considering the “dynamic equilibrium concept”, the goal would be to lead NK cells to their stimulation through activating receptors. In humans (Fig. 1.3), some of the receptors expressed by NK cells include the inhibitory and activating forms of KIRs, CD94/NKG2 receptors (CD94/NKG2A, hereafter NKG2A, and CD94/NKG2C, hereafter NKG2C), natural cytotoxicity receptors (NCRs), which include NKp30, NKp44 and NKp46, the 2B4 receptor (CD244), NKG2D, NKp80, DNAX accessory molecule-1 (DNAM-1), T cell immunoreceptor with Ig and ITIM domains (TIGIT), CD161, and CD16, which is the low affinity Fc gamma receptor for IgG (FcγRIIIa) ^{46–50}. The latter is responsible for antibody-dependent cell-mediated cytotoxicity (ADCC). The interactions between receptors and ligands are of two types: 1) the recognition of autologous determinants, such as human leukocyte antigens (HLA) class I antigens by the inhibitory KIR and NKG2A receptors, will result in the tolerance of the NK cells towards self; 2) the detection of stress-induced molecules, which are normally expressed at very low levels, but their expression is increased in virus-infected and cancer cells, leading to the activation of NK cells and, as a consequence, to the destruction of tumor and infected cells ^{46,49,50}. Among the stress-induced molecules are the NKG2D ligands: MHC class I chain-related protein A and B (MICA and MICB), and members of the UL16 binding protein (ULBP) family ⁵¹. Ligands for NK cell activating receptors also include viral encoded molecules ⁵² and a member of the B7 family ⁵³. Thus, NK cells do not usually lyse healthy cells expressing MHC class I molecules and/or low or no expression of stress-induced molecules and other activating receptor ligands. Rather, they selectively kill target cells that have low levels of MHC class I expression and/or that express adequate levels of stress-induced molecules and other ligands for activating receptors ^{46,49,50}.

In addition, it is well known that NK cell-mediated activity is regulated by cytokines. Examples of stimulating cytokines include IL-2 and IL-15. Both of these cytokines bind the intermediate

affinity receptor IL-2R $\beta\gamma_c$ (β chain and γ common chain heterodimeric IL-2 receptor)⁵⁴. Recently, several approaches are being developed in which recombinant cytokines are engineered to increase their affinity for their receptors in comparison with the original protein. Some examples include N-803 (formerly known as ALT-803), Neoleukin-2/15, superkine (IL-2), etc. All these modified interleukins trigger higher proliferation and cytotoxicity of NK cells and longer half-life of the cytokine in the circulation⁵⁵.

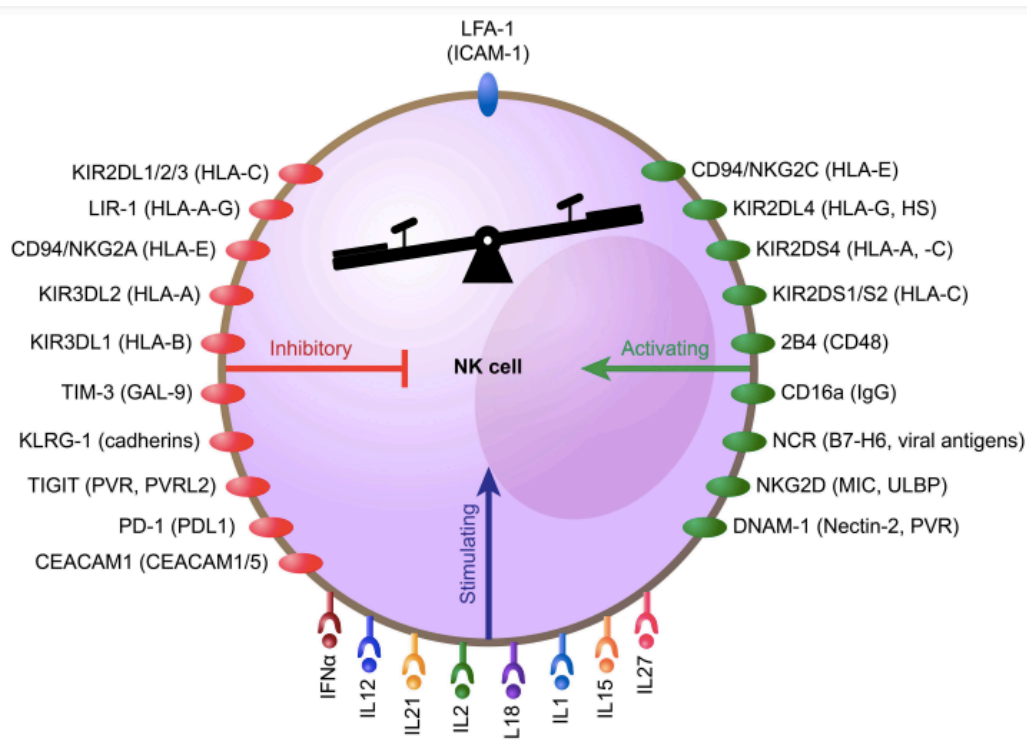


Figure 1.3. Activating and inhibitory receptors of human NK cells⁵⁶. Activating receptors are represented in green and inhibitory receptors are shown in red. The ligand for each receptor is written between brackets following the corresponding receptor. In the lower part cytokine receptors and cytokines pair that are able to stimulate NK cells are depicted. *Front. Immunol.* (2019), doi: 10.3389/fimmu.2019.02357⁵⁶

1.2.1.2. NK cells anticancer potential

Given NK cells potential to recognize and kill tumor cells, they have become a valuable tool in the fight against cancer and, therefore, several NK cell-based immunotherapies have been developed and are currently being used and tested in multiple clinical trials⁵⁷⁻⁶⁴. It is well known that the study of the interactions between HLA class I molecules and KIR receptors is very useful in allogeneic hematopoietic stem cell transplantation (HSCT) and in the design

Introduction. Harnessing the innate immune system through NP-based immunotherapy

of effective strategies of adoptive cell therapy. KIR-HLA class I molecules mismatch is of great relevance because donor NK cells expressing KIR that do not interact with host HLA class I molecules will be less inhibited and, therefore, they have superior ability to exert a graft versus leukemia (GvL) effect without inducing graft versus host disease (GVHD) ^{65,66}. Years ago, pioneering papers conclusively showed the ability of NK cells to mediate tumor regression *in vivo* in cancer patients. It was shown that NK cells from haploidentical donors can prevent relapse after haploidentical HSCT and can also induce remission after the infusion of haploidentical NK cells in patients with acute myeloid leukemia (AML) ^{66,67}.

To stimulate the immune response in cancer patients, the infusion of cytokines that have the ability to stimulate NK cells, as well as other cell types, are being used. The proof of concept that IL-2 has therapeutic potential was established long time ago ^{68,69}, although responses were limited and toxicity was very significant when used at high doses ⁶⁹. Low doses of IL-2, with fewer toxicity problems, are given to induce NK cell expansion *in vivo*, especially during adoptive cell therapy with NK cells ^{67,70,71}. On the other hand, since low doses of IL-2 can also stimulate regulatory T cells (Tregs) ⁷², new variants of this cytokine are being designed, such as the one that selectively binds to the β subunit of IL-2 receptor (IL-2R β) expressed on all NK cells, instead of the IL-2R α subunit which is highly expressed in Treg cells, and therefore it may provide better results ⁷³. Another relevant cytokine is IL-15, which stimulates CD8+ T cells and NK cells ⁷⁴. Administration of single-chain IL-15 (scIL-15) in cancer patients exhibited high dose-dependent toxicity ⁷⁵. Also, IL-15 super-agonists are being developed. An example is N-803, which is a complex that consists of a mutated IL-15 homodimer linked to a fusion protein formed by the α chain of the IL-15R (IL-15R α) and the Fc fragment of IgG1 ⁷⁶.

Checkpoint inhibitors have revolutionized cancer treatment and today they are a very relevant part of the therapeutic tools available to oncologists. There are checkpoints that are expressed primarily, though not exclusively, on NK cells. Among them, we can highlight KIR, NKG2A and TIGIT ^{46,49,50,77,78}. Clinical trials are testing the efficacy of blocking these

checkpoints with monoclonal antibodies (mAbs) in cancer treatment ⁷⁹. Anti-KIR mAbs, by blocking the interaction of HLA class I molecules on target cells with KIRs on NK cells, increase NK cell-mediated tumor cell lysis ⁸⁰. Several clinical trials are testing treatment of cancer patients with anti-KIR mAbs ^{79,81,82}. Also, by blocking the interaction of NKG2A on CD8+ T cells and NK cells with HLA-E on cancer cells, the mAb monalizumab is able to stimulate antitumor immunity by promoting the effector functions of those immune cells ⁸³. Also, blocking NKG2A expression by means of a single chain variable fragment (scFv) derived from an anti-NKG2A mAb linked to endoplasmic reticulum retention domains overcomes the resistance of HLA-E+ tumor cells to NK cell attack ⁸⁴. Tumor-associated NK cells express high levels of the TIGIT checkpoint inhibitory receptor, and therefore, blocking this receptor with mAbs prevents NK cell exhaustion and elicits potent antitumor immunity ⁸⁵. Several clinical trials are determining the safety and efficacy of anti-TIGIT mAbs alone or in combination with other mAbs ⁷⁹. Also, it is well known that other checkpoints, such as programmed cell death protein 1 (PD-1), are expressed on activated T cells, although NK cells can also express it ⁸⁶. Together with its PD-L1 ligand, it plays a central role in tumor recurrence and progression, since signaling through this pathway suppresses T cell and NK cell activation ⁸⁶. Experiments have shown that blocking PD-1 and PD-L1 stimulate a strong NK cell response, which could be very important for full therapeutic effect of these checkpoint inhibitors ^{87,88}. Thus, for example, blocking PD-1 enhances NK cell trafficking to tumors and also increases ADCC ⁸⁸.

Antibodies are also designed to direct NK cells to destroy tumors. mAbs induce tumor cell death through several mechanisms, including NK cell-mediated ADCC ⁸⁹. For example, rituximab, cetuximab and trastuzumab utilize ADCC as part of their mechanism of action ^{89,90}. The impact of polymorphisms in the gene that encodes CD16, and that affect its affinity for the Fc fragment of IgG1 and IgG3, has shown that the role of NK cells in mediating the antitumor response through ADCC is highly relevant ^{91,92}. On the other hand, the manufacture of mAbs that have different glycosylation patterns, in such a way that it also affects the affinity of their Fc fragment for CD16, adds relevance to the ADCC mechanism mediated by NK cells

Introduction. Harnessing the innate immune system through NP-based immunotherapy

^{93–95}. Regarding CD16, more recently have been designed bi- and tri-specific killer engagers (BiKEs and TriKEs). These are molecules that act through ADCC by cross-linking epitopes in tumor cells with CD16 on NK cells ^{57,96}. An example of TriKE consists of mAb fragments targeting the activating receptor NKp46 together with a tumor antigen and an Fc fragment to promote ADCC via CD16 ⁹⁷. Importantly, this TriKE has been shown to be more potent than clinical therapeutic antibodies targeting the same tumor antigen ⁹⁷.

Another therapeutic strategy consists in the adoptive transfer of NK cells. Compared to *in vivo* stimulation with cytokines, adoptive transfer allows manipulating NK cells prior to infusion and thus generating a more effective product. Some products include, for example, adoptive transfer of short-term *ex vivo* activated allogeneic NK cells that induce clinical responses in patients with multiple myeloma and AML ^{67,98}. *Ex vivo* activation of allogeneic NK cells for a short period of time has been carried out with cytokines such as IL-2 or IL-15 ⁹⁹. More recently, the efficacy and safety of cytokine-induced memory-like (CIML) NK cells have been explored ^{64,71}. CIML NK cells are generated after activation for approximately 18 hours with IL-12, IL-15 and IL-18. These cells are characterized by increased effector functions after a resting period and a longer half-life ^{36,64,100–102}. Importantly, clinical trials have demonstrated its safety and efficacy in treating patients with AML refractory to standard treatments ^{64,71}. Adoptive transfer of cultured and expanded NK cells with cytokines has also been used allowing the use of multiple infusions of highly activated NK cells ^{57,58,103,104}. Finally, the genetic manipulation of NK cells to optimize their persistence *in vivo*, as well as their location, overcome the resistant tumor microenvironment (TME) and cytotoxicity against tumor cells after adoptive transfer, is a very active research field at the present time ^{57,58,61,105,106}. Thus, NK cells expressing chimeric antigen receptors (CARs) (CAR-NK) are emerging as a complementary alternative to CAR-T cells. Some of the advantages of CAR-NK cells include greater safety, since the cytokine release syndrome and neurotoxicity are null or minimal, and the use of an allogeneic product does not pose the risk of developing GVHD. Another advantage is the feasibility for “off-the-shelf” manufacturing ^{107,108}. Numerous clinical trials with promising

results are being carried out with CAR-NK cells after having demonstrated their efficacy in preclinical models^{58,60,107,109–111}.

1.2.1.3. CIML (trained) and memory/adaptive NK cells.

Despite their classification as ILCs, NK cells exhibit memory properties, hinting the role of this cell type in adaptive immunity, long-term responses and contribution to cancer immunotherapy^{32,112–116}. NK cells exhibit three types of innate memory and memory-like responses depending on the initial stimulus: hapten-induced memory NK cells, viral-induced memory NK cells, also called adaptive NK cells, and CIML NK cells⁶⁴ (Fig. 1.4). The first two are antigen-specific, while CIML NK cells are not antigen-specific and have a flexible recall response.

In contrast to hapten-induced memory and adaptive NK cells, CIML NK cells more closely resembles trained immunity, in a similar manner as myeloid cells are trained by *Bacillus Calmette–Guérin* (BCG), β -glucan or lipopolysaccharide (LPS), and they also exhibit a long-term adaptation and persistence *in vivo*^{71,117,118}. Memory-like (or trained) properties of NK cells were first described by Cooper and Yokoyama¹⁰⁰. They found that after pre-activation of mouse NK cells with IL-12, IL-15 plus IL-18 for a short time, they can persist for a long time after adoptive transfer into syngeneic mice. Although the pre-activated NK cells proliferated, they returned to a resting state after one week of transfer and they were phenotypically similar to non-preactivated or endogenous NK cells and do not constitutively produced IFN- γ . However, these CIML NK cells produced significantly more IFN- γ upon restimulation¹⁰⁰. This enhanced ability to secrete IFN- γ was cell-intrinsic, independent of proliferative capacity, and persisted following cell division¹¹⁹. Similar to murine NK cells, human CIML NK cells have been also described¹⁰¹. The pre-activation of human NK cells with IL-12, IL-15 plus IL-18 followed by a resting period, enhanced cytokine and chemokine secretion, degranulation and cytotoxicity after restimulation with target cells and/or cytokines^{36,101,102,120–123}. In mouse models it has also been demonstrated that NK cells display memory-like properties following

Introduction. Harnessing the innate immune system through NP-based immunotherapy

systemic stimulation. Specifically, following LPS-induced endotoxemia, NK cells acquire cell-intrinsic memory-like features such as increased production of IFN- γ upon specific secondary stimulation¹²⁴. These memory-like NK cells persisted for at least 9 weeks and contributed to protection from *Escherichia coli* (*E. coli*) infection upon adoptive transfer¹²⁴.

Given the properties of CIML NK cells, they are becoming an important tool in the treatment of malignancies. First, it was reported that a single injection of IL-12/15/18-preactivated NK cells combined with radiation therapy substantially reduced growth of established mouse tumors, including solid tumors¹²⁵. Highly CD25 expressing preactivated NK cells proliferated *in vivo* in response to IL-2 produced by CD4+ T cells and persisted for a long time^{125,126}. Other studies have also shown that adoptive transfer of murine CIML NK cells suppressed GVHD and enhanced GvL after allogeneic HSCT^{122,127}. Regarding humans, several preclinical studies have demonstrated that CIML NK cells exhibited enhanced responses against tumor targets *in vitro* and *in vivo*^{36,64,71,101,118,128–130}. Very interestingly, it has been recently published that CAR-modified CIML NK cells displayed potent responses, including IFN- γ production, degranulation and killing, against NK cell resistant lymphomas when compared with conventional CAR-NK cells. Moreover, these CAR-modified CIML NK cells exhibit antigen-specific persistence and effectively control lymphoma targets *in vivo* in xenograft models¹¹⁰.

In the clinical practice, adoptive transfer of CIML NK cells is becoming a very important immunotherapy against hematological malignancies, mostly for patients with relapse/refractory AML⁷¹. Fludarabine and cyclophosphamide lymphodepleted patients were infused with a single CIML NK cell dose generated from a related HLA-haploidentical donor. After the transfer, low doses of IL-2 are given to support NK cell survival, expansion and function⁷¹. Clinical results were very encouraging, with approximately 50% of the patients achieving complete remission^{64,71,118}. Importantly, CIML NK cells infusion did not result in GVHD or cytokine release syndrome⁶⁴. Analysis have shown that the frequency of CD8 α + donor NK cells is negatively associated with the outcome after CIML NK cell therapy and that

the inhibitory NKG2A receptor is a dominant checkpoint for CIML NK cells, opening the possibility of targeting the NKG2A-HLA-E axis to improve its efficacy ¹¹⁸. Nonetheless, the infused haploidentical CIML NK cells will eventually be eliminated when the recipient's immune system recovers. Therefore, other approaches are being tested, as for example adoptively transferring CIML NK cells to patients that have previously received a standard of care haploidentical peripheral blood HSCT after reduced intensity conditioning with post-transplantation cyclophosphamide for GVHD prophylaxis. CIML NK cells are generated from a second leukapheresis from the same donor after the HSCT. Preliminary data have shown very promising results ⁶⁴. Other clinical trial is testing same donor CIML NK cells with donor lymphocyte infusion in patients that relapsed after allogeneic HSCT. Very possibly adoptive transferred cells will persist longer and improve the chances of complete remission ⁶⁴. Murine studies showing the synergistic interaction between T cells and CIML NK cells support this rationale ¹²⁶. Some of the clinical trials with CIML NK cells include NCT01898793, NCT02782546, NCT03068819, NCT04024761, NCT04290546, NCT04354025 and NCT04634435 (from clinicaltrials.gov).

The induction of a trained phenotype in CIML NK cells enables them to react rapidly and stronger when they are challenged with subsequent triggers. The molecular basis of this characteristic responsiveness is not very well known, but it is becoming clear that transcriptional, epigenetic and metabolic reprogramming occurs in CIML NK cells (Fig. 1.4).

Hapten-induced and virus-induced memory NK cells have been shown to be antigen-specific (Figure 1.4). Because these adaptive NK cell responses more closely look like T cell responses than the trained immunity exhibited by myeloid cells and CIML NK cells, it has been hypothesized that this distinctive NK cell response may represent an evolutionary bridge between the memory response of T cells and that of myeloid lineage ^{26,50,117}. The ability of NK cells to acquire antigen-specific memory was first described in the context of contact hypersensitivity (CHS) responses to chemical haptens ¹³¹. Hapten-induced CHS is an example

Introduction. Harnessing the innate immune system through NP-based immunotherapy

of adaptive immunity and it was found that mice lacking T and B cells, but not NK cells, were able to exhibit hapten-induced CHS responses and that these recall responses discriminated between different haptens and persisted for weeks¹³¹. Hapten memory NK cells reside in the liver and are dependent on the expression of CXCR6, which is critical for their persistence in the liver^{131,132}.

In humans, the pioneering works of López-Botet's group showed that healthy individuals seropositive for human cytomegalovirus (HCMV) exhibited higher frequencies of NKG2C+ NK cells¹³³. These cells expanded *in vitro* in response to HCMV-infected fibroblasts¹³⁴ and following acute HCMV infection *in vivo*¹³⁵. The expansion of these NKG2C+ adaptive NK cells requires, among others, IL-12 and the presentation of HCMV-encoded UL40 peptides by the non-classical MHC-I molecule HLA-E^{136,137}. Regarding cell surface markers, in addition to expressing NKG2C, human adaptive NK cells also express the late differentiation marker CD57, and higher levels of CD2, LIR-1 and CCR5 and low levels of NKp30, NKp46, and CD161, among other features¹³⁸. At the functional level, they have higher expression of granzyme B and Bcl-2, secrete higher levels of cytokines, and are capable of mediating strong ADCC responses and secrete cytokines against CMV infected cells¹³⁸. Very significantly, they have a very low or null expression of key components of cellular signaling molecules (FcεRγ, Syk, EAT-2) and transcription factors (PLZF, Helios)¹³⁸. Nevertheless, human adaptive NK cells are heterogeneous and several subpopulations can be distinguished based in the expression of different markers¹³⁹. For example, although the frequency of FcεRγ⁻ and NKG2C+ NK cells positively correlated, the FcεRγ⁻ and NKG2C+ NK cell populations did not exactly overlap¹⁴⁰. Moreover, different subsets exhibit somehow different properties: FcεRγ⁻NKG2C+ NK cells had weak natural effector function against K562 target cells but strong ADCC, while FcεRγ⁺NKG2C+ NK cells had strong effector functions in both settings¹⁴⁰. On the other hand, FcεRγ⁻NKG2C+ NK cells exhibited low Ki67 and high Bcl-2 expression, indicating the long-lived quiescent memory-like property¹⁴⁰. Interestingly, Liu et al have demonstrated that deleting FcεRγ reprograms conventional NK cells to display features of adaptive NK cells, while

deletion of PLZF had no significant effects¹⁴¹. It is also important to know that expansions of NKG2C⁺ NK cells have been also described in other infections such as HIV, hantavirus, chikungunya virus and SARS-CoV-2^{142–146}. However, in reports where HCMV status was assessed, the expansion of the NKG2C⁺ subset was almost entirely confined to individuals seropositive for HCMV^{142–146}. On the other hand, Nikzad et al. have found that human NK cells were able to display antigen-specific recall responses *in vitro* when isolated from livers of humanized mice previously vaccinated with HIV envelope protein¹⁴⁷. Furthermore, they also discovered that large numbers of cytotoxic NK cells were recruited to places of varicella-zoster virus (VZV) skin test antigen challenge in VZV-experienced people¹⁴⁷. Although they did not address by which mechanisms NK cells recognize HIV envelope protein and VZV specific NK cells are recruited to the challenge sites, they suggest that very likely is different from that of NKG2C expressing NK cells that expand upon HCMV infection and/or reactivation, highlighting the diversity of the human pool of virus-memory NK cells¹⁴⁷. Along these lines, Stary et al have also described a subset of human hepatic CD49a⁺CD16⁻ NK cells that exhibit antigen-specific cytotoxicity against B cells and dendritic cells pulsed with hepatitis A or hepatitis B proteins¹⁴⁸. Interestingly, the antigen-specific killing by these adaptive CD49a⁺CD16⁻ hepatic NK cells were able to bypass the KIR receptor-ligand system¹⁴⁸. In a similar way as to the hapten-induced memory NK cells shown in mice^{131,132}, Stary et al also showed that in patients sensitized against nickel, specific CD49a⁺CD16⁻ NK cells were recruited, very probably from the liver, to a nickel-induced epicutaneous patch test, highlighting the possibility of a liver-skin axis in the pathophysiology of hapten-induced adaptive NK cells¹⁴⁸.

Arguably, the best known model of adaptive NK cells involves the study of mouse CMV (MCMV) infection¹⁴⁹. Ly49H⁺ NK cells possess antigen specificity for the MCMV-encoded glycoprotein m157¹⁵⁰, undergo clonal proliferation^{151,152} and, in a similar manner to CD8⁺ T cells, persist during the contraction and memory phases²⁶. After reinfection, adaptive NK cells undergo a secondary expansion and they release cytokines and degranulate more rapidly,

Introduction. Harnessing the innate immune system through NP-based immunotherapy

which results in a more protective response against MCMV¹⁴⁹. The formation of robust effector and adaptive NK cells require proinflammatory cytokine signals such as IL-12 and IL-18^{153,154}. It has also been demonstrated the development of specific memory mouse NK cells after vaccination with antigens from influenza, vesicular stomatitis virus (VSV) or human immunodeficiency virus (HIV)-1. The adoptive transfer of virus-sensitized NK cells into naive recipient mice enhanced the survival of the mice after lethal challenge with the sensitizing virus but not after lethal challenge with a different virus¹³².

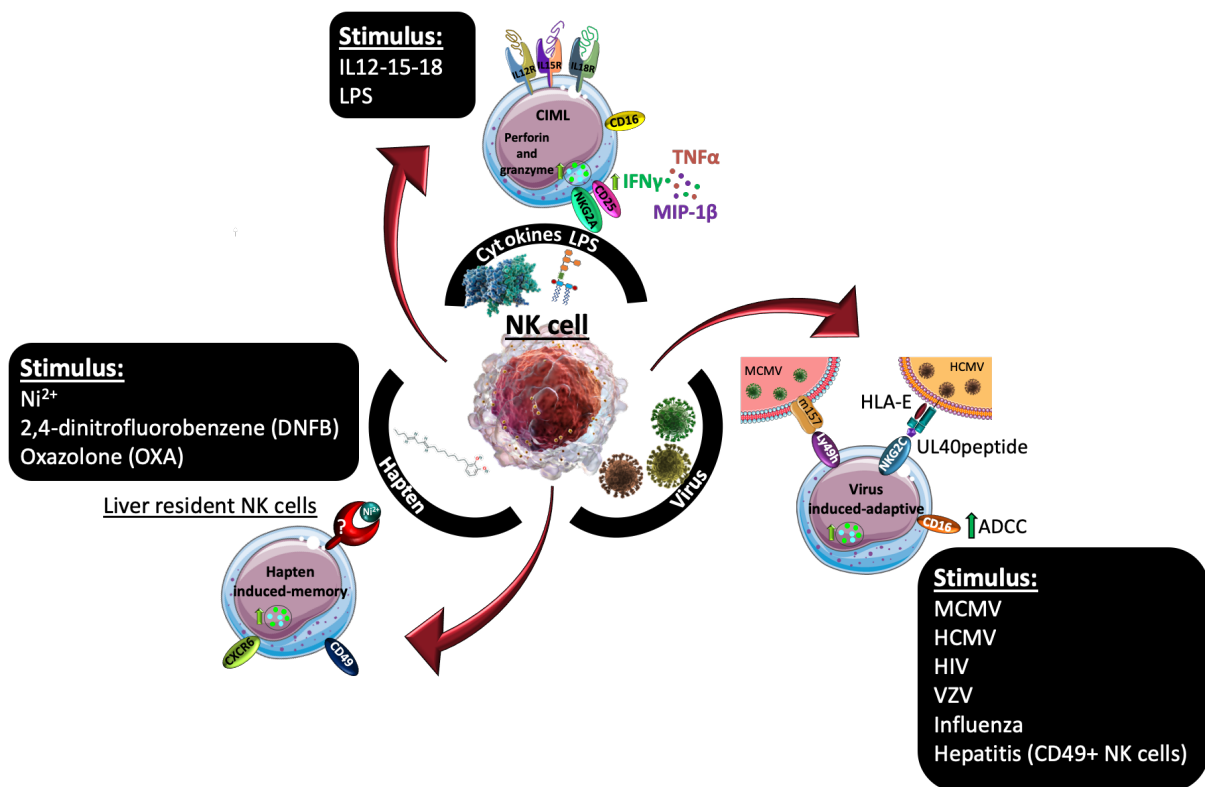


Figure 1.4. Heterogeneity of memory and memory-like NK cells. Three types of NK cells with memory properties are represented in the figure: CIML (cytokine-induced memory-like) or LPS-trained NK cells, virus-induced and hapten-induced NK cells. Black boxes depict the initial stimuli to induce the expansion of NK cells. ADCC (antibody-dependent cell-mediated cytotoxicity), CIML (cytokine-induced memory-like), HCMV (human cytomegalovirus), HIV (human immunodeficient virus), HLA (human leucocyte antigen), LPS (lipopolysaccharide), MCMV (murine citomegalovirus), VZV (varicella zoster virus). Adapted from Mikelez-Alonso et al., *Adv Drug Deliv Rev.* (2021) 10.1016/j.addr.2021.113860¹⁵⁵

1.2.2. Cytokines as stimulators of the innate immune system

Cytokines are molecules that play an important role in controlling the growth and activity of immune cells and other cells. The first described cytokine was related to fever pathogenesis in 1953¹⁵⁶. They are able to generate a response in picomolar to nanomolar concentrations and their size is between 6-30 kiloDalton (kDa) in almost all cases, and not more than 70 kDa¹⁵⁷. These molecules have a key role on the communication between immune cells and they can control the type and duration of the immune response¹⁵⁸. For example, IL-4 and IL-13 cause the polarization to M2 immunosuppressive phenotype of macrophages *in vitro* and in the TME *in vivo* ^{159,160}. These M2 macrophages release more immunosuppressive cytokines such as IL-10 or pro-metastatic proteins such as Chitinase-3-like protein 1 (CHI3L1), which shapes the TME in favor of tumor progression^{161–163}.

Many examples support the use of cytokines in cancer immunotherapy. For example, IFN- γ acts directly on cancer cells inhibiting hTERT (human telomerase reverse transcriptase). IFN- γ induces growth arrest which is translated on an inhibition of tumor cell growth¹⁶⁴. But IFN- γ is a pleiotropic cytokine and the mechanisms of its antitumor effect are numerous including, among others, increasing antigen presentation, favoring Th1 cell polarization and causing an inflammatory response^{165–168}. Interleukins are also studied as anticancer therapy and IL-2 is a good example of that. IL-2 exert antitumor effect in an indirect way where T cells are activated and expanded to become the final effector, but IL-2 also acts directly in the tumor area, by controlling the cell cycle of cancer cells or inducing tumor suppressor interleukins expression in melanoma cells^{169,170}. However, IL-2 is known to have limited efficacy, which is attributed to 1) toxicity induced by high doses of IL-2 that are needed to obtain beneficial results and 2) to the preferential expansion of Treg cells, due to their expression of the IL-2 high affinity receptor, which is translated on decreasing antitumor immunity¹⁷¹. Even so, IL-2 variants and other formulations such as the combined administration of IL-2 with TLR agonists are been investigated to avoid these limitations with successful results for application in antitumor

Introduction. Harnessing the innate immune system through NP-based immunotherapy

therapies^{172–175}. IL-2, IFN- γ and others, such as granulocyte-macrophage colony stimulating factor (GM-CSF) and IL-12, are used for the treatment of cancer^{176–180}. Additionally, it is well known that cytokine combinations induce functional and gene expression changes in many cell types, including in NK cells¹⁸¹. A good example is the pre-activation with IL-12, IL-15 and IL-18 generates CIML NK cells as it is described above.

However, as a consequence of the small size of the cytokines, their bioavailability is very low due to rapid clearance from plasma¹⁸². For this reason, many efforts are behind the goal of changing the pharmacokinetic of this kind of proteins *in vivo*. Introducing mutations in the sequence¹⁷⁵ or simply conjugating them with polymers¹⁸³ or loading them into nanoparticles are getting importance since the FDA started approving some of these organic and non-organic based nano-materials for their use in the clinic¹⁸⁴ (see Table 1.1).

Therefore, the strategy of nanovehiculization of cytokines try to achieve three goals:

- 1) increase the half-life of the cytokine in the circulation
- 2) increase the effective dose of the cytokine
- 3) and in consequence of the second goal, avoid the toxic effect of high doses of cytokines

Table 1.1. Examples of nanocomposites loaded with cytokines for antitumor immunotherapies.

Composition				
Nanoformulation	Cytokine	NP material	Therapeutic role	Ref.
DOTAP/MPEG-PLA-pIL-12	IL-12	DOTAP/MPEG-PLA	Lymphocytes proliferation and tumor cell killing after transfection of DMP-pIL12 into Ct26 cell. <i>In vitro</i> and <i>in vivo</i> model.	185
SPIONs-PAA-PEI+pDNA ^{IL-12}	IL-12	SPION and PAA and PEI	Magnetofection of pDNA ^{IL-12} into tumor cellstriggering IL-12 protein expression in the tumor area, activation of immune cells and then tumor cells death.	186
mPEG-Dlink _m -PDLLA	IL-12	PEG, PDLLA	Immunochemotherapy <i>in vivo</i> . The immune effect is produced by macrophage polarization from M2 to M1 and activation of T and NK cells cytotoxic functions, provoking tumor cell death. Chemotherapy effect is produced by paclitaxel.	187
TT-LDCP NPs	IL-2	DOTA, DOTAP, DSPE-PEG2000, cholesterol	Dual targeted immunogene therapy. siRNA for PD-L1 checkpoint and pDNA for IL-2 protein expression. The treatment triggers T and NK cells effector functions.	188

S(RA)_{IFN} + S(sulf)_{PIC}	IFN- γ	MSN	The treatment happens in two steps: first S(RA) _{IFN} enhances TLR3 expression, and then S(sulf) _{PIC} recognized TLR3 causing apoptosis.	189
DsNKG2D-IL-21 NPs	IL-21	Chitosan	NK and T cells activation by expression of NKG2D-IL-21 fusion protein from transfected tumor cells with pNKG2D-IL-21.	190
G-DOX/IL-2/IFN-γ	IL-2 IFN- γ	PELG ₇ -PEG ₄₅ -PELG ₇	Thermo sensitive hydrogel for melanoma treatment combining chemotherapy (doxil) and immunotherapy (IL-2 and IFN- γ) promoting T and NK cells proliferation.	191
PLE-IL-12 NPs	IL-12 IFN- γ	PLR, PLE, HA	Activation of T lymphocytes and mediation of Th1 type immune response.	192
NV-DOX_{IL-2}	IL-2	Cell derived membrane-based platform	Enhancement of DC maturation, T and NK cells cytotoxic function and recruitment of other immune cells in the tumor area.	193
IL-15 NP	IL-15	PLH-PEG-SPDP	Enhanced the cytotoxic effect of T and NK cells by activation of these cells.	194

DOTAP: Dioleoyl-3-trimethylammonium propane, MPEG-PLA: Methoxy poly(ethylene glycol)-poly(lactide), SN: supernatant, SPION: super paramagnetic iron oxide nanoparticles, PAA: polyacrylic acid, PEI: polietilenimina, PEG: poly(ethylene glycol), PDLLA: poly(D,L-lactide), DOPA: 1,2-dioleoyl-sn-glycero-3-phosphate, DOTAP: 1,2-dioleoyl-3-trimethylammonium-propane, DSPE-PEG2000: 1,2-distearoyl-sn-glycero-3-phosphoethanolamine-N-[methoxy(polyethylene glycol)-2000], MSN: mesoporous silica NPs, PELG: poly(2-aminoethyl-L-glutamate), PLR: poly-L-Arginine, PLE: poly-L-Glutamic acid, HA: hyaluronic acid, PLH: Polymer lipid hybrid, SPDP: succinimidyl 3-(2-pyridylthio)propionate.

1.2.2.1. IL-15 biology and its anticancer activity

IL-15 cytokine is a 12.5 kDa protein with structural similarities to IL-2¹⁹⁵ that is related to the binding to common receptor subunits. Both cytokines bind the complex of IL-2R β or CD122 with the common γ chain (γ_c) or CD132^{196,197}. In addition, a third chain may bind IL-2R $\beta\gamma_c$ to form a heterotrimeric receptor. IL-2R α chain or CD25 associates with IL-2R $\beta\gamma_c$ to conform the IL-2 high affinity receptor (IL-2R $\alpha\beta\gamma_c$), while IL-2 binds to IL2R $\beta\gamma_c$ with intermediate affinity¹⁹⁸. In physiological conditions, IL-15 is bound to IL-15R α and transpresented to lymphocytes expressing IL-2R $\beta\gamma_c$ by other cells such as epithelial cells, fibroblasts, monocytes and DCs^{199,200}. This is the reason why IL-15 is mostly undetectable in its soluble form. Although the two cytokines activate target cells through two common receptors, they dictate unique biologic outcome. As an example, IL-2 promotes the differentiation of effector cytotoxic T lymphocytes (CTL), and IL-15 promotes the development of memory T cells. In addition, the stimulation by IL-15 promotes enhanced antitumor capacity of CD8+ T cells and showed superior cytolytic activity by NK cells. This last effect could be associated with stronger signaling of the metabolic checkpoint kinase mammalian Target of Rapamycin (mTOR) following IL-15 stimulation of NK cells.^{201,202} In addition, it is known that the absence of IL-

Introduction. Harnessing the innate immune system through NP-based immunotherapy

IL-15 decreases the accumulation of effector cells, such as CD8⁺ T cells in the lymph node, down-regulating the immune response against the tumor mass as it happens in IL-15 deficient mice, highlighting the role of IL-15 in antitumor therapy and also in other diseases such as tuberculosis^{203–206}.

Regarding using IL-15 for anticancer therapy, it was initially sought as an alternative to IL-2, because of some limitations exhibited by the latter. For example, in contrast to IL-2, IL-15 does not stimulate Treg cells while it is able to activate and trigger NK and CD8⁺ T cells expansion²⁰⁷. Still, infusion of IL-15 single chain has a high toxicity profile and a rapid clearance from plasma²⁰⁶. Also, IL-15 superagonists are being developed and tested in clinical trials alone or in combination with other drugs. For example, the combination of the IL-15 superagonist N-803 with Nivolumab is being investigated for advanced or metastatic non-small cell lung cancer treatment (*NCT02523469*)²⁰⁸ and with BCG for BCG-unresponsive non-muscle invasive bladder cancer (*NCT03022825*). This IL-15 formulation is designed with the Fc domain of a human IgG1 bound to a complex of IL-15 and sushi domain of IL-15R α . These combinations of molecules to obtain N-803 confer to IL-15 1) prolonged half-life and 2) higher activity than IL-15 single chain^{209,210}.

1.2.3. Cancer nano-immunotherapy

A limitation of cancer immunotherapy consists in the difficulty of reaching the tumor location, which in many cases is away from the injection route. To overcome this limitation, the treatment dose is generally increased to achieve an efficient drug dose in the tumor²¹¹. However, this dose increase could trigger undesired side effects that are harmful to the patients. This limitation makes NPs ideal candidates for the delivery of cancer immunotherapies since they follow different pharmacokinetics and pharmacodynamics compared to free drugs^{212,213}.

Over the last two decades, NPs have been widely explored for their use in biomedical applications. Nevertheless, immunotherapy was not the first biomedical use of NPs. A few

years ago, editors from *Science* named immunotherapy as the “Breakthrough of the year”²¹⁴. Following this, the use of NPs in immunotherapy have increased tremendously. In addition, some anticancer treatments based on NPs have been approved by the FDA. In addition, more work is currently going on to achieve new anticancer therapy strategies based on nano-materials approved already by the FDA, such as Iron Oxide Nanoparticles (IONPs) (Table 1.2). However, these systems face issues concerning stability in physiological media, protein corona (PC) formation, and accumulation in the target tissues. The formation of a PC around the NPs in the presence of biological fluids plays an important role, mainly in changing the physicochemical properties of the nano-formulations, with consequent decrease in the therapeutic efficacy of nanomedicines. Furthermore, the modification of the surface of the particles is patient-specific and the formation of a PC may have additional undesired effects on the performance of the NPs including loss of efficacy of targeting moieties, undesired flagging by the complement, unspecific uptake by immune cells, and immunotoxicity^{215–217}.

Table 1.2. Recently studied nanoformulations for immunotherapy. Some nano-formulations are approved by Food and Drug Administration (FDA) and others are in clinical trials not necessarily for their use as anticancer therapy. QT: chemotherapy. Mikelez-Alonso et al., *Int. J. Mol. Sci.* 2020, 21(2), 519; <https://doi.org/10.3390/ijms21020519>²¹⁸

Name	Formulation description	QT	Target	Clinical Trials	FDA approval and indications	Ref
Ferumoxytol (Ferahem®)	Polyglucose sorbitol carboxymethyl ether-coated IONP.	No	TME → M2-like macrophages to M1-like.	-	MR imaging, anemia and kidney diseases.	219
eCPMV	Virus like particles (VLP) of cowpea mosaic virus.	No	Neutrophil activation in the TME	-	-	220, 221
RNA-LPX (Lipoplex®)	RNA-loaded liposomes.	No	DC maturation, T cell response, inflammatory response.	NCT02410733	-	222
MRX34	miRNA-34a-loaded liposome.	No	Downregulation of immune evasion tumor genes.	NCT01829971	-	223
nab-Paclitaxel (Abraxane®)	Paclitaxel-loaded albumin NPs.	Yes	DC maturation.	NCT01565499 NCT01667211	Breast cancer after failure of combination chemotherapy for metastasis or relapse within 6 months of adjuvant chemotherapy.	224, 225
aCD47@CaCO ₃	Anti CD47-loaded CaCO ₃ NP in fibrinogen solution.	No	After surgery, and with the addition of thrombin, aCD47@CaCO ₃ forms an immunotherapeutic gel in situ in the TME.	-	-	226
Sipuleucel-T (Provenge®)	Ex vivo DCs.	No	Vaccine.	-	Asymptomatic or minimally symptomatic metastatic castrate resistant prostate cancer.	227
Blinatumomab (Blincyto®)	Bi-specific T cell engager (BiTE). Specific to CD19 and CD3.	No	BiTE targeting CD19 (malignant B cell) and CD3 (T cell) for cytotoxicity against B cells.	NCT04521231 NCT04554485	Philadelphia chromosome-negative relapsed or refractory B-cell precursor acute lymphoblastic leukemia (ALL).	228
Talimogene laherparepvec (Imlygic™, T-VEC)	Injectable modified herpes virus encoding GM-CSF.	No	Local and systemic immune responses leading to tumor cell lysis and GM-CSF expression to DC activation. Liberation of tumor specific Ag and activation of tumor specific effector T lymphocytes.	-	Local treatment of unresectable cutaneous, subcutaneous, and nodal lesions in patients with melanoma recurrent after initial surgery.	229, 230
BIND-014	Docetaxel-loaded Poly-Lactic Acid (PLA) NP and Prostate-Specific Membrane Antigen (PSMA) in the surface.	Yes	-	NCT01812746	-	231, 232
Doxil®	Dox-loaded liposome.	Yes	-	-	Ovarian cancer, AIDS-related Kaposi's sarcoma and multiple Myeloma.	233
Marqibo®	vinCRISTine sulfate-loaded liposome	Yes	-	-	Ph negative ALL in second or greater relapse or whose disease has progressed following two or more anti-leukemia therapies.	234
Ontak®	Diphtheria toxin and IL-2 fusion toxin.	Yes	-	-	Persistent or recurrent cutaneous CD25 + T-cell lymphoma.	235

1.3. Anticancer nano-immunotherapy: “The good, the bad and the ugly”

New nanoparticles (NPs) based therapeutic strategies are emerging with the aim to enhance the efficacy of tumor immunotherapies. NPs exhibit different pharmacodynamic and pharmacokinetic properties compared with free drugs and enable the use of lower doses of immune-modulating molecules, somehow minimizing their side effects. It is well known that toxicity is an important problem associated with many immunotherapies²³⁶. In the context of using NPs for biomedical applications, it is important to understand the interactions occurring at the interface between NPs and biological fluids to predict the fate of injected NPs. It is commonly accepted that the interaction of the NPs and biological fluids is a consequence of several factors such as NP size, shape, charge, or coating agents are critical^{237–244}, but the characteristics of the biological fluids are also very important (ionic strength, protein concentration, pH, and temperature)²⁴⁵. Once NPs are exposed to biological fluids, they interact with active biomolecules (mostly proteins, but also sugars, nucleic acids, and lipids) and PC is formed around them by the unspecific adsorption of proteins on the surface of the NPs. This effect gives the NPs, upon PC formation, a different biological identity compared to bare NPs. The physicochemical properties of the bare NPs such as size, surface charge, surface composition, and functionality, change due to the PC formation. Therefore, the characterization of the properties of NPs after their exposure to a biological fluid has become mandatory for two purposes, to understand how these new characteristics affect the behavior of the nano-formulation *in vivo* and to design strategies to avoid the PC formation. In this context, Zhou et al. disclosed that the dynamic structure of NP surfaces can affect the protein adsorption kinetics and thus the interaction between nanoparticles/adsorbed proteins and cells²⁴⁶.

Recently, the scientific community has been moving from the mere evaluation of the impact of the PC on the physicochemical properties of NPs to the evaluation of the impact on their behavior in physiological systems. Furthermore, a large number of

Introduction. Harnessing the innate immune system through NP-based immunotherapy

studies have provided much insight into the layer thickness and composition of the PC, and the adsorption kinetics under different experimental setups. Many techniques have been used to measure the absorption of proteins around the NPs such as UV-visible spectroscopy (UV/Vis), dynamic light scattering (DLS), transmission electron microscopy (TEM), and fluorescence correlation spectroscopy (FCS) ^{247–249}. Another non-optical method that allows for the measurement of PC formation in complex media such as blood is ¹⁹F diffusion measured by nuclear magnetic resonance (NMR) ²⁵⁰. In addition, different techniques such as surface plasmon resonance (SPR), isothermal titration calorimetry (ITC), differential centrifugal sedimentation (DCS), and quartz crystal microbalance (QCM) have been used to quantify the affinities of proteins for NPs ^{251–255}. Nevertheless, liquid chromatography–mass spectrometry (LC-MS) is probably the most powerful tool to identify proteins present in the PC^{256,257}.

PC formation is especially relevant in the field of the immunotherapy, since in order to trigger an immune response, it is essential the interaction between antigens or other molecules and their receptors. In this sense, has been demonstrated that the PC can have a dual role in biomolecular recognition (Fig. 1.5). In some cases, the PC hides the antigen/molecule on the NPs surface, thereby inhibiting the interaction with its specific receptor (this immune-escape process could be defined as “*immune-blinding*”); and in other cases the PC contains proteins that act as ligands for receptors on specific immune cells and triggers undesirable immune responses (“*immune reactivity*”)^{258,259}. Additionally, PC can induce the phagocytosis of the NP by monocytes and macrophages ²⁵⁸ and in consequence could avoid the recognition of the molecules exposed on the surface of the NPs.

1.3.1. Immune-blinding as a consequence of PC formation

As shown in figure 1.5, immune-blinding could be promoted by two main mechanisms. On the one hand, PC may fully or partially cover the antigens/molecules present on the

surface of the NPs, and in consequence, the specific interaction and response will be low or fail and consequently the desired functions will not occur. Shanehsazzadeh et al. described a good example on how PC can induce immune-blinding on a nano-formulation *in vivo*. The uptake of NPs functionalized with anti-mucin1 (anti-MUC-1) antibody was nine times higher in MUC-1-positive cells than in the MUC-1 negative cells *in vitro*. However, in the *in vivo* mouse model, the antibody-functionalized NPs showed higher distribution in blood and muscle than in tumor. The conclusion of this work was that the PC covered the anti-MUC-1 antibody and in consequence, the specific tumor uptake *in vivo* was reduced^{260,261}. These difficulties *in vivo* evidence the importance of the NP composition in the possible immune-blinding effect promoted by the PC, as it was also shown in another study in which a different PC formation was observed depending on the PEGylation grade of NPs²⁶². In the case of nano-vaccine based therapies, the PC also plays a critical role in the uptake of the nano-formulation by DCs, which is a critical step for an effective therapeutic response^{237,263}.

On the other hand, the blinding effect can be due to the homeostatic function of immune cells. Macrophages have scavenger receptors that recognize biological patterns on strange bodies²⁶⁴. Sometimes, the structure of the proteins that formed the PC is altered during the PC formation on the surface of the NPs²⁶⁵, and in consequence usually unexposed epitopes are presented to the immune system. Macrophages could recognize these epitopes and phagocyte the NP–PC complexes through the scavenger receptors (Fig. 1.5)^{266,267}. This situation could be solved changing the physicochemical properties of the NPs and in consequence reducing the uptake of the NPs by macrophages²⁶⁸.

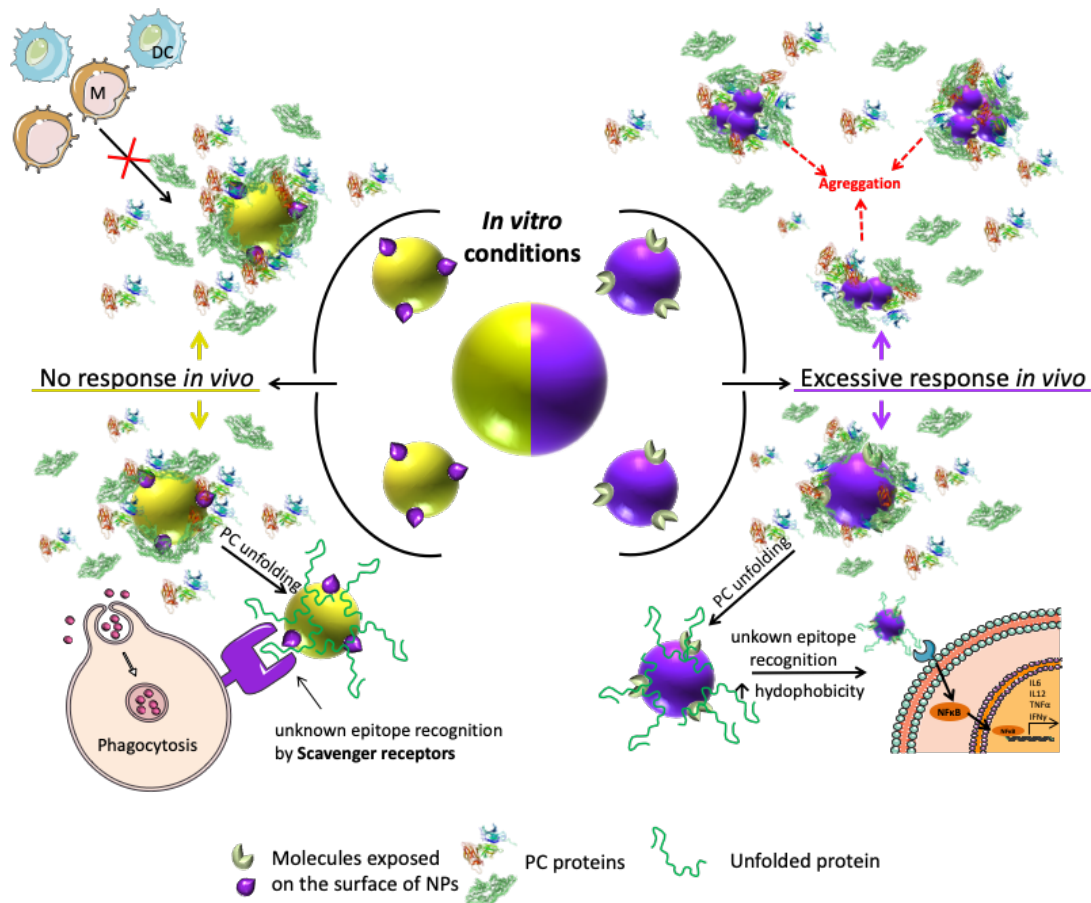


Figure 1.5. Nanoparticle-based immunotherapy failure because of protein corona (PC) formation. No-response (**left**) vs. excessive or uncontrolled response (Immune reactivity) (**right**). Top left panel: Immune cells are not able to recognize the molecules exposed on the surface of the NPs because the PC covers the NPs partially or totally. Bottom left: NP phagocytosis by macrophages because of the denaturalization of the proteins (in green) on the surface of the NPs. Top right: Aggregation of NPs triggers toxic effects by strange-body recognition by the immune system. Bottom right: Nuclear Factor κ B (NF- κ B) translocation to the nucleus because of the recognition of denatured proteins on the surface of the NPs. Mikelez-Alonso et al., *Int. J. Mol. Sci.* 2020, 21(2), 519; <https://doi.org/10.3390/ijms21020519>²¹⁸

1.3.2. Immune response or immune reactivity as a consequence of PC formation

The difference between a controlled and an uncontrolled and undesired immune response, which could be immune reactivity, as it is defined above, is not always clear. Immunotherapy in many cases, such as in cancer, seeks to strengthen the immune response, and it is very important to be carefully designed. In cancer nano-immunotherapy it is essential to consider that the contact of NPs with a biological fluid will most probably provoke the formation of a PC on the NPs surface. This PC could

trigger an acute inflammatory response after the interaction with immune cells. This phenomenon is commonly related to the excessive production of cytokines such as TNF- α , IFN- γ , IL-6, and IL-12 and the exacerbated inflammatory response associated to high levels of these cytokines. In this context, Dai et al. observed differences in pro-inflammatory cytokines secretion and immune cell apoptosis when studying the interaction of NP-PC complexes, formed in various biologically relevant environments, with macrophages. They observed that the NP-PC complexes either increased or mitigated the secretion of a specific cytokine, depending on the environment where the PC was formed²⁶⁹. On the other hand, although it has been demonstrated that the PC could trigger pro-inflammatory responses and tissue damage, some works suggest that PC could also have protective properties. Escamilla-Rivera et al. studied the role of the PC as potential protector for reactive oxygen species (ROS)-induced cytotoxicity and pro-inflammatory response in macrophages exposed to IONPs. They observed that the reduction in IONPs-induced cytotoxicity can be attributed to the PC shielding against ROS generation and pro-inflammatory response in macrophages²⁷⁰. It was also demonstrated that the formation of PC on the magnetic hydroxyapatite (MHA) scaffolds improved osteogenesis. PC causes an acute inflammation which turned into improved bone regeneration and it is related to the increased immune response against the scaffold²⁷¹.

The formation of PC on the NP surface does not always trigger an inflammatory response per se, as it has been previously described. Sometimes, the inflammatory responses could be associated with the presence of unfolded proteins in the NP-PC complexes. In the same way that macrophages can recognize some unfolded proteins present in NP-PC complexes through the scavenger receptors and phagocyte them, other specific receptors can recognize unfolded proteins present in NP-PC complexes and trigger an exacerbated inflammatory response. Deng et al. described that negatively charged poly(acrylic acid) (PLA)-conjugated gold NPs bind to and induce unfolding of fibrinogen,

Introduction. Harnessing the innate immune system through NP-based immunotherapy

which promotes interaction with the integrin receptor, Mac-1. The activation of Mac-1 receptor increases the NF- κ B signaling pathway, resulting in the release of inflammatory cytokines²⁷². However, not all NPs that bind to fibrinogen showed this effect, which illustrates the influence of the physicochemical properties of the NPs. The role of the physicochemical properties of the materials, such as surface chemistry and wettability, on the formation of PC in human serum and the subsequent effects on the innate immune response have been also investigated. Visalakshan et al. demonstrated that the amount and identity of proteins adsorbed on the surface of the different materials were strongly influenced by surface chemistry and wettability, which led to a distinct response from macrophages. Hydrophilic surfaces mostly adsorbed dysopsonin and albumin, which induced a greater expression of anti-inflammatory cytokines by macrophages. In contrast, hydrophobic surfaces mostly adsorbed IgG2 type opsonin, which caused increased production of pro-inflammatory signaling molecules²⁷³. Therefore, the identity of the adsorbed proteins on the surface of the NPs has also an important role in triggering excessive inflammatory responses. The administration of any nanomaterial to animals or humans results in the adsorption of proteins onto the nanomaterial surface and the subsequent complement activation, which may lead to exacerbated inflammatory response. This effect may be related to the observations that the presence in the PC of the third component of the complement protein (C3) affects the recognition of nanomedicines^{274–276}. To avoid the nanomaterial-induced complement activation, many researchers have used highly biocompatible materials such as zwitterionic polymers as well as hydrophilic NPs which decrease the protein adsorption²⁷⁷, and biomaterials already wrapped with “self” proteins such as CD200²⁷⁸. More recently, cell membrane coatings have emerged as a new class of coatings that enable the camouflage of NPs for evading immune clearance and lessen the complement activation by nanoparticles^{279–281}. For example, Fan et al. developed a coating based on red blood cell (RBC) membranes that was able to camouflage the particles from the immune system

and significantly reduced the number of infiltrating neutrophils in the scaffolds, which is translated into an elimination of the short-term inflammatory response²⁸².

These works and many others map out relationships between the physicochemical properties of the NPs and other materials, the PC formation, and subsequent immune responses²⁸³. The potential outcomes of these studies can guide the development of new nanomaterials to modulate serum protein adsorption and to avoid undesirable effects.

1.3.3. Gold standard of nano-immunotherapy strategies

Even though PC formation is presented as a drawback of NPs used *in vivo*, several scientific works support the feasibility of nano-immunotherapy strategies success. The principal advantage of using NPs in biomedical applications is the possibility to extract the intrinsic function that the use NP could have (Fig. 1.6). Their efficacy as delivery-system has been broadly demonstrated not only because they are carriers of molecules on the surface, but also because they can encapsulate molecules in the core, which is translated on intracellular drug administration. In that way, they can trigger the intracellular signaling pathways, such as stimulator of IFN genes (STING) expression, which is relevant in the PD-L1 limited response in certain cancers like triple-negative breast cancer (TNBC)²⁸⁴. The encapsulation is also interesting for *in vivo* applications as it makes possible also the i.v. treatment administration instead of intratumorally. Nonetheless, the use of NPs as poly-delivery systems known as engagers, are attracting more attention nowadays. The NPs can bind to different molecules on their surface and in this way, they can co-deliver them. This aspect is very relevant in the field of immunotherapy for two purposes: 1) to enhance the encountering of tumor and effector immune cells such as T cells²⁸⁵ and 2) to ensure the activation of immune cells with more than one signal. The combination of anti-PD1 (PD-1 antagonist) and anti-OX40 (tumor necrosis factor receptor (TNF receptor) agonist) in the same NP, called dual

Introduction. Harnessing the innate immune system through NP-based immunotherapy

immunotherapy nanoparticle (DINP), showed greater IFN- γ + T cells and also were more effective in killing B16F10-OVA cells than controls *in vitro*. The therapeutic effect of DINP was also validated *in vivo* in B16F10 bearing C57BL/6 mice and in 4T1 orthotopic breast cancer model, showing a synergistic effect of DINP. Interestingly, they were also able to change the phenotype of the TME to a hot tumor, which translated in an immunotherapy responsive tumor²⁸⁶.

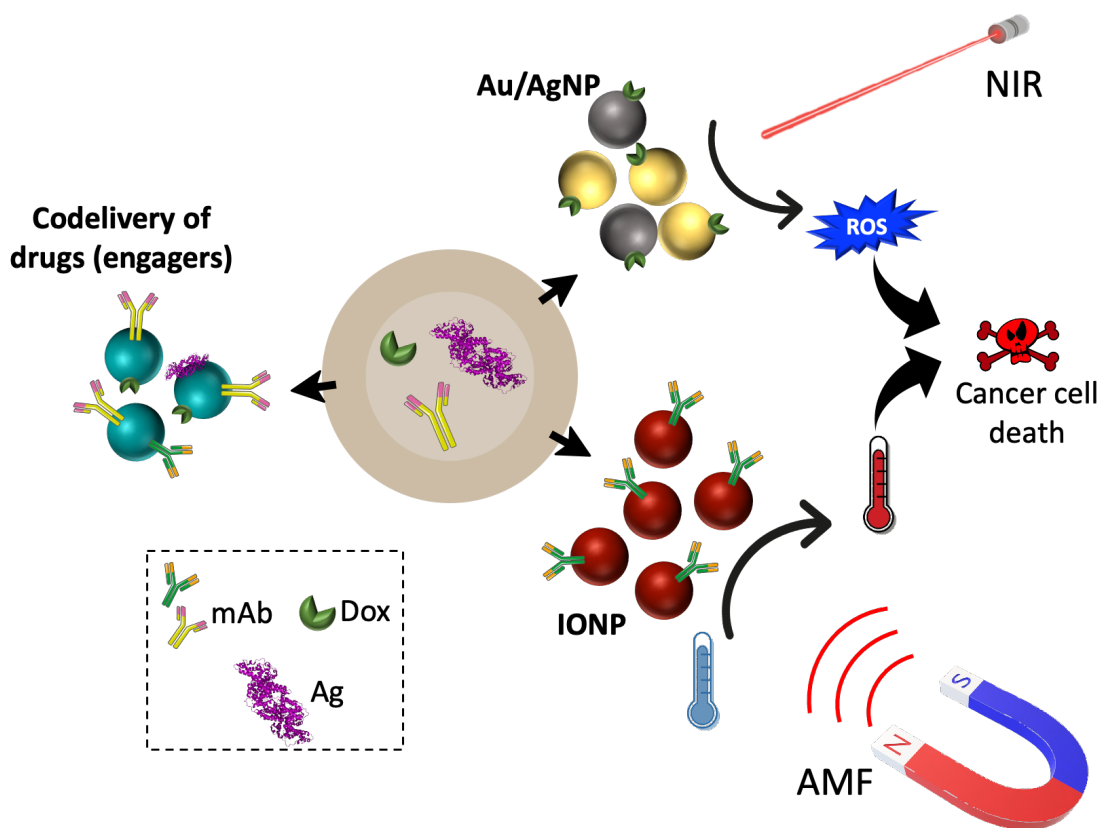


Figure 1.6. NPs contribution to antitumoral therapies. NPs are used for molecules administration and contributes in two principal ways. The first advantage is the codelivery of several molecules in the same device (e.g. engagers). The other contribution is the application of complementary therapies, such as phototherapy or magnetic hyperthermia, in addition to the therapeutic effect that the carried molecules triggers. *mAb*: monoclonal antibodies, *Dox*: doxorubicin, *Ag*: antigen, *Au/AgNP*: gold/silver nanoparticles, *IONP*: iron oxide nanoparticles, *NIR*: near-infrared, *ROS*: reactive oxygen species, *AMF*: alternating magnetic field.

In addition, the material with which the NPs are made or the additional molecules that can be loaded in the NPs (apart from drugs), turn the nano-immunotherapeutic formulations into poly-functional modules (Fig. 1.6). For instance, radiotracers or

photosensitizer (PS) can be loaded into NPs. Radiotracers convert these nano-formulations in theragnostic NPs^{287,288}. And interestingly, the addition of PSs adds extra antitumor therapy possibility to the system²⁸⁹. A PS is a molecule that absorbs light under electromagnetic stimulation (i.e. radiofrequency, near-infrared (NIR), microwave) and can trigger cell death, what is called phototherapy (PT). PSs loaded into NPs demonstrated favorable results. As an example, Poly Lactic-co-Glycolic Acid (PLGA)-NP loaded with indocyanine green (ICG) (PLGA-PEG-ICG-R837) stimulated with NIR irradiation was able to: 1) enhanced DC maturation, 2) provoke the infiltration of effector memory T cell (T_{EM}) into the tumor and 3) maintain long-term antitumor effect. These antitumoral responses happened with no cytokine levels increase, which is translated in an effective anti-tumor therapy without toxicity²⁹⁰. The strategy of using PSs is also applicable in CSC targeting therapies. PSs loaded NPs showed higher delivery to CSC compared with free PS administration, enhancing the anti-tumor effect by PT in CSC, which exhibits resistance to other anti-tumor therapies²⁹¹. Moreover, Au and Ag-based NPs showed exceptional properties for PT, as the material itself (Au and Ag) absorb light efficiently from 600 nm to 850 nm. The modules based on Au or Ag NPs do not need PS addition to the surface, so the biofunctionalization of molecules on Au and Ag based NPs is enough to construct a poly-functional module²⁹².

Similar to Au and Ag-based NPs, Fe-based nanomaterials also add functionality to the nano-therapeutic modules. IONPs exhibit magnetic properties and thus they can be used for magnetic guidance or magnetic hyperthermia. This last application is based on the cell death provoked by the heat generation under stimulation of IONPs with an alternative magnetic field (AMF)²⁹³.

1.3.3.1. Modulating NK cell effector functions by means of nanotechnology

NK cell-based immunotherapies have emerged as safe and effective approaches in cancer, especially in the field of hematological malignancies^{57-59,62,63}. In general, these

Introduction. Harnessing the innate immune system through NP-based immunotherapy

therapies could be divided in two major classes: adoptive NK cell therapy, including CIML (trained) NK cells, and *in vivo* enhancement of patient's NK cell effector functions⁵⁷⁻⁵⁹. Several challenges still persist for the full implementation of NK cell-based therapies, including their short *in vivo* life span, relatively poor expansion of NK cells *in vitro*, treatment complexities, and the cost burden of the treatment, among others. However, given the advancements in the development of immune cell-delivering nanosystems, targeting NK cells with NPs could be of great relevance for developing the best NK cell product to be infused into the patient and, on the other hand, to modulate NK cell activity *in vivo*^{294,295} (Table 1.3).

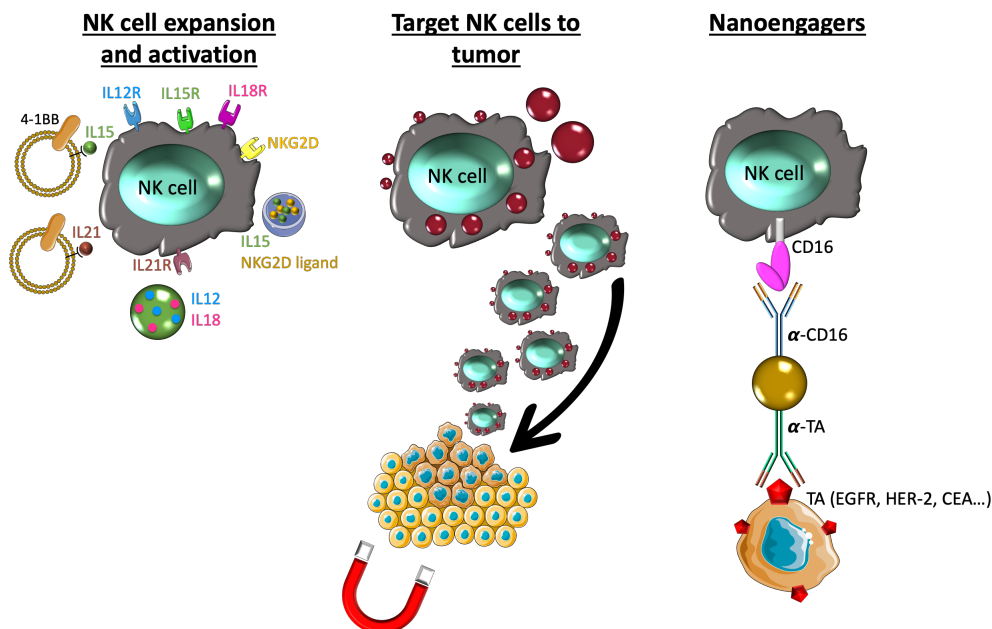


Figure 1.7. NPs used to modulate NK cells effector functions. Examples of three strategies are shown: Left panel, NK cells are expanded and/or activated with liposomes and NPs, such as IL-12 and IL-18-loaded polylactic acid microspheres, plasma membrane particles derived from K562-mbIL15-41BBL or K562-mbIL21-41BBL feeder cells and DCs-derived exosomes expressing IL-15Ra and NKG2D ligands. Middle panel, directing NK cells to the tumor by means of magnetic NPs and application of external magnetic fields. Right panel, targeting NK cells to tumor cells with nanoengagers decorated with anti-CD16 and anti-tumor antigen (TA) antibodies. From Mikelez-Alonso et al., *Adv Drug Deliv Rev.* (2021) 10.1016/j.addr.2021.113860¹⁵⁵.

Table 1.3. Examples of nanoplatforms targeting NK cells. From Mikelez-Alonso et al., *Adv Drug Deliv Rev.* (2021) 10.1016/j.addr.2021.113860¹⁵⁵

Formulation	Formulation description-Stimulus	Application	Ref.
STRATEGIES FOR NK CELL ACTIVATION			
PLAM	IL-12 and IL-18 loaded polylactic acid microspheres.	Local and systemic tumor immunotherapy.	296
dsNKG2D-IL21 NPs	Chitosan NPs loaded with plasmid encoding NKG2D-IL21.	NK cell and T cell activation for cancer therapy.	190
DMA-pIL15	DOTAP and MPEG-PLA self-assembly loaded with plasmid encoding IL15.	Antitumor therapy against colon cancer.	297
NK-EV _{SIL15} NB-ex	Isolation of exosomes from neuroblastoma primed NK cells.	NK cells treated exosomes for cancer immunotherapy.	298,299
Dex Dex (OVA+plC)	DC derived-exosomes.	Activation of NK cells through NKG2D, IL15Ra and other receptors for cancer treatment.	300,301
PM-mb15-41BBL PM21	Plasma membrane particles derived from K562 mbIL15(21)-41BBL feeder cells.	Expansion of NK cells for adoptive transfer.	302,303
cMLV	Multilamellar liposomal vesicles charged with drug able to attached to NK cell surface.	Combination therapy (chemotherapy and NK cell activation).	304
Lipo-IL2-Fc Lipo-aCD137	IL2 and a-CD137 conjugated PEGylated liposomes.	Combination therapy activating T and NK cells.	305
NGO-a-CD16	Graphene Oxide based NK cell activating cluster.	Activation of NK cells through CD16 cross-linking.	306
αHSP70p-CM-CaP	NPs loaded with cancer membrane proteins, aHSP70p and CpG.	NK and T cell activation and expansion. Increased effector functions.	307
NK CELL AND NPs ENRICHMENT IN TUMOR AREAS OR IN LYMPH NODES			
MNP@SiO ₂	Silica coated magnetic NP.	Targeting NK cell to tumor sites.	308
Fe3O4@polydopamine	Magnetic nanoparticles for loaded in NK cells.	Targeting NK cells to tumor sites.	309
SVNP-OVA or IC	Liposomes decorated with OVA antigen or poly (I:C)	Targeting of NPs to lymph nodes enhance T cell and NK cells expansion and stimulation.	310
cdGMP/MPLA-NP	cdGMP and MPLA loaded NP.	Antitumor therapy and increase migration of NK cells to tumor area.	311
NANOENGAGERS			
HGNP	α-GD2 Abs decorated Gold NP.	Enhancement of ADCC by enhancing the contact of NK cells and tumor cells.	312
HMRu@RBT-SS-Fc	NP loaded with EPI and decorated with α-EGFR, α-CD16 and α-4-1BBL Abs.	Combination therapy targeting NK cells and tumor cells. PDT effect on tumor cells.	313
α-EGFR/α-CD16/α-4-1BB EPI NPs	NP loaded with EPI and decorated with α-EGFR, α-CD16 and α-4-1BBL Abs.	Combined antitumor therapy through NK cell effector functions and chemotherapy.	314
pBIAb-AuNP	α-gp120 and α-CD16 Abs decorated gold NPs.	NK cells mediated killing of HIV infected cells.	315

Abs (antibodies), ADCC (antibody-dependent cell-mediated cytotoxicity), cdGMP (cyclic diguanylate monophosphate), CEA (carcinoembryonic antigen), DC (dendritic cell), Dex (DC derived exosomes), DMA (DOTAP and MPEG-PLA), DOTAP (1,2-dioleoyl-3-trimethylammonium-propane (chloride salt)), EGFR (epidermal growth factor receptor), EpCAM (epithelial cell adhesion molecule), EPI (epirubicin), GD2 (disialoganglioside carbohydrate antigen), HIV (human immunodeficiency virus), MPEG-PLA (methoxy poly (ethylene glycol)-poly(lactide)), MPLA (monophosphoryl lipid A), NB (neuroblastoma), NGO (nanoscale graphene oxide), NK (natural killer), NPs (nanoparticles), OVA (ovalbumin), PDT (photo-dynamic therapy), PEG (polyethylene glycol), PLAM (polylactic acid microspheres), PTT (photothermal therapy), RBT (rice brand stored at 400C in the dark), SVNP (synthetic vaccine nanoparticles), TA (tumor antigen).

Introduction. Harnessing the innate immune system through NP-based immunotherapy

For example, NPs have been developed to expand NK cells for adoptive transfer^{294,316}. Nanocarriers have been used to incorporate various cytokines and other molecules such as membrane-bound IL-15³¹⁷, membrane-bound IL-21³¹⁸ and anti-CD16 antibodies³¹⁹ to activate and expand NK cells (Fig. 1.7). More specifically, it has been developed a technology to expand NK cells that is based in plasma membrane (PM) particles derived from K562-mbIL15-41BBL feeder cells (PM15)³¹⁷. These feeder cells were engineered to express the NK cell stimulating molecules IL-15 and 4-1BBL in the erythroleukemia K562 cell line. The PM15 particles induced selective expansion of NK cells from unsorted peripheral blood mononuclear cells (PBMCs). The efficiency and rate of NK cell expansions with PM15 particles were far better than stimulation with soluble 4-1BBL, IL-15, and IL-2. These expanded NK cells exhibited high cytotoxicity against several leukemia cell lines and also against patient AML blasts³¹⁷. PM particles derived from K562-mb21-41BBL cells (PM21), expressing 4-1BBL and membrane-bound IL-21 have also been developed³¹⁸. *Ex vivo*, PM21 particles caused specific NK-cell expansion from PBMCs from healthy donors and AML patients and also stimulated *in vivo* human NK cell expansion in mice injected with human PBMCs preactivated with PM21 particles³¹⁸.

NPs are also being used to direct NK cells to tumor tissues²⁹⁴. One approach consists in the application of external magnetic fields to guide engineered NK cells with magnetic NPs to the tumor. In this regard, Jang et al. have shown that silica decorated superparamagnetic iron oxide ($\text{Fe}_3\text{O}_4/\text{SiO}_2$) NPs conjugated with the fluorophore Cy5.5 into the NK-92MI cell line allowed to visualize and control the movement of the cells by an external magnetic field. NK-92MI cell infiltration in tumors bearing mice was increased by 17-fold when applying the magnetic field and nanoparticle labeling and their killing activity still remained the same as NK-92MI cells without the NPs³²⁰. Other study has used NPs consisting of a magnetic Fe_3O_4 core and a shell of polydopamine (PDA) for magnetic targeting therapy. *In vitro* and *in vivo* studies showed that Fe_3O_4 @PDA NP-labeled NK cells significantly inhibited tumor growth³²¹. In addition to

magnetic methods, NK cells can be recruited to the tumor sites by other means. For example, it has been shown that the delivery of double-gene fragments encoding the extracellular domains of NKG2D and IL-21 to the TME by means of chitosan-based NPs resulted in retarded tumor growth and elongated the life span of tumor-bearing mice by activating NK and T cells *in vivo*³²². Also, it has been developed a PEGylated liposome co-loaded with cyclic diguanylate monophosphate, a STING agonist, and the adjuvant monophosphoryl lipid A, a toll like receptor (TLR)4 agonist, which synergize to produce high levels of IFN β ³²³. The systemic delivery of these NPs resulted in increased production of type I IFN and, among others, a high recruitment of NK cells into the tumor³²³. On the other hand, other study has proposed to use NK cells to guide drug loaded NPs to the tumor³²⁴. In this work, NK92 cells were engineered to express a CAR and were used as carriers for paclitaxel loaded NPs. In a mouse model, the tumor volume was significantly more reduced when animals were treated with CAR-NK92 cells conjugated with drug-loaded NP than when they were infused with CAR-NK92 cells and paclitaxel NPs separately³²⁴.

In addition to activate and increase the number of T cells, nano-vaccines targeting DCs also promote NK cell activation and proliferation. DC-targeted poly(γ -glutamic acid)-based vaccines co-delivering ovalbumin (OVA) and poly (I:C), a TLR3 agonist, markedly increased the NK cell population and their activation *in vivo*³²⁵. Others have generated TLR7/TLR8 agonist loaded NPs that enhanced co-stimulatory molecules expression on DCs and stronger pro-inflammatory cytokine response³²⁶. This led to a stronger degranulation, cytotoxicity, including ADCC, and prolonged activation of NK cells compared to that with the soluble agonist. *In vivo*, the TLR7/8 agonist-loaded NP treatment significantly enhanced the anti-tumor efficacy of cetuximab and an anti-HER2/neu antibody in mouse tumor models³²⁶. Also, it has been shown that necroptotic cancer cell mimetic vaccines, designed as flexible platforms for delivering cancer membrane proteins, danger-associated molecular patterns (DAMPs) signal-augmenting

Introduction. Harnessing the innate immune system through NP-based immunotherapy

element α -helix HSP70 functional peptide (α HSP70p) and CpG to both NK cells and DCs, were able to induced expansion of IFN- γ -producing CD8+ T cells and NK cells³²⁷. Furthermore, a combination of the vaccine with anti-PD-1 therapy resulted in significant tumor regression in a mouse model³²⁷.

Other studies had the goal to activate NK cells *in vitro* or *in vivo*. As example, there are studies that have revealed how DC derived-exosomes (Dex) also promote activation of NK cells^{328,329}. For example, it has been shown that Dex-expressing IL-15R α and NKG2D ligands lead to proliferation and activation of NK cells *ex vivo*. Furthermore, in a phase I trial, Dex based-vaccines restored the number of circulating NK cells and their NKG2D-dependent functions in half of the patients with melanoma³²⁸. In the same context, Dex purified from tumor antigens pulsed DCs and matured with poly(I:C), stimulated and recruited both antigen specific CTLs and NK cells to the tumor, significantly inhibiting its growth in a mouse model of melanoma³²⁹.

Other NP-based methods, for NK cell activation strategy, included the encapsulation of plasmids encoding cytokines, such as IL-15, into DOTAP and MPEG-PLA (DMA) nanoparticles. Treatment of tumor bearing mice with DMA-IL15 NPs significantly inhibited tumor growth *in vivo* by inhibiting angiogenesis, promoting apoptosis, and reducing tumor cells proliferation through activation of the host lymphocytes³³⁰. Also, it has been shown that primary intratumor delivery with IL-12 and IL-18-loaded polylactic acid microspheres (PLAM) led to a significant tumor suppression, decrease in metastases and improvement in survival compared with either cytokine alone. The observed responses were dependent on the activation of CD8+ T cells and NK cells³³¹.

In addition to cytokines-induced stimulation, NK cells are also activated through the ligation of activating receptors, such as CD16 (Fc γ RIIIa). In this context, it has been used nanoscale graphene oxide (NGO) as a template to mimic the signaling receptor nanoclusters to activate NK cells by targeting the CD16 receptor³¹⁹. The NGO

functionalized with mAbs that bind human CD16 were confirmed to specifically bind NK cells via the CD16 receptor. More importantly, they function as an activating reagent, enhancing NK cell effector functions in terms of degranulation and IFN- γ secretion³¹⁹. Other authors have shown that conjugated gold nanoparticles to an anti-GD2 antibody was able to both enhance computerized tomography imaging contrast and to stimulate the killing of GD-2 positive neuroblastoma and melanoma cells by NK cells³³². These anti-GD2 conjugated gold particles also triggered NK-mediated ADCC against the GD2 positive cells with a two-fold higher efficacy compared to that elicited by the antibody alone³³².

BiKEs and TriKEs are new types of immunotherapeutic agents capable of simultaneous recognition of target cells and lymphocytes, including NK cells^{57,96,97,333,334}. These therapeutics are designed to increase specificity and facilitate a more direct interaction between immune cells and tumor cells, leading to a more effective target elimination. Recently, nanoengagers are being developed to direct NK cells to tumor and infected cells^{335–337}. Xu et al. manufactured PEGylated hollow mesoporous ruthenium NPs as a carrier to load the fluorescent anti-tumor complex ([Ru(bpy)₂(tip)]²⁺ or RBT) and a conjugate with bispecific antibodies designed to recognize on one arm the carcinoembryonic antigen on colorectal cancer cells and on the other arm CD16 on NK cells³³⁵. These functionalized NPs effectively engaged NK cells and possessed excellent NIR-sensitive cytotoxicity and *in vivo* fluorescence imaging studies demonstrated high tumor targeting and therapeutic effects³³⁵. Also, a NP-based trispecific NK cell engager (nano-TriNKE) expressing anti-epidermal growth factor receptor (EGFR), anti-CD16 and anti-41BB mAbs have been developed. This platform targets EGFR-overexpressing tumors and promote the recruitment and activation of NK cells to eliminate the cancer cells³³⁶. Importantly, the nanoengagers are more effective than free antibodies. Moreover, the nano-TriNKE can deliver cytotoxic drugs to further increase their therapeutic efficacy³³⁶. In addition to targeting tumor cells, nanoengagers have been

Introduction. Harnessing the innate immune system through NP-based immunotherapy

also designed to target human HIV infected cells. Astorga-Gamaza et al. have developed bispecific gold nanoparticles (BiAb-AuNPs) conjugated with both anti-HIVgp120 and anti-human CD16 antibodies³³⁷. These BiAb-AuNPs significantly enhanced the contact between NK cells and HIV-expressing cells and elicited a potent cytotoxic response against HIV-infected cells. What is even more significant is that the BiAb-AuNPs were able to significantly reduce latent HIV infection after viral reactivation in a cell model of HIV latency³³⁷.

Directing NPs to the tumor sites using NK cell derived materials is another therapeutic tool that is being investigated. NK cell-derived extracellular vesicles, including exosomes, have a big impact within the TME and are starting to be exploited as novel drug delivery systems, mediators of antigen presentation, modulators of cell signaling, as well as biological targeting agents and diagnostic tools in cancer therapy³³⁸⁻³⁴⁰. Pitchaimani et al. isolated the cell surface receptor proteins from activated NK-92 cells and infused them into liposomes to form NKsomes that exhibited a higher affinity towards cancer than normal cells as well as enhanced tumor homing *in vivo*. Furthermore, doxorubicin-loaded NKsomes shows promising antitumor activity *in vivo* against MCF-7 induced tumor model³⁴¹. On the other hand, exosomes derived from NK-92MI cells were able to induce apoptosis of melanoma cells *in vitro* and after intratumoral injection they were able to inhibit tumor growth *in vivo*³⁴². Furthermore, exosomes isolated from NK-92MI cells cultured in the presence of IL-15 significantly inhibited the growth of glioblastoma xenograft cells in mice when compared with exosomes derived from cells cultured in the absence of IL-15³⁴³. Others have shown that naive NK cells exposed to the exosomes derived from NK cells, which were previously cocultured with neuroblastoma cells, had greater cytotoxicity against neuroblastoma cells³⁴⁴. Kang et al. have developed a microfluidic system to collect patient-specific NK cells and on-chip biogenesis of NK cell derived exosomes³⁴⁵. In a cohort of patients with lung cancer they found that they had higher numbers of NK cell derived exosomes than

healthy people. Interestingly they found that the NK cell derived exosomes harvested from the chip exhibited cytotoxic effect on circulating tumor cells³⁴⁵. This system has the potential to be used for patient-specific NK cell-based immunotherapies.

Despite the growing number of publications on the modulation of NK cell effector functions by means of nanotechnology, still this field is in its early stage. In fact, current adoptive NK cell transfer-based therapy still remains challenging due, among others, to difficulties to their poor delivery into the tumor, mass production for “off-the-shelf” use, and a relatively fast reduction in number upon adoptively transferred. Therefore, mobilization of host NK cells by engineered NPs might help to improve this therapy. Delivery of antibodies, cytokines and other agents capable of promoting NK cell proliferation, expansion and homing to the tumor would be of great help. Furthermore, targeting specific NK cell subsets, as for example cytokine-induced memory-like and adaptive NK cells, is worthy to explore.

1.4. Justification and objectives of the research

Interest in immunotherapy has considerably grown in recent decades. The reason for the increasing attention is because immunotherapy has achieved very successful clinical results such as checkpoint inhibitors and engineered T cells (CAR-T cells)^{346,347}. These strategies have emerged as alternatives to the more traditional chemotherapy. However, there are occasions in which they are not as effective as expected³⁴⁸. A clear example of that is the TNBC, in which anti-PD-L1 treatment failed^{349,350}. On the other hand, the use of NPs is becoming more common, especially in preclinical settings. Among other reasons, the use of nano-formulations contribute to the increase of the circulation time of drugs. In addition, in the field of antitumor immunotherapy, the use of NPs makes the recognition of molecules on their surfaces more efficient. It can even induce greater effector functions from immune cells. Therefore, NP-based immunotherapy could contribute the expansion of tools to fight cancer.

The aim of this thesis was to develop and test a nano-module (IONP@hIL15HIS) able to stimulate NK and T cells *in vitro* and *in vivo* (Figure 1.7). The aim was to mimic the physiological transpresentation of IL-15 by monocytes and DCs to NK cells. For that, IONP@hIL15HIS would work as a lab-made IL-15 transpresentation system and its effects on immune cells were compared with commercial IL-15.

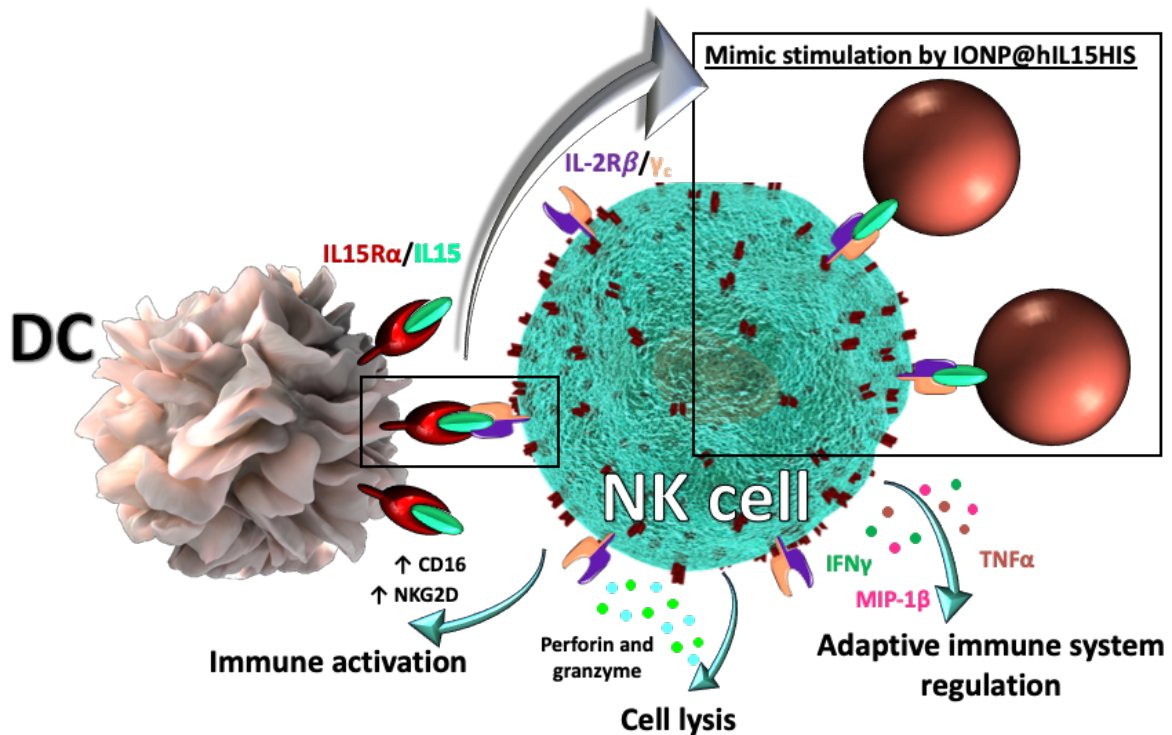


Figure 1.7. Physiological and NP-mediated IL-15 stimulation of NK cells. IL-15 is transpresented by the alpha subunit of its receptor (IL-15R α) by immune cells such as DCs and monocytes. In that way, IL-15 is able to bind the other two subunits of the receptor (IL-2R β / γ_c dimer) on NK cells leading to their activation. On the right part, IONP@hIL15HIS can mimic the transpresentation of IL-15 that is linked to the surface of the NPs.

The specific objectives are:

- ◆ To develop and characterize water-soluble IONP micelles able to provide anchoring sites to IL-15.
- ◆ To select the appropriate bioconjugation strategy for the His-tagged lab-made human IL-15 cytokine to IONP micelles.
- ◆ To characterize the effect of IONP@hIL15HIS on T lymphocytes and NK cells from healthy donors *in vitro*.
- ◆ To study and analyze the *in vivo* distribution of the IONP@hIL15HIS primed cells.
- ◆ To study the *in vivo* therapeutic effect of IONP@hIL15HIS in tumor bearing mice.

Chapter II

Design, synthesis and characterization
of the hIL-15HIS coated PEGylated
IONP

Chapter II Design, synthesis and characterization of the hIL-15HIS coated PEGylated IONP

2.1. Introduction

The applicability of Iron Oxide Nano-Particles (IONPs) has been widely demonstrated in environmental science or engineering.^{351,352} In particular their biocompatibility, good size control, and low toxicity convert the Fe based nano-formulations in one of the most widespread materials in nanomedicine, making possible their use *in vivo*, including in the clinic³⁵³. Nevertheless, as other gadolinium, manganese, cobalt, zinc or nickel^{354,355} based materials, iron materials present magnetic properties which provides them wider potential in biomedicine since it opens the possibility to design multimodal systems³⁵⁶.

The main applications in nanomedicine of the IONPs which are based on their intrinsic properties are the following (Fig. 2.1):

1. Magnetic Resonance Imaging (MRI). IONPs can diminish the relaxation time of water protons in the surrounding media where they are accumulated and in consequence generating T2 contrast in the MRI images. Some compounds have been approved by the Food and Drug Administration (FDA) for their use in clinics, this is the example of Resovist which is the second superparamagnetic IONP contrast agent approved by FDA³⁵⁷, although is not available in United States and Europe. Fe based materials tend to accumulate in determine tissues depending on their composition, and therefore they could use for diagnosis because they will generate different contrast of healthy or damage tissue³⁵⁸. For example, cited Resovist compound accumulated in liver so it was used for diagnose liver lessions. The main use of IONP as contrast agent is for T₂ imaging, which is the white or bright contrast comparing with the surrounding tissues. But depending on the tissue studied, the black or dark contrast is preferred, therefore there is a high interest on using as T₁ contrast agent which will display black or dark contrast³⁵⁹. These T₁ contrast from IONP based materials is also possible when

their size is up to 3 nm. In addition, dual contrast agents are also studied which could act as T₁ or T₂ contrast, opening the diagnostic in a wide range of tissues³⁶⁰.

2. Magnetic guidance. With this strategy is possible to enhance the accumulation of the magnetic nanoparticles (NPs) to certain interest area such as tumor *in vitro* and *in vivo* using focused magnetic field^{361,362}. As consequence, the accumulation will be faster than without magnetic guidance of NPs and the adverse effect could be diminished. In addition, magnetic NP could be bound to a cell or acquired by cells and hence, these cells could field attracted by a magnetic field. This is useful for certain cell enrichment *in vitro* for following injection *in vivo*, what is known as adoptive cell transfer therapy (ACTT)^{363–365}. Moreover, magnetic NP acquired cells could be guided to a desired area through the body by focused magnetic field³⁶⁶, as is explained in the beginning for the magnetic NP guidance.

3. Magnetic hyperthermia. IONPs are also able to produce heat under an alternative magnetic field (AMF). The resulting temperature increase will trigger cell death within the surrounding tissue. If the NPs are able to migrate to a tumor area, the magnetic hyperthermia effect will mainly affect the tumor cells triggering apoptosis^{367,368}. Therefore, the magnetic hyperthermia can be used as an on-off effect with relative specificity, since the tissue damage would happen only when the AMF is applied and on the areas of application.

4. Delivery system. As other nanoparticles with different compositions, IONPs could be used also for targeted drug delivery towards selected areas resulting in higher local effective doses^{369–371}. The increase in effective dose is a consequence of different factors such as: 1) the decrease in the clearance of the drug when is linked to the surface of the nanoparticle; 2) the avoidance of the phagocytosis of the NPs designed for immune scape; and 3) the high drug payloads that can be achieved on nanoparticles, among others.

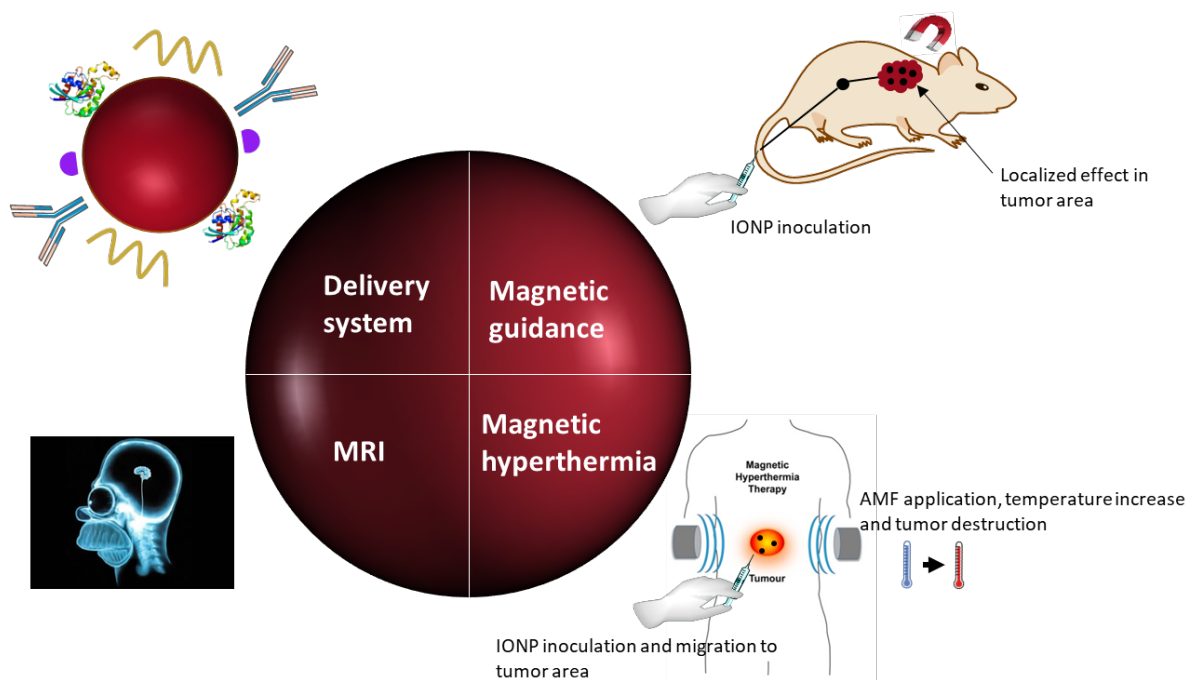


Figure 2.1. Current applications of IONP in biomedicine. Above commented 4 principal applications are represented: Magnetic Resonance Imaging (MRI), magnetic guidance, magnetic hyperthermia, and delivery system.

Considering the aforementioned features of IONP, IONPs-based systems are very attractive platforms for a wide range of biomedical applications^{372–374}.

2.1.1. Anticancer therapies using IONPs

Current applications of IONPs are very extend in terms of therapeutics, as previously mentioned. However, the first application of these NPs was in diagnosis as contrast agents for MRI, since Fe based nanomaterials display magnetic properties. In addition to their use as simple contrast agents a lot of effort has been put in developing them as delivery systems, and as dual delivery and imaging systems (theranostic agents). The latest application is possible because Fe-based can be coated with biocompatible components such as polyethylene glycol (PEG) molecules and anti-cancer drugs, while magnetic properties are not affected^{375–377}.

The intrinsic magnetic properties of IONPs are used also for tumor cell killing³⁷⁸. In this process, named *magnetothermal therapy* or *magnetic hyperthermia*, the magnetic NPs can

generate local heat under an AMF and thus provoke tumor cells death by oxidative deoxyribonucleic acid (DNA) damage³⁷⁹. Additionally, the resulting high temperature could trigger synergistically tumor cells killing by other mechanisms such as sensitization to apoptosis induced by chemotherapeutic molecules, such as doxorubicin,³⁸⁰ or tumor cell differentiation which will imply the inhibition of their auto-renewal³⁸¹. Furthermore, NP-induced magnetic hyperthermia could be exploited for advanced delivery systems, for example through their interfacing with smart heat-responsive materials for controlled and local drug release.

For example, by loading a smart heat-responsive material with drug-loaded NPs for the temperature-dependent release of the drug.

this high temperature could have an effect in smart drug delivery systems used in cancer therapies, such as , and in consequence release the drug loaded in NPs³⁸², meaning that a local drug delivery is guaranteed.

The use of IONPs as magnetotherapy is applicable *in vitro* but also *in vivo*³⁸³. What is more, several clinical trials support the relevance of this therapy^{384–389} since first application in clinic in 2005 was reported in a recurrence prostate cancer case³⁹⁰. Although there are many reported works supporting the effect of magnetotherapy and the success is irrefutable, it is important to consider that it is not totally specific process. There is a possibility to damage healthy tissue surrounding the area in where the temperature is increasing, because the heat did not discriminate between tumoral or non-tumoral cells. This is especially important in the case of bone cancers because of the need to occupy the gap to support strength to the bone after tumor removal, which in the case of a nanomaterial based therapy will be also required and thus a bioactive material able to regenerate bone tissue will be needed^{391,392}.

In addition, as IONPs are magnetic materials, they are attracted by magnets and they could be guided under a magnetic field *in vitro* and *in vivo*^{393,394}. An interesting *in vitro* application of this magnetically guidance is the stimulated cell enrichment in the field of immunotherapy.

In this sense, the enrichment of certain immune cell population such as T cells or NK cells could trigger higher immune response because the absence of other cell populations that inhibit the functions of these cells^{395–397}. For *in vivo* application, one of the major interest is to achieve selective guidance of NPs to the tumoral areas, resulting in an increased therapeutic effect related to the higher NP effective dose^{398,399}.

In addition to the magnetic intrinsic property of IONPs, it has been observed that the presence of Fe in the IONPs is able to inhibit tumor growth without any decoration with anti-cancer drugs or immune-stimulating molecules. So, it is considered that the effect of the drug loaded or conjugated on the IONP will be maximize with the adjuvant effect of the Fe. The specific process through Fe is able to trigger tumor cell death, is known as ferroptosis^{400,401}. An interesting work about resistance against radiotherapy in glioblastoma demonstrated the anti-tumor effect of IONPs. This work showed that IONPs are able to increase the ROS species which affected not only glioblastoma (GBM) cells but also GBM stem-like cells, which are responsible for the treatment-resistance^{402,403}.

Additionally, the IONPs, as other type of NPs, are in the nanometer scale and thus they can act as nanocarriers delivering molecules of interest such as drugs to the desired targets^{404,405}. For that purpose, the drugs can be conjugated to the surface of the NPs but also can be encapsulated in the inner part of the NPs. The selected drug loading strategy will depend on the target and biologic process in which the nano-formulation will act. If the drug or molecule must be recognized by receptors present on the cell membrane, the conjugation is prioritized. However, if the molecule to be delivered is a chemotherapy drug, the encapsulation is usually preferred since the goal is usually the controlled release of the drug. Also, the encapsulation is normally selected when the particle is pH- or thermo-responsive. When using this class of NPs the drug is protected in the inner part of the NPs until the area at certain pH or temperature value is reached, where the NP will release the drug^{387,406–408}.

The intrinsic properties of IONPs opens multiple possibilities for multimodal nanoformulations as anticancer therapies; where the effect of the NPs could be enhanced by the effect of the drugs or molecules, resulting in a synergistic effect.

2.1.2. Synthesis of biocompatible IONP

There are several IONPs synthesis protocols, and the difference between them eradicated on the size control, NPs shape, and even the magnetic properties of the resulting nanomaterials. In the literature could found that the size of the IONP can be tuned from 4 to 20 nm for example by changing the reaction parameters^{409,410}. The control in the synthesis reaction is based on the LaMer model in which it is postulated that the precipitation of the nanoparticles is guided by 3 principal processes: nucleation, crystal growth, and maturation^{411,412}.

The most commonly used methods for the synthesis of IONPs are the following: coprecipitation, microemulsion, hydrothermal synthesis, sonochemical synthesis, and thermal decomposition^{413–418}. The size is the most common characteristic of NPs that is desired to control, and therefore thermal decomposition is the preferred method. The IONPs obtained by this method have a monodisperse distribution and good crystallinity. In addition, the reaction is done in one step with high yields, which traduces in short time and low consumption of reagents.

Even if the size and shape of the nanoparticles are critical parameters for their applicability, the principal aspect of the IONPs for their use in clinics, even in cells growth medium, is that they must be biocompatible and so on, water soluble^{419–422}. In the above named commonly used thermal decomposition protocol, the resulting NPs are hydrophobic, which is a drawback for biomedical application as it is mentioned. For that, after the synthesis step of IONPs, water transfer phase is needed to obtain biocompatible nanoformulations. Continued efforts are done for this purpose⁴²³, surprisingly, more than in improving the magnetic properties of the IONPs⁴²⁴. Most used materials for water transfer of hydrophobic NPs and converting them to biocompatible systems are polymers, proteins, and phospholipids.

Below are listed three main methods to transfer the hydrophobic IONPs to water:

1. Inorganic coating method. IONPs could be coated by gadolinium, gold, or silica among other materials for example. The most common and broadly known material for inorganic method is the silica (Aminosilane)⁴²⁵. The problem on this kind of NPs coating method is that the coating material is not biodegradable, and this is a downside for biomedical applications.

2. Ligand exchange method. This method is based on a chemical reaction of ligand replacement. The substitution is produced under two-phases ligand exchange method in a compound (i.e. NP surface), where the hydrophobic ligand is replaced by a hydrophilic one presenting higher affinity to the compound⁴²⁶. The most commonly used materials for this purpose are dimercaptosuccinic acid (DMSA) and polyethyleneimine (PEI)⁴²⁷. The problem in this case is it involves chemical reactions that could lead to poor ligand exchange yields, that could be traduced in a partial ligand exchange and therefore a poor water solubility.

3. Ligand addition method.^{428,429} This could be an alternative for ligand exchange method. In this method, the idea is to add hydrophilic molecules that have affinity or react with the hydrophobic surfactant that IONPs have on the surface from the synthesis. In these case PEG^{430,431} is the most used material because of the biocompatibility and the capacity to retard the uptake by macrophages by the broadly known mononuclear phagocytic system (MPS)⁴³².

In addition, to the selection of the more suitable transfer protocol, another important aspect to consider when designing the NPs is the selection of the coating molecules, since they will strongly affect the NP biocompatibility and their fate in the biological medium. The type of coating molecule will determine the potential side effects that could trigger systemic failures *in vivo* or other processes. One of the most common and very well-known process is the protein corona (PC) formation around the surface of the NPs by absorption of proteins. In the field of immunotherapy, the PC could avoid the desired effect of the nanoparticle because of the blinding effect⁴³³, but also could trigger an exacerbate response through immune system⁴³⁴.

Furthermore, the biocompatibility must be considered not only for the NP coating molecules on the NP surface but also for the NP core⁴³⁵. This consideration is relevant because the NPs will eventually degrade and all components including molecules and metals, could be exposed to the biological medium and as results, toxic effects could appear. This effect may have been overlooked, since commonly synthesized materials not always are composed by entirely biocompatible elements, and unexpected cytotoxic effects may arise hampering the use of those nanomaterials in biomedicine.

2.1.3. Biofunctionalization strategies

Different strategies could be used to charge the nanoparticles with the desired molecule, but always, the strategy depends on the objective of the study as it is mentioned before.

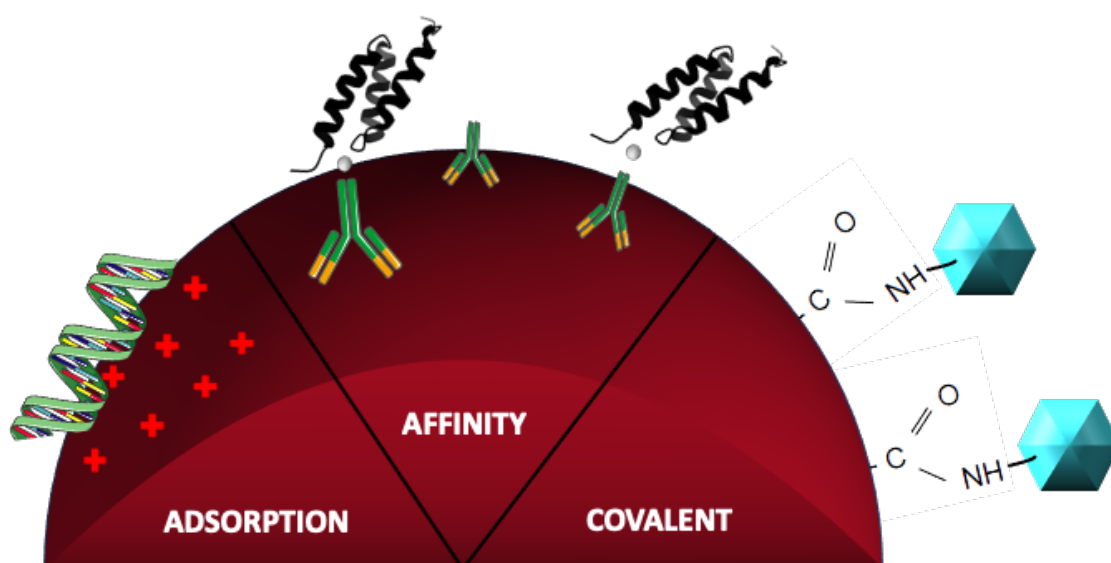


Figure 2.2 Common biofunctionalization strategies. Electrostatic (Adsorption) which is based on the attraction of the molecules to the NP surface based on charge complementarity, affinity-based immobilization of molecules such as protein A to the Fc region of IgG, or covalent linkage such as selective bond generated between the particle surface molecules and the biomolecules, for example an amide bond between carboxy groups on the surface and amine groups in proteins.

1. Adsorption. This kind of binding is based on the attraction between molecules. This attraction could be because of hydrophobicity or electrostatic forces between the molecules⁴³⁶. The most used is the electrostatic force effect. Molecules that have opposite

charge to the ones on the surface of the NPs are attracted and will be attached to the NPs. The main problem of this strategy is the poor stability of the conjugates since this binding is not covalent and for example the electrostatic interactions could be easily destroyed in high ionic force media.⁴³⁷ This strategy is widely used for the attachment of DNA molecules (negatively charged) to positively charged NPs. Moreover, this strategy is also used for environmental cleanup; for example, the adsorption of organophosphorus pesticides in metal NPs is used to clean the contaminated waters⁴³⁸.

2. Affinity. It is based on the strength of the binding interaction between two molecules. The most common affinity example is the receptor-ligand affinity, but the coordination of molecules by metals is also an affinity-based biofunctionalization strategy. The coordination of nitrilotriacetic acid (NTA) molecule with his-tag sequence by Ni metal is a well-known example of this kind of binding interaction⁴³⁹. Moreover, affinity-based strategies could be used as facilitator for a following covalent linkage, by bringing molecules close in space to facilitate a further covalent linkage reaction⁴⁴⁰. Anyway, this method is not as strong as covalent linkage, and is usually stronger than adsorption method, providing a wide range of affinities described for different systems based on their K_d from fM-mM

3. Covalent linkage. This strategy is based on the selective reactivity between a chemical group on the surface of the NPs and a chemical group present in the molecule to be attached. Amide bond between a primary amide and a carboxylic group and the reaction of thiol group with maleimide molecule in which this last molecule act as cross-linker are the two covalent reactions mostly used for NP biofunctionalization^{441,442}. Covalent linkage is irreversible unless other reactants attack the bond chemically. This method is commonly used in the functionalization of nanoparticle with receptors, for their correct display in receptor-cell interaction assay.^{443,444}

In this chapter the results of the synthesis of the hydrophobic IONPs (hIONPs), coating method, his-tagged human interleukin (IL)-15 (hIL-15HIS) protein expression and conjugation of IONP@hIL15HIS are shown.

2.2. Result and discussion

2.2.1. Synthesis of IONP-based micelles and magnetic characterization

The first step to prepare the IONP-based micelles is the synthesis of the hIONPs by thermal decomposition (Figure 2.3). These hIONPs were synthesized in Prof. J.C. Mareque lab following previously published protocol⁴⁴⁵. The hIONPs were used as the core of the micelles and their size were around 6 nm (Figure 2.4).

As it is mentioned in the introduction of this chapter, the first step once hIONPs are synthesized is their transfer to a water phase solution. For that, a micelation protocol was carried out following the ligand exchange method (Fig. 2.3), which is based on the addition of PEG- phospholipid (PEG-PL) to the hydrophobic surface of the nanoparticle. The phospholipids are amphiphilic molecules, so the hydrophobic part could be in contact with the hydrophobic surface of the nanoparticle.

The protocol resemble to the used for liposomes because the aim of the micelation protocol is to create a film with the hydrophobic molecules and then, do a hydration phase, in which the micelles are generated by self-assembly⁴⁴⁶. The final product is organized in a way which the hydrophobic part will be in the core of the nanoparticle, so in this case, the hIONPs will be in the inner part of the NP (Fig. 2.3).

The resulting micelles were characterized by Inductively Coupled Plasma Mass Spectrometry (ICP-MS), dynamic light scattering (DLS), Transmission Electron Mycroscopy (TEM) and absorbance spectrometry (Fig. 2.4). The ICP-MS measurements provided the concentration of Fe present in the sample, which in all batches was around 20 mM of Fe. The DLS provided the size and charge, showing a size of around 50-60 nm and a charge of -30 mV approximately, as shown in figure 2.4. TEM and absorbance characterization were used as control where aggrupation of hIONPs were visible in TEM images and the characteristic peak of absorbance appeared around 480 nm.

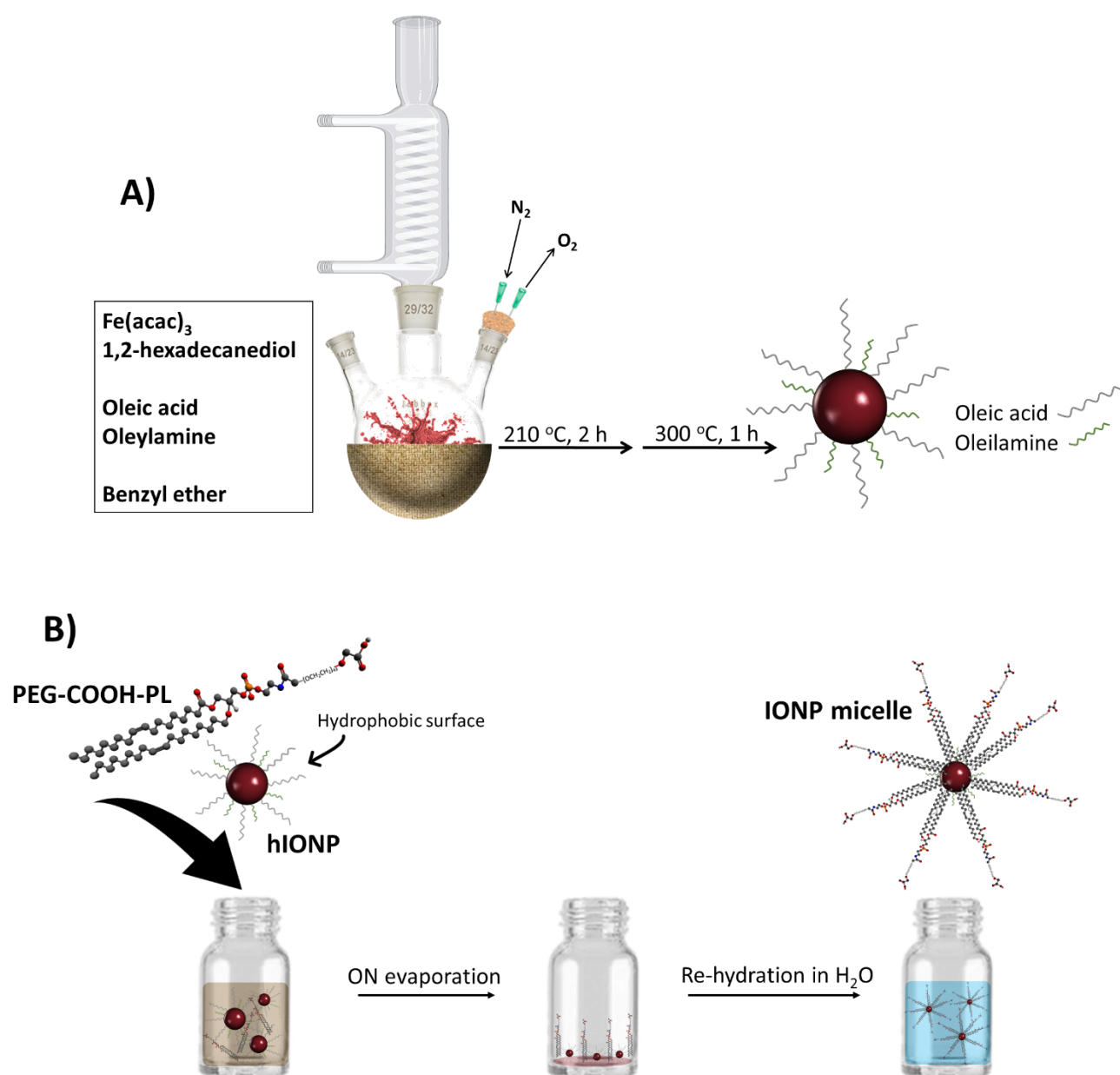


Figure 2.3. Synthesis and water transfer of hIONPs scheme. (A) The hydrophobic IONPs were synthesized by thermal decomposition under N_2 atmosphere. (B) Self-assembled micelles scheme showed the two-step protocol of water transfer of hIONP consisting in solvent evaporation and re-hydration in H_2O .

The best ratio to form micelles was 1:2 ratio (NP:PEG-PL). The mixture was performed in chloroform and then it was let it dry overnight for solvent evaporation. To avoid any presence of solvent the sample was dried under N_2 gas. After complete evaporation, the film was heated and hydrated with an aqueous solution.

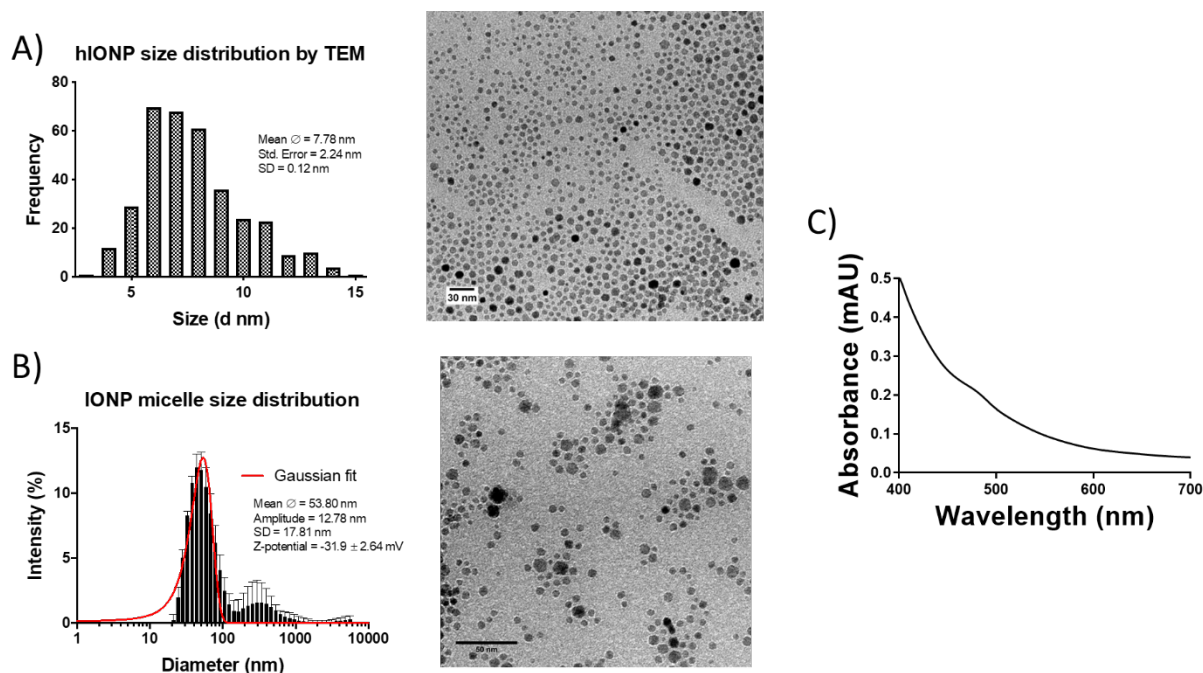


Figure 2.4. hIONP and IONP micelles characterization by TEM, Z-sizer, and spectrophotometer. (A) hIONP size frequency distribution on bar-graph and TEM image are shown. (B) IONP micelle size distribution by intensity is represented in bar-graph and TEM image is shown. (C) The absorbance spectrum of IONP micelle showed the peak at 480 nm.

In addition, the characterization of the magnetic properties of the IONP micelles was performed since these NPs may have also potential for their use as contrast agents *in vivo*⁴⁴⁷. The characterization of IONP micelles suspension was carried out measuring T_1 and T_2 at 1.5 T in Bruker Minispec mq60 TD-NMR spectrometer and at 7 T in the Bruker Biospec 7 T (Fig 2.5). These parameters are measured at different concentration of a material to define the longitudinal (r_1) and transverse (r_2) relaxivities ($r_1 = \text{slope of linear fitting of measured } 1/T_1$ and $1/T_2$ values, respectively at different Fe concentrations. T_1 is the time constant that approximately 65% of proton spins take to reach the magnetization or equilibrium (signal recovery time) and T_2 is the time that approximately 65% of proton spins take to decay away the signal (signal persistence away). Contrast agents will decrease T_1 and T_2 and in consequence the r_1 or r_2 will increase. When T_1 or T_2 decrease, the signal of the tissue or surrounding media in the image become darker (T_1 agents) or brighter (T_2 agents), generating positive or negative contrast in the image.

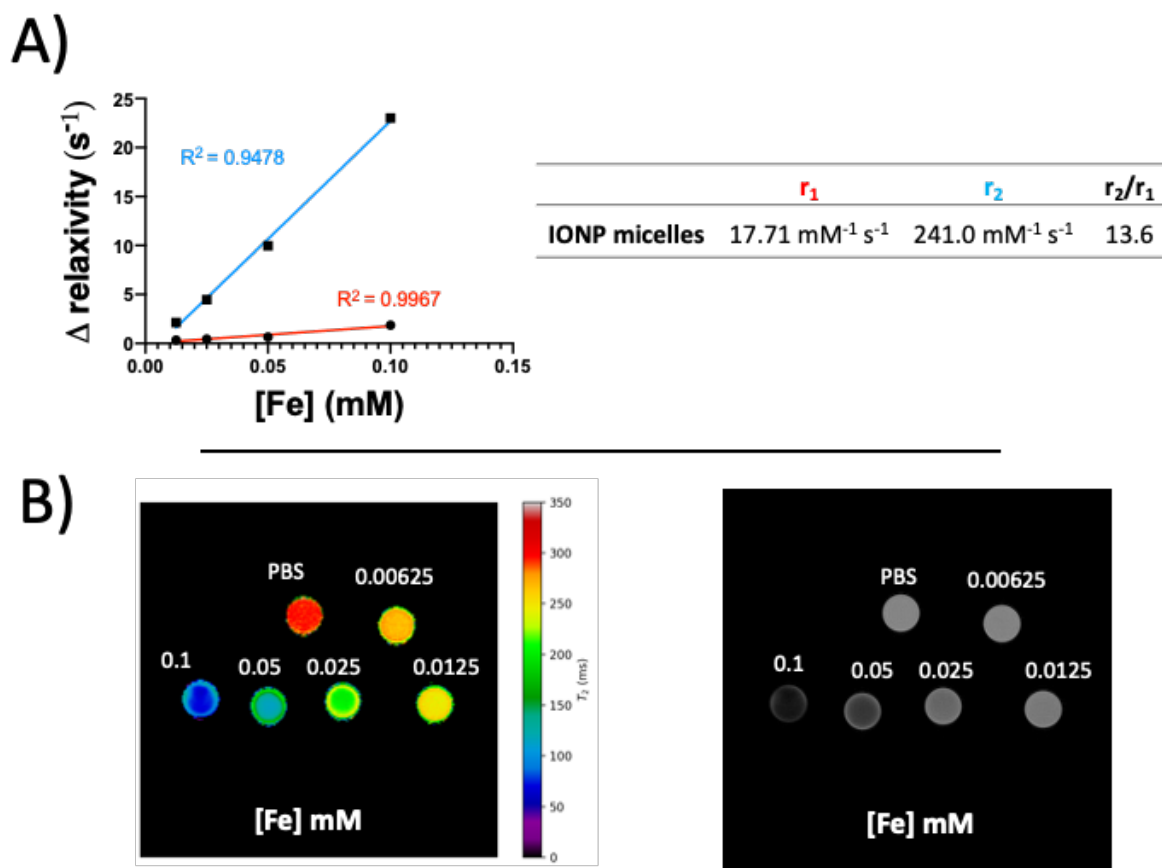


Figure 2.5. Magnetic characterization of IONP micelles. (A) Delta relaxation rates ($R_1=1/T_1$) (connected with red line) and $1/T_2$ (connected with blue line) values at different Fe concentrations was represented in XY graph and linear fitting was performed slope (r_1 and r_2) calculation, represented in a table. (B) MR images of IONP micelles at different Fe concentration in T2 maps is shown.

Although it is common to say that a material is T_1 or T_2 type contrast agent, actually these values are tissue dependent and are not related to a material. The point is that as it happened in pathologies such as cell density changes, edema or necrosis, the presence of a contrast agent in a given tissue, will affect T_1 and T_2 which is translated in different contrast in the image. For example, IONPs are classified as negative (T_2) contrast agents, but in some cases could have properties as positive (T_1) agents when the size of nanoparticles is ultrasmall (3 nm in diameter) or when the NP is doped with other metals such as Gd, Mn or Cu^{448–450}.

In the case of the IONP micelles used in this thesis, the r_1 and r_2 values were $17.71 \text{ mM}^{-1} \text{ s}^{-1}$ and $241.0 \text{ mM}^{-1} \text{ s}^{-1}$, respectively. The value of r_2 was very high indicating that the IONP micelles can be considered T_2 contrast agents⁴⁵¹, which is translated into a darker signal than

the PBS (media in which the particles are suspended). It was also calculated the ratio r_2/r_1 which defines T_1 agents as $r_2/r_1 < 3$, T_2 agents as $r_2/r_1 > 10$ and dual contrast agents (which could display T_1 and T_2 properties) as r_2/r_1 between 3 and 10. For IONP micelles r_2/r_1 was 13.6 which confirms the T_2 properties of the material. In addition, the T_2 map of the MR images of known concentrations of the IONP micelles showed the capacity of this material to increase the contrast of the PBS while the concentration of IONPs micelle increases as it could see in the figure 2.5C.

In principle, for the clinic, T_1 contrast agents are getting relevance, but the rapid accumulation of the IONPs on lymph nodes, liver and spleen or the capacity to homogenize the bowel content signal make IONPs as ideal negative contrast for the study of those tissue alterations⁴⁵². For example, in the case of Crohn disease lesions diagnosis with superparamagnetic oral contrast agent, the signal of T_2 displays same accuracy as Gd-enhanced T_1 - and T_2 -weighted sequences⁴⁵³. This similar accuracy demonstration and the fact that Fe based materials are less toxic than Gd or Mn based ones, convert IONPs in the almost unique contrast agent for MRI in clinic^{454,455}.

2.2.2. Expression and the biofunctionalization of protein

The first step was defining the biofunctionalization strategy for the NP decoration. Several efforts in the field of conjugation reactions showed complications in the conjugation by covalent binding related to the orientated binding of molecules. This problem is especially important in the case of molecules that need to exhibit certain part of the molecules, as it happened with antibodies (Ab), because they will recognize certain molecules or cell membrane receptors^{456,457}. As in this case the molecule is a protein and will be recognized receptors on cell membrane, it was selected an affinity attachment of the biomolecule to ensure the contact between the receptors and protein recognition site. There are several well-established affinity systems, such as the protein A that binds the Fragment crystallizable region (Fc) of immunoglobulin (Ig) G, or 6x his-tag sequence that binds Ni or Co-NTA⁴⁵⁸⁻⁴⁶⁰.

This last affinity system is usually used for protein purification, but in this work, will be also employed as the basis of the biofunctionalization strategy⁴⁶¹.

His-tagged human IL-15 protein expression (called hIL-15HIS from now on):

Human IL-15 was expressed in bacteria following an optimized method based on a previously published protocol⁴⁶². This protein is a cytokine type protein which can stimulate immune cells (see further details on the biological role of IL-15, and interest for immunomodulatory therapies in Chapter 3).

hIL-15 gene was ordered to Biomatik (<https://www.biomatik.com/>) cloned in the pUC57 expression vector flanked by the BamHI and HindIII restriction sites for re-cloning. Then, the gene was re-cloned into a pProEX-HT vector as a His-tag fusion, for further purification and bioconjugation. The digestion of two vectors (IL-15 gene containing pUC57 and pProEx-HT) was carried out with BamHI and HindIII restriction enzymes. Thus, IL-15 gene could be ligated in the his-tag containing expression vector (pProEX-HTa) (see appendix I: A2.1 and A2.2). Upon cloning in the pProEX-HT vector the IL-15 gene presents the his-tag sequence at the N-terminal (Figure 2.6).

After the ligation, the pProEX HT-IL15 vector was transformed in *Escherichia coli* DH10 β strain to extract the plasmidic DNA. To ensure that the gene was in frame of the 6x- his-tag sequence, the vector was sent for sequencing to StabVida (Fig. 2.6 A) as indicated in the experimental section. The sequences are described in Appendix I.

For protein expression *E. coli* C41 strain was used. First a standard protocol for purification of his-tagged proteins was applied, but the protein remained mostly in the insoluble fraction after the lysis (Fig. 2.6B). Therefore, alternative protocols were applied to improve the solubility of the protein by adding urea as reducing agent to the lysis buffer. When using 6 M urea the protein appeared in the soluble fraction as can be observed in the sodium dodecyl sulphate-poly-acrylamide gel electrophoresis (SDS-PAGE) (figure 2.5 C). In addition, the

sonication step from the original protocol was eliminated since the protein yield was higher without sonication.

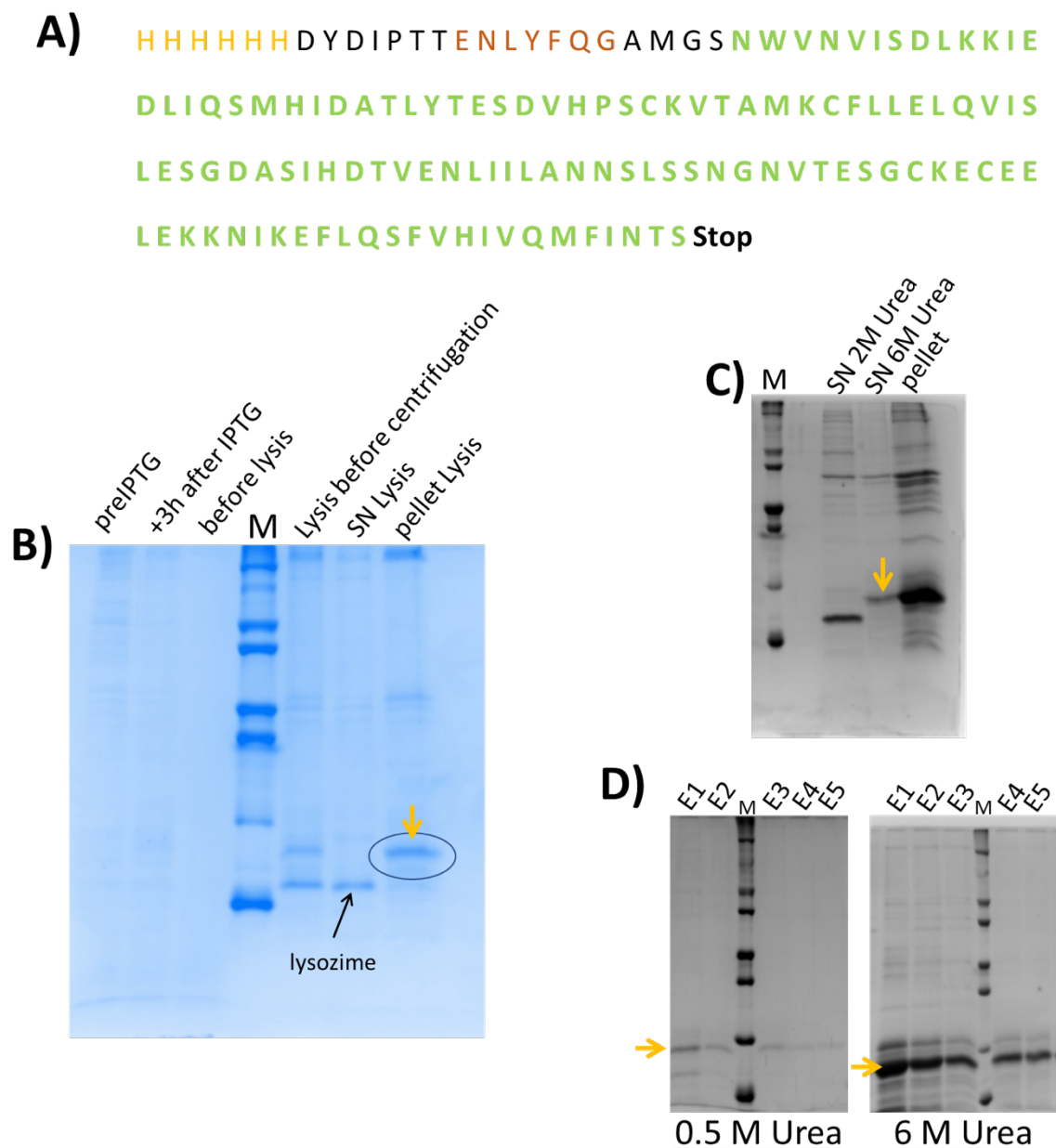


Figure 2.6. IL-15 sequence and purification. (A) Designed hIL-15HIS gene sequence with the his-tag sequence in N terminal and tobacco etch virus nuclear inclusion-a endopeptidase (TEV) cleavage sequence is showed. (B) Failed protein purification is showed with pointing at with an arrow the IL-15 in the insoluble fraction (pellet lysis). (C,D) Urea concentration contribution on protein extraction from the insoluble fraction was checked by polyacrylamide gel. (C) The protein extracted from the insoluble fraction after incubation in a buffer at 6 M Urea confirms the ability of reducing agents on the extraction of protein from pellet. (D) Protein lysis with 0.5 vs. 6 M urea was compared from same batch of cells that express the protein.

After SDS-PAGE, the protein sample is run through a high load gel filtration column in which the proteins are separated by size. This step should eliminate every protein that was bound to the Ni column in an unspecific way. After that, the protein was characterized by different techniques. Circular dichroism (CD) is used for the confirmation of the secondary structure and the folding properties of the protein. In this case, the CD spectra displays two peaks between 200 and 220 nm and a decrease of CD signal at 250 nm which starts going up again at 205 nm. This spectrum is related with an alpha helical structure of protein which is related to the structure of IL-15 protein⁴⁶³ (Fig. 2.7. A).

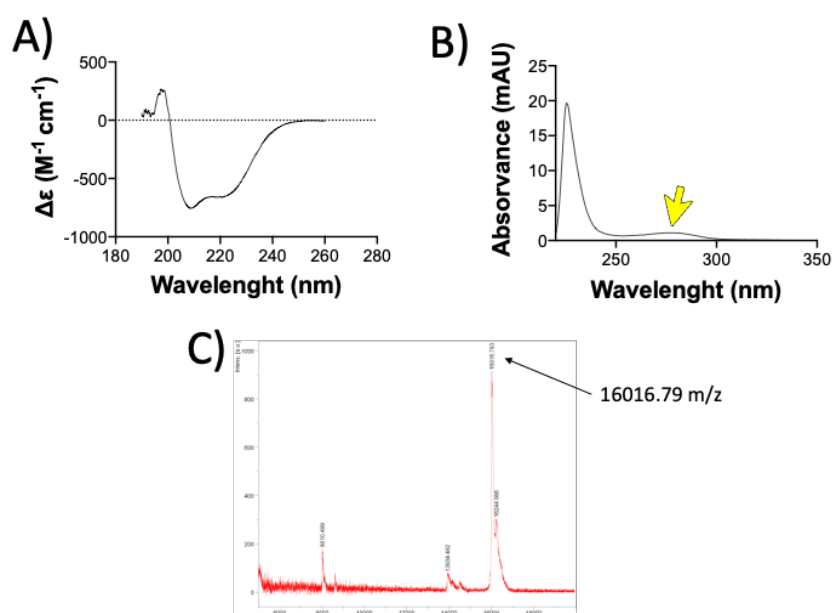


Figure 2.7. Lab made IL-15 (hIL-15HIS) characterization. (A) Circular Dichroism (CD) confirmed the alpha helical structure of the protein, (B) absorption spectroscopy was used to obtain the protein concentration by absorption peak at 280 nm (yellow arrow) and (C) MALDI-ToF mass spectrometry confirmed the mass of the protein which was 16016.79 m/z.

The exact mass of the protein was also characterized by matrix-assisted laser ionization joined to a time-of-flight mass analyzer (MALDI-ToF MS) (Fig. 2.7 C). The MALDI-ToF MS showed a 16016.79 m/z which is near to the theoretical his-tagged IL-15 protein mass (16144.18 Da). This small difference would be owing to some molecule separation in the fly when the protein is measuring in the MALDI-ToF MS, so the mass was considered to related to the his-tagged IL-15 protein. Finally, the protein concentration was calculated by measuring the absorbance

of the protein at 280 nm by absorbance spectroscopy (Fig. 2.7 B) and calculating the extinction coefficient by amino acid composition. The yield of protein expression was calculated as total protein obtained from a batch of bacteria in 1 L.

The immunomodulatory purpose of the expression of hIL-15HIS become essential its comparison with commercial IL-15, already use for the same purpose. The aim of this comparison was principally to check the purity of the sample produced. Polyacrylamide gel showed pure proteins and Maldi-ToF MS sizes were what was expected in both hIL-15HIS and commercial IL-15 (Fig. 2.8 A, B).

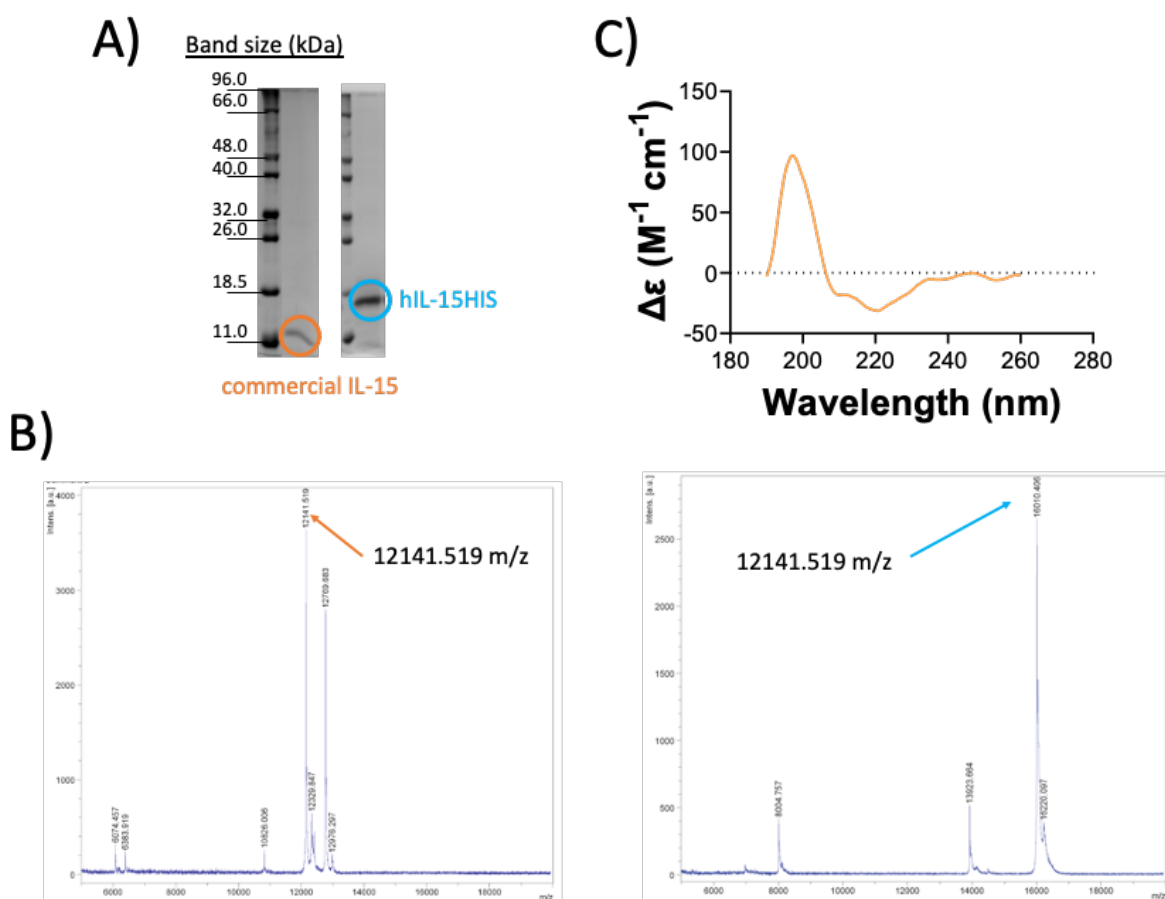


Figure 2.8. Comparison of commercial IL-15 and hIL-15HIS. (A) Polyacrylamide gel shows the purity and the approximate size of the commercial IL-15 (orange) and hIL-15HIS (blue). (B) Maldi-TOF-TOF shows the difference in size of commercial (orange arrow) and lab made (blue arrow) protein which is related to what was expected (B). (C) The CD spectra of commercial protein shows the secondary structure of the commercial IL-15 at 10 μ M.

The secondary structure of the commercial protein was measured by CD (Fig. 2.8 C), and unless the CD spectrum was not valuable, it could observe that the structure seems to be like the hIL-15HIS (Fig. 2.7 A) and displayed the peaks observed in alpha helical structured proteins.

The comparison of the lab made IL-15 with the commercial IL-15 demonstrated success expression and purification of the protein. The conclusion is that the hIL-15HIS is as pure as the commercial one and the mass and structure is comparable considering the presence or absence of the His-tag.

Protein biofunctionalization

The strategy to decorate the protein on the surface of the nanoparticle is based on the affinity of the His-tag sequence with the NTA molecule⁴⁶⁴, already used in the protein purification protocol. For this purpose, the NTA molecule needs to be attached to the particles, and this will be achieved through the modification of the carboxylic group of the PEG-PL. In this thesis, two ways of modifications were carried out: modification of the PEG-PL before and after micelation.

In both cases, NTA molecule attachment to the PEG-PL was performed through a covalent linkage (Fig. 2.9). The amino group of the Lys containing NTA molecule will react with the carboxylic (COOH) group of the PEG-PL. To accelerate the reaction between the NH₂ and COOH, the carboxylic group was activated with 1-ethyl-3-(3-dimethylaminopropyl) carbodiimida (EDC) and N-Hydroxysuccinimide (NHS). In the case of the modification before micelation, the modified phospholipid (PEG-NTA-PL) was characterized and quantified by electrospray ionization source and a time-of-flight analyzer mass spectrometer (ESI-ToF-MS). The ultra-performance liquid chromatography (UP-LC) chromatogram of the modified sample showed two peaks. As it can be observed, after the MS spectrum analysis (Fig. 2.10), the calculated and the experimental isotopic profiles of the spectrum for the peak assigned to the PEG-NTA were similar. The retention time of the PEG-NTA-PL was larger than the observed for the PEG-

COOH (PEG-PL). This increase in the retention time can be explained by the lower polarity of the functionalized PEG-NTA-PL compound (in reverse phase chromatography, the less polar, the more retained). The best ratio of reagents to obtain at least 50% of PEG-NTA phospholipid modification was 1:6:2:3 (PEG-PL:EDC:NHS:NTA).

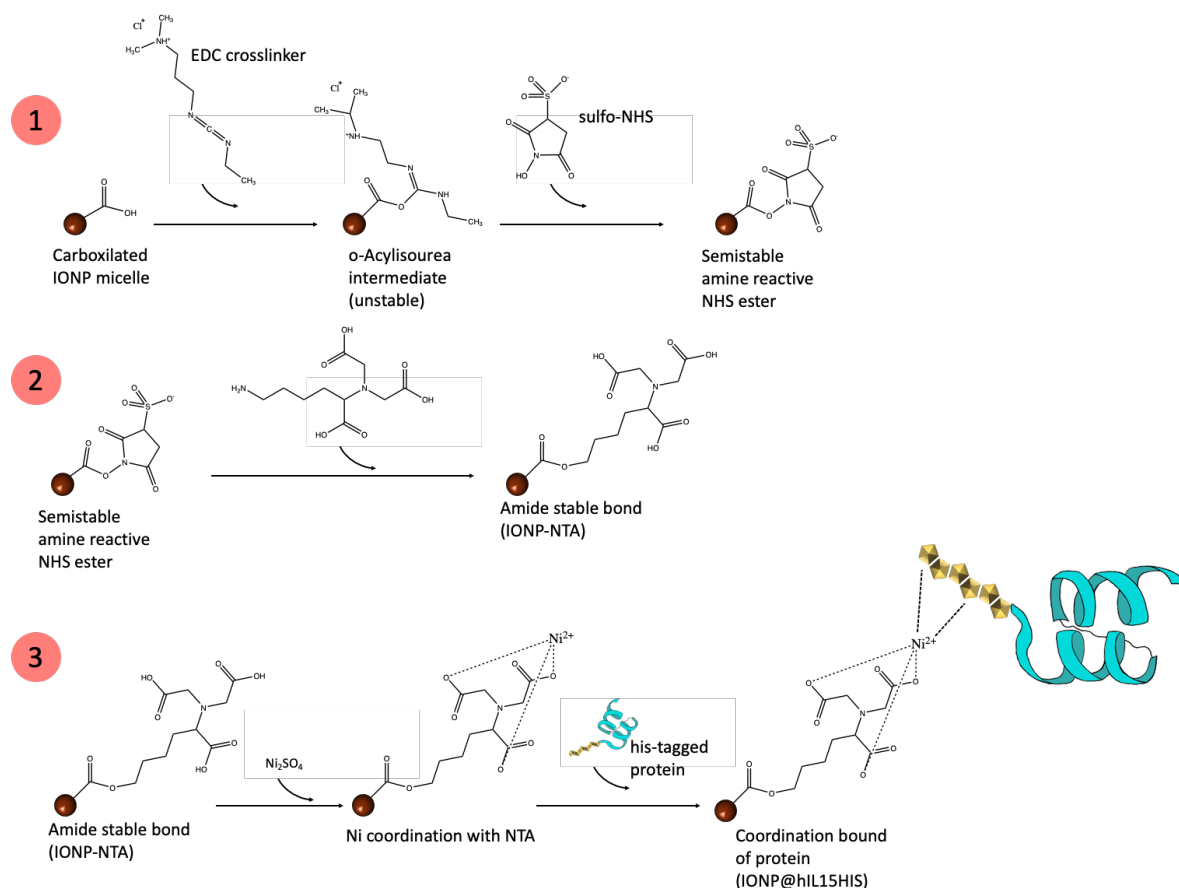


Figure 2.9. Conjugation strategy step by step. Biofunctionalization of the protein was carried out following three steps 1) activation of carboxylic group on the surface of the IONP micelle; 2) covalent binding of NTA-Lys molecule with the carboxylic group of PEG-PL (IONP-NTA); 3) hIL-15HIS binding through coordination bond with Ni^{2+} and NTA.

Once the PEG-PL was modified, the next step was to make the micelle using the modified molecule, but micelation with this PEG-NTA-PL was as efficient as the micelles formed using the original PEG-PL (with COOH) (Fig. 2.10 C). The low Fe concentration and the poor stability observed by precipitation of the samples after a week, were the fact to speculate low efficiency on PEG-NTA micelles (NP@NTA). Therefore, the modification of the PEG-PL after micelation was the method selected to fabricate all batches of the nanoformulation.

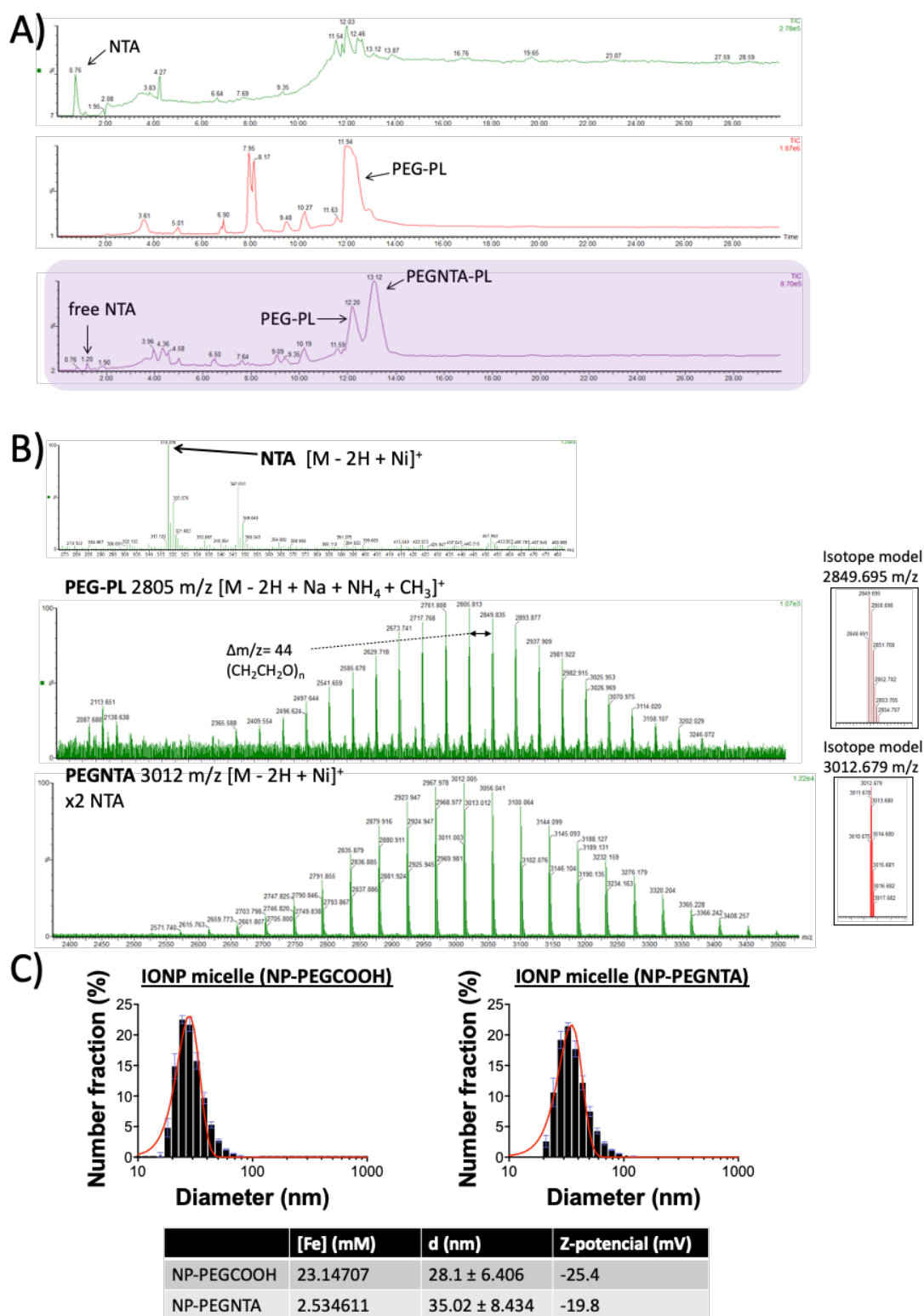


Figure 2.10. PEG-NTA-PL molecule and forming micelles characterization. (A) The differential retention time in UPLC-MS chromatograph of NTA alone, PEG-PL alone and modified PEG-PL with NTA (PEG-NTA-PL) are showed. (B) Mass of NTA, PEG-PL and PEG-NTA-PL detected by electrospray ionization was analyzed comparing the MS spectra of the experimental isotope models. (C) The capacity of micelation was measured by Fe concentration, size and z-potential.

The principal advantage of the modification of the phospholipid after the micelation consist on the cross-reactions are avoided because the excess of reagents can be easily eliminated. This reagents wash was possible because the structure in which the reaction is happening (surface of the NP), is big enough to separate from the reagents in a standard buffer exchange column (NAP-5 prepaccked column (GE healthcare Life Science). The best reaction ratio for PEG-PL modification on the surface of the micelle was 1:100:50:21 (PEG-PL:EDC:NHS:NTA). After PEG-PL modification the conjugation processed was continued, first the Ni_2SO_4 was added in a molar ratio of 1:20 (NTA: Ni_2SO_4) and then the protein was added in 1:1 (PEG-PL:protein) molar ratio.

The final step of biofunctionalization was the purification of protein by filtration through a 6cLB Sepharose gel filtration column. The obtained fractions from the column were evaluated by spectrophotometer to determine the scattering of the nanoparticle and the absorbance of the protein at 280 nm (Fig. 2.11 B). In all batches, IONP@hIL15HIS containing fractions was between 7-8 fraction which was correlated with bigger size than bare IONP micelle which eluted in the 10th fraction (Fig 2.11A). The 6cLB column fractions absorbance spectra (red and green in figure 2.11 B) confirmed the presence of the NP by scattering and the protein by absorbance at 280 nm in the fractions which is related with the presence of IONP@hIL15HIS.

The fractions from the 6cLB column were also monitored by protein concentration performing Bradford or Bicinchoninic assay (BCA) protein quantification assays. Considering the protein concentration from these assays in combination with the fractions where the protein peak and the scattering of the NP appeared, the IONP@hIL15HIS containing fractions were selected, that are between 7-10 fractions in all batches.

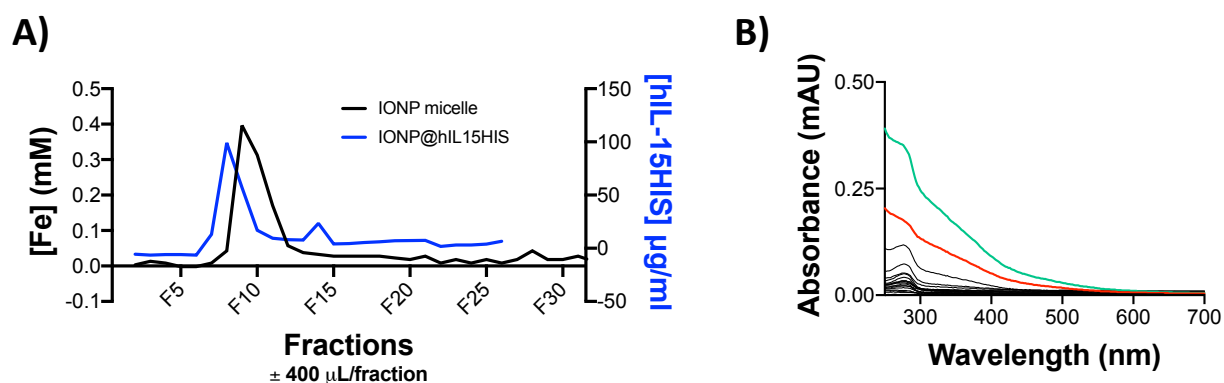


Figure 2.11. Purification of IONP@hIL15HIS with Sepharose 6cLB resin column. (A) IONP micelle chromatogram of 6cLB column (representing Fe concentration measured by ICP) and IONP@hIL15HIS chromatogram (representing protein concentration measured by BCA assay) is showed. Micelles alone eluted at 10 fraction (black line) and IONP@hIL15HIS retain slightly more in the column and elute at F7-F9 (blue line). (B) All fractions from the purification step on 6cLB Sepharose resin were characterized by absorbance spectra to select fractions that displays absorbance at 280 nm and the NP scattering (red and green lines).

2.2.3. IONP@hIL15HIS characterization

In the field of bio-nanotechnology the resulted system characterization gain importance because of the interest on anticipating to the fate of NPs. Nevertheless, in terms of bioconjugation the interest lies in characterizing all steps of the reaction to be able to follow the bioconjugation at least in some point. Therefore, it was decided to follow the reaction by size and charge in three different steps: beginning (bare micelle), micelle with the NTA molecule bound covalently and final sample in where the protein is coordinated with the NTA molecule. These three steps were selected assuming they are the steps in where the sample is stable enough to do some characterizations and are the steps in where it can see differences in size and charge.

The measurements of these three different steps revealed clearly in the figure 2.12.A how the size increased by adding the NTA molecule and the protein, while the z-potential changed in every step. The z-potential of the bare nanoparticle (IONP micelle) was the most negative between all characterized bioconjugation steps. When the NTA molecule was bound covalently to the surface of the nanoparticle, the z-potential value changed to -4.63 ± 1.16 mV and after protein coordination with the NTA molecule, the system turned to a slightly more

negative charge. The net charge of the final sample was -9.63 ± 1.76 mV, which could be considered a value close to 0. It is demonstrated that when the charge of a NP is not so far from 0 the fate of the particles is guaranteed. By contrast, when the size is clearly positive or negative some processes such as protein corona formation and immune-sequestration could stop the circulation time of NP^{242,465–468}.

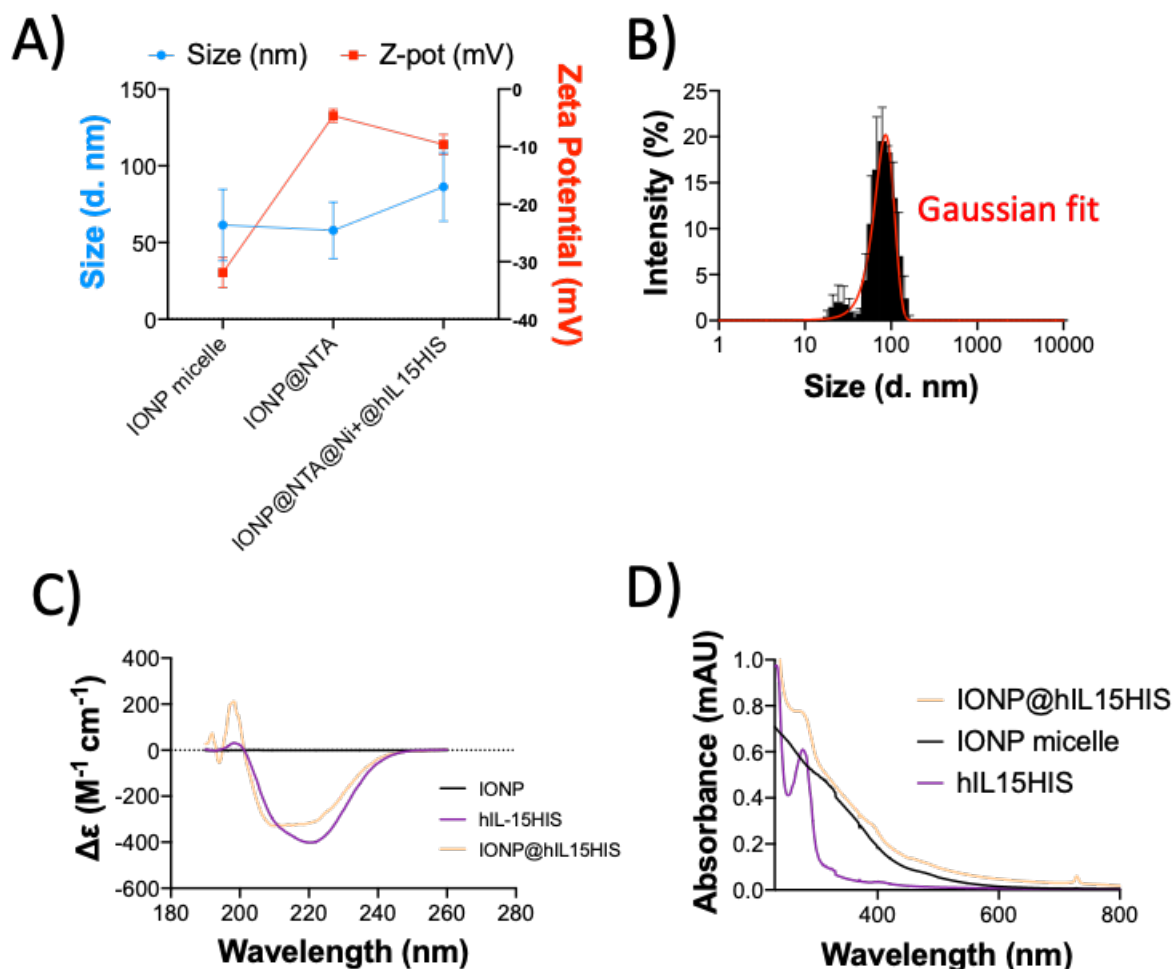


Figure 2.12. Characterization of IONP@hIL15HIS. (A) Size and z-potential of all steps of bioconjugation are showed. (B) The size of a representative IONP@hIL15HIS batch sample is showed. (C) CD spectra displaying the alpha helical secondary structure of the protein and (D) absorbance spectrum showing the absorbance or protein at 280 nm and the NP scattering of final sample is represented comparing with IONP micelles and protein alone as controls.

Once IONP@hIL15HIS size and z-potential was evaluated, the system was characterized by CD, absorbance spectrometry and ICP-MS (Fig. 2.12). The CD spectra (Fig. 2.12.C) showed that the chirality is only displayed in the protein containing samples (hIL-15HIS and

IONP@hIL15HIS). Specifically, absence of CD signal in IONP sample and the presence of the active chiral molecule in IONP@hIL15HIS demonstrated the biofunctionalization of the protein in the surface of the NP and its structure preservation. The absorbance spectrum verified the presence of the protein and the NP in the sample and ICP-MS data was performed to know the Fe concentration in the final sample which was around 0.5 mM in all batches.

Additionally, DLS measurement also confirmed the presence of the protein considering the difference in size of IONP and IONP@hIL15HIS. As it could see in the table 2.1, IONP micelle was around 20 nm smaller than IONP@hIL15HIS, and this matched approximately with the size of one molecule of protein as DLS results confirmed.

Table 2.1. Size difference between micelle and IONP@hIL15HIS. Size and charge data provided by dynamic light scattering (DLS) reveals the difference between IONP micelles and IONP@hIL15HIS is approximately the size of protein alone.

Sample	Size (diameter)
hIL-15HIS	17.95 ± 2.048 nm
IONP micelle	59.87 ± 5.072 nm
IONP@hIL15HIS	82.66 ± 4.274 nm

The final system characterization means also in the quantification of how much of the molecule is finally biofunctionalized. This is specially importance in this case, as hIL-15HIS will trigger immunomodulation in the *in vitro* and *in vivo* studies. The protein concentration in IONP@hIL-15HIS final sample was performed by an indirect quantification (Fig 2.13). Just before doing the protein excess purification in the 6cLB Sepharose column (not-purified IONP@hIL15HIS), 100 µL were taken and centrifuged to make NP precipitating to the pellet and the supernatant was measure by absorbance spectroscopy to measure the unbound protein. The same process was performed with a protein sample (hIL-15HIS) diluted to a comparable volume and the resulting difference between the protein concentration of the hIL15HIS SN and IONP@hIL15HIS supernatant (SN) was assumed as the protein amount bound to the NP.

In parallel, 20 μL from the same non-purified IONP@hIL15HIS was taken to digest and quantify the Fe concentration by ICP. The data from ICP in combination with the indirect protein concentration data from the non-purified IONP@hIL15HIS let it obtain the ratio of μM of hIL15HIS/mM Fe which let us know the concentration by measuring the Fe concentration on the final sample (around 20-40 μM hIL-15HIS/0.5 mM Fe).

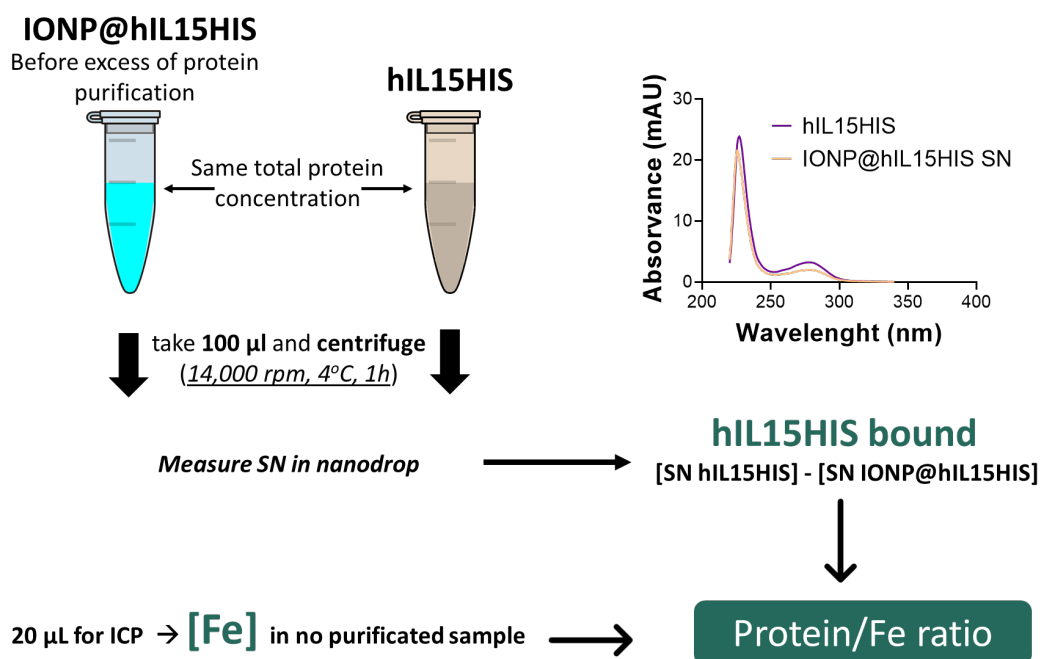


Figure 2.13. Indirect quantification of hIL-15HIS bound to the IONP. IONP@hIL15HIS and hIL-15HIS samples were centrifuged and the protein amount of the SN was calculated from the absorbance of protein at 280 nm. The difference between hIL-15HIS and IONP@hIL15HIS SN protein concentration was considered as bound protein (hIL-15HIS bound). Measuring the Fe by ICP from the same sample it could get the protein/Fe ratio in green box in the figure.

Finally, the stability of the IONP@hIL15HIS was studied measuring the size of the system by DLS (Fig. 2.14). It was observed that the size distribution of IONP@hIL15HIS did not vary in a 23 days period of time, and it was considered that the system was at least stable in terms of colloidal stability for 23 days stored at 4°C.

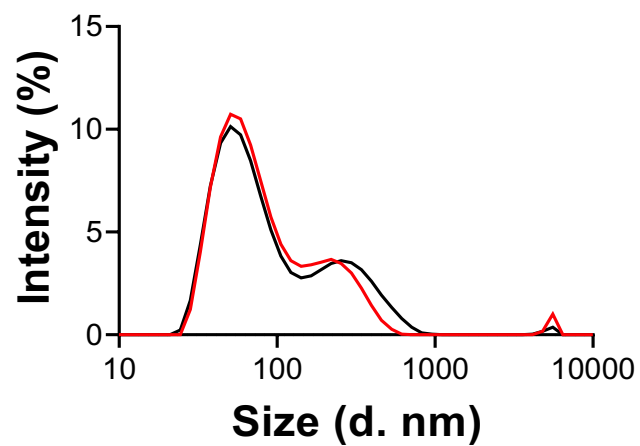


Figure 2.14. Size distribution of IONP@hIL15HIS by DLS. Black line shows the size distribution of a fresh sample and red line represented the same sample after 23 days stored at 4°C.

2.3. Conclusion

The designed, synthesis and characterization of hIL-15 delivery system were successfully achieved. The first approach was to do the water-soluble transfer of hydrophobic IONPs following a very simple protocol based on the self-assembly of the hydrophobic structures similar to the liposome synthesis. Then the bioconjugation was carried out combining two strategies of binding in two consecutive steps: covalent binding of NTA molecule on the surface of the IONP micelle and then NTA and his-tag affinity-based binding of his-tagged hIL-15HIS protein. In all batches of IONP@hIL15HIS produced in this thesis the size was ideal for *in vivo* application (size between 70-100 nm). The charge also is an important aspect to consider in the systems that are for biological applications. The final system used in this thesis (IONP@hIL15HIS) is negatively charged but the value was considered to be close to 0, which seems to be related with higher circulating time, and also in a low clearance by the immune system as several scientific works demonstrated^{434,469}.

The characterization of the final system was done by different techniques and in all of them the presence of the Fe and the protein was confirmed. Furthermore, stability checked by DLS indicate that IONP@hIL15HIS was stable for at least 23 days in terms of stability. In addition, *in vitro* experiments were repeated 7 times in order to get representative results and all repetitions were carried out with the same sample stock of IONP@hIL15HIS during 2 months. Considering that IONP@hIL15HIS did not manifest any decrease in stimulation capacity in all this period, it was concluded that the system denoted a functional stability for almost 1 month. The colloidal and functional stability evidences indicated that IONP@hIL15HIS endured with easy storage requirements.

In this chapter it is shown the successful synthesis of recombinant his-tagged IL-15, stable IONP micelles and a robust and versatile biofunctionalization strategy for the decoration of IONPs with hIL-15HIS.

Chapter III

In vitro assays with IONP@hIL15HIS

Chapter III In vitro assays with IONP@hIL15HIS

3.1. Introduction

Interleukin (IL)-15 is a cytokine able to activate natural killer (NK) and T cells through the recognition of the β subunit of IL-2/IL-15 receptor (IL-2/IL-15R β or CD122) and common gamma chain (γ_c or CD132) on the surface of those cell types⁴⁷⁰. IL-15 induces proliferation of T and NK cells and has a fundamental role in the development and survival of NK cells and CD8 effector/memory T cells⁴⁷¹. In the field of cancer immunotherapy IL-15 has showed antitumor effect in preclinical models⁴⁷². This antitumor effect, in addition to its effect on NK and CD8 T cells, is also related, among other reasons, to the almost null effect on regulatory T cells (Tregs) that IL-15 exhibits, which is the opposite to the related cytokine IL-2 that is able to activate Tregs due to their expression of the high affinity receptor for IL-2⁴⁷³. As Tregs inhibit antitumor immunity, the antitumor effect triggered by IL-15 on other effector cells is practically not restrained by Tregs⁴⁷⁴. On the other hand, it has been shown that therapies based on the infusion of IL-15 may cause an increased expression of checkpoint receptors such as programmed death-ligand 1 (PD-L1) and cytotoxic T-lymphocyte antigen-4 (CTLA-4)^{475,476}. Therefore, combined therapies of IL-15 with monoclonal antibodies against these receptors have been proposed^{477–479}(Table 3.1).

Table 3.1. Examples of ongoing clinical trials with IL-2 and IL-15 as part of combination therapy for cancer treatment. There are approximately 601 ongoing clinical trials with IL-2 and 147 with IL-15. *The information is from ClinicalTrials.gov (<https://clinicaltrials.gov/ct2/home>).*

Cyokine	Intervention/treatment	Cancer Type	Clinical trial
IL-2	○ IL-2	● Melanoma stage IV	NCT03991130
	○ Nivolumab	● Metastatic RCC	
	○ IL-2	● Cutaneous metastatic melanoma	NCT03928275
	○ BCG		
	○ IL-2	● NSCLC	NCT03474497
	○ Pembrolizumab	● Metastatic melanoma	
	○ Radiotherapy	● Metastatic RCC	
		● HNSCC	
	○ FT516 (allogeneic NK cells, expressing high affinity non-cleavable CD16)	● Ovarian cancer	NCT04630769
	○ IL-2	● Fallopian tube adenocarcinoma	
○ Enoblituzumab	● Primary peritoneal cavity cancer		
○ Aldesleukin (IL-2)	● III and IV stage RCC	NCT03260504	
○ Pembrolizumab	● Advanced Clear Cell RCC		
	● Metastatic Clear Cell RCC		
○ Re-stimulated TIL	● Recurrent/platinum resistance:	NCT01883297	
○ IL-2	○ Ovarian cancer		
○ Cyclophosphamide	○ Fallopian tube cancer		
	○ Primary peritoneal cancer		

	<ul style="list-style-type: none"> ○ TIL ○ IL-2 ○ Anti PD-1 	<ul style="list-style-type: none"> ● Advanced melanoma 	NCT04165967
	<ul style="list-style-type: none"> ○ Radiotherapy ○ IL-2 	<ul style="list-style-type: none"> ● Metastatic RCC ● Malignant/metastatic melanoma 	NCT01884961
IL-15	<ul style="list-style-type: none"> ○ N-803 (IL-15 superagonist) ○ PD-L1 t-haNK (NK-92 cells expressing PD-L1-targeting CAR, high affinity CD16 and IL-2 retained in ER) ○ Chemotherapy drugs ○ SBRT 	<ul style="list-style-type: none"> ● Advanced/metastatic pancreatic cancer 	NCT04390399
	<ul style="list-style-type: none"> ○ BCG ○ N-803 	<ul style="list-style-type: none"> ● Non-muscle Invasive Bladder Cancer 	NCT02138734
	<ul style="list-style-type: none"> ○ Donor IL-15 stimulated NK cells infusion 	<ul style="list-style-type: none"> ● Acute leukemia 	NCT03669172
	<ul style="list-style-type: none"> ○ ALT-803 (N-803) ○ Nivolumab 	<ul style="list-style-type: none"> ● NSCLC 	NCT02523469
	<ul style="list-style-type: none"> ○ rhIL-15 ○ Avelumab 	<ul style="list-style-type: none"> ● Clear cell RCC 	NCT04150562
	<ul style="list-style-type: none"> ○ GTB-3550 TriKE® (trispesific scFv killer cell engager: anti-CD16, anti-CD3, modified IL-15) 	<ul style="list-style-type: none"> ● High-risk Myelodysplastic Syndromes ● Acute Myelogenous Leukemia ● Systemic Mastocytosis ● Mast Cell Leukemia 	NCT03214666
	<ul style="list-style-type: none"> ○ N-803 ○ CIML NK cell Infusion ○ Ipilimumab 	<ul style="list-style-type: none"> ● HNSCC ● Recurrent HNSCC 	NCT04290546
	<ul style="list-style-type: none"> ○ NIZ985 (IL-15/IL-15Rα heterodimer) ○ PDR001 (Spartalizumab, anti-PD-1) 	<ul style="list-style-type: none"> ● Metastatic and advance solid tumors 	NCT02452268
	<ul style="list-style-type: none"> ○ iC9.GD2.CAR.IL-15 T-cells (CAR-T cell against GD2, expressing inducible caspasa 9 and IL-15) ○ Cyclophosphamide ○ Fludarabine 	<ul style="list-style-type: none"> ● Neuroblastoma ● Osteosarcoma 	NCT03721068

IL: interleukin, RCC: renal cell carcinoma, BCG: Bacillus Calmette-Guérin, NSCLC: non-small cell lung cancer, HNSCC: head and neck squamous cell carcinoma, TIL: tumor-infiltrating lymphocytes, ER: endoplasmic reticulum, SBRT: Stereotactic Body Radiotherapy, CIML: cytokine-induced memory-like, IL-15R α : IL-15 receptor α .

3.1.1. IL-15 application in the clinic

Nearly 150 clinical trials (<https://clinicaltrials.gov/ct2/home>) are initiated in which IL-15 has been used as mono or combined therapy (Table 3.1). In addition to clinical trials in where IL-15 is administered to patients⁴⁸⁰, there are other trials in which this cytokine is used in the context of adoptive cell transfer therapy (ACTT)⁴⁸¹, for the manufacturing of cell products. ACTT is based on the pre-activation and/or expansion of cells before infusion into the patient. Some examples include the generation of cells with higher effector functions such as T cells and NK cells that are infused into patients^{482,483}. The adoptive transfer of short-term (overnight) *ex vivo* activated and/or expanded autologous or allogeneic NK cells are able to induce clinical responses in patients with multiple myeloma and acute myeloid leukemia (AML)^{484,485}. *Ex vivo* activation of allogeneic NK cells for a short period of time (overnight) has been carried out with cytokines such as IL-2 or IL-15⁴⁸⁶. More recently, the efficacy and safety

of cytokine-induced memory-like (CIML) NK cells is being explored^{487,488}. CIML NK cells are generated after activation for approximately 18 hours with a combination of IL-12, IL-15 plus IL-18 as first stimulus. These cells are characterized by increased effector functions in response to a second stimulus (i.e. cancer cells, ILs stimulation) after a resting period, in addition to exhibiting a longer half-life^{487,489–492}. Importantly, clinical trials have demonstrated its safety and efficacy in treating patients with relapsing/refractory AML^{487,488}. In these trials, IL-12/15/18 pre-activated NK cells are infused into lymphodepleted patients, followed by subcutaneous low doses of IL-2 to induce the *in vivo* expansion of CIMLs^{487,488}. Adoptive transfer of cultured and expanded autologous NK cells with cytokines has also been used, allowing the use of multiple infusions of highly activated NK cells^{493–496}.

3.1.2. Engineering IL-15 to improve its therapeutic effect

Despite the success of IL-15-based therapies, its effectiveness is limited in part by the low half-life of the protein *in vivo*⁴⁹⁷. To reverse this situation, IL-15 molecular modifications and conjugates are proposed^{209,498}. The best known is N-803 (formerly known as ALT-803) formulation that consists of the fragment crystallizable region (Fc) domain of immunoglobulin (Ig) G (IgG) bound to a complex of IL-15 and the sushi domain of IL-15 receptor α (IL-15R α). This modified cytokine is more stable in circulation, and shows better anti-tumor effect^{499,500}.

Those encouraging results with modified cytokines have led us to think about including nanoparticles (NPs)-based technology among the IL-15-based therapies aimed to stimulate the immune response. It is expected that NPs can also increase the bioavailability of the protein acting as an effective delivery system transporting the adequate and effective dose to the tissue and cells of interest. Additionally, depending on the material of the NP (Fe, Au, Ga...), they can be also used for other complementary applications such as imaging. In the case of Iron Oxide Nanoparticles (IONPs), they could be used as molecular resonance imaging (MRI) contrast agent. Furthermore, the composition of the NPs could also generate an adjuvant effect⁵⁰¹. For example, Fe based NPs could act as adjuvants by the process named

ferroptosis. This process is a type of programmed cell death that occurs after an accumulation of lipid peroxides and is differentiated biochemically and genetically from apoptosis⁵⁰².

In this chapter, a set of experiments are designed to *in vitro* study the effector functions of NK and T cells after pre-activation of peripheral blood mononuclear cells (PBMCs) with human IL-15 with His-tag (hIL-15HIS) expressed in the lab in its soluble or immobilized form (IONP@hIL-15HIS). hIL-15HIS protein and IONP@hIL15HIS are also combined with IL-12 and IL-18 cytokines to study the contribution of the biofunctionalization of the protein in the generation of CIML NK cells. The goal of the experiments was to determine the phenotype of NK and T cells just after the activation (priming) with the combination of IL-12, IL-18 and the two forms of IL-15 (hIL-15HIS protein and IONP@hIL15HIS) (day 0) and after an expansion phase (day 4).

3.2. Results and discussion

To evaluate the effect of IONP@hIL15HIS, an *in vitro* culture protocol was established. A scheme is shown in Figure 3.1 and is explained in detail in the experimental section (Fig. ES3). Overall, this protocol is divided in two principal steps: 1) pre-activation phase (16-18h) and 2) expansion phase and lasts for 4 days. The expansion phase with cytokines aims to simulate the administration of IL-2 (and in our experiments IL-15 as well) to patients who have received CIML NK cells, with the aim of expanding them *in vivo*^{488,489}. For convenience, the day in which the experiment starts is called day -1 and the day after 16-18h of pre-activation phase is identified as day 0. Also, this day 0 is the day when the expansion phase starts. Following this *in vitro* protocol, we will determine the role of IONP@hIL15HIS in both the pre-activation and expansion phases.

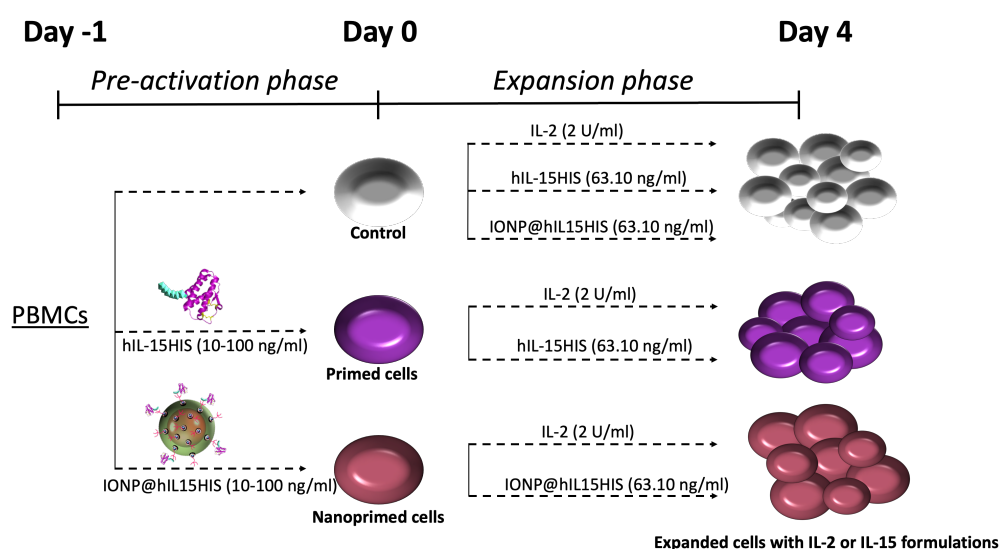


Figure 3.1. Schematic representation of pre-activation and expansion phases. PBMCs cultured in the presence of soluble (hIL-15HIS) and functionalized (IONP@hIL15HIS) forms of IL-15. Following the stimulation during 16-18 hours with hIL-15HIS or with IONP@hIL15HIS, cells were named primed and nanoprimered PBMCs, respectively. After this pre-activation phase, PBMCs were washed and expanded with IL-2 or with IL-15 formulations (hIL-15HIS or IONP@hIL15HIS). At the end of this phase, cells are named expanded PBMCs with IL-2, soluble or functionalized IL-15.

3.2.1. IONP toxicity determination by a proliferation assay

Before we started performing experiments with biofunctionalized IONPs, we first tested if T, T56 and NK cell proliferation was affected by the presence of bare Iron Oxide Nanoparticles micelles (IONPm), without any decoration on the surface. IONPm were similar in composition to those used for the rest of experiments in the thesis and the only difference was in the phospholipids (PLs) that compound the micelle. As it is described in chapter II, micelles are formed in a manner where PLs exhibit their polar head to the surface because of the water transfer of lipids, and this is where the difference lies. For these experiments, three types of micelles were studied, each micelle differs in the polar head radical group of the PL (Figure 3.2): 6 nm IONP covered with polyethylene glycol-carboxylic group (PEG-COOH) and PEG-amino (PEG-NH₂) lipids (NCA.6S), 6 nm IONP covered with PEG-methoxy (PEG-CH₃) and PEG-NH₂ (NMA.6S) and 6 nm IONP covered with PEG-CH₃ and PEG-COOH (NMC.6S). The difference between lipids polar head group could change the charge of the micelle and this is an important property of the NP for using them in biological media, as it is described in Chapter II.

There are several protocols to test newly emerging nanomaterials-induced toxicity to cells and/or organisms⁵⁰³⁻⁵⁰⁷. In our experiments, IONPm toxicity was analyzed by determining the proliferation capacity of NK, T and T56 cells within PBMCs after the incubation in the presence of the mentioned micelles. It was reasoned that if IONPm were toxic for PBMCs, they were not able to adequately proliferate. Then, cells were cultured with a high dose of IL-2 (1000 IU/ml) in the presence of IONPm at different Fe concentrations (5 and 10 µg/ml) for 4 days.

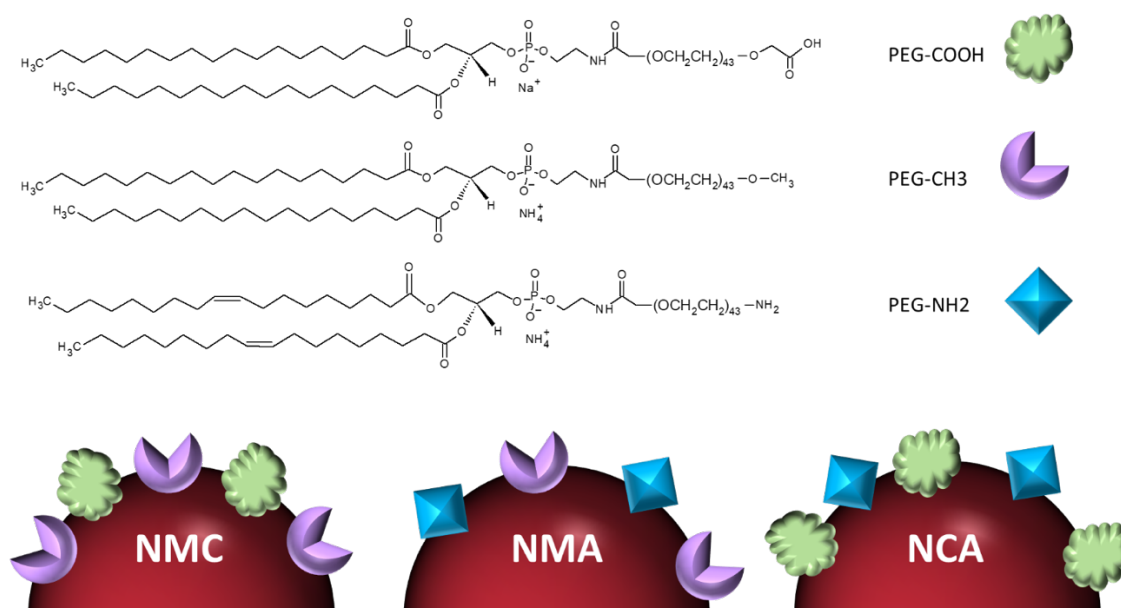


Figure 3.2. Scheme of different lipid composition of micelles. The 3 different PEG-phospholipid structure used for micelles formation are showed and the combination of PEG-PL is illustrated in the bottom of the figure. PEG-COOH: phospholipid with polyethylene glycol chain and carboxylic group in the polar head; PEG-CH3: phospholipid with polyethylene glycol chain and methoxy group in the polar head; PEG-NH2: phospholipid with polyethylene glycol chain and amino group in the polar head; NMC: Iron Oxide NP micelle composed with PEG-CH3 and PEG-COOH; NMA: Iron Oxide NP micelle composed with PEG-CH3 and PEG-NH2; NCA: Iron Oxide NP micelle composed with PEG-COOH and PEG-NH2.

Figure 3.3 shows that IONPm did not induce significant death in lymphocytes cultured with NPs coated with different compositions. The frequencies of the three studied cell subsets (NK, T and T56) were not affected, in general. These results are in agreement with other works in where IONP toxicity was only observed when 200 $\mu\text{g}/\text{ml}$ of Fe content was used during 3 days of lymphocyte cultures⁵⁰⁸. The PEG molecule, incorporated on IONPm nanoformulation, also contributes to the biocompatibility as it is reported^{509,510}. Nevertheless, the NMA.6S micelle, which consists of methoxy and amine group PLs, seems to have a toxic effect only at a concentration of 5 $\mu\text{g}/\text{ml}$ Fe. Although this effect could be explained by the charge of the micelle, it was thought that probably was an artefact or a punctual contamination of the well, considering that the same composition did not have a negative effect when the highest Fe concentration condition was tested (Figure 3.3, 3.4). Furthermore, proliferation of lymphocyte subsets was studied by carboxyfluorescein succinimidyl ester (CFSE) staining.

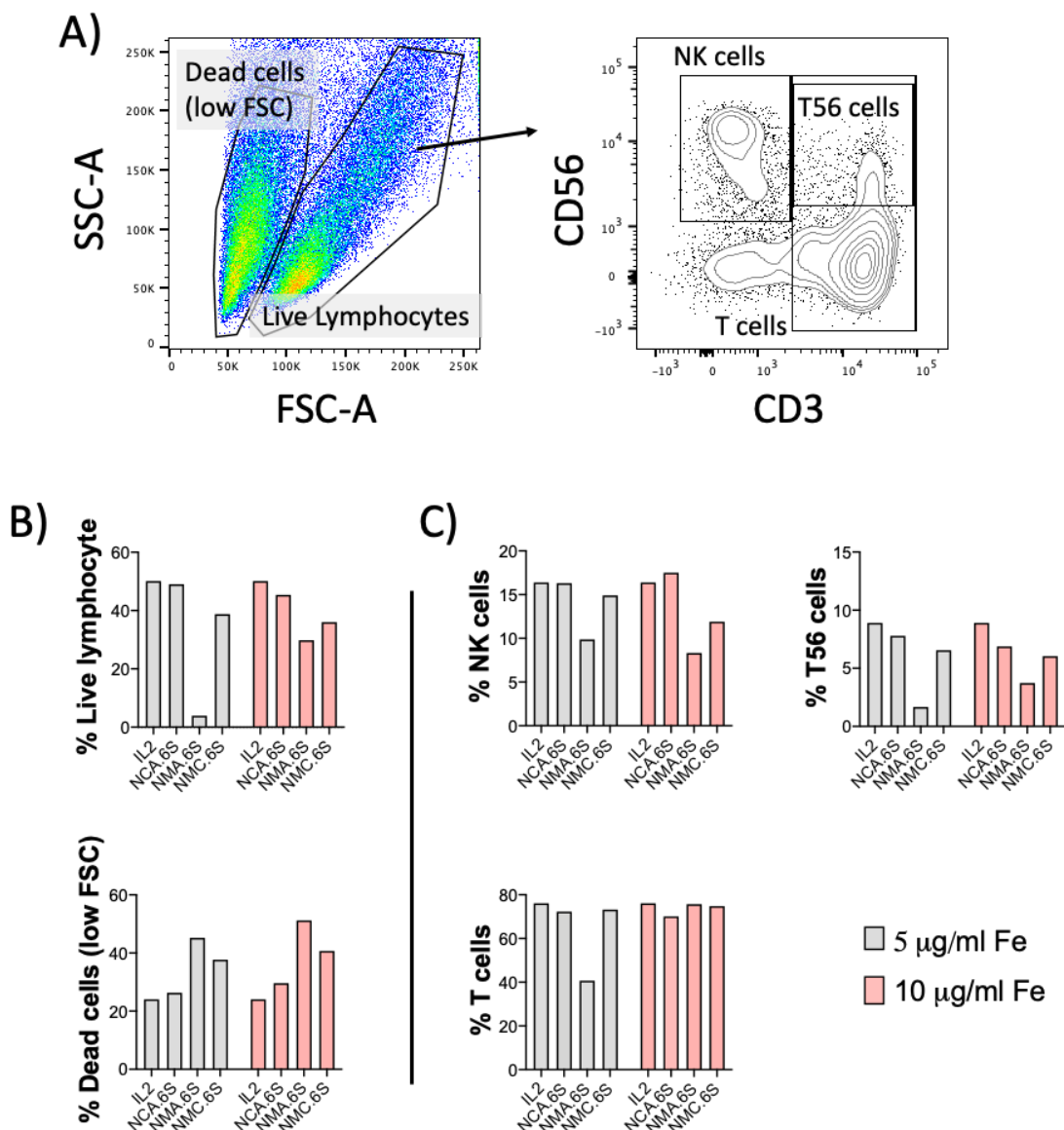


Figure 3.3. IL-2 (1000 IU/ml) cultured PBMCs during 4 days in the presence of IONPm covered with different lipid composition (n=2). (A) Gating strategy: live and dead lymphocytes were identified according to the forward scatter (FSC) and side scatter (SSC) parameters (left) and NK cells (CD56+CD3-), T56 cells (CD56+CD3+) and T cells (CD56+/-CD3+) were analyzed within the live lymphocytes (right). (B and C) Bar graphs representing (B) the percentage of live and dead cells and (C) of NK cells, T56 and T cells within the live lymphocytes.

CFSE stably binds to amine groups present in cytoplasmic molecules, conferring a stable fluorescence intensity to cells which is equally divided between daughter cells after each division, and therefore, cells that are dividing have reduced fluorescence intensity. Proliferation modeling was carried out with FlowJo software (v7.6.5). First, undivided cells were gated and peak 0 (division 0) was set. The number of peaks was adjusted for each sample and it was checked if the model fits the data in every sample. After this, the model was

compared with all histograms to check if the model fits the data in all samples⁵¹¹. The output of this modeling are parameters such as proliferation index (PI), which is the average number of divisions excluding undivided cells.

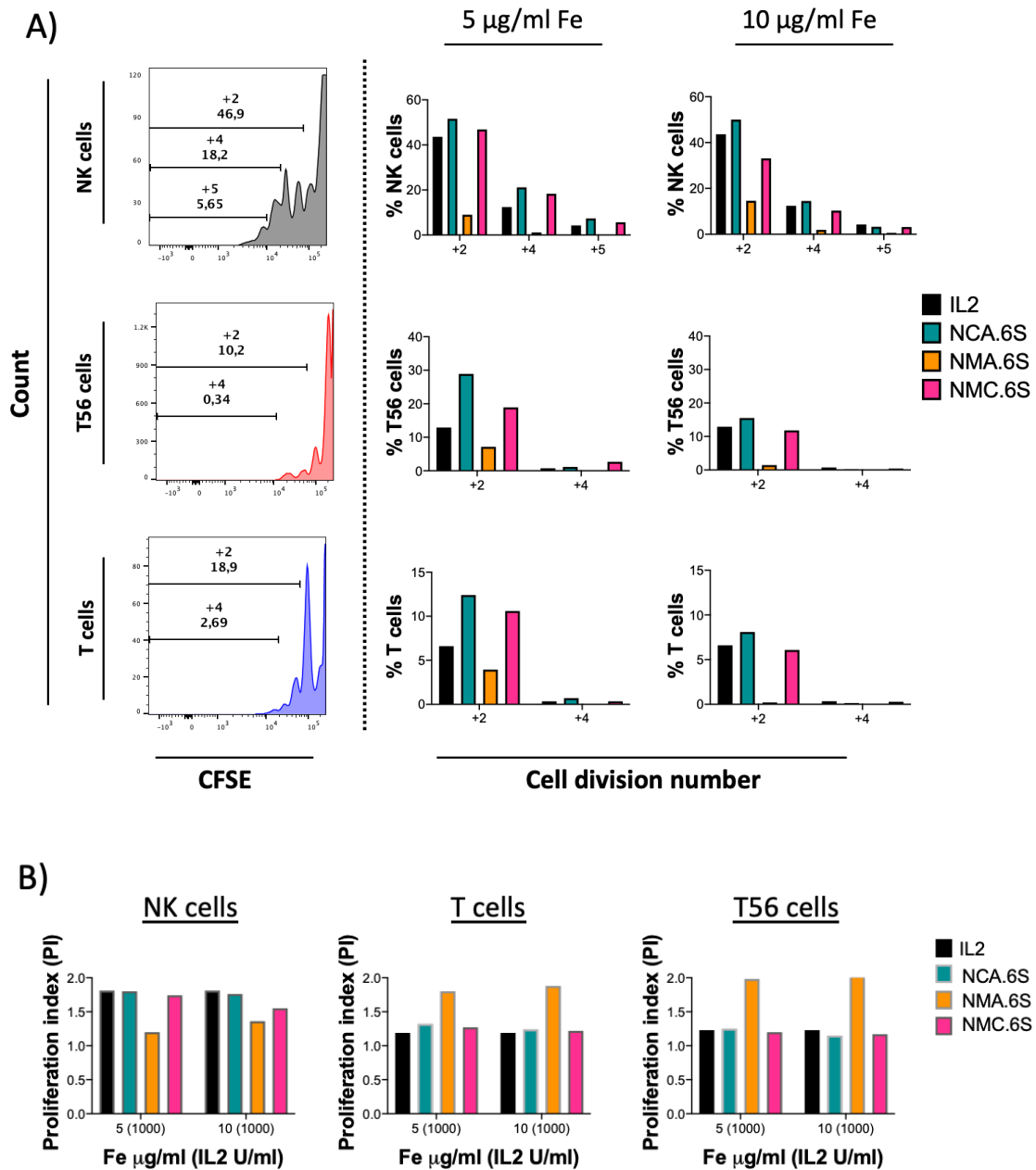


Figure 3.4. PBMCs subsets (NK, T56 and T cells) proliferation after incubation with IONPm for 4 days (n=1). (A) Histograms of IL-2 stimulated cell subsets showing cell divisions determined by CFSE dilution (left) and bar graphs showing percentage of cells undergoing more than 2, 4 and 5 divisions. (B) Bar graphs showing the proliferation index of cell subsets cultured with IL-2 and IONPm. Proliferation modeling was done with FlowJo software (v.7.6.5).

After this modeling no significant differences in the PI were observed, although there were some differences in the percentage of cells reaching the 4th generation (Figure 3.4). Given the higher proliferation index of NCA.6S and NMC.6S on NK cells and the higher percentage of cells reaching the 4th generation under this condition, it was decided that PEG-COOH was a good composition for micelling the IONPs.

3.2.2. Determination of hIL-15HIS activity.

The last purification step was performed by gel filtration chromatography using a Fast Protein Liquid Chromatography (FPLC) equipment and Superdex 75 HiLoad column. This technique allows proteins to be separated by size, thus purifying the desired protein from aggregates or other proteins present in the sample. After gel filtration, the purity of the protein within the different fractions was evaluated by Sodium Dodecyl Sulphate-Poly-Acrylamide Gel Electroforesis polyacrylamide (SDS-PAGE) gels and Maldi-ToF. Figures 3.5. A and B show the absence of other proteins in the sample, concluding that the recombinant IL-15 purity was similar to the IL-15 purchased from Miltenyi Biotec (cIL-15).

The gel filtration chromatogram of IL-15 showed two main peaks (Fig. 3.5.C). When fractions from those peaks were evaluated by polyacrylamide SDS-PAGE gel and Maldi-ToF mass spectrometry, both peaks displayed a molecular weight that corresponds to the one of the hIL-15HIS protein (Fig. 3.5.B). Considering the elution volumes in the gel filtration chromatogram it was thought that the peak elution first (elution volume (Ve) = 46 ml) may correspond to a protein aggregate (peak 1)⁴⁶², and the second peak may correspond to the monomeric hIL-15HIS (Ve = 71 ml) (peak 2). A native gel of those peaks was run using a recombinant Consensus TetratricoPeptide Repeat (CTPR) protein with the His-tag sequence (CTPRHIS) protein as MW control (MW, 17 kDa) (Fig. 3.5. C). There is a band in the peak 2 column which runs more than the control band. This band was expected to be the IL-15 monomer (16.14 kDa) and is only visible in the sample corresponding to the peak 2. The sample of the peak 1 shows a smear at high MW, indicating the presence of aggregated or forming higher order oligomers. Nevertheless, samples from the two peaks were transparent with no visible aggregates.

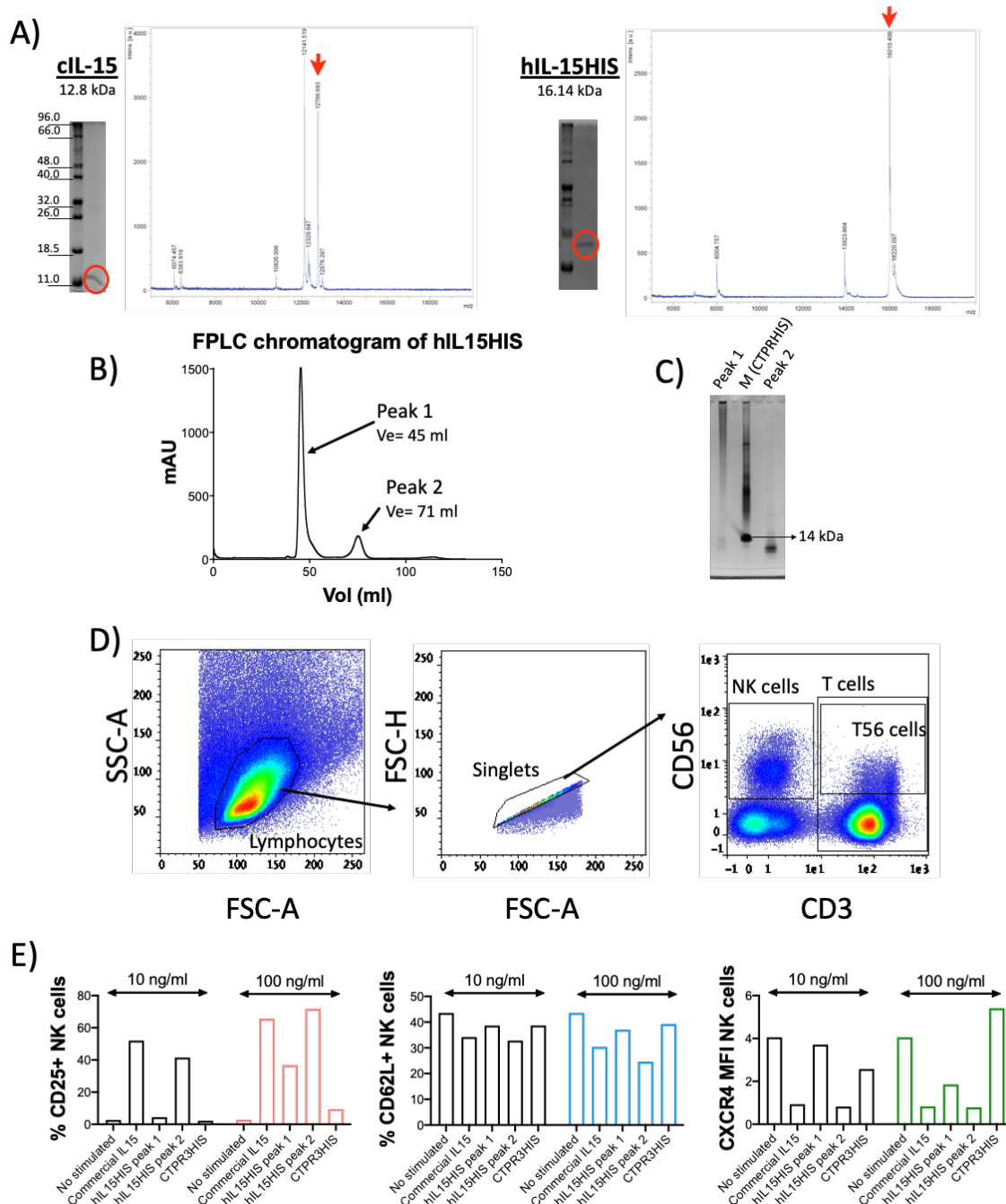


Figure 3.5. Expression, purification, and characterization of his-tagged human IL-15 (hIL-15HIS). Purity and activity of hIL-15HIS is compared with cIL-15 (n=1). (A) Characterization of the purity and mass of hIL-15HIS by polyacrylamide SDS-PAGE gel and MALDI-ToF. cIL-15 is used for comparison. (B) Gel filtration chromatogram of hIL-15HIS using a Superdex 75 HiLoad column. (C) Native polyacrylamide gel (4-12 %) of the gel filtration fractions corresponding to the peaks at 45 ml (peak 1) and 71 ml (peak 2) elution volumes (Ve). CTPRHIS protein (MW = 17 kDa) was used as molecular weight marker. (D) Gating strategy of NK, T and T56 cells starting from the lymphocyte gate is showed in pseudocolor plots. (E) Effect of IL-15 samples on NK cell surface markers expression. Bar graphs representing the MFI of CXCR4 and the frequency of CD25 and CD62L positive NK cells stimulated with different conditions (*cIL-15*: commercial interleukin 15, *hIL-15HIS peak 1*: His-tagged human IL-15 from peak 1 of chromatogram, *hIL-15HIS peak 2*: His-tagged human IL-15 from peak 2 of chromatogram, *CTPRHIS*: His-tagged Consensus Tetratricopeptide Repeat protein).

Next, the effect on NK cell activation was checked after incubation with IL-15 protein. It was determined the frequency of NK cells that expressed CD25 (the α subunit of IL-2 receptor or IL-2R α) and CD62L (homing receptor), and the MFI of CXCR4 (chemokine receptor) on NK cells (Fig. 3.5.E). PBMCs were incubated with 3 different protein samples during 18 h: 1) cIL-15, 2) hIL-15HIS from peak 1, and 3) hIL-15HIS from peak 2 (Fig. 3.5.B). The recombinant CTPR3HIS, produced in the lab following the same protocol, and with no stimulating capacity, was used as a control.

The goal of the experiment was to compare the activity of cIL-15 with the activity of the two peaks obtained for hIL-15HIS. The reported IL-15 action is to increase the expression of CD25 and to decrease the expression of CXCR4 and CD62L according to literature⁴⁸⁹. Figure 3.5 shows that hIL-15HIS peak 1 did not activate NK cells as determined by CD25 expression levels. On the contrary, hIL-15HIS peak 2 was able to induce NK cell activation in a similar manner to cIL-15. Regarding CXCR4 and CD62L expression, hIL-15HIS peak 2 showed an activity comparable to cIL-15, while hIL-15HIS peak 1 did not show a significant effect.

The activity assays indicates that within this aggregated form the IL-15 site recognized by the IL-15 receptor⁴⁶² is not exposed, thus impairing its activity. Therefore, it was concluded that peak 2 was the hIL-15HIS monomeric form and, consequently, it was selected for the following experiments.

3.2.3. NK cell activation and polyfunctionality in response to IONP@IL15his pre-stimulation at day 0

In this section, the activation markers (CD25, CD69), homing receptors (CXCR4, CD62L), functional markers such as degranulation (CD107a) and cytokines production (IFN- γ , TNF- α and MIP-1 β) following cytokine pre-activation (day 0) were studied by flow cytometry (Experimental section, Table ES1). Day 0 is the moment when the pre-activation phase is finished and the expansion phase starts, as it is explained in the beginning of the results section (Figure 3.1) and in the experimental section (Figure ES3). CD25 is the α subunit of the IL-2 receptor, which leads to the proliferation of NK and T cells in response to low doses of

IL-2⁵¹². CD69 is an activation marker that is expressed at the very early stages of NK cell activation. CD69 is able of inducing cytotoxicity and cytokine release, so it was selected to determine the activation state of NK and CD56 expressing T (T56) cells^{513–515}. CXCR4 and CD62L are homing receptors that are required for cell migration to the bone marrow and to secondary lymphoid organs such as lymph nodes, respectively⁵¹⁶.

Regarding to functional markers, CD107a was selected as a degranulation marker of NK and T56 cells. When these cells are activated, for example in response to cytokines or after interacting with a target cell, they start degranulating and secreting cytotoxic components, i.e. perforin and granzymes, and consequently the CD107a receptor is exposed on the outer leaflet of the plasma membrane^{517,518}. IFN- γ , TNF- α and MIP-1 β were selected as pro-inflammatory mediators. IFN- γ is a key cytokine because is responsible for the recruitment of other immune cells to infected/affected areas (i.e. tumor) and also polarizes the adaptive immune response towards a Th1 phenotype^{519,520}. In addition, IFN- γ together with TNF- α liberated from NK cells, promote DC activation and maturation, providing the evidence that NK cells have a role in the regulation of both innate and adaptive immune responses⁵²¹. Regarding MIP-1 β , besides its role as chemoattractant, is also able to trigger macrophage activation⁵²².

For these experiments, 10 ng/ml protein concentration was tested. Cell viability was measured by staining with LIVE/DEAD™ Fixable Near-IR (NIR) Dead Cell Stain Kit and the viable cell percentage is around 80 % in all cases. Results in figure 3.6 shows that NK and T56 cell subpopulation frequencies did not significantly change in response to hIL-15HIS or IONP@hIL-15HIS (hIL-15HIS functionalized IONP micelle) stimulation for 18 hours.

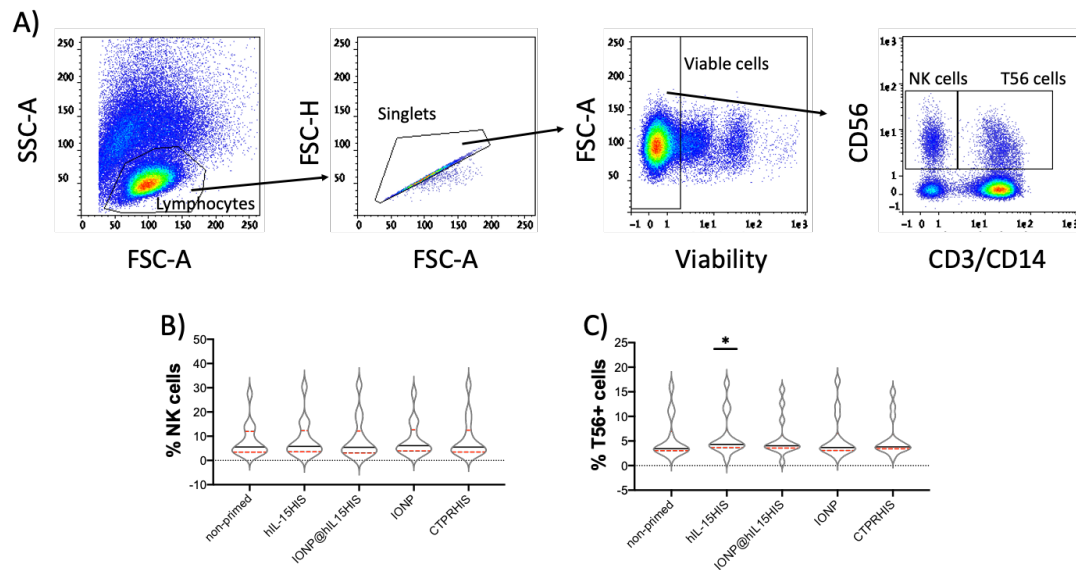


Figure 3.6. Lymphocyte cell subsets frequencies at day 0 (n=14). (A) The gating strategy of hIL-15HIS pre-activated PBMCs as a representative example is shown. (B) The percentage of NK and (C) T56 cells are expressed in violin graphs (black line: median, dashed red line: quartile). PBMCs were pre-activated with 10 ng/ml of IL-15 protein and 0.1 μ M of Fe. Significance of data in (B-C) was determined by comparing each sample with IONP@hIL15HIS condition using Dunn's multiple comparison test after Friedman test for paired samples application. * $p < 0.05$.

Regarding the activation markers expression after the pre-activation phase, IONP@hIL15HIS can activate NK and T56 cells in a very similar manner compared with the soluble form of hIL-15HIS protein (Figure 3.7). Although there were significant differences ($p < 0.0001$) in the CD25 and CD69 expression between non-primed vs. IONP@hIL15HIS pre-activated NK cells, there are no statistical differences between the stimulation with the soluble or immobilized form of the protein (Fig. 3.7 B-C). Similar results were obtained when we analyzed CD25 and CD69 expression in T56 cells (Fig. 3.7 D-E). In addition, given the low expression of both activation markers, CD25 and CD69, in NK and T56 cells following incubation with the controls CTPRHIS and bare IONP, it could be concluded that the material used for NK and T56 cell stimulation is pure enough for the study of the CD69 and CD25 expression rates, and cell activation depends specifically on IL-15 recognition and signaling.

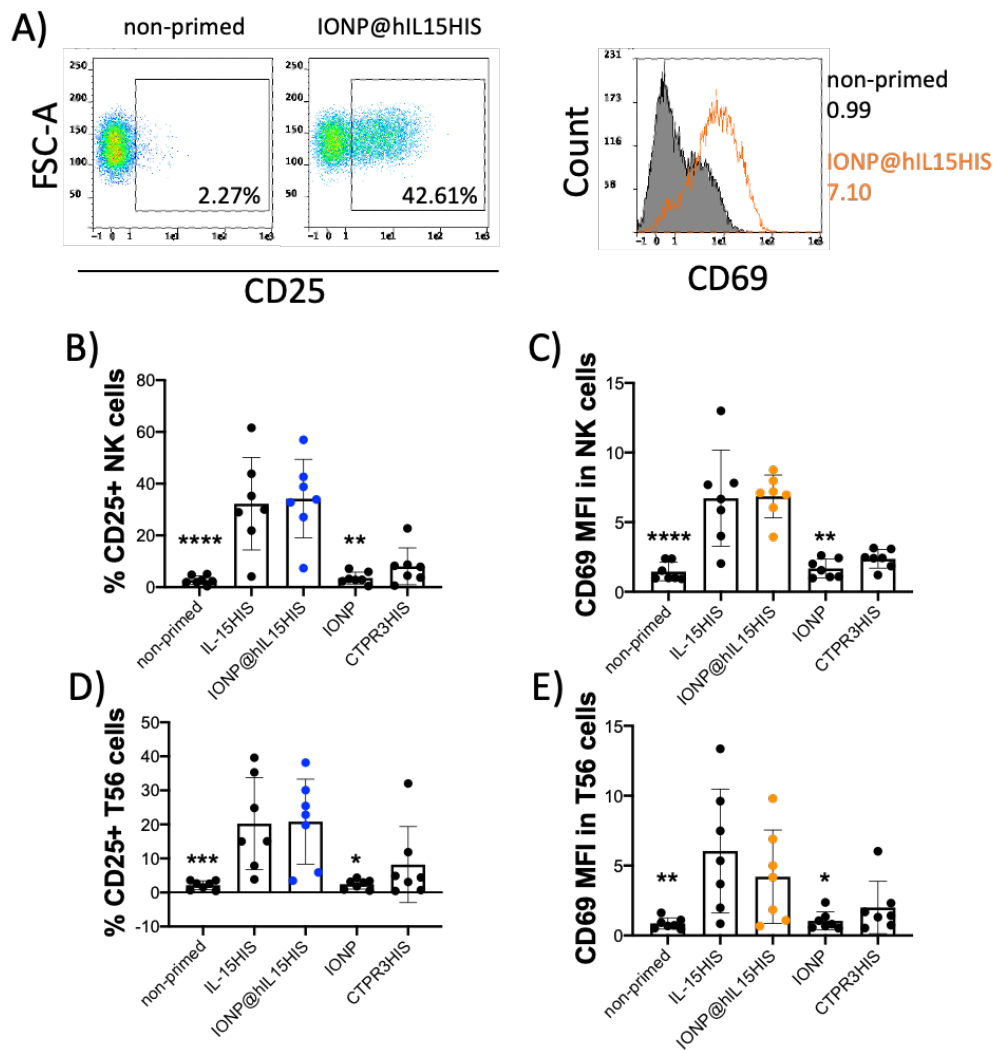


Figure 3.7. CD25 and CD69 activation markers expression in lymphocytes at day 0 after pre-activation phase (n=7). (A) Examples of dotplot for CD25 expression and histogram for CD69 expression on NK cells are shown. (B,D) Blue and black points bar graphs: percentage of CD25 positive NK (top) and T56 (down) cells; and (C,E) orange and black points bar graphs: CD69 Mean Fluorescence Intensity (MFI) on total NK (top) and T56 (down) cells. PBMCs were pre-activated with 10 ng/ml of protein and 0.1 μ M of Fe. Data are shown as mean \pm SD where each point is the data from one donor. Significance of data in (B-E) was determined by comparing each sample with all other conditions using Dunn's multiple comparison test after Friedman test for paired samples application. * $p < 0.05$, ** $p < 0.01$, *** $p < 0.001$, **** $p < 0.0001$.

Regarding the homing receptors expression (Fig. 3.8), the biofunctionalization of IL-15 protein on IONPs gave more interesting results than when the expression of activation markers was analyzed. CD62L expression showed a significant decrease after pre-activation with hIL-15HIS when compared with IONP and CTPR3HIS controls on NK cells. The expression of CD62L hardly changed in the case of T56 cells, and it was maintained around 20% in all conditions. Moreover, CXCR4 expression was significantly decreased when cells were stimulated with hIL-

15HIS in its soluble form compared with controls in both cell types (NK and T56 cells). It is known that the pre-activation of NK cells with cytokine cocktails or with target cells (tumor cells) decreases the expression of CXCR4 and CD62L⁵²³.

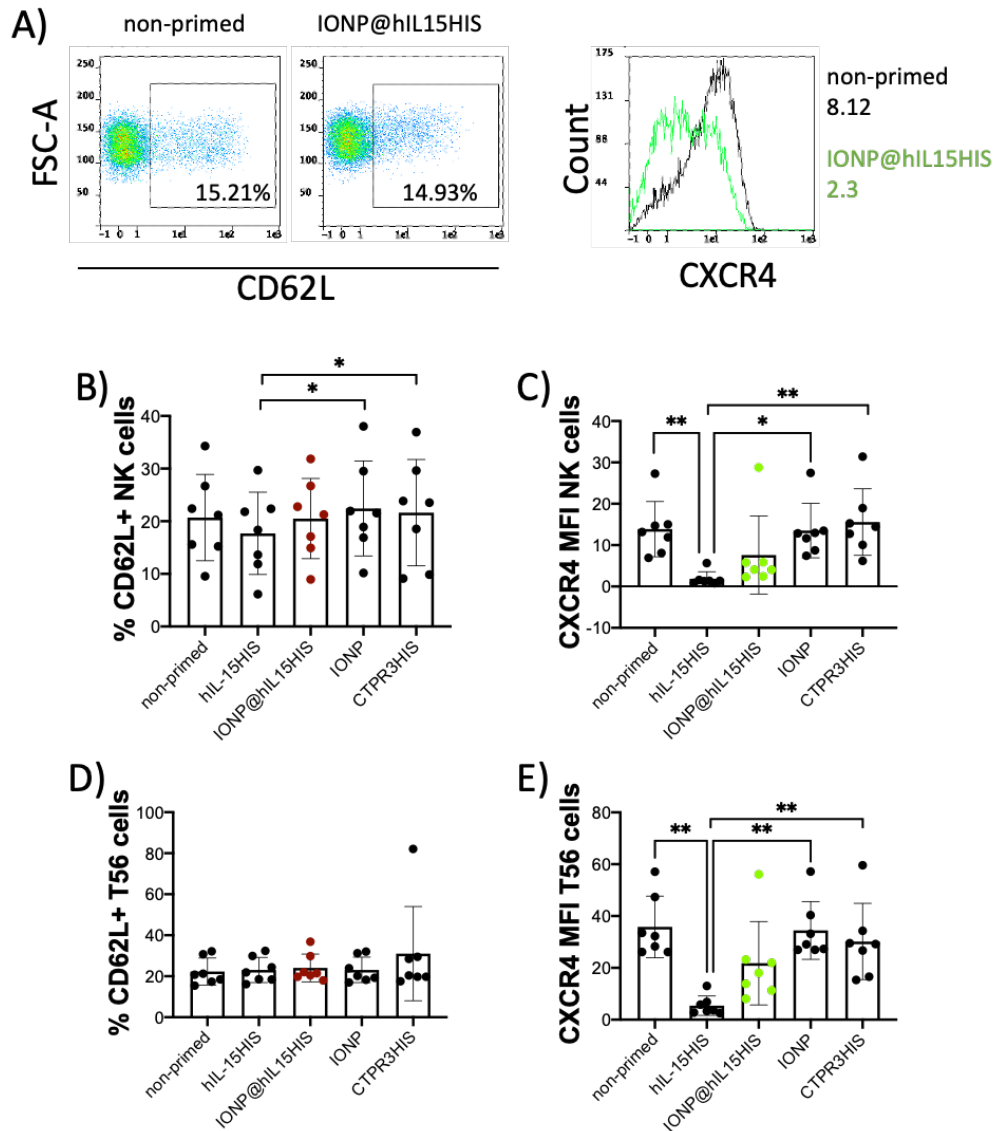


Figure 3.8. CD62L and CXCR4 homing markers expression on lymphocytes at day 0 after pre-activation phase (n=7). (A) Example of dotplot for CD62L expression and histogram for CXCR4 expression on NK cells are shown. (B, D) Maroon and black points graphs: percentage of CD62L positive NK (top) and T56 (down) cells; and (C, E) green and black points graphs: CXCR4 Mean Fluorescence Intensity (MFI) on total NK (top) and T56 (down) cells. PBMCs were pre-activated with 10 ng/ml of protein and 0.1 μ M of Fe. Data are shown as mean \pm SD where each point is the data from one donor. Significance of data in (B-E) was determined by comparing each sample with all other conditions using Dunn's multiple comparison test after Friedman test for paired samples application. * $p < 0.05$, ** $p < 0.01$.

This dramatic decrease in CXCR4 expression was observed following hIL-15HIS stimulation, but not with the immobilized form of the protein (IONP@hIL15HIS), at least not in such dramatic way. This effect could confer cells stimulated with IONP@hIL15HIS a greater capacity for migration to, at least, the bone marrow because activation with this IL-15 formulation partially preserved higher CXCR4 expression⁵²⁴.

Effector functions were determined by degranulation (CD107a) and by the production of cytokines: IFN- γ , TNF- α and MIP-1 β . Data were analyzed and represented in two formats: comparing the expression of each effector function individually and analyzing the polyfunctionality (explained below) with the SPICE free software (v6 or SPICE 6; developed by M. Roederer, National Institutes of Health)⁵²⁵.

First, we observed that degranulation and MIP-1 β production by NK cells was statistically higher after IONP@hIL15HIS stimulation compared with the non-primed condition (Fig. 3.9 A, D). Nevertheless, degranulation and cytokine production in response to hIL-15HIS stimulation did not show any significant differences with cells pre-activated with IONP@hIL15HIS (Fig. 3.9 A-D). In general, it could be said that degranulation (CD107a) and IFN- γ , TNF- α and MIP-1 β production is relatively similar following the stimulation with both soluble and immobilized form of IL-15 protein, given that there are no significant differences when the two stimuli are compared. Additionally, the significant differences between the controls (non-primed, IONP and CTPR3HIS) and IONP@hIL15HIS (Fig. 3.9. A, D) shows that IL-15 significantly triggers the degranulation and the production of MIP1- β .

Cytokine production and degranulation are also analyzed in the context as polyfunctionality using a Boolean analysis, which means that the four effector functions are measured all in all. The highest polyfunctionality consists in cells that are positive for the four tested parameters (CD107a+, TNF- α +, IFN- γ + and MIP-1 β +). Results showed that there are no significant differences in the polyfunctionality of NK cells independently of how they were stimulated. It was calculated with the permutation test in SPICE 6 free software (Fig. 3.9 E).

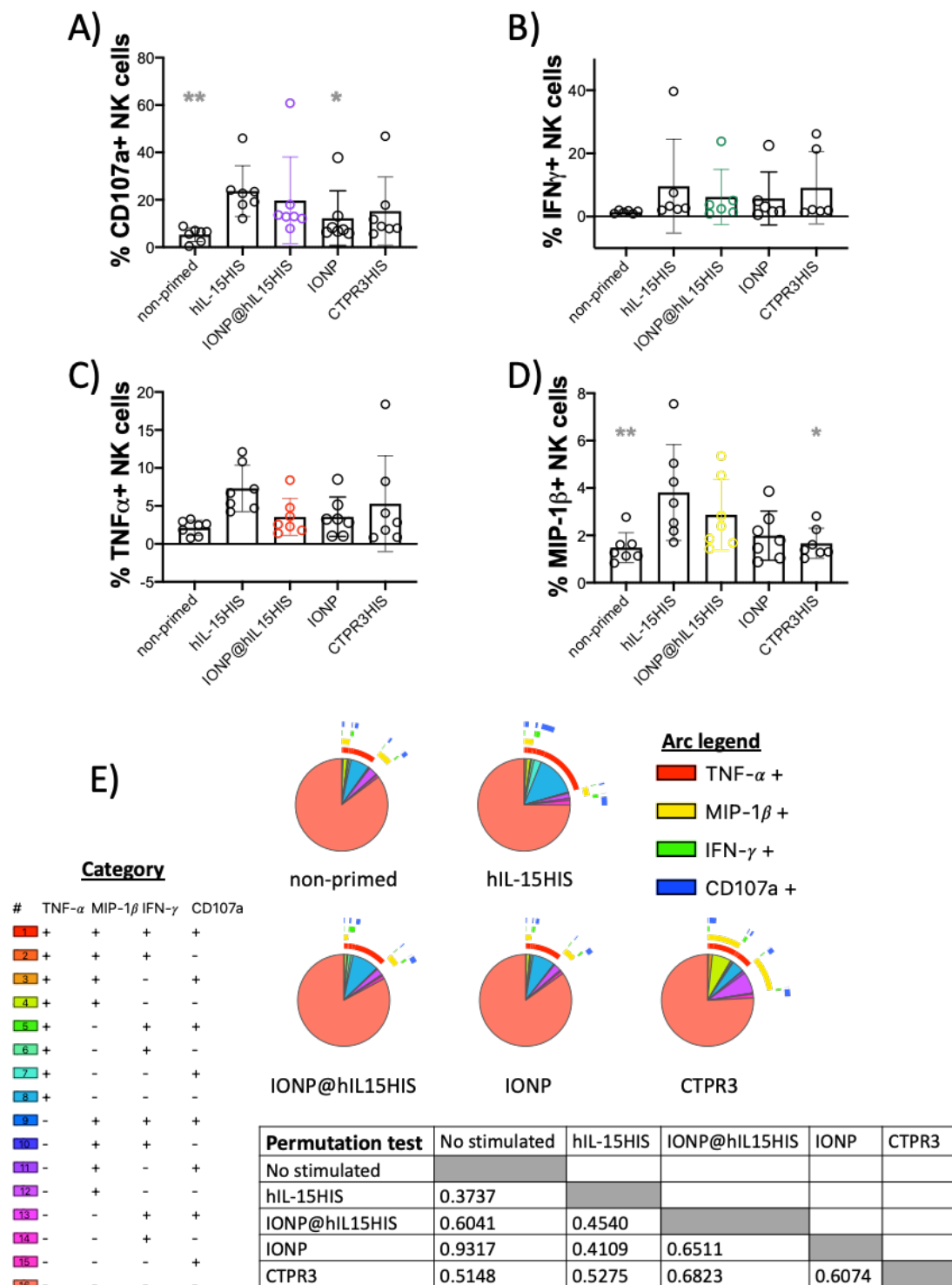


Figure 3.9. Functional profile and polyfunctionality of NK cells at day 0 (n=7). (A-D) CD107a, IFN- γ , TNF- α and MIP-1 β production. Data are shown as mean \pm SD, where each point is the data from one donor (n=7). Significance of data in (A-D) was determined by comparing each sample with IONP@hIL15HIS condition using Dunn's multiple comparison test after Friedman test for paired samples application. *p<0.05, **p<0.01. (E) Pie charts representing the percentages of non-primed, IL-15 formulations (hIL-15HIS, IONP@hIL15HIS) and control (IONP and CTPR3) pre-activated NK cells in the presence of 10 ng/ml of protein and 0.1 μ M of Fe (n=7). Differences between pie charts were established with non-parametric permutation test. The p-values are in the boxes below the pie charts. Arc legend is the positivity for each marker and is represented as bars around pie chart graphs.

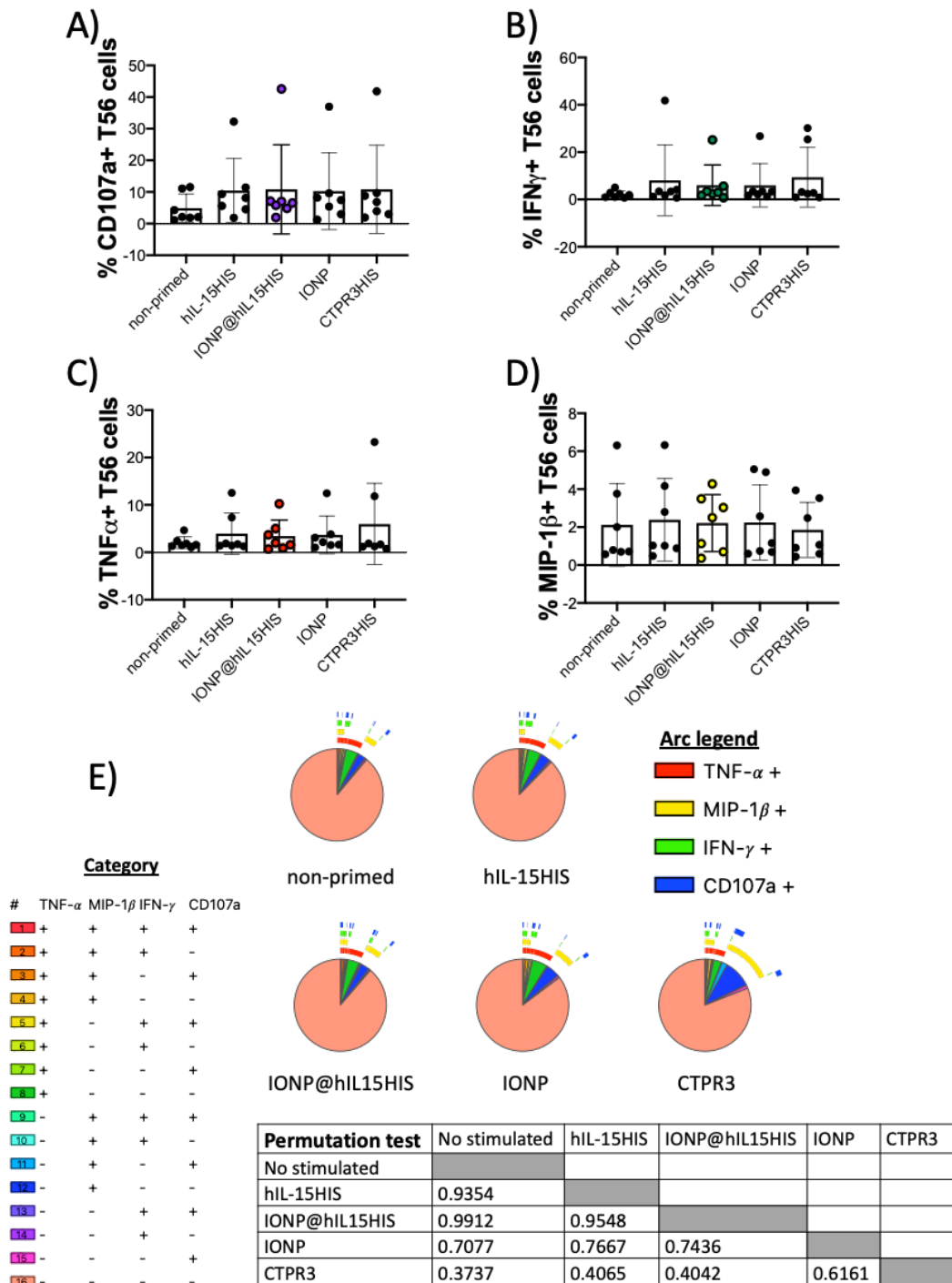


Figure 3.10. Functional profile and polyfunctionality of T56 cells at day 0 (n=7). (A-D) CD107a, IFN- γ , TNF- α and MIP-1 β production. Data are shown as mean \pm SD where each point is the data from one donor. Significance of data in (A-D) was determined by comparing each sample with IONP@hIL15HIS condition using Dunn’s Friedman test for paired samples application but no significant differences were observed between stimuli conditions. (E) Pie charts representing the percentages of non-primed, IL-15 formulations (hIL-15HIS, IONP@hIL15HIS) and control (IONP and CTPR3) pre-activated T56 cells in the presence of 10 ng/ml of protein and 0.1 μ M of Fe (n=7). Differences between pie charts were established with non-parametric permutation test. The p-values are in the boxes below the pie charts. Arc legend is the positivity for each marker and is represented as bars around pie chart graphs.

The degranulation and cytokine production were also evaluated in T56 cells (Fig. 3.10). Comparing with NK cells, T56 cells showed lower levels of degranulation (CD107a) and cytokine production, which could be related with their different way to respond to stimuli. The production of cytokines was similar in all conditions (Fig. 3.10 B-D), and the degranulation slightly, but similarly, increased in all conditions when compared with non-primed cells (Fig. 3.10 A). In general, it could be said that both soluble and IONP immobilized IL-15, at the tested dose, did not significantly induce effector functions on T56 cells. As expected, the polyfunctionality analysis also showed no statistical differences between stimulation with soluble hIL-15HIS or IONP@hIL15HIS, neither between any IL-15 formulation compared with controls (no stimulated, IONP, CTPR3HIS) (Fig. 3.10 E).

3.2.4. NK and T56 cell activation and polyfunctionality in response to IONP@IL15HIS priming at day 4

In the same manner that it was performed for the analysis of stimulated cells at day 0, PBMCs were pre-activated with IL-15 different formulations (soluble or immobilized) and with controls (non-primed/cell media and IONPm). Next, after the pre-activation phase, IL-2 (2 U/ml) was added to expand NK and T56 cells (Fig. 3.1). Activation, functional markers and cytokines were studied by extracellular and intracellular staining and cells were acquired in the flow cytometer (experimental section Table ES1.D). In addition to CD69 and CD25 activation markers, it was also studied CD16 and perforin expression. Through its ability to bind the Fc fragment of IgG, CD16 is responsible for antibody dependent cellular cytotoxicity (ADCC) and perforin is one of the principal components of the cytotoxic granules of NK and CD8+ T cells that, after degranulation, causes pores on target cells, including tumor and infected cells^{526,527}. Also, both cell proliferation, which was determined by CFSE dilution assay, and expression of homing receptors expression (CXCR4, CD62L), which may give information about cell migration potential, were studied. Regarding functional markers, once again we studied CD107a (degranulation) and IFN- γ , TNF- α and MIP-1 β production.

First, lymphocyte subsets frequencies were evaluated. Results in figure 3.11 shows that NK cell frequency was statistically lower in PBMCs pre-activated with IONP@hIL15HIS than in other conditions, while T56 cell frequency was statistically higher following IONP@hIL15HIS stimulation compared with non-primed and IONP but not comparing with hIL15HIS. NK and T56 cells frequency were around 10% and around 5%, respectively, except in response to IONP@hIL15HIS. Cell frequency was lower than 10% for NK cells and higher than 5% for T56 cells following IONP@hIL15HIS stimulation. This difference in the frequency of cells after stimulation with IONP@hIL15HIS may be due to the fact that IONP@hIL15HIS has a tendency to expand T56 cells more than NK cells (Figure 3.15; see below). Alternatively, and for some unknown reason, IONP@hIL15HIS pre-stimulation may render NK cells more susceptible to apoptosis^{528,529}. Undoubtedly, additional studies are required to identify the mechanisms by which IONP@hIL15HIS promotes cell activation and proliferation.

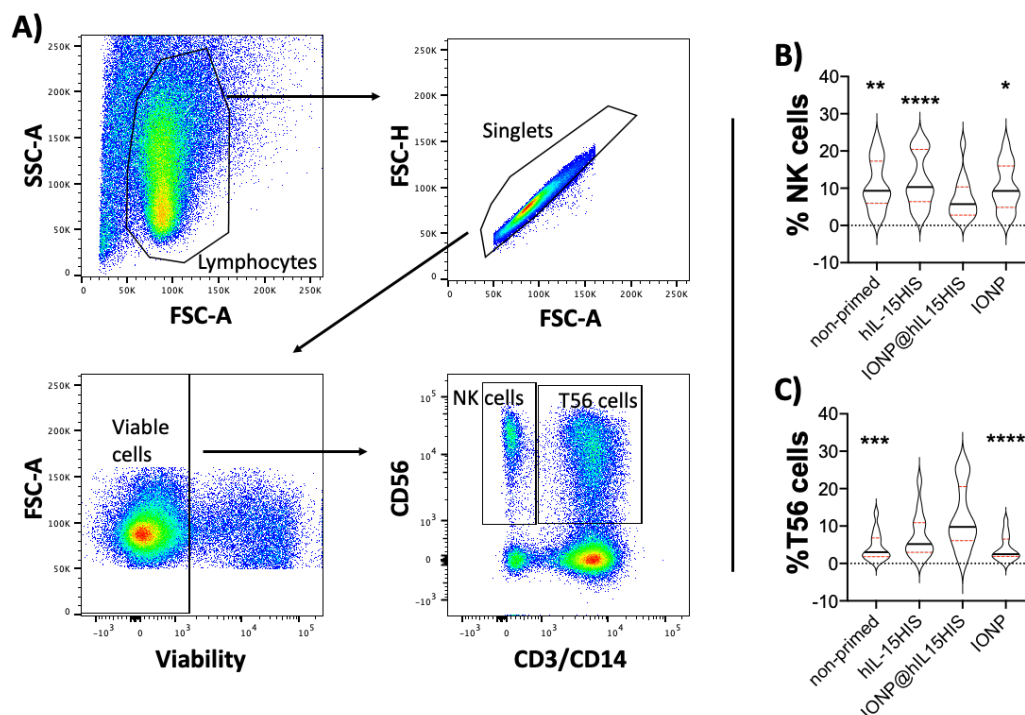


Figure 3.11. Cell subpopulations percentage at day 4 (n= 14). (A) Gating strategy to identify NK cells and T56 cells. (B) Total NK cell and (C) T56 cell percentage after PBMCs priming with IL-15 at 63.10 ng/ml (soluble or immobilized form) and 0.12 μ M Fe. Next, cell expansion was carried out with IL-2 (2 U/mL) for 4 days. Data are represented in violin graphs (black line: median, dashed red line: quartile). Significance of data in (B, C) was determined by comparing each sample with IONP@hIL15HIS condition using Dunn's multiple comparison test after Friedman test for paired samples application. * $p < 0.05$, ** $p < 0.01$, *** $p < 0.001$, **** $p < 0.0001$.

Activation markers expression was higher in response to IONP@hIL15HIS than other priming condition (Fig. 3.12). Nevertheless, the differences were statistically significant only between non-primed vs IONP@hIL15HIS and IONP vs IONP@hIL15HIS for the expression of CD69 in NK cells and for the CD25+ T56 cell frequency (Fig. 3.12 B and E). The difference of CD25+ NK frequency was also significant when compared IONP vs IONP@hIL15HIS (Fig. 3.12 D).

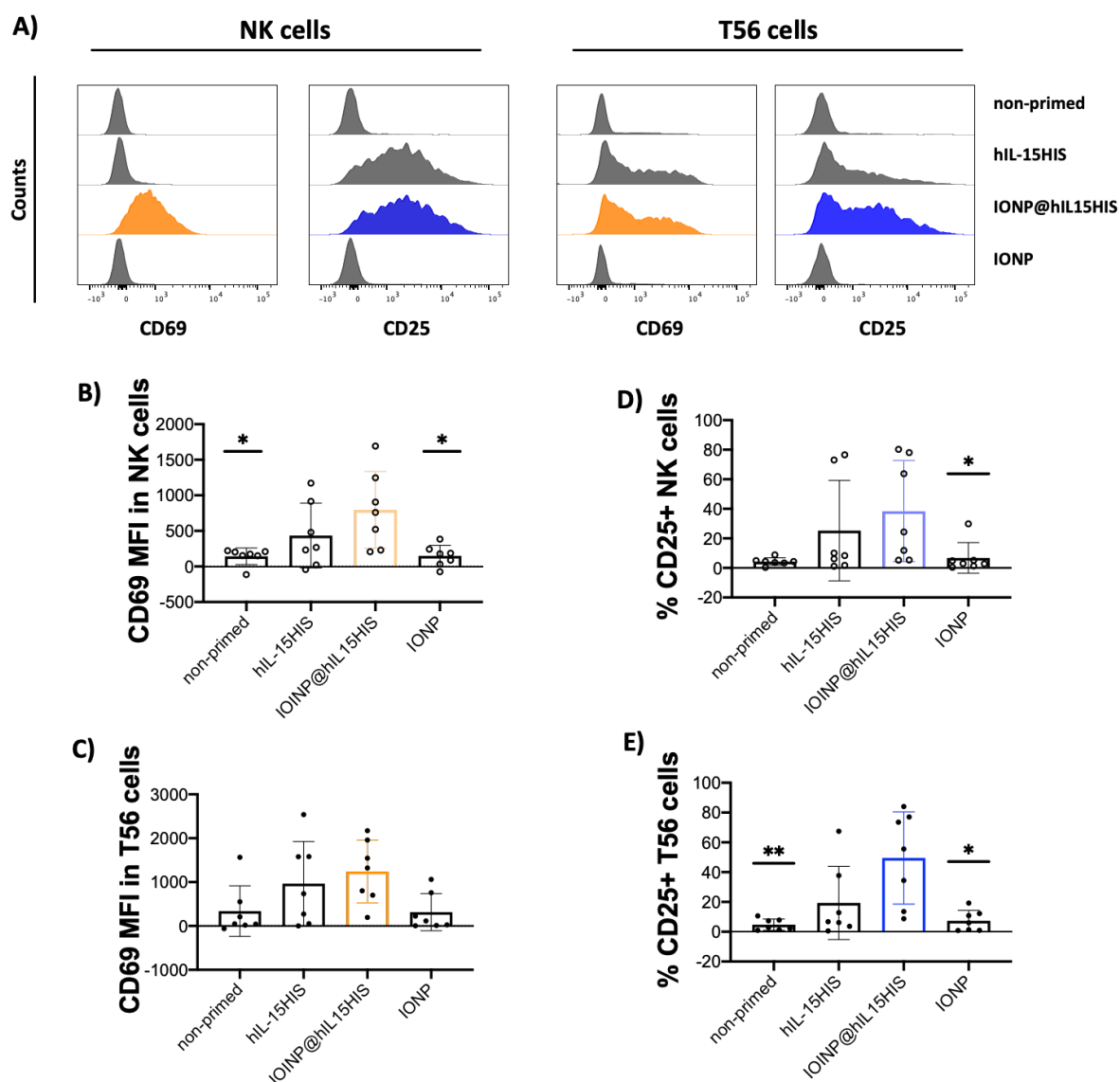


Figure 3.12. CD25 and CD69 activation markers expression at day 4 (n=7). PBMCs priming was done with 63.10 ng/ml of IL-15 and 0.12 μ M Fe. Next, cell expansion was carried out with IL-2 (2 U/mL) for 4 days. (A) Representative histograms are showed. (B-C) Bar graphs representing the MFI of CD69 expression on NK and T56 cells. (D-E) CD25 is expressed as percentage of NK and T56 positive cells. Data are shown as mean \pm SD where each point represents one donor. Significance of data in (B-E) was determined by comparing each sample with IONP@hIL15HIS condition using Dunn's multiple comparison test after Friedman test for paired samples application. * $p < 0.05$, ** $p < 0.01$.

The higher activating receptors expression could be a consequence of the higher affinity of IONP@hIL15HIS for the IL-15 receptor composed by β and γ_c chains (IL2/IL-15R $\beta\gamma_c$), when compared with the affinity of hIL-15HIS for the same receptor. The higher affinity of other formulations of IL-15 such as RLI (IL-15R α sushi domain linked to IL-15), resulted in an enhanced functionality⁵³⁰. The functionalization of the hIL-15HIS on the IONP, could be triggering the same effect, resulting in a higher activation markers expression. Nevertheless, experiments must be performed to determine if IONP@hIL15HIS exhibits a higher affinity for IL2/IL-15R $\beta\gamma_c$ than hIL-15HIS.

On NK cells, CD16 expression at day 4, measured as MFI and frequency of CD16+ cells, was very similar in all tested conditions (Fig. 3.13 B-C), except for a significant difference in the frequency of CD16+ NK cells between the non-primed and IONP@hIL15HIS conditions (Fig. 3.13 B). As expected, CD16 expression was lower on T56 cells, and all studied conditions revealed similar levels of CD16 expression (Fig. 3.13 D-E). On the contrary, perforin expression at day 4 was higher in cells that were primed with IONP@hIL15HIS, although significant differences were only observed in T56 cells when compared with the non-primed condition (Fig. 3.13 F-G). In any case, there was not statistically significant differences between cells that were pre-activated with hIL-15HIS and IONP@hIL15HIS.

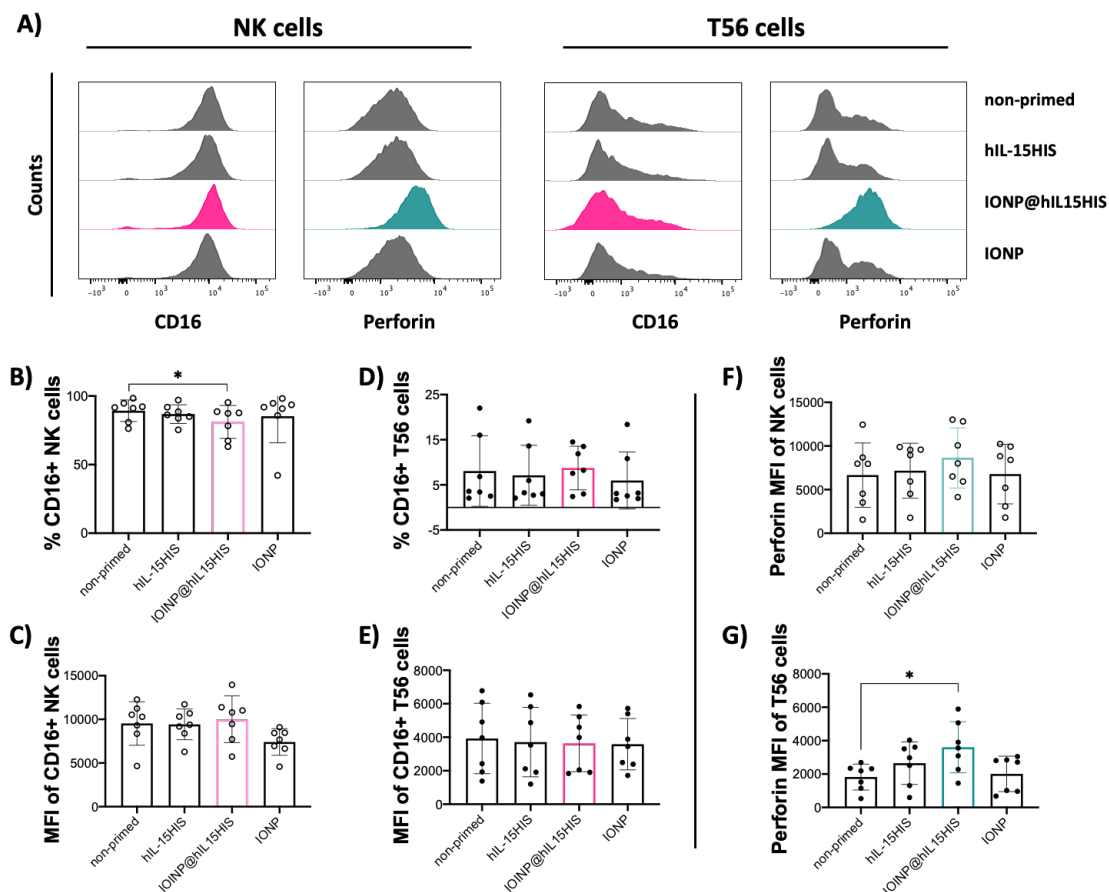


Figure 3.13. CD16 expression and perforin at day 4 (n=7). PBMCs priming was performed with 63.10 ng/ml of IL-15 and 0.12 μ M Fe. Next, cell expansion was carried out with IL-2 (2 U/mL) for 4 days. (A) Representative examples of histograms showing CD16 and perforin expression on NK and T56 cells. (B-E) CD16 expression is represented as mean fluorescence intensity (MFI) and as percentage of positive cells. (F, G) NK and T56 cells perforin expression (MFI). Bar graphs represent the mean \pm SD. Each point represents one donor. Significance of data in (B-G) was determined by comparing each sample with all other conditions using Dunn's multiple comparison test after Friedman test for paired samples application. * $p < 0.05$.

As above mentioned, it is known that homing receptors expression decreases after stimulation with cytokines^{489,531}. Results in figure 3.14 B-E showed that CXCR4 expression tended to decrease at day 4 on both NK and T56 cells that were pre-activated with hIL-15HIS. Very interestingly, NK cells primed with IONP@hIL15HIS did not exhibit a decrease in CXCR4 expression when compared with controls (Fig. 3.14 B, C). On the other hand, CD62L expression did not change in all tested conditions (Fig. 3.14 F,G).

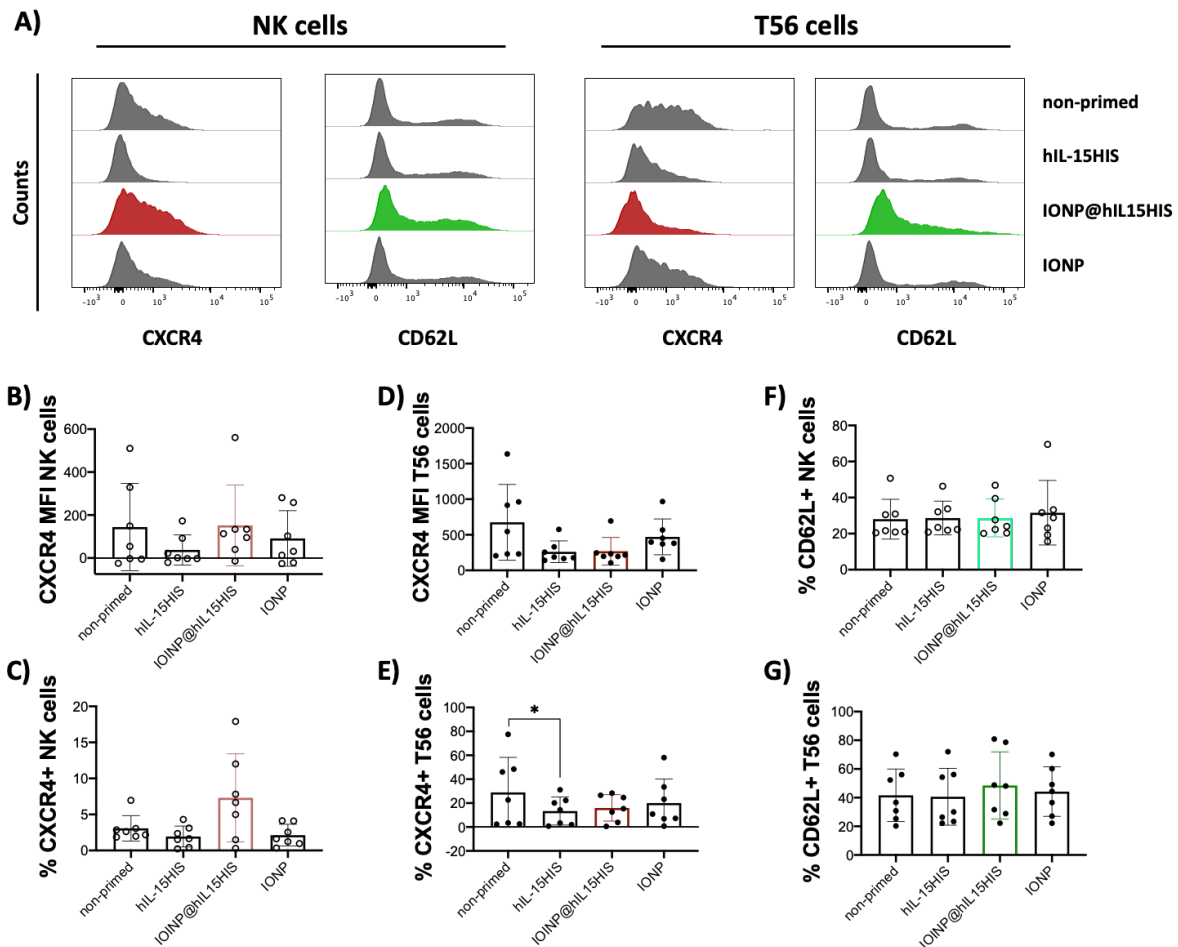


Figure 3.14. CXCR4 and CD62L homing receptors expression at day 4 (n=7). PBMCs priming was done with 63.10 ng/ml of IL-15 and 0.12 μ M Fe. Next, cell expansion was carried out with IL-2 (2 U/mL) for 4 days. (A) Representative examples of histograms showing CD62L and CXCR4 expression on NK and T56 cells. (B-E) CXCR4 expression is represented as mean fluorescence intensity (MFI) and as percentage of positive NK cells (B,C) and T56 cells (D,E). (F-G) Frequencies of CD62L+ NK cells (F) and T56 cells (G). Data are shown as mean \pm SD where each point represents one donor. Significance of data in (B-G) was determined by comparing each sample with all other conditions using Dunn's multiple comparison test after Friedman test for paired samples application. * $p < 0.05$.

It was also analyzed cell proliferation at day 4⁵¹¹, as it was done before at day 0 using CFSE staining and modeling in FlowJo software (v 10.7.2) (Fig. 3.15 A). The percentage of cells that underwent 1 or more divisions was analyzed (Fig. 3.15 B-E). In general, it was observed that cells pre-activated with both formulations of IL-15 divided more than control cells. While there were no statistical differences when NK cells were taken into account (Fig. 3.15 B-C), there were significant differences when T56 cells were analyzed (Fig. 3.15. D-E). Although the cell percentage in the 1st and 2nd division was higher following IONP@hIL15HIS stimulation (Fig. 3.15 B-E), the PI did not show significant differences (Fig. 3.15 F, G).

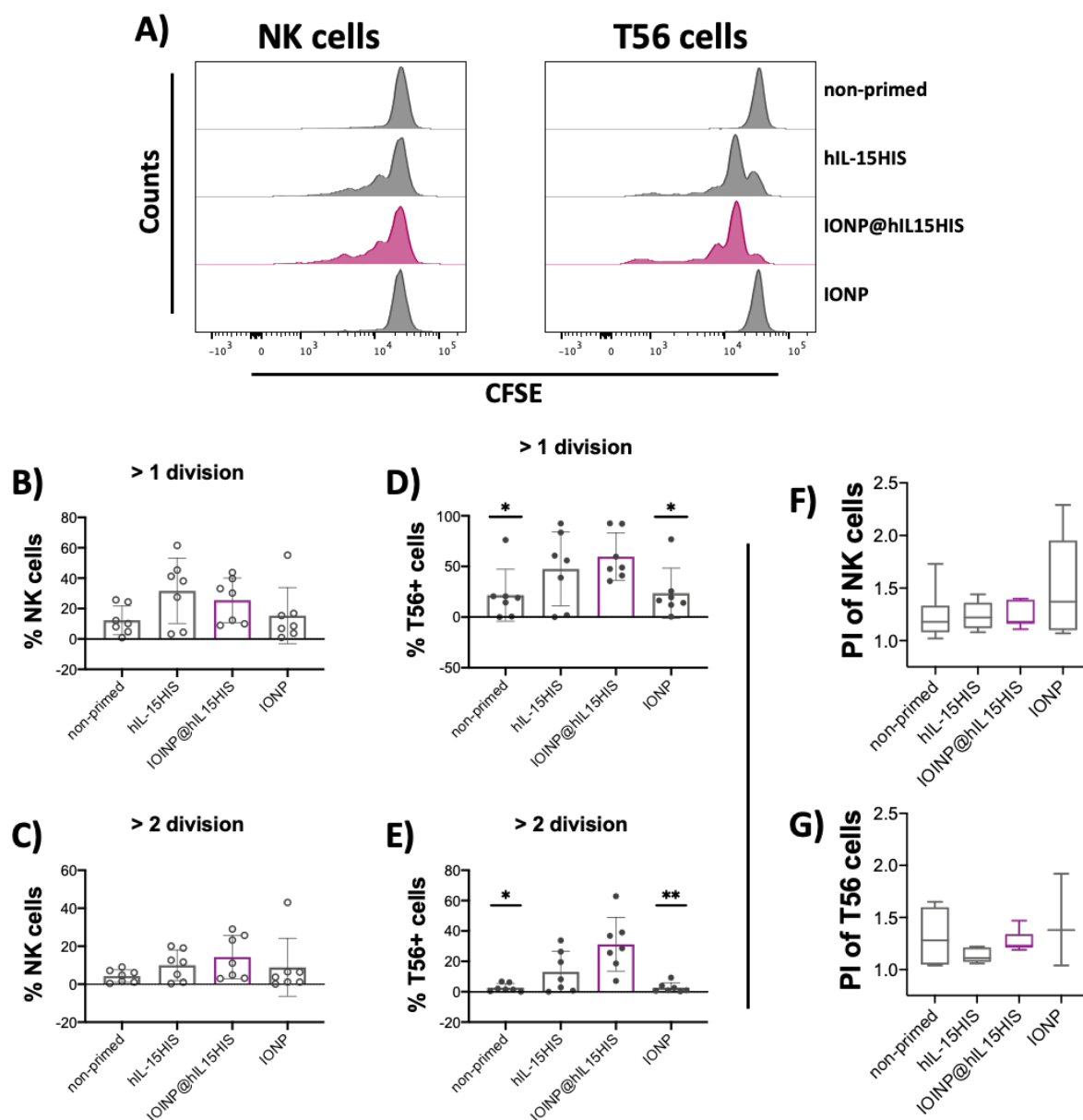


Figure 3.15. NK and T56 cells proliferation at day 4 (n=7). PBMCs priming was done with 63.10 ng/ml of IL-15 and 0.34 μ M Fe. Next, cell expansion was carried out with IL-2 (2 U/mL) for 4 days. (A) CFSE histograms are shown to compare peaks of proliferation between different conditions. (B-E) Cell percentage from 1st and 2nd division is showed for NK (B-C) and T56 (D-E) cells. Data are shown as mean \pm SD where each point is the data from one donor. (F-G) Proliferation index (PI) is represented in box and whiskers graphs (line: median and error bars: maximum to minimum) calculated by modeling in FlowJo (10.7.2)⁵¹¹. Significance of data in (B-G) was determined by comparing each sample with all other conditions using Dunn's multiple comparison test after Friedman test for paired samples application. *p<0.05, **p<0.01.

Effector functions of NK and T56 cells at day 4 were also analyzed. Regarding NK cells, it could be said that degranulation (CD107a) and TNF- α and MIP-1 β production were slightly higher in cells pre-activated with IONP@hIL15HIS compared with cells primed with hIL-15HIS and controls, but the differences between hIL-15HIS and IONP@hIL15HIS were statistically not-

significant. The only significant difference is in the percentage of CD107a+ NK cells when non-primed and IONP conditions are compared with IONP@hIL15HIS (Fig. 3.16. A, C). In contrast, the frequency of IFN- γ + NK cells was significantly higher when cells were primed with hIL-15HIS, resulting in a statistically significant difference when compared with IONP@hIL15HIS (Fig. 3.16. B).

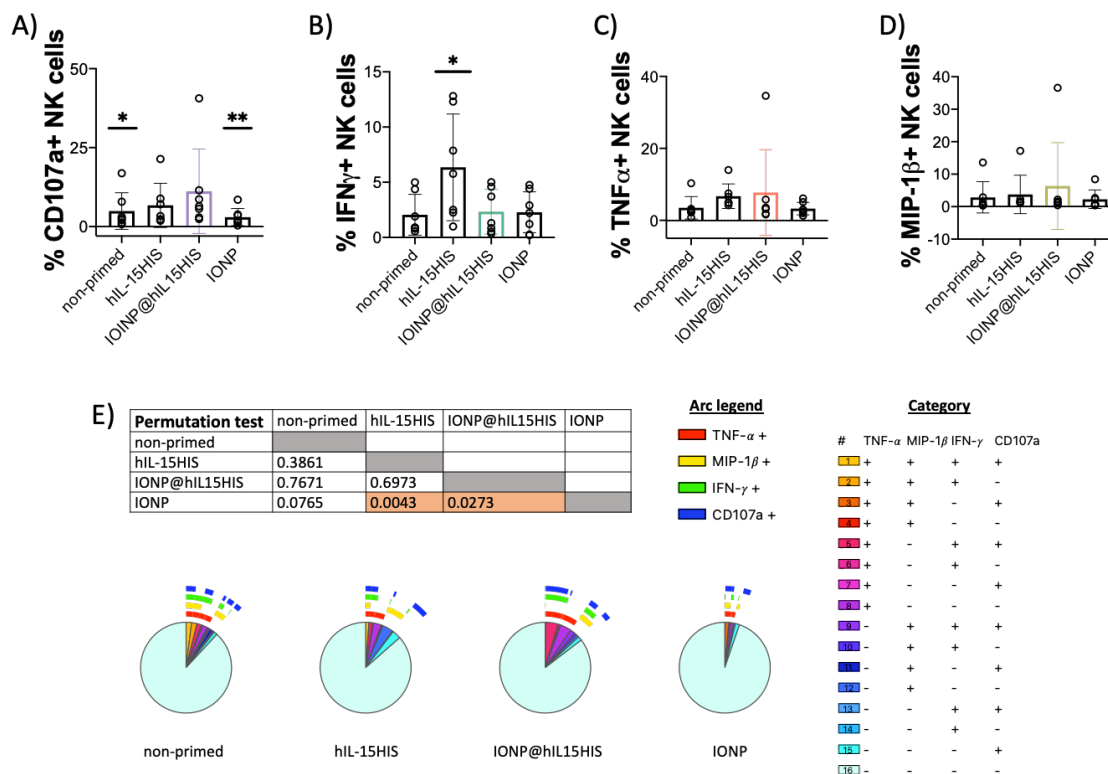


Figure 3.16. NK functional profile after expansion phase at day 4. PBMCs priming was with 63.10 ng/ml of IL-15 and 0.34 μ M Fe. Next, cell expansion was carried out with IL-2 (2 U/mL) for 4 days. (A-D) CD107a, IFN- γ , TNF- α and MIP-1 β production by NK cells at day 4. Data are shown as mean \pm SD, where each point represents one donor (n=7). Significance of data in (A-D) was determined by comparing each sample with IONP@hIL15HIS condition using Dunn's multiple comparison test after Friedman test for paired samples application. *p<0.05, **p<0.01. (E) Pie charts representing the percentages of NK cells at day 4 (n=7). Differences between pie charts were established with non-parametric permutation test. The p-values are in the box on top of the pie charts. Arc legend is the positivity for each marker and is represented as bars around pie chart graphs. Significant differences are in the orange cells.

Regarding T56 cells no significant differences in effector functions at day 4 were observed with cells pre-activated with both IL-15 formulations and control cells (Fig. 3.17 A-B). Small non-significant differences in degranulation and cytokine production should not be translated into low NK and T56 cells cytotoxicity potential against target cells. For example, it has been

shown that CD107a- NK cells are able to eliminate tumor cells with the same efficiency as those CD107a+ NK cells⁵³². In addition, this similar cytotoxic effect occurs not only in the first contact with the target cell but also in a second contact, meaning that the NK cells exhibit a long-term viability and killing potential⁵³².

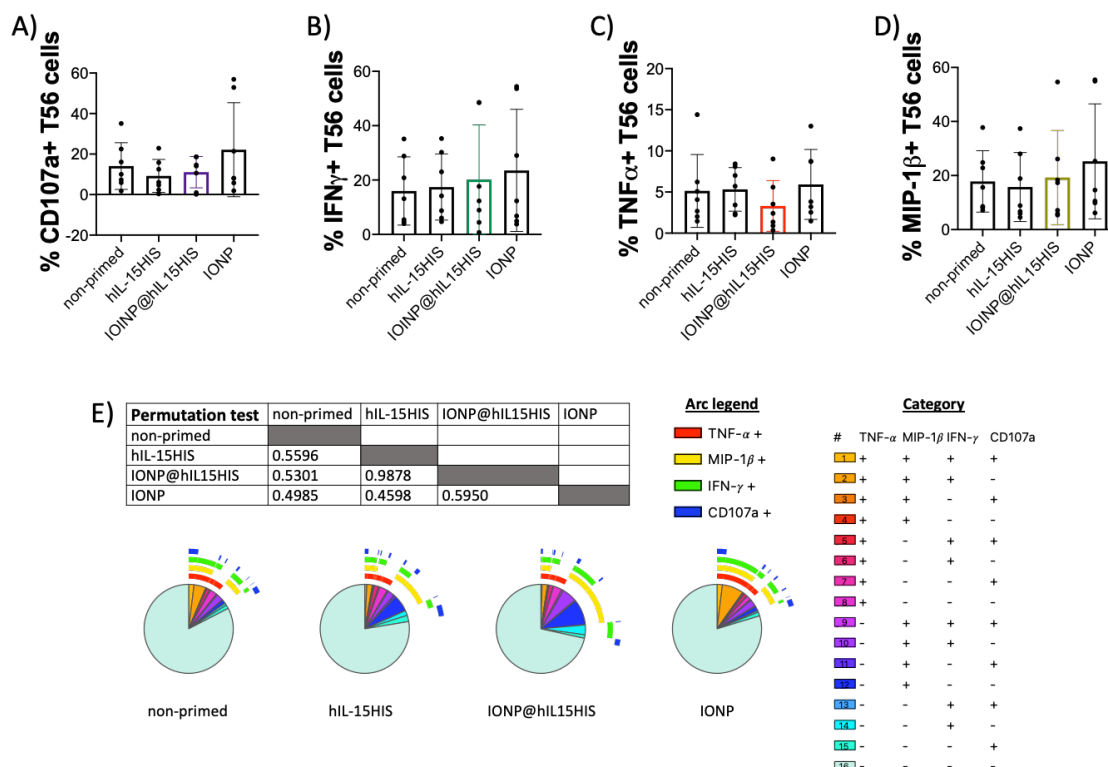


Figure 3.17. T56 functional profile after expansion phase at day 4 (n=7). PBMCs priming was with 63.10 ng/ml of IL-15 and 0.34 μ M Fe. Next, cell expansion was carried out with IL-2 (2 U/mL) for 4 days. (A-D) CD107a, IFN- γ , TNF- α and MIP-1 β production by T56 cells at day 4. Data are shown as mean \pm SD, where each point represents one donor (n=7). Significance of data in (A-D) was determined by comparing each sample with IONP@hIL15HIS condition using Dunn's multiple comparison test after Friedman test for paired samples application. (E) Pie charts representing the percentages of T56 cells at day 4 (n=7). Differences between pie charts were established with non-parametric permutation test. The p-values are in the box on top of the pie charts. Arc legend is the positivity for each marker and is represented as bars around pie chart graphs.

Finally, polyfunctionality analysis was performed with SPICE 6 software. The permutation test did not show significant differences when T56 cells were analyzed (Fig. 3.17. E). On the contrary, hIL-15HIS or IONP@hIL15HIS pre-activated NK cells were significantly more polyfunctional than NK cells primed only with IONP (Fig. 3.16. E). In general, cells did not show a good polyfunctionality profile at day 4. This could be because they were not re-stimulated at day 4 with a tumor cell or a combination of cytokines. It is well known that after the pre-

activation phase, the stimulation with a second stimuli with a target (or the same stimulus of the first contact) cells respond faster and stronger, two features of immunological memory^{489,533–536}.

3.2.5. Phenotype of NK and T56 cells primed with a combination of IL-12, IL-15 and IL-15: role of IONP@hIL15HIS

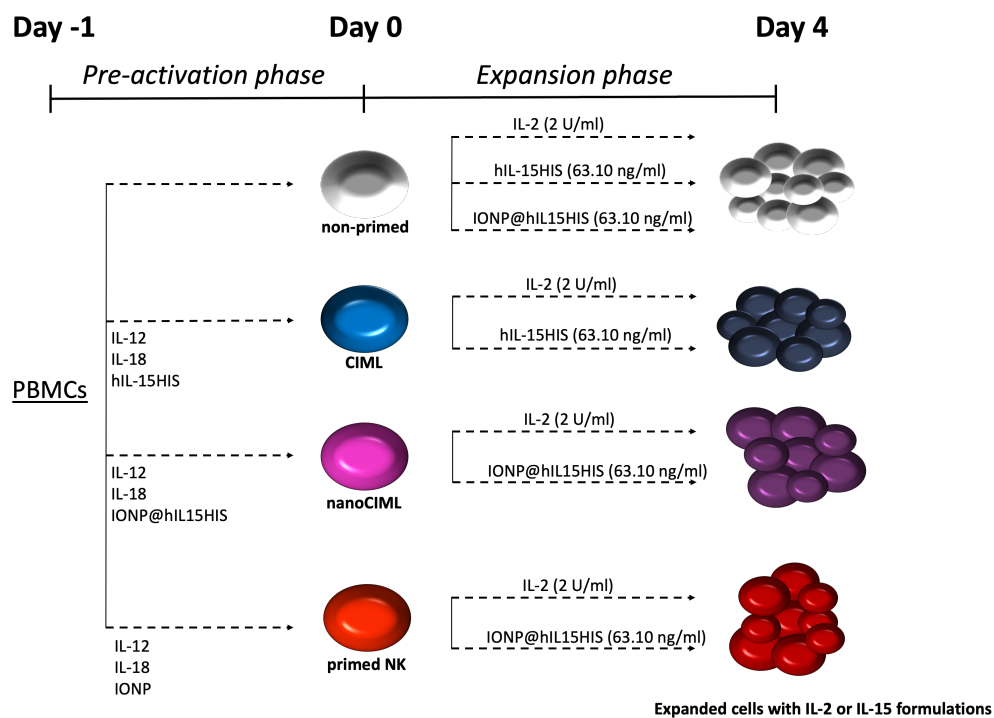


Figure 3.18. Schematic representation of pre-activation and expansion phases of CIML-NK cells. PBMCs were cultured in the presence of soluble (hIL-15HIS) and functionalized (IONP@hIL15HIS) form of IL-15 protein along with IL-12 and IL-18 for 16-18 hours. After stimulation with IL-12, IL-15 and IL-18 combination cells are called cytokine-induced memory-like (CIML) cells. After this pre-activation phase, PBMCs are expanded with IL-2 or with IL-15 formulations (hIL-15HIS or IONP@hIL15HIS).

Figure 3.18 shows the timing protocol of PBMCs priming with a cytokine combination (IL-12, IL-18, and IL-15). The priming with these cytokines generates what is called cytokine-induced memory-like (CIML) NK cells^{488,489,537,538}. Traditionally, immune memory was a feature ascribed to the adaptive immune system, but currently, it is well known that cells from the innate immune system also exhibit memory-like responses, that is enhanced effector functions weeks after pre-activation with certain stimuli, as for example cytokines^{155,539}.

The aim of these sets of experiments was to explore if the immobilization of IL-15 on IONP has some specific effects when cells are pre-activated with IL-12, IL-15 and IL-18. Results at day 0, following the priming with the cytokine combination, revealed that the expression of CD25 and homing receptors following IL-12/IL-18/IONP@hIL15HIS stimulation were higher when compared with IL-12/IL-18/hIL-15HIS stimulation in all cases, except for CD25 expression on NK cells, which it is higher in response to this last stimulation condition (Fig. 3.19).

Regarding the expression of homing receptors, the tendency is similar to the experiments performed with only IL-15 pre-stimulation. It is known that following cytokines stimulation, the expression of CXCR4 and CD62L on NK cells decreases⁴⁸⁹. In this thesis it has been shown that stimulation with IL-15 immobilized in the IONP micelle (IONP@hIL15HIS) leads to a smaller decrease in the expression of CXCR4 and CD62L compared with the more pronounced decrease following the stimulation with the soluble form of IL-15 protein (hIL-15HIS). Interestingly, this effect was also observed in response to stimulation with the cytokine combination in which IONP@hIL15HIS is present (figure 3.19). Because of the low number of experiments (n=2), it was not possible to perform a statistical analysis. Therefore, more experiments are required to conclude if the observed differences are significant or not.

On the other hand, degranulation (CD107a) and the production of IFN- γ , TNF- α and MIP-1 β production tended to be lower when cells were pre-activated with IL-12/IL-18/IONP@hIL15HIS than with IL-12/IL-18/hIL-15HIS (Fig. 3.20), although the differences were not statistically significant neither in NK nor in T56 cells. The only significant differences were observed when non-primed cells were compared with IL-12/IL-18/IONP@hIL15HIS cells for CD107a, IFN- γ and MIP-1 β in NK cells and for IFN- γ in T56 cells. Therefore, it can be concluded that the presence of IONP@hIL15HIS in the cytokine combination did not contribute to a higher activation (CD25) and better functional profile (CD25, CD107a, IFN- γ , TNF- α and MIP-1 β) of NK and T56 cells at day 0.

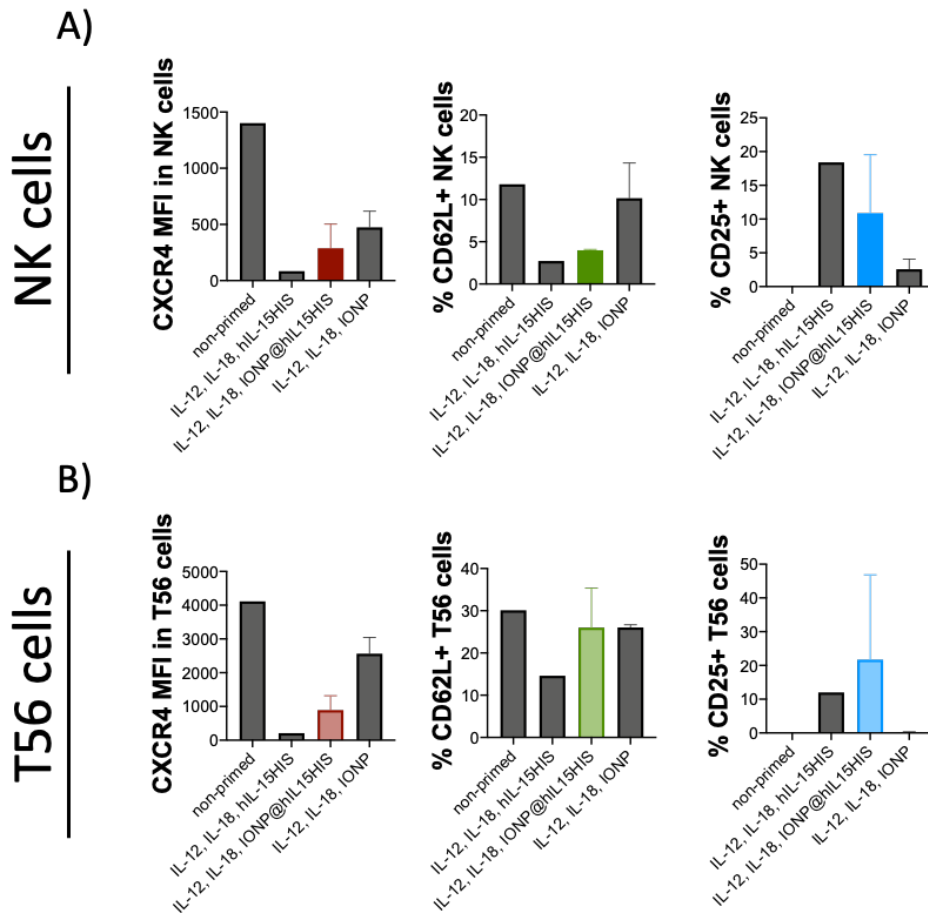
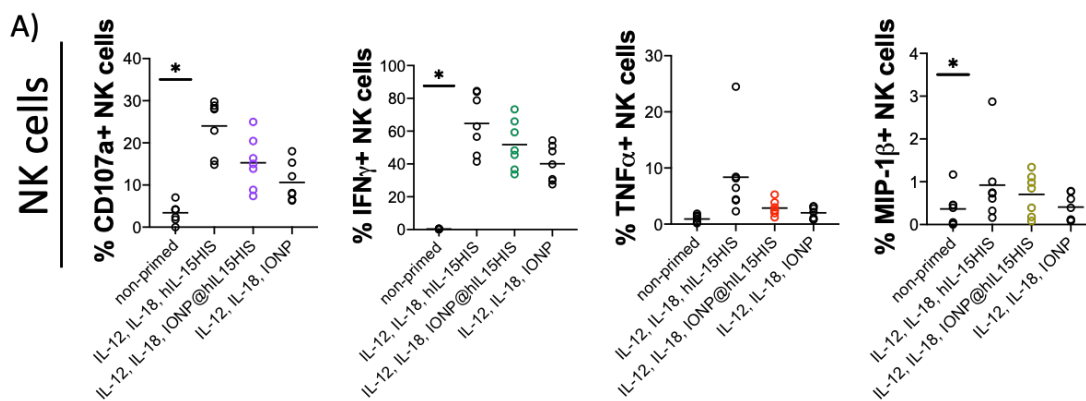


Figure 3.19. CD25 and homing receptors (CXCR4 and CD62L) expression after PBMCs priming with a cytokine combination at day 0 (n=2). IL-12 (10 ng/ml), IL-18 (50 ng/ml) and IL-15 (soluble or immobilized at 63.10 ng/ml and 0.23 nM of Fe) cytokine combinations were used to prime PBMCs and the expression of CD25, CXCR4 and CD62L was analyzed after 18 hours of culture. Data from (A) NK and (B) T56 cells are represented as mean \pm SD in bar-graphs.



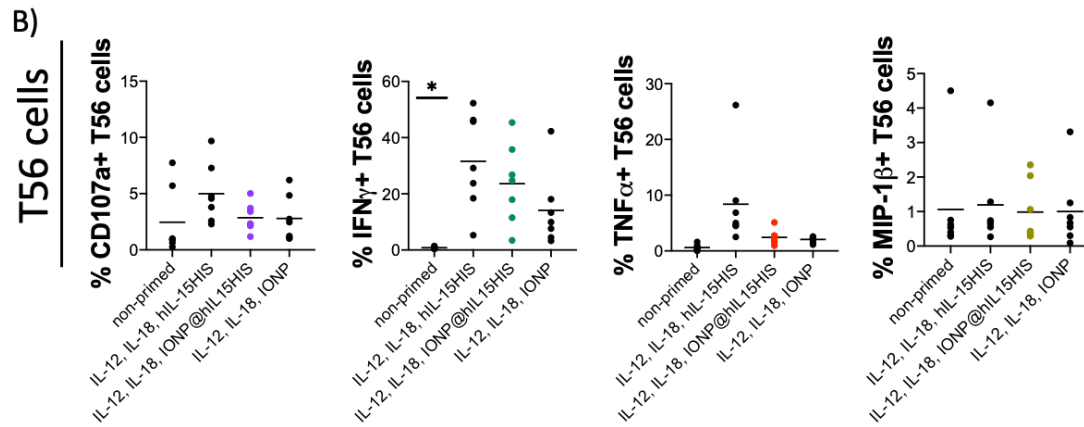


Figure 3.20. Degranulation (CD107a) and cytokine production after PBMCs priming with a cytokine combination at day 0 (n=7). IL-12 (10 ng/ml), IL-18 (50 ng/ml) and IL-15 (soluble or immobilized at 63.10 ng/ml and 0.34 of Fe) cytokine combinations were used to prime PBMCs and the expression of CD107a, IFN- γ , TNF- α and MIP-1 β was analyzed after 18 hours of culture. Data from (A) NK and (B) T56 cells are represented in scatter plots where each point represents one donor (line: mean). Significance of data was determined by comparing each sample with IL-12/IL-18/IONP@hIL15HIS condition using Dunn's multiple comparison test after Friedman test for paired samples application. * $p < 0.05$.

Next, activation markers (CD25, CD69) and homing markers (CXCR4, CD62L) expression and proliferation were studied at day 4 following non-primed, IL-12/IL-18/IONP@hIL15HIS, IL-12/IL-18/hIL-15HIS and IL-12/IL-18/IONP stimulation (Fig. 3.21, and Fig. 3.22). First of all, it was observed that, in general, CD25 and CD69 expression levels were higher when cells were pre-activated with the cytokine combination rather than only with IL-15 formulations, with the only exception of CD69 expression on T56 cells (Fig. 3.12), which somehow was unexpected according to the literature^{489,540}. In any case, it was concluded that the contribution of IONP@hIL15HIS in the cytokines cocktail did not show significant differences regarding the expression of CD69 and CD25 when compared with hIL-15HIS, although it tended to be a slightly higher expression when the immobilized IL-15 was administered in combination with IL-12 and IL-18 (Fig. 3.21).

The proliferation capacity of cells was compared by the percentage of cells that divided more than two times. The frequency of NK cells which divided more than two times was higher following IL-12/IL-18/hIL-15HIS pre-stimulation, but it was not statistically significant compared with IL-12/IL-18/IONP@hIL15HIS pre-activated NK cells. On the contrary, the

frequency of T56 cells dividing more than two times was significantly higher following IL-12/IL-18/IONP@hIL15HIS pre-activation (Fig. 3.22 A,B right graphs in purple).

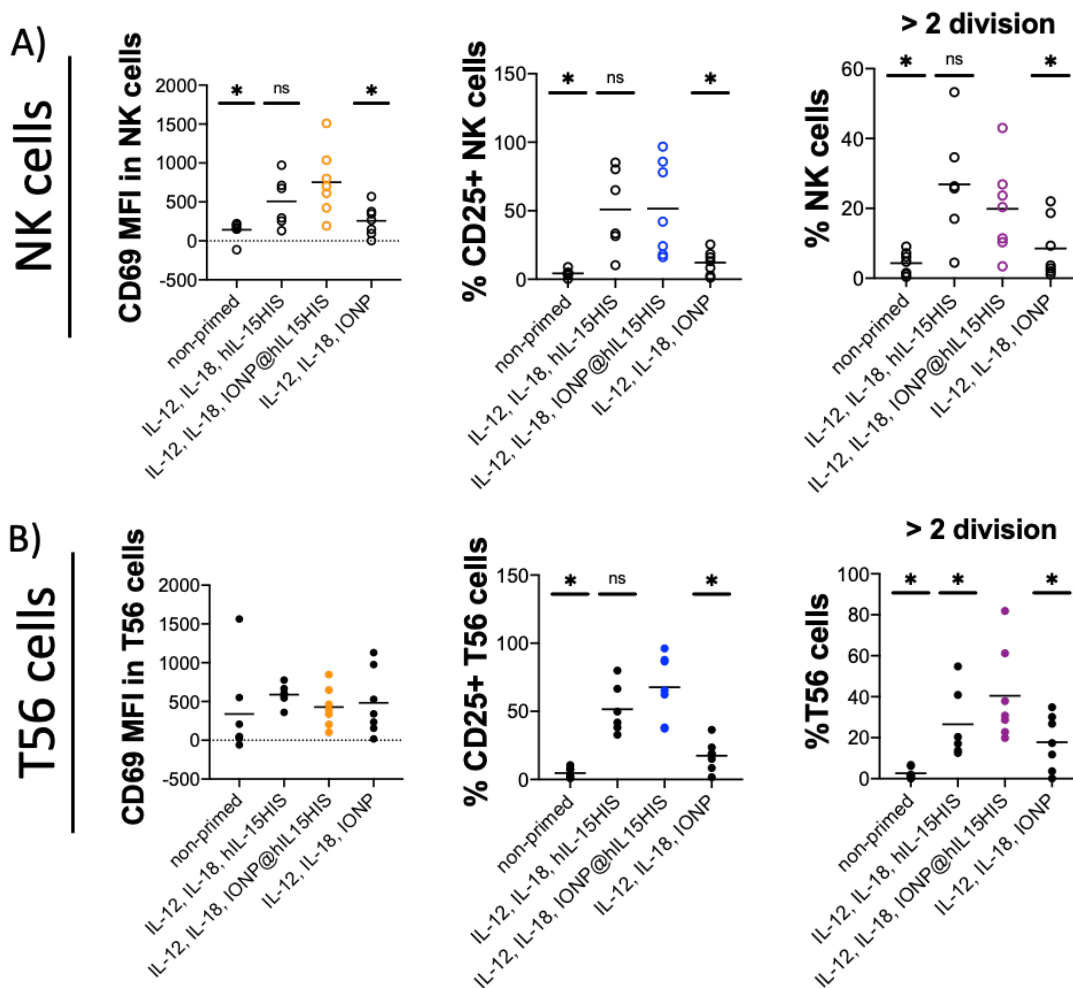


Figure 3.21. Activation markers expression and proliferation after PBMCs priming with a cytokine combination and expanded with IL-2 at day 4 (n=7). IL-12 (10 ng/ml), IL-18 (50 ng/ml) and IL-15 (soluble or immobilized at 63.10 ng/ml and 0.23 nM of Fe) cytokine combinations were used to prime PBMCs for 18 hours and IL-2 (2 U/ml) was used to expand cells for 4 additional days. The expression of CD69 and CD25 were determined as activation markers and CFSE staining was used for the proliferation assay. Data from (A) NK and (B) T56 cells are represented in scatter plots where each point represents one donor (line: mean). Significance of data in (A-D) was determined by comparing each sample with IL-12/IL-18/IONP@hIL15HIS condition using Dunn's multiple comparison test after Friedman test for paired samples application. * $p < 0.05$, ns=not significant.

The study of homing receptors was central in this project because the immobilization of IL-15 appears to be beneficial for the maintenance of CXCR4 and CD62L expression, as it was showed in previous experiments (Fig. 3.5, 3.8, 3.14 and 3.19). In the current set of experiments, CXCR4 expression levels were very similar following both IL-12/IL-

18/IONP@hIL15HIS and IL-12/IL-18/hIL-15HIS pre-activation and IL-2 expansion. CXCR4 expression was slightly lower than non-primed and IL-12/IL-18/IONP controls. In contrast, the expression of CD62L was higher than the controls in both cell subsets, and in T56 cells the difference in CD62L expression between cells pre-activated with IL-12/IL-18/hIL-15HIS and pre-activated with IL-12/IL-18/IONP@hIL15HIS was statistically significant (Fig. 3.22 B).

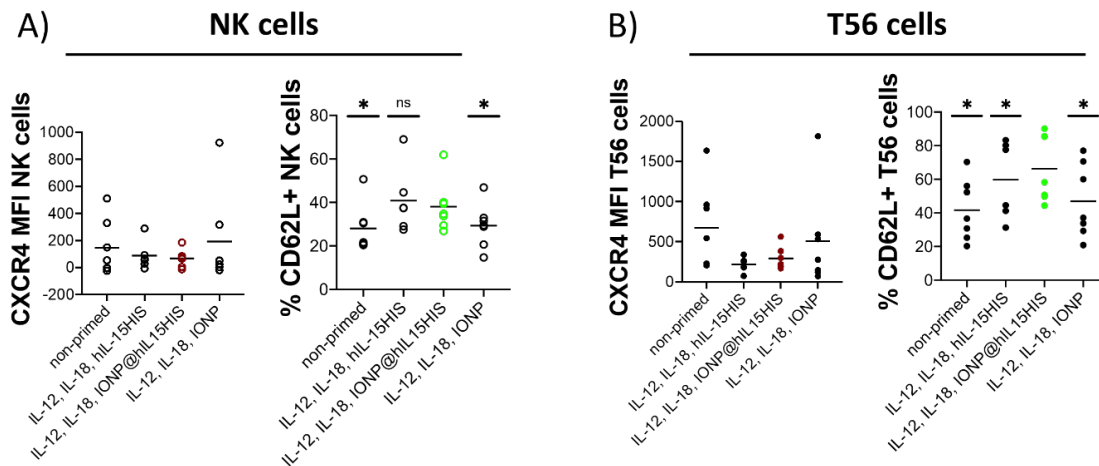


Figure 3.22. Homing receptors expression after PBMCs priming with a cytokine combination and expanded with IL-2 at day 4 (n=7). IL-12 (10 ng/ml), IL-18 (50 ng/ml) and IL-15 (soluble or immobilized at 63.10 ng/ml and 0.23 nM of Fe) cytokine combinations were used to prime PBMCs for 18 hours and IL-2 (2 U/ml) was used to expand cells for 4 additional days. The expression of CXCR4 and CD62L was analyzed. Data from NK (A) and T56 (B) cells are represented in scatter plots where each point represents one donor (line: mean). Significance of data in (A-D) was determined by comparing each sample with IL-12/IL-18/IONP@hIL15HIS condition using Dunn's multiple comparison test after Friedman test for paired samples application. * $p < 0.05$, ns=not significant.

Functional profile of NK and T56 cells was determined by degranulation (CD107a) and IFN- γ , TNF- α and MIP-1 β production. The only significant difference was observed between non-primed and priming with IL-12/IL-18/IONP@hIL15HIS for CD107a and TNF- α production by NK cells (Fig. 3.23 A). Moreover, the cell frequency of cells that exhibited effector functions was lower when compared with day 0 results. This was expected because the functional profile of NK and T56 cells was studied following a strong stimuli consisting in the combination of three cytokines, while at day 4 cells were studied following an expansion phase with a very low amount of IL-2 and in the absence of a second stimulation with a cytokine combination or target cells (such as tumor cell)^{541–543}.

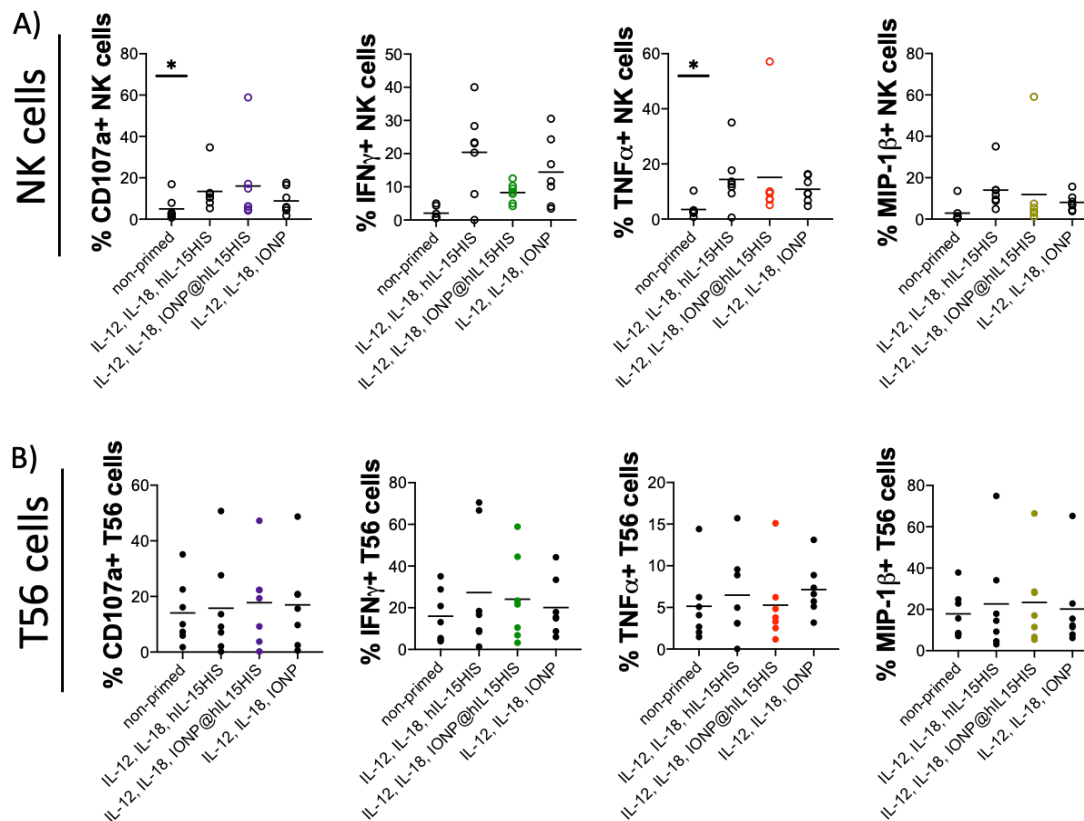


Figure 3.23. Degranulation (CD107a) and cytokine production after PBMCs priming with cytokine combination at day 4 (n=7). IL-12 (10 ng/ml), IL-18 (50 ng/ml) and IL-15 (soluble or immobilized at 63.10 ng/ml and 0.34 of Fe) combinations were used to prime PBMCs and the expression of CD107a, IFN- γ , TNF- α and MIP-1 β was analyzed. Data from NK (A) and T56 (B) cells are represented with scatter plots where each point represents one donor (line: mean). Significance of data in (A-D) was determined by comparing each sample with IONP@hIL15HIS condition using Dunn's multiple comparison test after Friedman test for paired samples application. * $p < 0.05$.

3.2.6. T56 and NK cells expansion with IL-2 or IL-15 in its soluble or immobilized forms

As figure 3.1 shows, the expansion phase was carried out with IL-2 or with IL-15 in its soluble or in the immobilized form. This was done because: 1) Taking into account that IL-2 and IL-15 share the IL2/15R $\beta\gamma_c$, it was thought that IL-15 will also be able to expand cells in a similar manner to IL-2 and also will have the ability to maintain the same levels of functional and activation markers expression; and 2) the previous results show that IONP@hIL15HIS stimulation of NK and T cells exhibits certain differences in terms of expression of activation markers and homing receptors compared to the stimulation with its soluble form. It was assumed that if the immobilization of IL-15 somehow modulates the expression of some receptors in comparison with soluble IL-15, it could be useful for cell expansion and for the

acquisition of a different phenotype that could be better for carrying out their effector functions.

The experiments were designed in a manner that PBMCs primed with IL-15 in its soluble form (hIL-15HIS) were expanded with IL-2 or hIL-15HIS, and PBMCs primed with immobilized form of the protein (IONP@hIL15HIS) were expanded with IL-2 or IONP@hIL15HIS. For control, non-primed PBMCs were expanded with IL-2, hIL-15HIS or IONP@hIL15HIS. Expansion of cells with IL-2 versus the two formulations of IL-15 showed different results in the expression of activation markers (CD25 and CD69), in degranulation (CD107a) and in the production of IFN- γ . Non-primed cells (Fig. 3.24 left column graphs) expanded with IL-15 formulations (soluble and immobilized forms) exhibited higher expression levels of CD25 and CD69 activation markers, although it was statistically significant only when the frequency in CD25⁺ T56 cells was taken into account (Fig. 3.25 left graph). It was also observed a statistically significant increase of degranulation (CD107a) and IFN- γ production between non-primed expanded with IL-2 and expanded with IONP@hIL15HIS NK cells, while degranulation (CD107a) and IFN- γ production was higher in response to IONP@hIL15HIS expansion compared with hIL-15HIS, but with no statistical significance.

When cells were pre-activated with different formulations of IL-15, it was observed that the expansion with its respective formulation (pre-activated with hIL-15HIS, expanded with hIL-15HIS; pre-activated with IONP@hIL15HIS, expanded with IONP@hIL15HIS) showed a significant increase in the expression of all markers when compared with the expansion with IL-2 (Fig. 3.24 and 3.25 second and third graphs). The exception was the frequency of CD69⁺ NK cells that did not show significant differences (Fig. 3.24 first line second and third columns graphs).

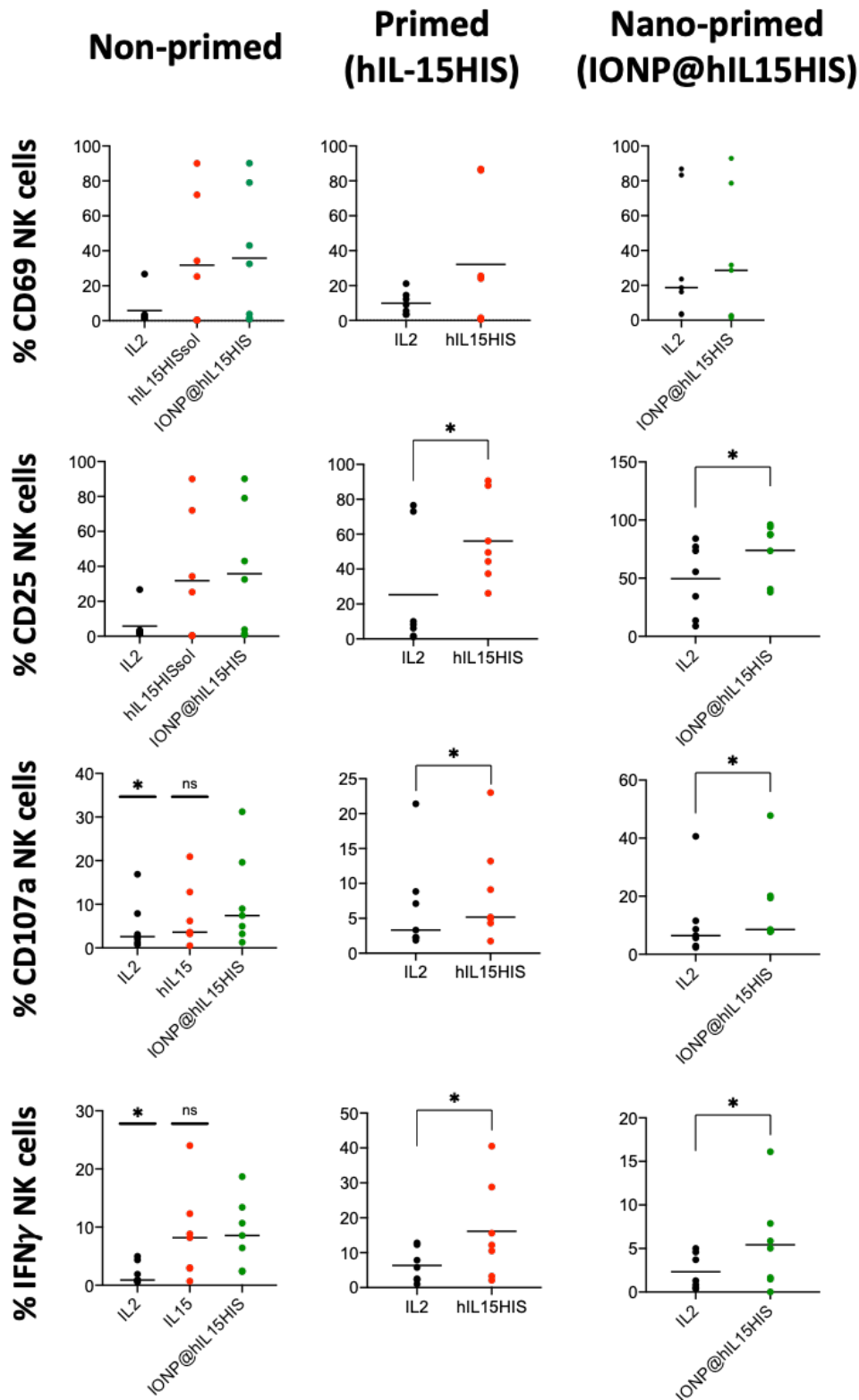


Figure 3.24. PBMCs expansion with IL-2 and IL-15 formulations: functional profile and activation markers on NK cells at day 4 (n=7). PBMCs were expanded with IL-2 (2 U/ml) or with IL-15 formulations (hIL-15HIS or IONP@hIL15HIS at 63.10 ng/ml and 0.23 nM Fe) after pre-activation with IL-15 formulations at 63.10 ng/ml and 0.23 nM Fe. Then, the expression of CD69, CD25, degranulation (CD107a) and IFN γ production was analyzed. Data are represented in scatter plots where each point represents one donor (line: mean). Significance of data of non-stimulated (left column graphs) was determined by comparing each sample

with IONP@hIL15HIS condition using Dunn's multiple comparison test after Friedman test for paired samples application and by Wilcoxon matched-pairs signed rank test for paired samples (middle and right columns graphs). * $p < 0.05$, ns= not significant.

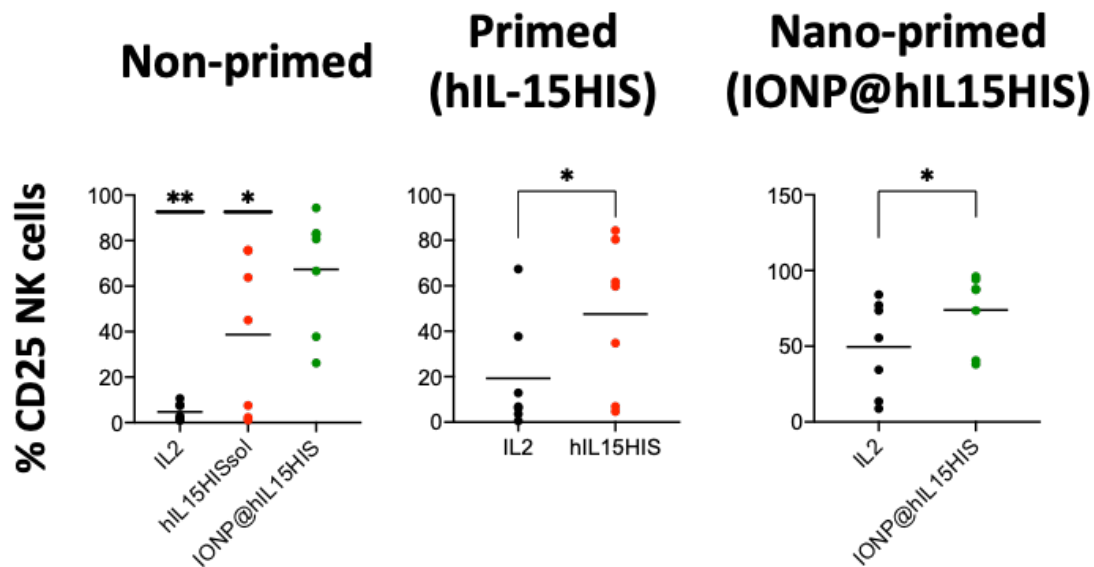


Figure 3.25. PBMCs expansion with IL-2 and IL-15 formulations: functional profile and activation markers on T56 cells at day 4 (n=7). PBMCs were expanded with IL-2 (2 U/ml) or IL-15 formulations (hIL-15HIS or IONP@hIL15HIS at 63.10 ng/ml and 0.23 nM Fe) after pre-activation with IL-15 formulations at 63.10 ng/ml and 0.23 nM Fe. Then, the expression of CD25 was analyzed. There were no significant differences between the frequencies of CD107a+, CD69+ and IFN γ + on T56+ cells (data not shown). Data are represented in scatter plots where each point represents one donor (line: mean). Significance of data of non-stimulated (left column graphs) was determined by comparing each sample with IONP@hIL15HIS condition using Dunn's multiple comparison test after Friedman test for paired samples application and by Wilcoxon matched-pairs signed rank test for paired samples (middle and right columns graphs). * $p < 0.05$, ** $p < 0.01$.

It was also studied the effect of the expansion with IL-2 or IL-15 formulations following T56 and NK cells priming with cytokines combination (Fig. 3.19). Figure 3.26 shows expression levels of activation markers and expanded cells that have divided more than two times in response to IL-2 or IL-15 formulations after pre-activating them with IL-12/IL-18/hIL-15HIS or IL-12/IL-18/IONP@hIL15HIS. Results from the expansions with IL-15 formulations showed that NK cells have a tendency to express higher levels of activation markers compared with NK cells expanded with IL-2, although statistically significant differences were not always observed (Fig. 3.26 A, C). Regarding T56 cells, it was only observed significant differences when the percentage of CD25+ cells was taken into account (Fig. 3.26 D), while the expression of CD69 on T56 cells was the same after the expansion with IL-2 and IL-15 (data not shown).

Regarding cell proliferation, there were no significant differences when compared IL-2 with IL-15 formulations mediated expansions. Graphs representing the NK and T56 cells frequencies that have divided at least two times are shown in figure 3.26 E and F, respectively. It was observed that the expansion with IL-2 or IL-15 formulations did not alter the proliferation capacity of NK and T56 cells, with the exception of T56 proliferation expanded with IL-2 following IL-12/IL-18/IONP@hIL15HIS pre-activation. The cell frequency after cell expansion with IL-2 vs IL-15 formulation and in response to this pre-activation condition (IL-12/IL-18/IONP@hIL15HIS) is statistically higher (Fig. 3.26 F).

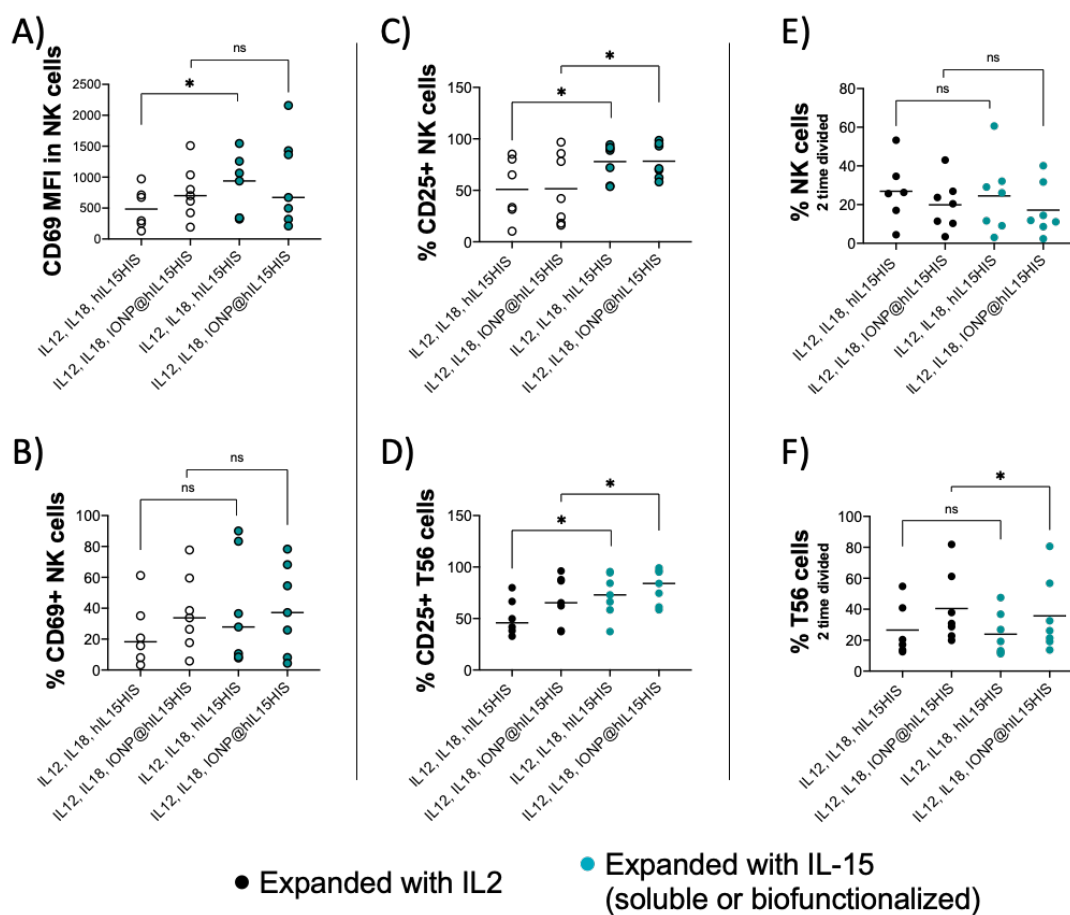


Figure 3.26. Effect of IL-2 and IL-15-mediated expansions in NK and T56 cells pre-activated with cytokines combination: Activation markers and proliferation at day 4 (n=7). PBMCs were expanded with IL-2 (2 U/ml) or IL-15 formulations (hIL-15HIS or IONP@hIL15HIS at 63.10 ng/ml and 0.23 nM Fe) after pre-activation with IL-12 (10 ng/ml), IL-18 (50 ng/ml) and IL-15 (soluble or immobilized at 63.10 ng/ml and 0.23 nM of Fe) cytokines combination. (A-D) CD69 and CD25 activation markers expression was studied in NK and T56 cells. (E, F) Percentage of NK and T56 cells that have divided at least 2 times is shown. Data are represented in scatter plots where each point represents one donor (line: mean). Significance of data was determined as follows: on the one hand was compared the condition of priming with IL-12/IL-18/hIL-15HIS

and expansion with IL-2 vs expansion with IL-15 formulations, and on the other hand, the priming with IL-12/IL18/IONP@hIL15HIS and expansion with IL-2 vs expansion with IL-15 formulations using Wilcoxon matched-pairs signed rank test for paired samples * $p < 0.05$, ns= not significant.

Regarding CD16 and perforin expression it could be said that, in general, there are no differences between cells expanded with IL-2 and cells expanded with IL-15 formulations, no statistical differences at least. Although it seems that perforin expression levels are slightly higher when cells are expanded with IL-15 formulations (Fig. 3.27 E).

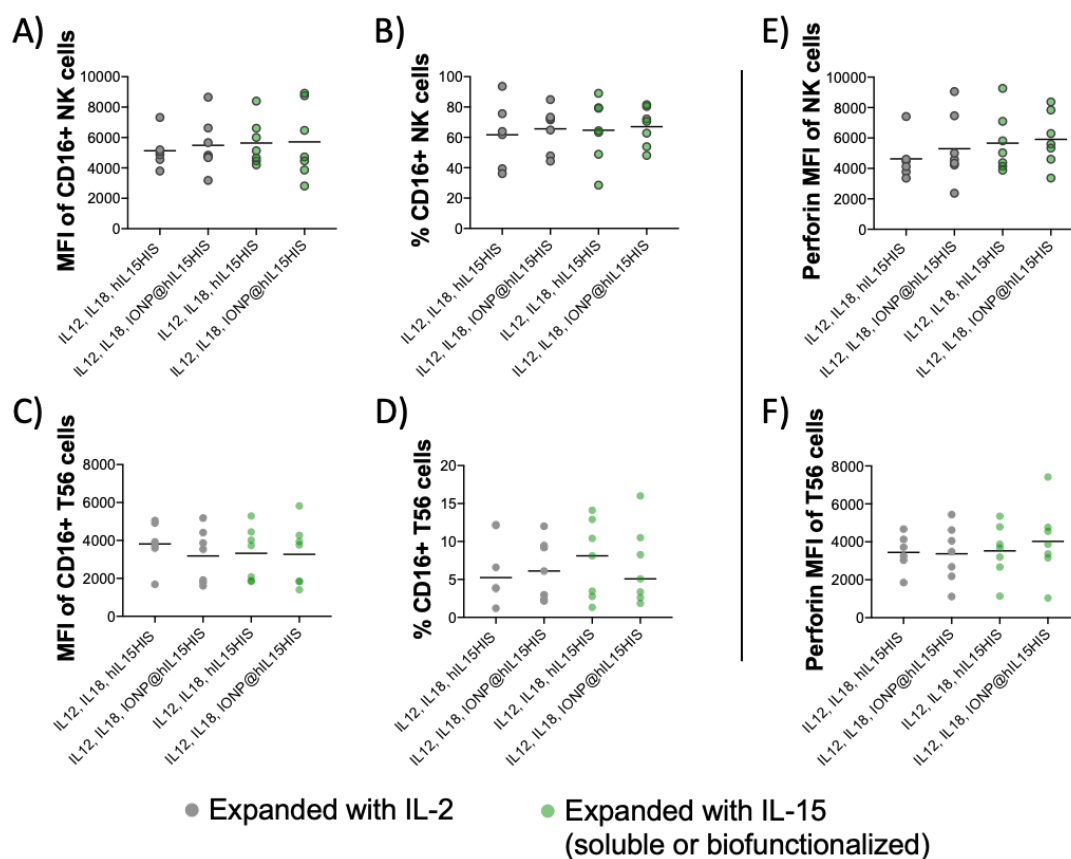


Figure 27. Effect of IL-2 and IL-15-mediated expansions in NK and T56 cells pre-activated with cytokines combination: Effector markers at day 4 (n=7). PBMCs were expanded with IL-2 (2 U/ml) or IL-15 formulations (hIL-15HIS or IONP@hIL15HIS at 63.10 ng/ml and 0.23 nM Fe) after pre-activation with IL-12 (10 ng/ml), IL-18 (50 ng/ml) and IL-15 (soluble or immobilized at 63.10 ng/ml and 0.23 nM of Fe) cytokines combination. CD16 and perforin expression were analyzed as effector markers of NK (top graphs) and T56 (down graphs) cells. (A-D) CD16 expression is represented as Mean Fluorescence Intensity (MFI) (A,C) and as cell percentage (B, D). (E, F) Perforin expression by NK and T56 cells. Data are represented in scatter plots where each point represents one donor (line: mean). Statistical analysis revealed no significant differences.

Functional markers were also studied in NK and T56 cells primed with cytokines combination and expanded with IL-2 and IL-15 formulations at day 4 (Fig. 3.28). Some effector functions,

i.e. degranulation (CD107a) and cytokines production (IFN- γ , TNF- α and MIP-1 β), of NK and T56 cells expanded with IL-15 formulations, were increased when compared with cells expanded with IL-2.

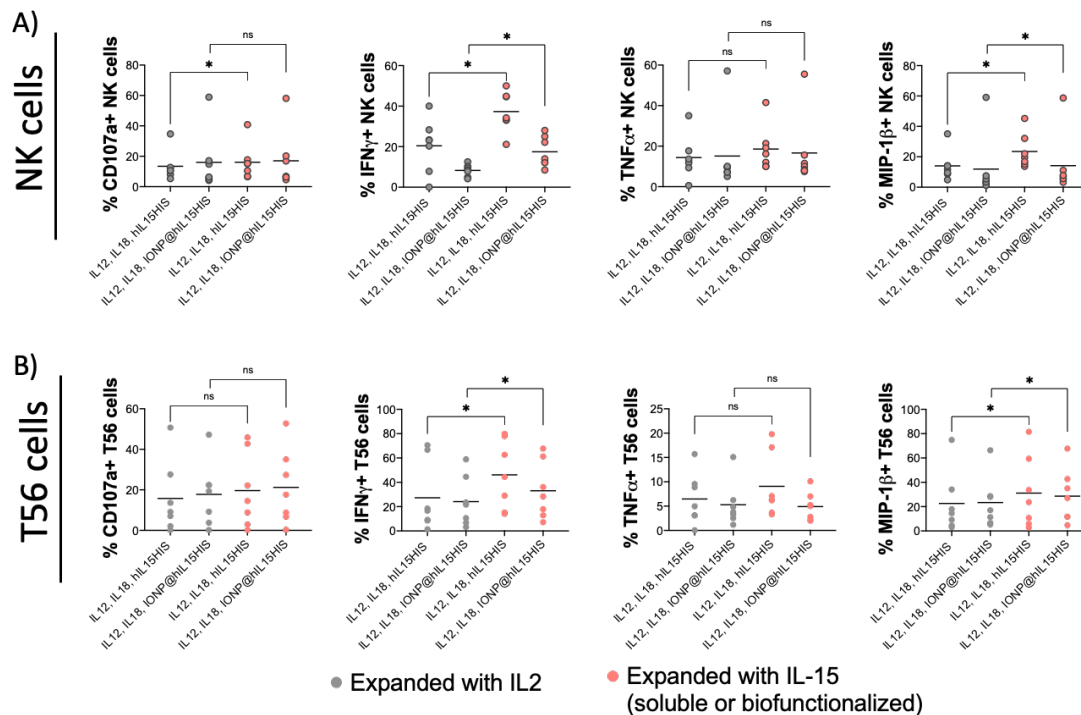


Figure 3.28. Effect of IL-2 and IL-15-mediated expansions in NK and T56 cells pre-activated with cytokines combination: Functional markers at day 4 (n=7). PBMCs were expanded with IL-2 (2 U/ml) or IL-15 formulations (hIL-15HIS or IONP@hIL15HIS at 63.10 ng/ml and 0.34 nM Fe) after pre-activation with IL-12 (10 ng/ml), IL-18 (50 ng/ml) and IL-15 (soluble or immobilized at 63.10 ng/ml and 0.34 nM of Fe) cytokines combination. The expression of CD107a, IFN- γ , TNF- α and MIP-1 β was analyzed in (A) NK cells and (B) T56 cells. Data are represented in scatter plots where each point represents one donor (line: mean). Significance of the data was determined as follows: pre-activation with IL-12/IL-18/hIL-15HIS and then expansion with IL-2 vs hIL-15HIS and, from the other, pre-activation with IL-12/IL-18/IONP@hIL15HIS and then expansion with IL-2 vs IONP@hIL15HIS, using Wilcoxon matched-pairs signed rank test for paired samples * $p < 0.05$, ns= not significant.

3.3. Conclusions

Laboratory made IL-15 was expressed and characterized successfully reaching a grade of purity similar to commercial IL-15 measured by Maldi-ToF and SDS-PAGE. Furthermore, the ability to activate NK cells of laboratory-made IL-15 was also similar to commercial IL-15.

When cells were stimulated, the bioconjugation of IL-15 on the IONPm (IONP@hIL15HIS) provided this cytokine with some biological effects that were somehow different in comparison with soluble IL-15 (hIL-15HIS). Activation markers (CD69, CD25) and homing receptors (CXCR4, CD62L) were expressed at similar or higher levels on NK and T56 cells at day 0 following IONP@hIL15HIS stimulation and also at day 4 after an expansion with low doses of IL-2. Results were similar when cells were pre-activated with IONP@hIL15HIS in combination with IL-12 and IL-18 in comparison with cells pre-activated with hIL-15HIS in combination with IL-12 and IL-18. In addition, the functional markers (CD16 and perforin) at day 4 were expressed also at similar or higher levels following IONP@hIL15HIS stimulation, with the exception of the frequency of CD16 positive NK cells that was lower in response to IONP@hIL15HIS.

It is of special interest that the expression of the CXCR4 and CD62L is different depending if cells were stimulated with any strategy where IONP@hIL15HIS is present (IONP@hIL15HIS, IL-12/IL-18/IONP@hIL15HIS). This effect is very interesting for two reasons: 1) hIL-15HIS induces a significant decrease of the two homing receptors, especially CXCR4, which is partially reverted by the nanovehiculization of the protein and 2) the diminished decrease in homing receptor expressions could be associated with a higher migration capacity of cells to different locations (to the bone marrow in the case of CXCR4 and to the lymph nodes in the case of CD62L).

Regarding cell functionality, the stimulation with IONP@hIL15HIS did not result in significant differences in the studied effector functions (CD107a, IFN- γ , TNF- α and MIP-1 β) when

compared with hIL-15HIS. The functional profile of T56 cells practically did not change in response to any stimuli. NK cells tended to exhibit increased effector functions at day 0 following hIL-15HIS stimulation compared with IONP@hIL15HIS stimulation. At day 4, the picture was reverted for all functions except for IFN- γ production. Regardless, the differences were not statistically significant between the frequencies of positive cells in response to hIL-15HIS vs. IONP@hIL15HIS. However, given that effector functions were analyzed in many cases following an expansion phase (day 4), it is important to keep in mind that the low functional profile of the cells does not necessarily mean a lower ability to deal with a possible encounter with target cells.

On the other hand, it was also studied the ability of IL-15 formulations to expand cells. Results showed that cell expansion with IL-15 formulations is also possible and, what is more relevant, the expression levels of activation and functional markers in NK and T56 cells was increased when they were expanded with IL-15 formulations in comparison with IL-2.

In conclusion, it could be postulated that IL-15 formulations could be a good alternative to IL-2, because they were able to also expand cells and maintain the expression of certain markers and increase the expression of others. In addition, the results presented in this chapter are of special interest because they open the door to perform more studies with immobilized IL-15 by means of nanotechnology and its possible role in future immunotherapy regimes, alone or in combination with other drugs.

Chapter IV

In vivo application of IONP@hIL15HIS

Chapter IV In vivo study of IONP@hIL15HIS as antitumoral immunotherapy

4.1. Introduction

In vitro experiments are useful to understand the interactions between different cell types, as for example between cancer cell lines and immune cells. Nevertheless, until a few years ago, the limitation of mimicking a multicellular system was a problem with *in vitro* studies, but it has been partially solved by using organoids, which are providing very good information. In fact, organoids are able to model the tumor microenvironment (TME)⁵⁴⁴. However, the lack of an immune system, stroma and/or blood vessels represents a limitation of organoids⁵⁴⁵. Therefore, *in vivo* models are still needed today.

4.1.1. State of the art of the nano-immunotherapy *in vivo*

One of the principal problems of many therapies is the high doses that are required to adequately reach target cells due to molecule clearance. This problem is a consequence of the pharmacokinetics of the drugs. Nanoparticles (NPs) may have an important role in avoiding this problem, and the main contributions of NPs in nano-immunotherapy are described below:

1) Efficient drug delivery into the tumor area. NPs are good candidates because they can carry hydrophilic and hydrophobic molecules while they enhance the half-life of the carried molecule (fig. 4.1 box 1 and 2). Therefore, the delivery of molecules is more efficient with NPs (fig. 4.1 box 3)^{546–548}. In addition, NPs can be designed with specific polymers or components which are responsive to pH, temperature and/or hypoxia⁵⁴⁹. These smart nanomaterials are tumor-specific because the delivery occurs only under particular situations such as temperature, pH or O₂ concentration variations.

2) Mimic ligand-receptor interactions through NPs bioconjugation. The main goal is mimicking the cell membrane to resemble the expression of molecules on the surface

of cells (fig. 4.1 box 3). For example, NPs decorated with T-cell receptors and loaded with chemotherapeutic drugs work as biomimetic nano-constructs for chemo-immunotherapy⁵⁵⁰. This strategy has gotten interest during the last years for cancer nano-vaccines because it can promote a tumor-specific immune response, *i.e.*, antigen (Ag) carriers^{551,552} (Figure 4.1).

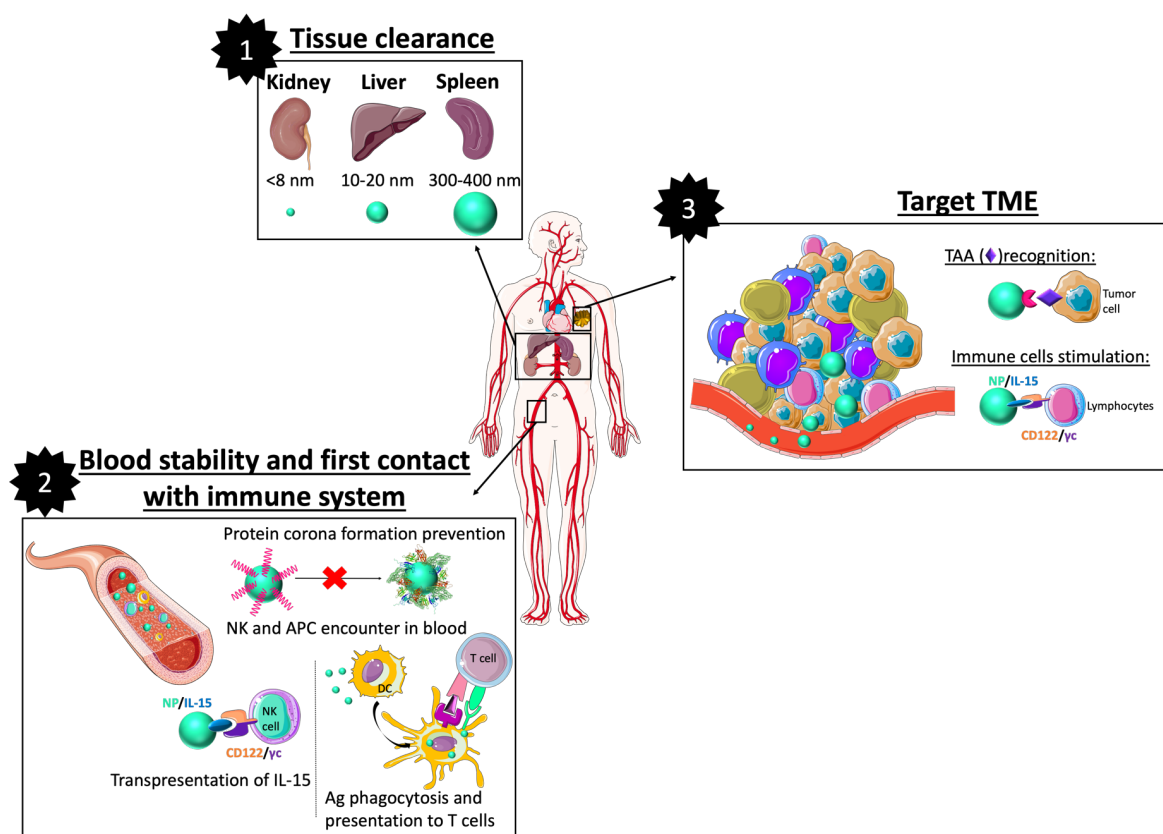


Figure 4.1. NPs-based formulations *in vivo*. NPs enhances drug availability in the tumor area by two mechanisms. 1) It can avoid tissue clearance because of their size. Molecules smaller than 8 nm will be secreted by the kidney, molecules in the range of 10-20 nm will be eliminated by the liver, and molecules ranged between 300-400 nm by the spleen (box 1). 2) It increases blood stability by avoiding protein corona formation (box 2)^{553,554}. Moreover, NPs could transport molecules and drugs of interest to the tumor area triggering the activation of immune cells (box 3). In that way, it could mimic naturally existing biological processes such as cell membrane receptors expression (*i.e.* IL-15 trans-presentation) or just enable the contact of tumor cells with NP, and in consequence, get closer the drug entrapped into the NP.

Apart from drug delivery for immunotherapy, NPs by themselves may have an adjuvant effect and also are able to trigger ferroptosis (if they are Fe-based materials) as it is mentioned in chapter III^{555,556}. The use of IONPs for these two effects, adjuvant and ferroptosis, point them out as engaging tools for their use in antitumoral immunotherapies.

In this chapter, IL-15 biofunctionalized IONPs are tested in two *in vivo* models. The first model is based on adoptive cell transfer therapy (ACTT), where *in vitro* primed peripheral blood mononuclear cells (PBMCs) with IL-15 formulations (hIL-15HIS and IONP@hIL15HIS) are injected into mice. In the second model we have studied the therapeutic effect of IL-15-based formulations in tumor-bearing mice.

In vivo application of IONP@hIL15HIS

4.2. Results and discussion

4.2.1. ACTT *in vivo* model with IONP@hIL15HIS primed PBMCs

Many ACTT are based on priming and/or culturing cells *in vitro* followed by their infusion into the patient. In this section we have studied the *in vivo* expansion capacity of PBMCs after priming with hIL-15HIS in its soluble or immobilized form (IONP@hIL15HIS). This priming was carried out in the same manner as in chapter III. The difference in this Chapter is that the expansion phase happened *in vivo* in NOD.Cg-Prkdc^{scid} Il2rg^{tm1Wjl}/SzJ mice (most often known by their branded name, NOD scid gamma or NSGTM). The timing of the experiment was designed according to the literature^{557–560}. The protocol depicted in figure 4.2 was carried out.

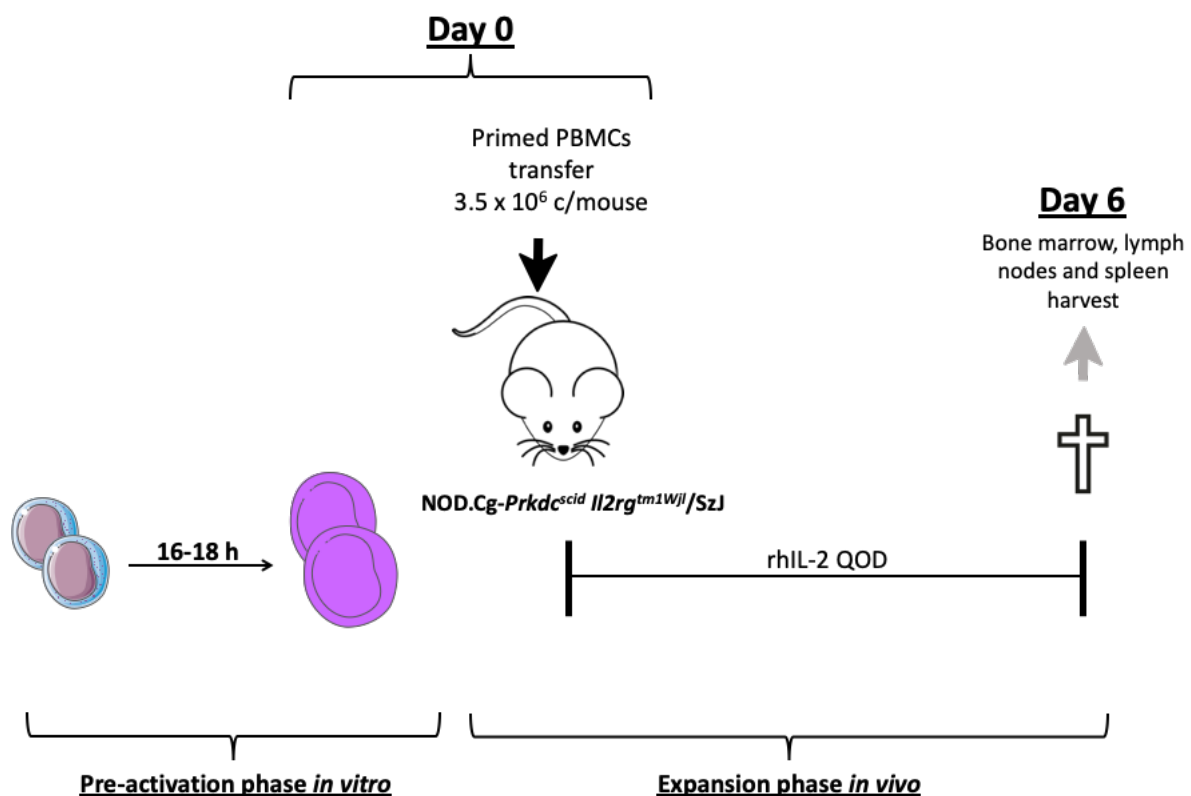


Figure 4.2. Schematic representation of ACTT protocol. PBMCs were primed with hIL-15 and IONP@hIL15HIS at 50 ng/ml protein concentration in the pre-activation phase *in vitro*. After that, cells were washed and inoculated into mice (3.5×10^6 cells/mouse). After 6 days, mice were euthanized and bone marrow, lymph nodes, and spleen were harvested for further flow cytometry-based analysis. PBMCs: peripheral blood mononuclear cells, QOD: every two days.

As it is represented in Fig. 4.2, organs (bone marrow, spleen and lymph nodes) were harvested and processed at day 6. Cells suspensions were done, then stained and acquired in a flow cytometer for further analysis (flow cytometry panel in the experimental section on table ES.2). The gating strategy is represented in figure 4.3. First, single cells were selected. Then, in the absence of a viability marker, dead cells were identified as low forward (FSC-A) and side (SSC-A) scatter parameters and excluded from live cells. Next, lymphocytes were gated based on their FSC-A and SSC-A features and, finally, human hematopoietic cells were identified (figure 4.3.A). Human and mouse hematopoietic cells were discriminated using anti-human CD45 (hCD45) and anti-mouse CD45 (mCD45) monoclonal antibodies (mAbs) respectively. The human/mouse ratios were calculated by dividing the percentage of hCD45+ cells by the percentage of mCD45+ cells (Fig. 4.3.B). Next, the expression of other human markers (CD25, CD62L and CXCR4) was determined only in human cells with specific anti-human fluorochrome-conjugated mAbs.

A ratio hCD45+/mCD45+ higher than one means that there is a higher frequency of human hematopoietic cells than mouse hematopoietic cells. In figure 4.3 B, it could be seen that only in lymph nodes from mice that received primed PBMCs with hIL-15HIS and IONP@hIL15HIS there were more human than mouse CD45+ cells. Although the differences were not statistically significant, we would like to propose that there is a tendency of primed hIL-15HIS and IONP@hIL15HIS human cells that migrate to the lymph nodes to slightly exhibit an expansion when compared with cells treated with controls (PBS and IONP). In the case of the bone marrow and spleen samples, the hCD45+/mCD45+ ratio was no higher than 1, indicating that in these two organs there were less human cells than mouse cells. Also, no significant differences were observed when human cells were primed with hIL-15HIS or IONP@hIL15HIS in comparison with the controls (PBS and IONP).

NSG mice are immunodeficient. They carry two mutations: severe combined immune deficiency (*scid*) and a null allele of the IL-2 receptor common gamma chain or IL-2R γ c

(*IL2rgnull*). The *scid* mutation is in the DNA repair complex protein *Prkdc* which results in B and T cell deficiency. The *IL2rgnull* mutation prevents cytokine signaling through multiple receptors, leading to a deficiency in NK cells. Given the absence of T, B and NK cells, a higher expansion of adoptively transferred human PBMCs was expected (Fig.4.3.B), due in part to an increased homeostatic proliferation⁵⁶¹. Nevertheless, it could be possible that human PBMCs did not adequately respond to mouse homeostatic cytokines, such as IL-7 and IL-15⁵⁶².

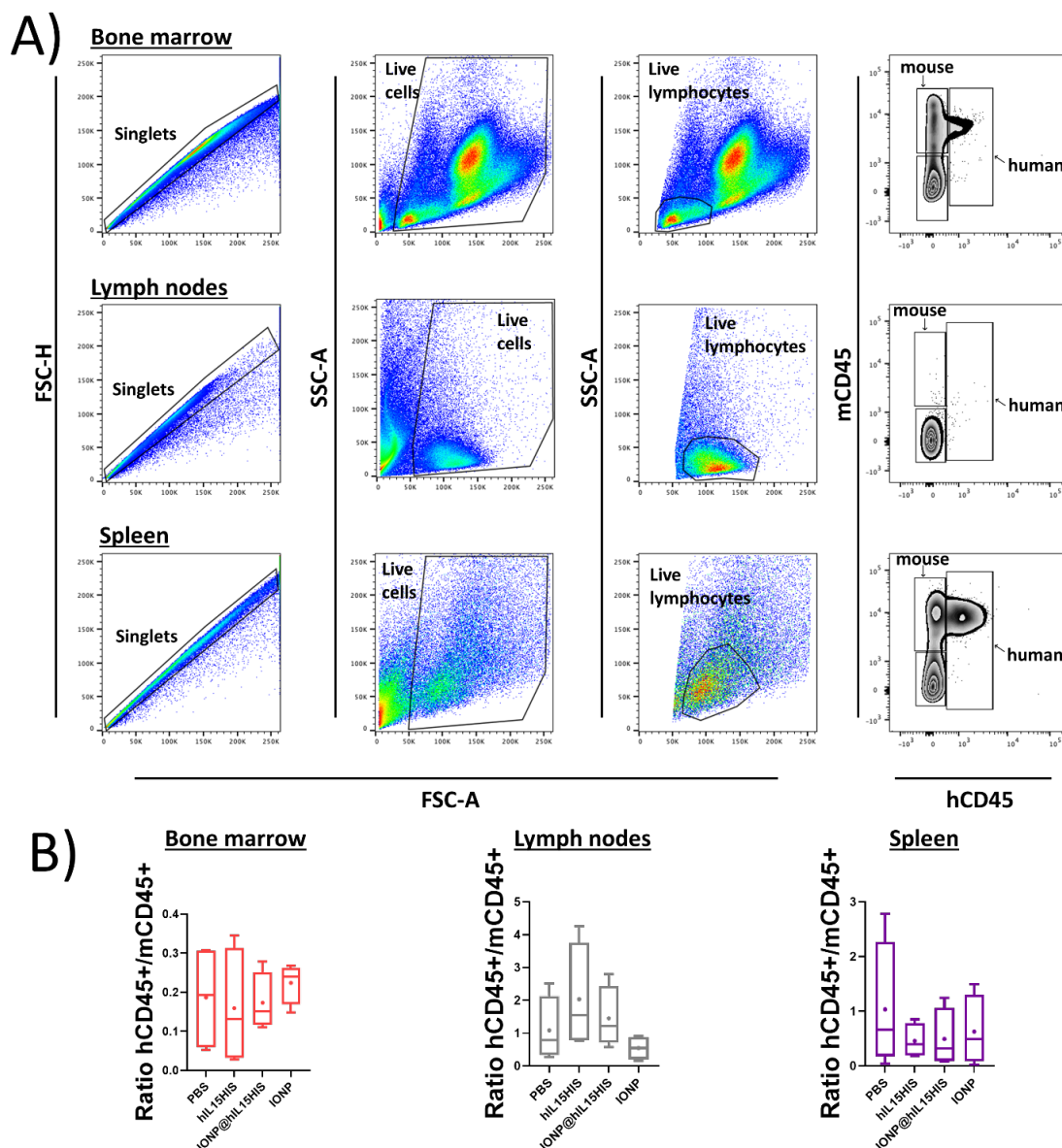


Figure 4.3. The ratio between human CD45+ and murine CD45+ cells. (A) Dot plots show the gating strategy used for the identification of hCD45+ cells. (B) Box and whiskers graphs represent the hCD45+/mCD45+ ratio in bone marrow, lymph nodes and spleen (horizontal lines in the boxes represent the mean and the points are the median; the lower part of the box is the Q1 and the top part of the box is the Q3, whiskers are the maximum and minimum data value). Statistical analyses were performed using

Wilcoxon matched-pairs signed rank test. No significant differences were observed between stimuli conditions (n=4).

Next, the homing receptors (CXCR4 and CD62L) and the CD25 activation marker expression of hCD45⁺ cells were studied. First, it was observed that the migration of cells to the different organs was related with the expression of the homing receptors. Cells expressing higher levels of CXCR4 and low levels of CD62L were found in the bone marrow and those expressing higher levels of CD62L and low levels of CXCR4 were predominantly found in the lymph nodes (Fig. 4.4). This association of homing receptor expression pattern and migration was expected. CXCR4 and CD62L expression is a requirement to traffic to the bone marrow and to the lymph nodes, respectively^{563,564}. Regarding CD25 expression, the frequency of CD25⁺ cells exhibited a tendency to be higher, although not significant, when PBMCs primed with IONP@hIL15HIS were transferred into mice when compared with other conditions. On the other hand, there were no differences in the mean fluorescence intensity (MFI) in the four tested conditions.

Within the PBMCs, we also wanted to determine how T (CD3⁺) and NK (NK1.1⁺, CD3⁻) cells migrated and expanded, because both cell types respond to IL-15 as well as to the IL-2 that is used for *in vivo* cell expansion¹⁸³. The frequencies of T cells stimulated with different conditions were not statistically different (Fig. 4.5 B). We found that the majority of hCD45⁺ cells were CD3⁺ (Fig. 4.5 A). Therefore, it was assumed that only T cells were able to expand under the studied conditions. Nevertheless, it must be considered that NK cells may have migrated to other locations rather than bone marrow and secondary lymphoid organs (spleen and lymph nodes). In fact, most NK cells within PBMCs are characterized by a CD56^{dim} phenotype and they are known to traffic to peripheral organs, while the very minor CD56^{bright} subset migrates to secondary lymphoid organs⁵⁶⁵.

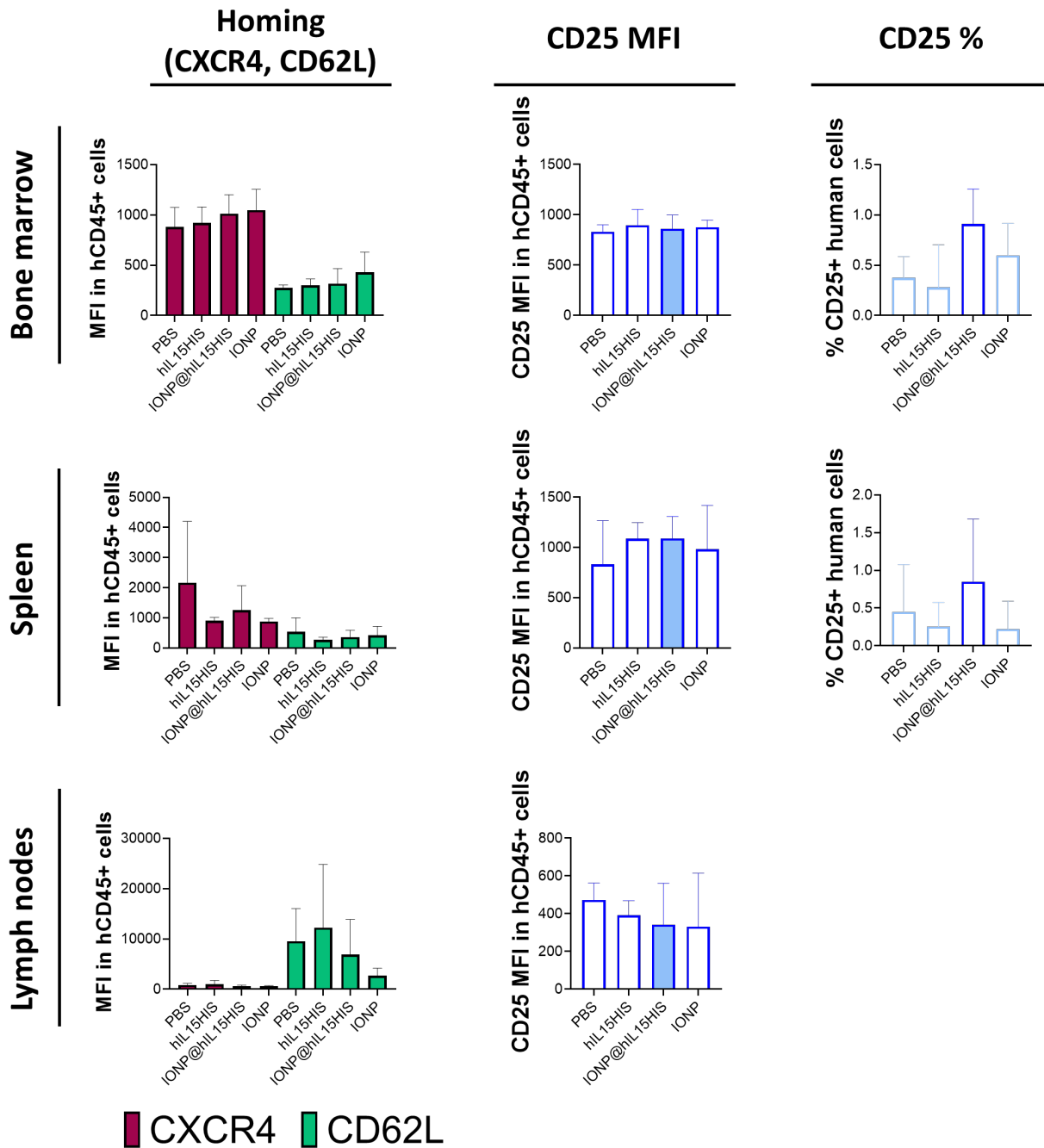


Figure 4.4. CXCR4 and CD62L homing receptors and CD25 activating receptor expression on human CD45+ cells. Mean fluorescence intensity (MFI) of CXCR4, CD62L from hCD45+ cells means are represented in bar graphs (maroon and green). CD25 MFI from hCD45+ cells and percentage of CD25+ cells are represented in bar graphs (blue). Bone marrow, lymph nodes and spleen tissues were analyzed. Error bars represent the standard deviation. Statistical analyses were performed using first with Friedman test (non parametric for paired data) with no significant differences between stimuli conditions (n=4).

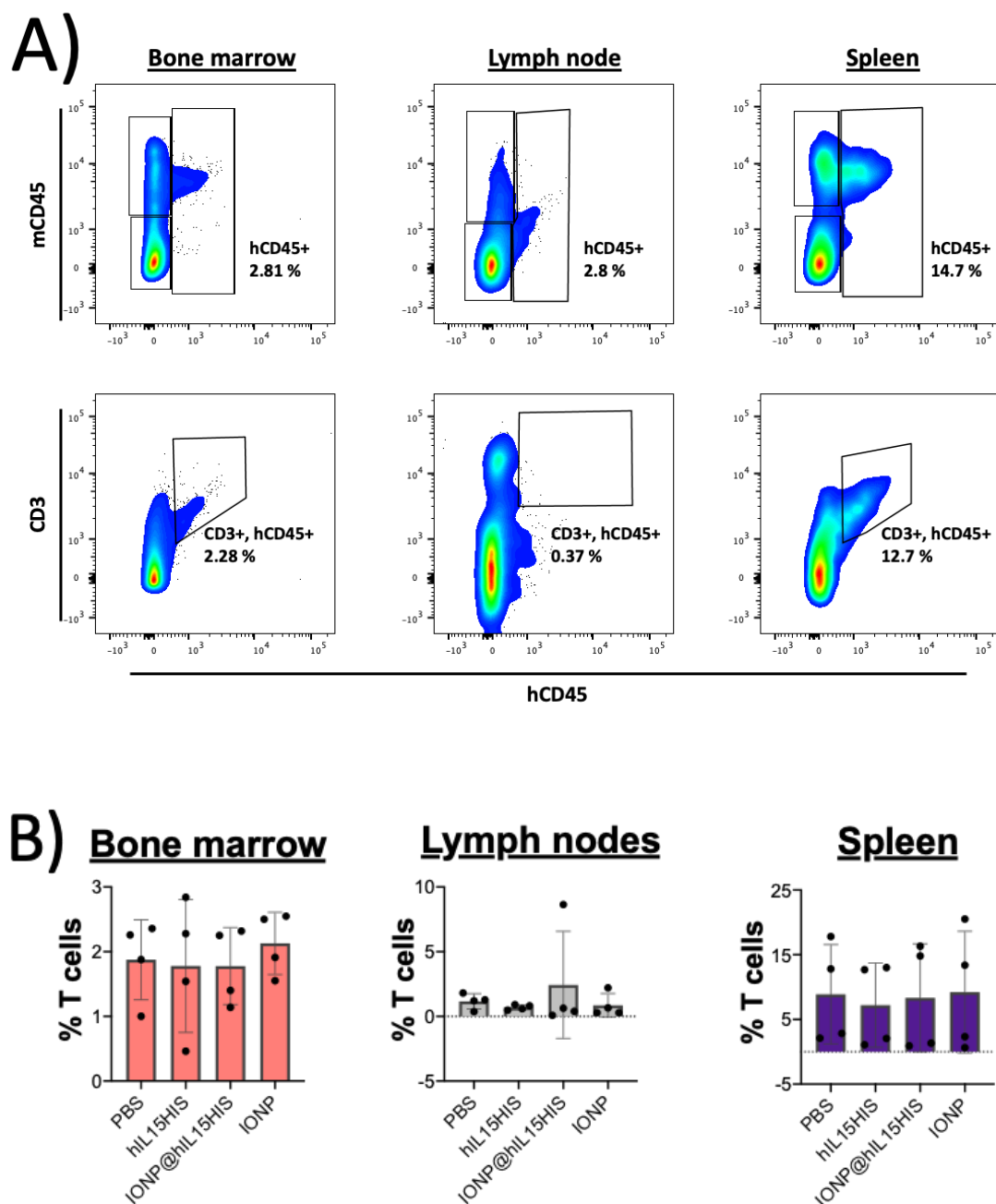


Figure 4.5. Human T cells in bone marrow and secondary lymphoid organs. (A) Most cells present in the three organs are T cells. The percentage of hCD45+mCD45⁻ cells (upper panel) and hCD45+CD3⁺ cells (lower panel) is similar. T cells are identified by the expression of CD3. (B) The frequency of T cells (hCD45+CD3⁺ gate) in the three studied organs is showed in bar graphs. Mean and standard deviation is represented by bars and error bars, and each point represents different mouse data. Statistical analyses were performed using first with Friedman test (non parametric for paired data) with no significant differences between stimuli conditions (n=4).

We thought that one of the reasons of the poor proliferation of the adoptive transferred cells possibly was that we performed the analysis after few days of the inoculation and expansion

with IL-2. Another reason could be that the dose of IL-2 was too low. Priming of PBMCs was carried out in the presence of IL-15 while the expansion was done with IL-2. It is known that IL-2 is able to trigger NK and T cell proliferation, but *in vivo*, other factors, such as Bcl-2 downregulation⁵⁶⁶, could be responsible for the low rate of proliferation. Other possibility is that more days of expansion probably are needed, including a previous expansion phase *in vitro* before cell transfer⁵⁶⁷. It was also thought that using IL-15 in the expansion phase *in vivo* could lead to higher proliferation. This tentative affirmation was based on other works where IL-15 formulations induced the expansion of T (especially CD8+ memory T cells) and NK cells in *in vivo* experiments and in ongoing clinical trials with IL-15 (NCT01385423, NCT02395822)⁵⁶⁸⁻⁵⁷⁰. In addition, it was also expected that the priming of PBMCs with IONP@hIL15HIS could have contributed to higher proliferative rate of PBMCs⁵⁷¹. But similarly, this higher proliferation would be higher if IL-15 formulations (hIL-15HIS or IONP@hIL15HIS) were also used in the expansion phase *in vivo* instead of IL-2. Clearly, more studies are required to define the best conditions for IL-15 primed cells expansions in this mouse model.

It was also compared the expression of CXCR4, CD62L and CD25 on human T cells before the transfer of PBMCs to the mice and after cell expansion for 6 days *in vivo* in bone marrow, lymph nodes and spleen (Fig. 4.6). Homing receptors (CXCR4 and CD62L) expression decreased after 6 days, which is in agreement with the bibliography and with what was observed in the *in vitro* experiments in this thesis (see Chapter III). In addition, the decrease of the CD62L expression from day 0 to day 6 was considerably less in lymph nodes than the decrease in bone marrow and the spleen, confirming the relationship of this homing receptor expression with the migration to the lymph nodes⁵⁷². However, the decrease in the CXCR4 expression is similar in cells from all organs.

CD25 expression in cells before transfer and after 6 days of expansion was also studied by analyzing the frequency of CD25+ cells within the hCD45+ cell population. CD25+ cell

percentage is lower at day 6 than before cell transfer and the highest decrease was observed under IL-15 formulations priming conditions.

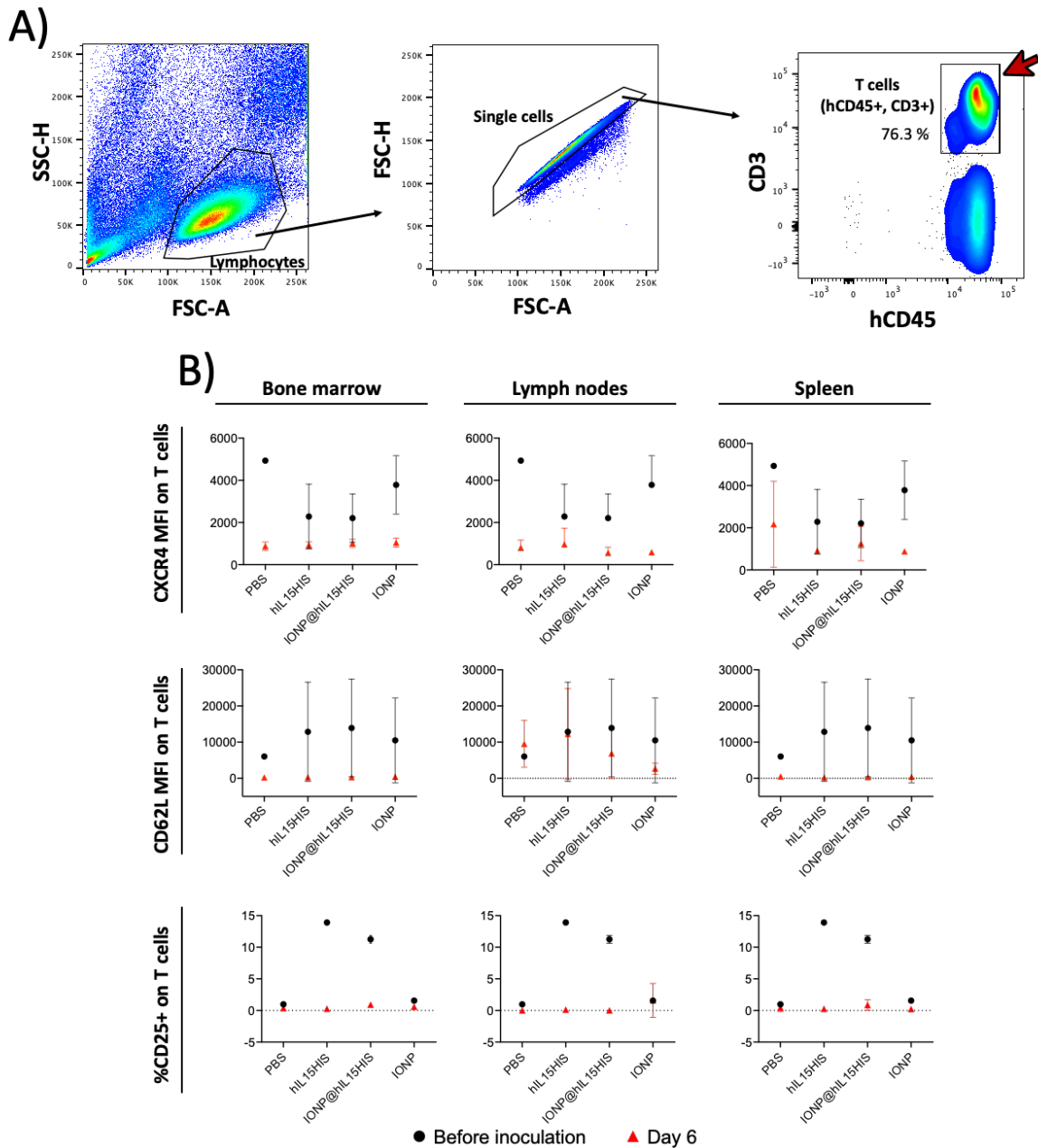


Figure 4.6. Mean fluorescence intensity (MFI) of homing markers (CXCR4 and CD62L) and activation marker (CD25) on T cells before transfer (day 0) and at day 6. (A) The gating strategy of T cells is showed in dot plots. The population of T cells, identified as CD3+ and hCD45+ cells (red arrow) was selected to compare day 0 vs. day 6 data. (B) Comparison of the MFI values of CXCR4 and CD62L and the percentage of CD25+ cells from day 0 and day 6 (gating strategy represented on Figure 4.3) is represented in XY graphs where black circles are data from day 0 and red triangles are day 6 data. (n=4)

4.2.2. Antitumor therapeutic effect of IONP@hIL15HIS

The potential of IL-15 formulations to trigger tumor cell killing by different means has been demonstrated in leukemia but also in solid tumors^{573,574}. Different strategies such as gene therapy, cancer cell vaccines or IL-15 protein containing engagers have been used^{575–578}. In addition, in chapter III it has been shown that the stimulation of PBMCs with IL-15 and IONP@hIL15HIS activates NK and T56 cells, leading to the production of cytokines such as TNF- α and IFN- γ and presumably to the death of tumor cells⁵⁷⁹. In our system, IONP@hIL15HIS somehow resembles a cell presenting IL-15 to NK and T cells (transpresentation), where the NP acts as the cell bearing IL-15 receptor α (IL-15R α). NP-mediated IL-15 transpresentation activate NK and T cells since they express the β subunit of IL-2/IL-15 receptor (IL-2/IL-15R β or CD122) and the gamma common chain (γ_c or CD132), leading to an increase in NK and T cells effector functions and to hamper tumor growth.

The therapeutic effect of IONP@hIL15HIS was studied in B16F10 tumor bearing C57BL/6 mice. Tumor size and animal weight were monitored over time. Blood samples from the temporal superficial vein were harvested one day before mice were administered intravenously (i.v.) with IL-15 formulations and controls (Fig. 4.7). Tumor volume results did not show any statistically differences between all treatments, but it appeared to be a trend to slow down the tumor growth using the IONP@hIL15HIS formulation (Fig. 4.8 A). In addition, the tumor growth slopes were transformed analyzing them by simple linear regression in GraphPad Prism v8 and the slopes of the lines were represented and compared in bar graphs (Fig. 4.8 B). There were not statistically significance differences, but the slope is lower when IONP@hIL15HIS was used compared with other conditions (Fig. 4.8 B). Although results did not show significant differences, it could be proposed that IL-15 cytokine administration tend to slightly inhibit tumor progression comparing with the PBS group, which is in agreement with the literature^{580,581}. In addition, the biofunctionalization of IL-15 seemed to hamper tumor size in a slightly higher efficient manner than the soluble form of IL-15 suggesting that

the transpresentation of IL-15 by the NP may result in higher antitumor effect⁵⁸². The limited antitumor effect of IONP@hIL15HIS could be also enhanced using another route of administration, such as intratumorally instead of intravenously⁵⁸³.

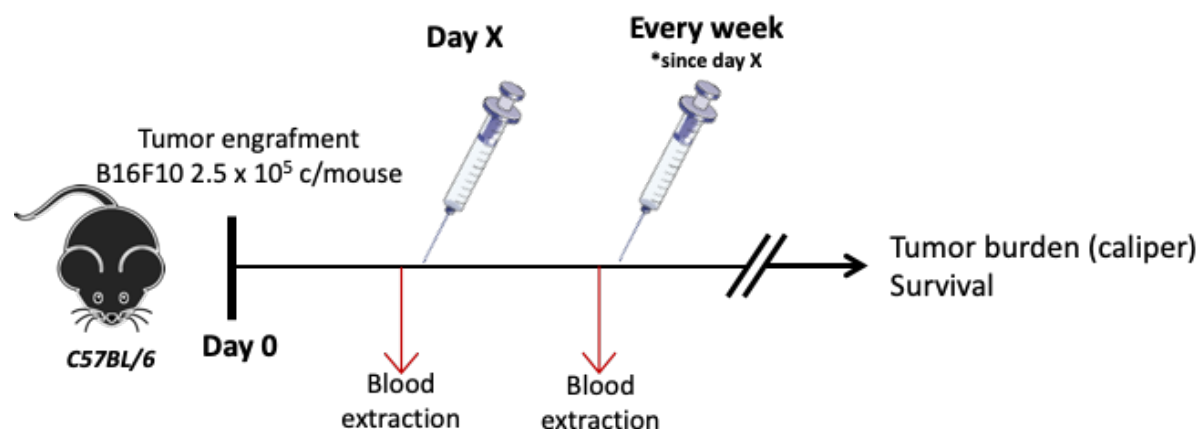


Figure 4.7. Schematic representation of antitumor therapy schedule. B16F10 tumor bearing C57BL/6 mice were treated with hIL-15HIS in its soluble or immobilized form in IONP micelles (IONP@hIL15HIS) at Day X. Then IL-15 treatment and controls were administered once a week. One day before treatment, blood extractions were carried out for flow cytometry-based analyses. Day 0: tumor engraftment; Day X: day when tumor volume reaches 300 mm³.

The probability of survival was also studied and it was not found significant differences. Nevertheless, the IONP@hIL15HIS treated group showed the highest probability of survival (Fig. 4.8 C). The weight was used to monitor the mice (Fig. 4.8 D). The hIL-15HIS treated animal group displayed a tendency to increase their weight. This tendency to gain weight when animals were treated with soluble form of IL-15 (hIL-15HIS) could be related with an inflammation reaction⁵⁸⁰, associated with the presence of the protein in its soluble form^{584,585}. In fact, this increase in animal weight was not observed in the IONP@hIL15HIS treated group.

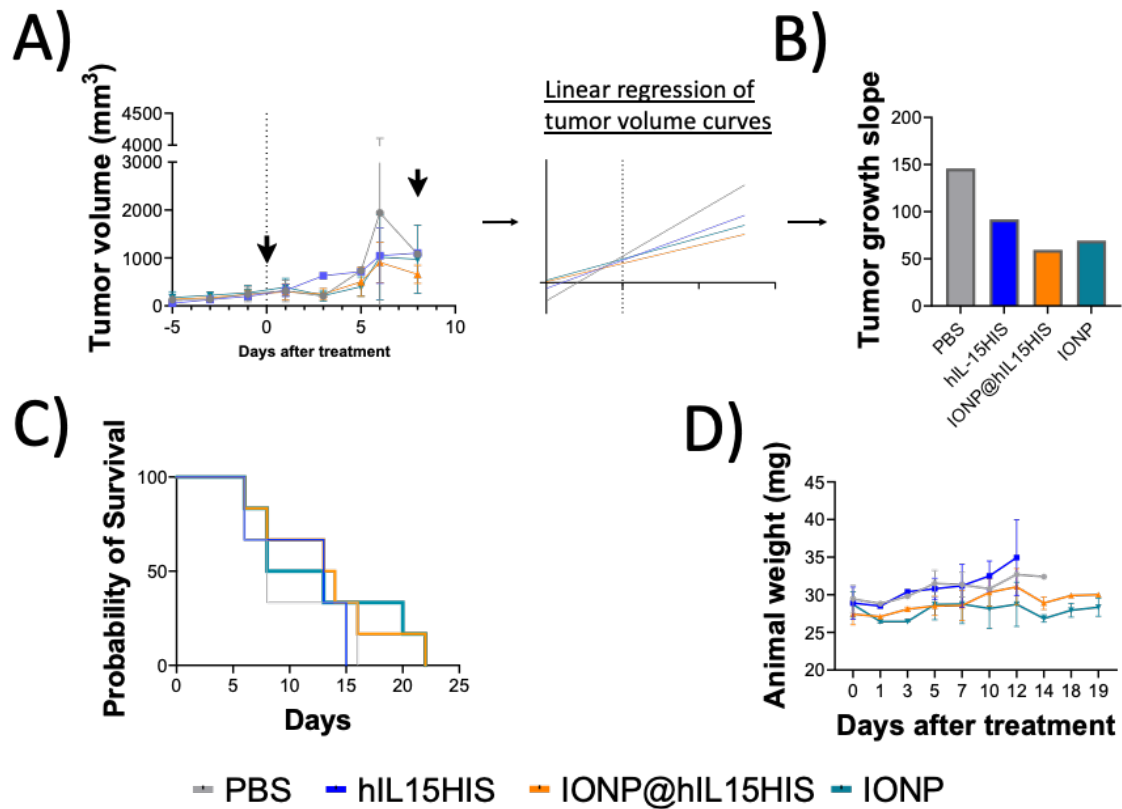


Figure 4.8. Therapeutic effect of systemically administered hIL-15HIS and IONP@hIL15HIS in the mouse B16F10 model. B16F10 tumor bearing C57BL/6 mice were treated with hIL-15HIS in its soluble or immobilized form in IONP micelles (IONP@hIL15HIS). (A) Tumor size mean (dots) and standard deviation (error bars) are represented in XY graph. Arrows in the graph represent the day of treatment. Also, the analysis of the linear regression of the means is showed. (B) The resulting slope of the linear regression analysis of the size mean curve is represented in the bar graph. (C) The survival rate (represented as probability of survival in percentage) is showed. (D) Animal weight expressed as mean and standard deviation in error bars is showed in XY graph. No statistical analysis was possible to perform in the tumor size curves due to the small sample size. Statistical analysis of survival curves did not show significant differences (n=3-6).

The results did not show significant differences, but we would like to suggest that the IONP@hIL15HIS formulation may show some potential. Not only because the tumor growth moderately decreased, but also because the NP formulation appears to be biocompatible as it was demonstrated on chapter III and because, it has not caused big damage in animals in the *in vivo* models. However, as it has been reported in other scientific works, even in clinical trials, IL-15 monotherapy shows limited efficacy. Therefore, the combination with other

immunotherapy strategies such as checkpoint inhibitors, as for example anti-PD-L1^{586,587}, is getting attention with promising results.

In addition to monitor tumor growth, blood samples were acquired one day before each IL-15 infusion and NK and T cell populations were analyzed (Fig. 4.9). Regarding NK cells, it could be said that in the groups treated with IL-15 formulations (soluble or immobilized) there is a tendency to an increase in cell frequency. Regarding total T cells, the frequency of them appear to decrease at day 7 (after 1 dose) in all conditions but, at day 14, hIL-15HIS and IONP@hIL15HIS caused an increase in T cell frequency, probably due to an increase in the percentage of CD4+ (hIL-15HIS) and CD8+ (IONP@hIL15HIS) T cells. The CD8/CD4 T cell ratio is lower than 1 under all conditions, and the highest ratio was observed in the IONP@hIL15HIS treated group. It is accepted that an antitumor effect is achieved mostly by CD8+ T cells^{588,589}, suggesting that the increase frequency in this subset when animals receive IONP@hIL15HIS could help to better control tumor growth. Nevertheless, others have shown that treatment with an anti-OX40 agonist (provides a survival signal to activated T cells) and programmed cell death-1 (PD-1) blockade that the CD4+ T cell population was essential for tumor elimination and also for antitumor memory⁵⁹⁰.

The activation profile of circulating NK and T cells was evaluated by CD69 expression levels (Fig. 4.10). It was observed that CD69 expression was increased by day 7, after the first infusion of IL-15 and controls, in all conditions with a tendency to be higher in mice receiving IONP@hIL15HIS, although the differences were not statistically significant. This increase in CD69 expression at day 7 was observed in both cell subsets, but only persisted until day 14 on NK cells, while on T cells CD69 expression returned to day 0 levels. These results suggest that NK cells are activated longer time than T cells. There is a work in where the high expression of CD69 in human *in vitro* cultured NK cells at day 7, predicted augmented cytotoxicity against human breast cancer cells⁵⁹¹. Therefore, it could be suggested that the CD69 high expression (not statistically) observed at day 7 in NK cells from mice receiving

IONP@hIL15HIS (Fig. 4.10 B), will be translated into higher cytotoxicity against tumor cells as it happens in the cited article.

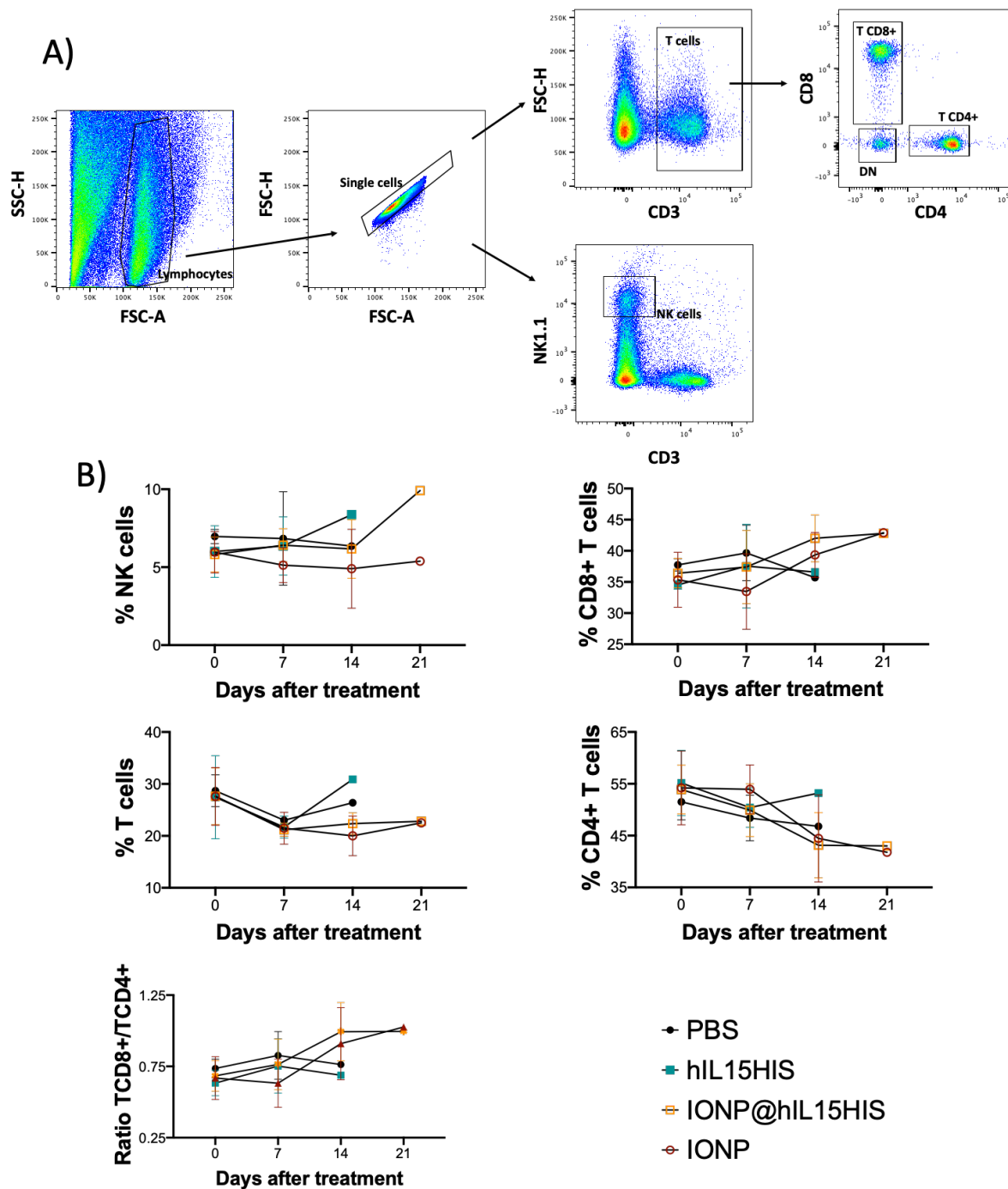


Figure 4.9. NK and T cells frequencies in blood. Blood samples of mice were collected one day before treatment (50 $\mu\text{g}/\text{mouse}$ of IL-15 formulations) administration during the course of the experiment (day 0, 7, 14 and 21). (A) Gating strategy for the identification of NK, T and CD8+ T and CD4+ T cells from an IONP@hIL15HIS treated mouse at day 7. (B) The percentages of cells are represented in XY graphs. Points represents the mean and the error bars represents the standard deviation. (n= 3-6).

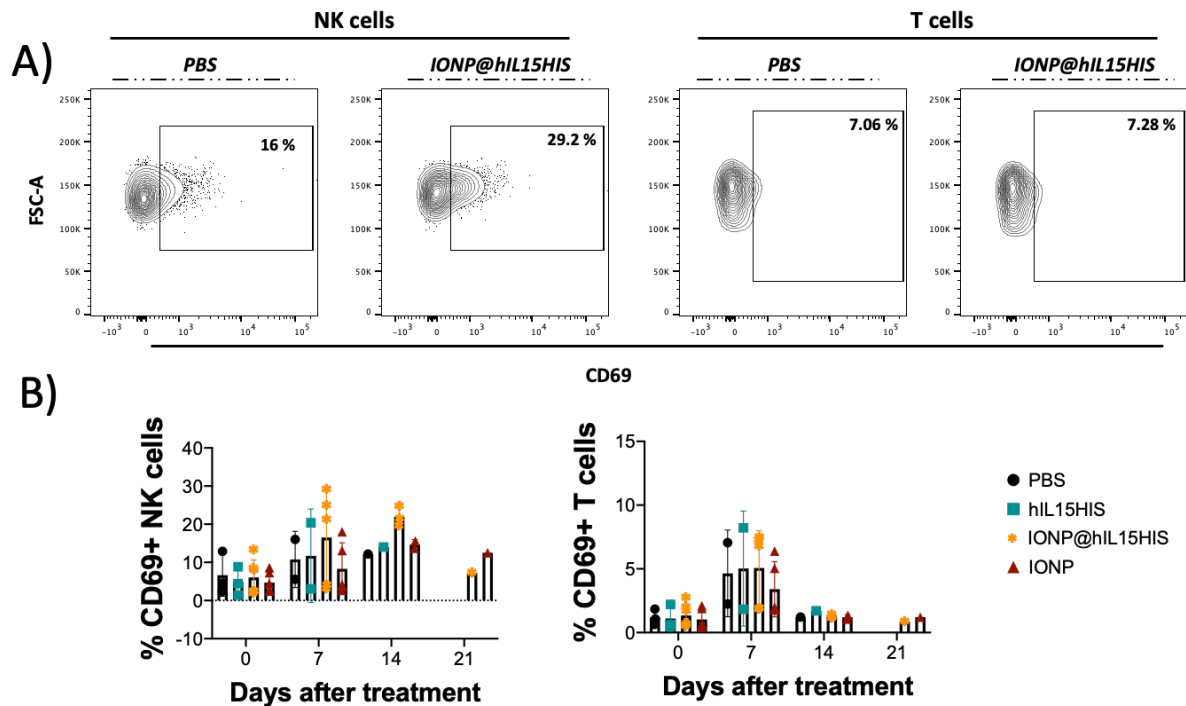


Figure 4.10. Expression of CD69 activation marker in circulating cells the day before treatment. (A) Representative example of contour plots showing CD69 expression on NK and T cells from PBS and IONP@hIL15HIS treated mice. (B) Mean of CD69+ cell percentage is showed in bar charts, where mean is represented in bars and the standard deviation by error bars. Each animal data is showed in points, squares, stars and triangles. Treatment: 50 μ g/mouse of IL-15 formulations. (n= 3-6).

Mouse T cells are a heterogeneous pool of cell subsets with different phenotypes and functions. CD8+ and CD4+ T cells can be separated in different subsets such as memory, effector and naïve T cells. Some cell membrane receptors, such as CD62L and CD44, allow discriminating between these subsets. CD44+ T cells (CD8+ and CD4+) are classified as memory T cells, and CD44- are considered naïve T (T_N) cells⁵⁹². Memory T cells also could be subdivided in effector and central memory cells depending on the low (effector memory, T_{EM}) or high (central memory, T_{CM}) expression of the CD62L lymphoid trafficking marker^{593,594}.

T_{EM} and T_{CM} CD8+ T cells subsets behave in a similar way in response to hIL-15HIS and IONP@hIL15HIS at days 0 and 7 (Fig. 4.11). There is a tendency of a small increase of T_{CM} cell frequency compared with PBS control at day 7 when mice are treated with hIL-15HIS and IONP@hIL15HIS. On the contrary, the frequency of T_{EM} cells did not change over the time in hIL-15HIS and IONP@hIL15HIS treated groups. T_N cell frequency was lower under

IONP@hIL15HIS at day 0 and 7, but at day 14 increased in percentage to a higher level than hIL-15HIS treated group. In general, these results suggest that the IL-15 formulations caused a redistribution of T cell subpopulations with an increase of memory T cells, which is in agreement with the literature⁵⁹⁵.

Regarding CD4+ T cells subsets (Fig. 4.12), both T_{EM} and T_{CM} percentages tended to be higher in the IONP@hIL15HIS treated group than in the hIL-15HIS group at day 0 and at day 7. At day 14, highest T_{EM} and T_{CM} cells frequencies were observed in the hIL-15HIS group, although it is not possible to conclude anything from day 14 since there was one single mouse per condition. CD4+ T_N cell frequency was generally maintained at all time points at similar values independently of the treatment mice received.

The finding of higher frequencies, although not significant, of T_{EM} and T_{CM} cells in animals receiving IONP@hIL15HIS, more evident at day 7, could suggest that T cells may exert a better antitumor effect. Considering all data together, it may be that increased T cell memory/effector frequencies are associated with slower tumor growth. At day 0 and 8 mice received the infusion of formulations. Between those two infusions days the tumor grows slower in the IONP@hIL15HIS treated group, which could be associated with the higher T subpopulations frequencies observed at day 7. In addition, IONP@hIL15HIS group showed higher probability of survival. T_{EM} and T_{CM} would protect against tumor progression because their response will be faster and bigger⁵⁹⁶, and maybe they could contribute to avoid metastasis, as it has been shown in other tumor models⁵⁹⁷⁻⁵⁹⁹. Nevertheless, this affirmation must be taken very carefully because all solid tumors with higher tumor immune cell infiltration did not display the same good prognosis⁶⁰⁰. In fact, it has been described that in renal cell carcinoma the tumor infiltration by memory T cells is associated with poor prognosis⁶⁰¹.

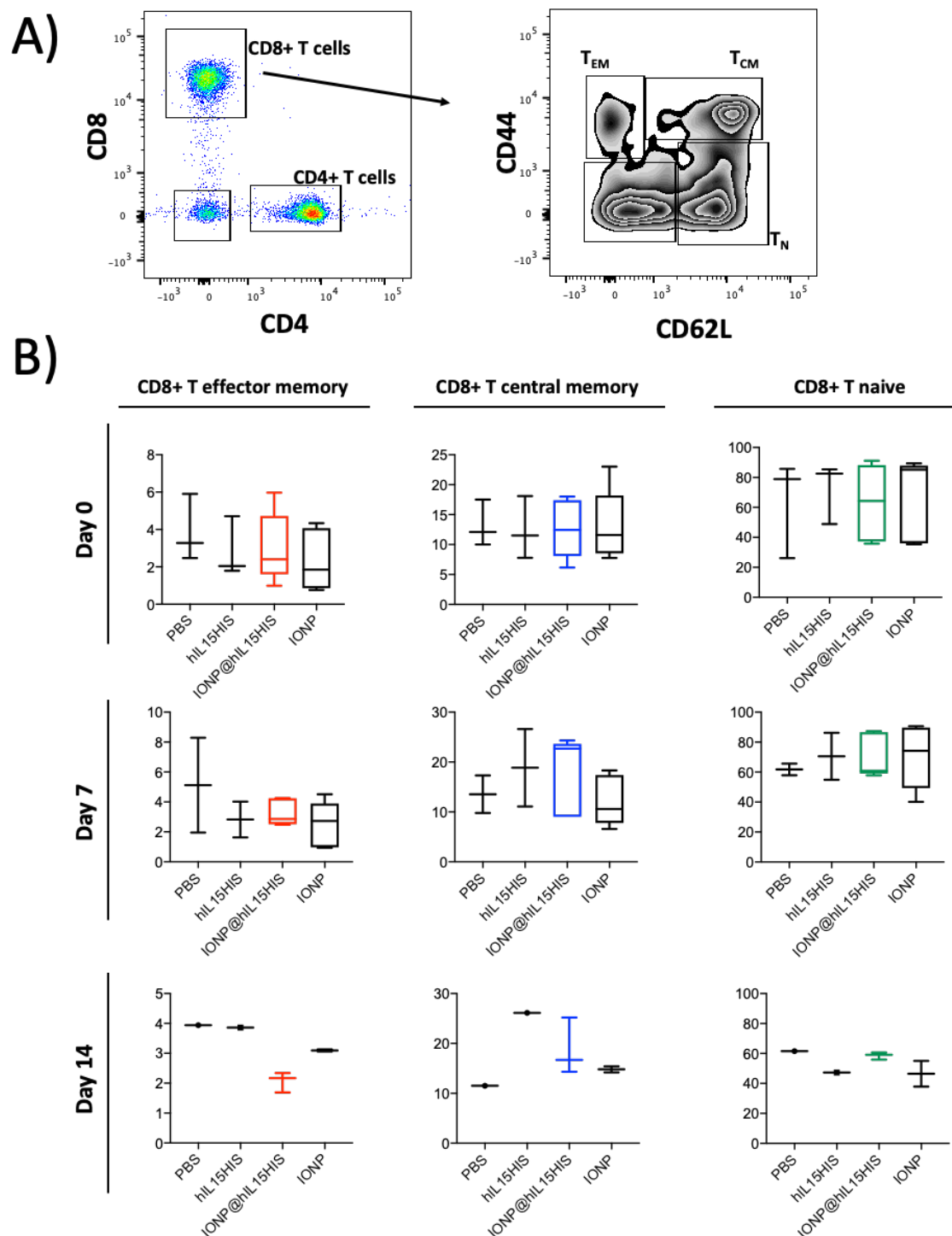


Figure 4.11. CD8+ T cells subpopulations frequencies in blood the day before treatments. (A) T cell subpopulations (T_{EM}, T_{CM} and T_N) were identified by the differential expression of CD62L and CD44 as it is showed in dot and zebra plots. (B) Frequencies of these populations are showed in boxes and whiskers plots (horizontal line represents the median, the lower part of the box is the Q1 and the top part of the box is the Q3, whiskers are the maximum and minimum data value) at different time points during the *in vivo* experiment: day 0, day 7 and 14 after treatment. Treatment: 50 µg/mouse of IL-15 formulations. T_{EM}: effector memory T cells, T_{CM}: central memory T cells and T_N: naive T cells. (n=3-6).

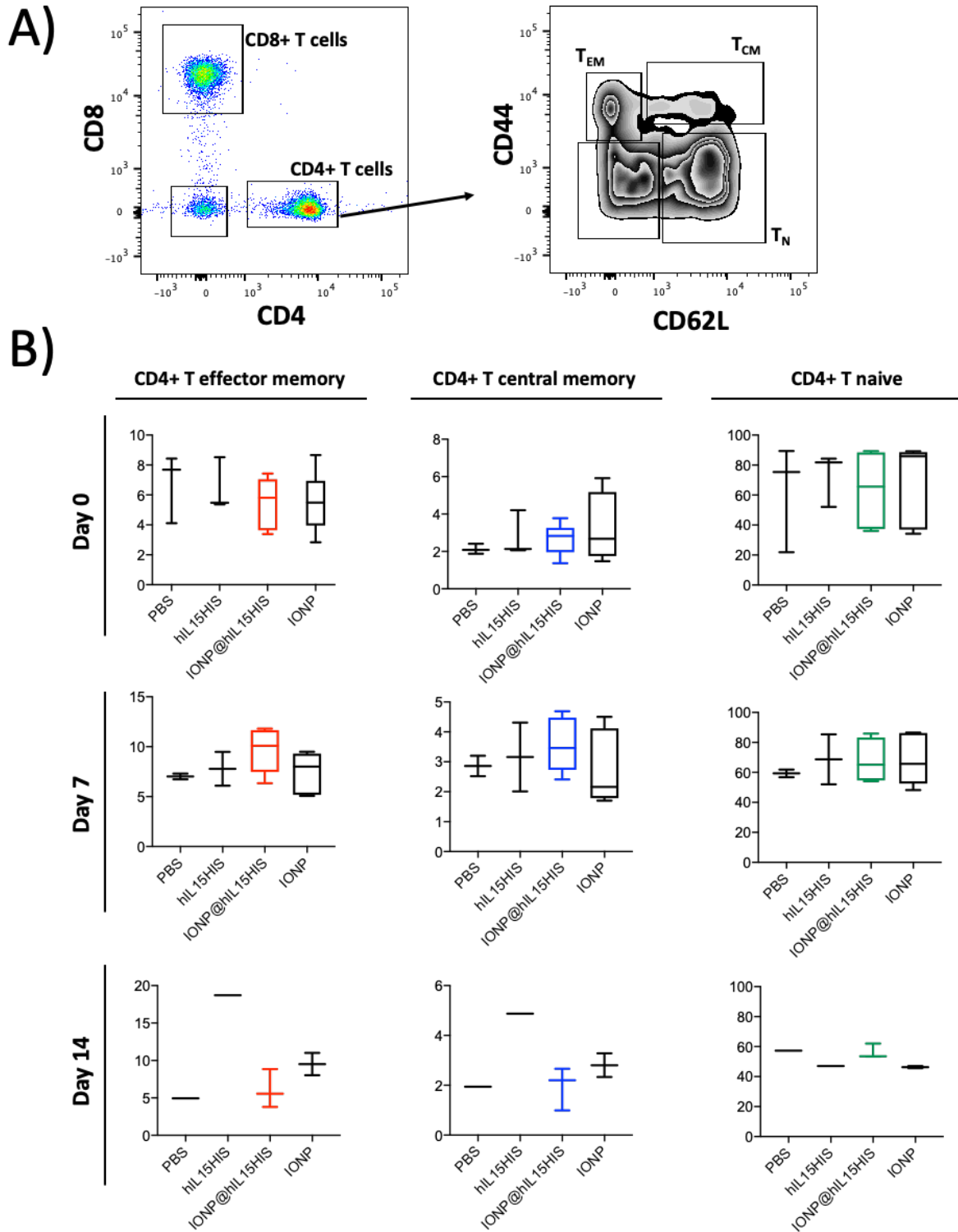


Figure 4.12. Percentages of CD4+ T cells subpopulations in blood the day before treatment. (A) T cell subpopulations (T_{EM} , T_{CM} and T_N) were identified by the differential expression of CD62L and CD44 as it is showed in dot and zebra plots. (B) Frequencies of these populations are showed in boxes and whiskers plots (horizontal line represents the median, the lower part of the box is the Q1 and the top part of the box is the Q3, whiskers are the maximum and minimum data value) at different time points during the *in vivo*

experiment: day 0, day 7 and 14 after treatment. Treatment: 50 $\mu\text{g}/\text{mouse}$ of IL-15 formulations. T_{EM} : effector T memory cells, T_{CM} : central memory T cells and T_N : naive T cells. (n=3-6).

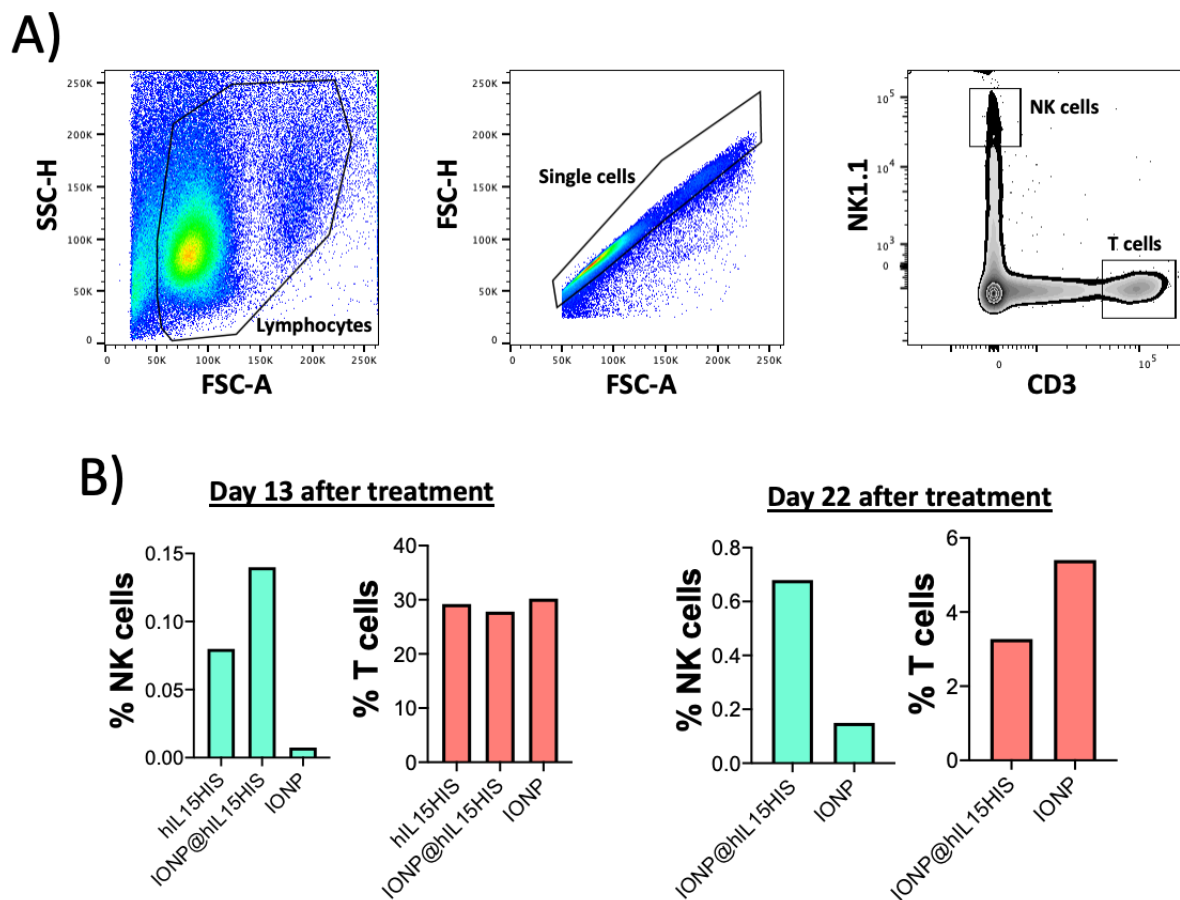


Figure 4.13. Tumor infiltrating cell quantification. (A) NK and T cells were identified by the expression of NK1.1 and CD3 as it is showed in dot and zebra plots. (B) Bar charts represent the percentage of NK and T cells in tumors. n=1 per condition.

Finally, tumors were collected for further flow cytometry-based analyses. However, the experiment design did not allow us to sacrifice all the mice on the same day. Still and all, we analyzed some tumors from mice that were sacrificed on the same day by humane endpoint (Fig. 4.13). Tumors were processed and samples were acquired in the flow cytometer. The data presented in the figure 4.13 B shows the percentage of NK and T cells within the tumor. Higher tumor infiltration of NK cells was observed in mice receiving IONP@hIL15HIS. Although very preliminary, this is quite interesting because functionalization of IL-15 in the IONP based micelle may enhance NK cell infiltration into the tumor. Publications have shown that high NK

cell infiltration in solid tumors is associated with better prognosis^{602,603}. However, it is also known that the success of NK cell antitumor activity will be defined by the TME⁶⁰⁴. T cell frequency did not show differences at day 13, although at day 22 seems that the mouse receiving IONP exhibited more T cells in the tumor than the one that received IONP@hIL15His treatment. This higher total T cell frequency must be carefully considered because T cell subsets are not properly characterized. Undoubtedly, more experiments need to be performed to obtain conclusive data.

In vivo application of IONP@hIL15HIS

4.3. Conclusions

After *in vitro* experiments where NK and T cells enhanced effector functions were observed following IL-15 formulations stimulation, *in vivo* experiments were carried out with two different purposes: 1) IL-15 primed ACTT-based biodistribution study and 2) antitumoral effect of IONP@hIL15HIS against B16F10 tumor.

Regarding to the ACTT model, it was expected higher expansion rates of NK and T cell populations in the analyzed tissues after human PBMCs infusion in NSG mice. As it is suggested in the result section, with longer expansion (including an expansion phase *in vitro*) and other cytokines such as IL-15 for the expansion phase could lead to higher cell expansion rates. Remarkably, homing receptors expression (CXCR4 and CD62L) and cell migration to the specific tissue (bone marrow or lymph node) was correlated. Cells expressing CXCR4 were localized in the bone marrow and no in the lymph node. In the same way, cells expressing CD62L were localized in the lymph nodes and no in the bone marrow. In addition, the expression of those homing receptors tended to be higher in IONP@hIL15HIS condition. Interestingly this effect was also observed *in vitro* with higher expression of homing receptors when cells were treated with IONP@hIL15HIS. This higher expression of homing receptors could suggest a higher migration capacity of cells under this stimulating condition to each respective tissue (CD62L, lymph node; CXCR4, bone marrow).

The antitumor effect was studied in a B16F10 tumor bearing C57LB/6 mouse model and the therapeutic effect was monitored measuring the tumor size and the animals weight. Blood extractions also were carried out to better understand the systemic effect of IONP@hIL15HIS infusion. B16F10 tumor is very aggressive, and it was not possible to study the therapeutic effect for more than 21 days after tumor reached 300 mm³ in volume. Mice displayed ulcers or big tumor size (>1500 mm³) and they must be euthanized as specified by the approved protocol by the Ethics Committee. The results presented showed a slightly therapeutic effect

In vivo application of IONP@hIL15HIS

in the IONP@hIL15HIS treated group with higher survival probability and smallest slope of tumor size increase. It could also be concluded that, at least, the material with which the NP is made up do not affect dramatically the wellbeing of the animals and no loss of animal weight was observed.

Taken all together, these findings suggest that IONP@hIL15HIS could be an effective vehicle for promoting cell stimulation *in vivo* against cancer disease. Nevertheless, experiments performed with, at least, higher number of animals and different dosage must be performed to obtain more conclusive results.

Summary of results and general conclusions

This thesis demonstrates the feasibility of an IL-15-based nanoformulation that may have the potential to become an anti-tumor immunotherapy tool. The results obtained in this thesis lead to the following main conclusions:

- ◆ Nanomicelles of approximately 50 nm in size can be obtained by the encapsulation of hydrophobic IONP with PEG-PLs with carboxylic group as terminal groups for further functionalization.
- ◆ Recombinant IL-15 protein produced and purified in the laboratory exhibited a purity grade similar to commercial IL-15. This protein is capable of activating NK and T cells at a similar degree as commercial IL-15.
- ◆ IONP micelles functionalized with IL-15 protein were achieved through the subnanomolar affinity binding of NTA to the His-tag protein, resulting in a simple and reproducible protocol for His-tagged proteins functionalization onto nanoparticles containing carboxylic groups.
- ◆ The nanoformulation IONP@hIL15HIS showed colloidal on shelf stability according to size distribution measurements over almost 1 month.
- ◆ *In vitro* stimulation with soluble IL-15 and the immobilized form (IONP@hIL15HIS) induce T and NK cells activation as shown by changes in the expression levels of several markers. While the expression of certain markers was similar following stimulation with both IL-15 formulations, other markers exhibited higher expression after IONP@hIL15HIS stimulation compared with soluble IL-15. Homing receptors expression exhibits a tendency to be less downregulated when NK and T cells were stimulated with IONP@hIL15HIS, which may be associated with a higher migration capacity of cells to the tissues of interest.
- ◆ B16F10 tumor-bearing mice treated with IONP@hIL15HIS tended to exhibit slower tumor growth and an increased survival rate, although the results were not statistically significant. The administration of IONP@hIL15HIS does not cause significant harm to mice, making the nano-formulation safe for *in vivo* experimentation.

- ◆ Homing receptors expression associates with cell migration to tissues and organs. Human cells which migrate to the bone marrow express CXCR4 and those that migrate to the lymph nodes express CD62L.
- ◆ The expansion of human PBMCs in NSG mice was lower than expected, not achieving a human/mouse hematopoietic cell ratio (hCD45+/mCD45+ cell ratio) higher than 1 in almost all tested conditions and analyzed tissues.

Although the *in vitro* and *in vivo* results are not conclusive, the work carried out in this thesis is a valuable contribution to the current knowledge in immunotherapy, specifically to the use of IL-15 as an anti-tumor agent. Moreover, a Fe-based NP formulation has been designed, developed and tested as a vehicle for IL-15 on the NP surface, in an attempt to mimic the physiological transpresentation of the protein by monocytes and dendritic cells to NK and T cells.

EXPERIMENTAL SECTION

Experimental section

1. Synthesis and characterization of hydrophobic IONPs and IONP-filled micelles

- **Hydrophobic IONPs.** Hydrophobic magnetite (Fe_3O_4) nanoparticles (named iron oxide nanoparticles, IONP) were synthesized by thermal decomposition method. The synthesis was carried out with iron (III) acetylacetonate (2 mmol), 1,2-hexadecanediol (10 mmol), oleic acid (6 mmol), oleylamine (6 mmol) and benzyl ether (20 ml). These reagents were mixed under nitrogen flow and heated at 210°C during 2h. After that, the mixture is heated until 300°C for 1h. Then, the synthesis was kept cooling down to room temperature (RT) and ethanol (40 ml) was added in order to precipitate nanoparticles (NP). These precipitated NPs were separated by centrifugation (3000 xg, 30 min). The pellet was dissolved in hexane (10 ml) with oleic acid (0.05 ml) and oleylamine (0.05 ml). Sample was centrifuged (3803 xg, 10 min) to remove any undispersed residue. Then, ethanol (20 ml) was added and, finally, sample was centrifuged again (3803 xg, 10 min) and kept evaporating the remaining ethanol. Resulting hydrophobic Fe_3O_4 nanoparticles (hIONPs) were characterized by Transmission Electron Microscopy (TEM) and the hIONP size were analyzed in Image J software where a minimum of 200 nanoparticles were measured.
- **Water soluble IONP micelles.** 1 mg of 6 nm diameter hIONP and 2 mg of PEG-COOH (1,2-distearoyl-sn-glycero-3-phosphoethanolamine-N-[carboxy(polyethylene glycol)-2000], Avanti, CAS 1403744-37-5) were dissolved in chloroform (500 μL) and it was allowed to evaporate overnight (ON) at RT. In this process, a film of phospholipid and nanoparticles was formed stuck to the vial. This film was heated in a water bath at 80°C for 30 seconds and rehydrated with 1 ml of nanopure water, causing the micelation of hydrophobic nanoparticles into phospholipid monolayer. The solution was centrifuge at 7300 xg for 5 minutes in order to discard the large NPs formed in the self-assembling process of micelation. The pellet was discarded, and the supernatant was filtered (0.45 μm). The filtered supernatant (SN) was ultracentrifuged 3 times at 369000 xg during 45 minutes in order to eliminate free liposomes formed. The final pellet was resuspended in a desired volume of water or saline buffer and stored at room temperature. The resulting IONP micelles (IONPm) were characterized measuring 3 times the Dynamic Light Scattering (DLS) and the intensity data was plotted in GraphPad Prism 9 and analyzed with Gaussian fit to obtain the size mean.

2. Protein design, expression, and purification

Based on the human IL-15 (hIL-15) sequence available in Ensemble genome browser web page, the following complementary DNA (cDNA) and protein sequences were selected: NM_172175 and NP_751915. The gen construct was purchased to Biomatik with BamHI at 5' and HindIII at 3' in a pUC57 vector.

A) Coding DNA sequence (CDS) of hIL-15 gene cloned into pUC57 vector and the sequence of the protein:

hIL-15 CDS

```
ggatccAACTGGGTGAATGTGATTAGTGATCTGAAAAAGATTGAGGATCTGATTCAGAGTATGC
ATATTGATGCCACCCTGTATACCGAAAGTGATGTGCATCCGAGTTGTAAAGTGACCGCAATGAA
ATGTTTTCTGCTGGAAGTGCAGGTTATTAGCCTGGAAAGCGGTGACGCAAGTATTCATGATACC
GTGAAAAATCTGATTATTCTGGCAAATAATAGCCTGAGCAGCAATGGTAATGTTACCGAAAGTG
GTTGCAAAGAATGCGAAGAAGTGGAAAAGAAAAATATTAAGGAGTTCCTGCAGAGTTTTGTTC
ATATTGTGCAGATGTTTATCAACACCAGCTAAaagctt
```

hIL-15 protein sequence

```
GSNWVNVISDLKKIEDLIQS Met HIDATLYTESDVHP SCKVTA Met KCF L
LELQVISLES GDASIHDTVENLIILANNSLSSNGNVTESGCKECEELEKK
NIKEFLQSFVHIVQ Met FINTS Stop
```

B) CDS of hIL-15 gene cloned into pProEX-HTa vector and the sequence of the protein:

hIL-15 DNA

```
CATCACCATCACCATCAGATTACGATATCCCAACGACCGAAAACCTGTATTTTCAGGGCGCCAT
GggatccAACTGGGTGAATGTTATTAGTGATCTGAAAAAGATTGAGGATCTGATTCAGAGCATGC
ATATTGATGCAACCCTGTATACCGAAAGTGATGTTTCATCCGAGCTGTAAAGTGACCGCCATGAA
ATGCTTTCTGCTGGAAGTGCAGGTTATTAGTCTGGAAAGTGGTGACGCCAGCATTTCATGATACC
GTGAAAAATCTGATTATTCTGGCCAATAATAGTCTGAGCAGCAATGGCAATGTTACCGAAAGTG
GCTGTAAAGAATGCGAAGAAGTGGAAAAGAAAAATATTAAGGAGTTCCTGCAGAGTTTTGTGC
ATATTGTGCAGATGTTTATTAACACCAGCTAA
```

Histidine-tagged hIL-15 protein sequence

```
HHHHH DYDIPTTENLYFQGA Met GSNWVNVISDLKKIEDLIQS Met HI
DATLYTESDVHP SCKVTA Met KCF LLELQVISLES GDASIHDTVENLIIL
ANNSLSSNGNVTESGCKECEELEKKNIKEFLQSFVHIVQ Met FINTS Stop
```

Figure ES1. DNA and protein sequences of hIL-15 cloned in pUC57 and pProEX-HTa vectors. It is marked in blue the hIL-15 CDS and the corresponding aminoacids (aa) sequence. Green and maroon highlighted small sequences are BamHI and HindIII restrictions sites respectively. Pink highlighted letters correspond to the His-tag encoding DNA sequence and the corresponding 6x histidine sequence.

hIL-15 CDS from pUC57 vector was cloned into a pProEX-HTa vector for the fusion of a His-tag for affinity purification and for the IONP biofunctionalization strategy. The His-tag was designed to be at N-terminal of IL-15 based on 4GS7 and 2Z3Q pdb structures. It was confirmed that the addition of His-

tag sequence did not affect the binding of IL-15 to the $\beta\gamma_c$ receptor. All sequences were confirmed using SnapGene software and protein structure visualization was carried out in PyMol.

Once the hIL-15 coding sequence was cloned in pProEX-HTa vector, the vector was transformed into *Escherichia coli* C41 strain for the expression of the His-tagged protein. A single colony was used to inoculate an ON culture of 10 ml of fresh LB medium containing 100 $\mu\text{g/ml}$ of ampicillin and then grown ON at 37°C in a shaking incubator. 10 ml of overnight pre-culture was used to inoculate 1 L of fresh LB medium containing 100 $\mu\text{g/ml}$ of ampicillin (Amp). The culture is kept until reaches an optical density (OD) of 0.8-1 at 600 nm. Then, protein expression was induced with isopropyl- β -D-1-thiogalactopyranoside (IPTG) at a final concentration of 0.4 mM. Protein expression was performed ON at 20°C. The cells were centrifuged at 550 $\times g$ during 15 minutes at 4°C and pellet was resuspended in a denaturing lysis buffer (500 mM NaCl, 6M urea, 5 mM Tris pH= 8) and was frozen at -20°C ON. After cold incubation of lysis solution, lysozyme (1 mg/ml of culture) (Merck), DNase I 10x (5 μL) (ThermoScientific) and protease inhibitor (1 tablet) (Roche) were added and incubated at 4°C for 30 minutes. The lysate was centrifuge at 1050 $\times g$ for 45 minutes and SN was incubated with High Density Nickel Agarose (Jena Bioscience) (1ml/L of culture) mixing at 4°C for 45 minutes. The protein purification was carried out by gravity flow through High-Density Nickel Agarose pre-incubated with lysate SN. The washing step was carried out using two buffers: 1) With high NaCl concentration buffer and Triton (1 M NaCl, Imidazol 10 mM, Triton 0.1%, 50 mM Tris pH= 7.4) and 2) Same as buffer 1, but without Triton. The protein elution was carried out in a buffer with Urea at low concentration (300 mM NaCl, Imidazol 300 mM, 0.5 M Urea, 50 mM Tris pH= 7.4) and the eluted protein was dialyzed ON in PBS buffer (50 mM NaCl, 150 mM phosphate buffer pH 7.4). Depending on the degree of purity observed in the electrophoresis gel, the sample was re-purified in an additional Ni affinity column or was applied a Fast Protein Liquid Chromatography (FPLC) step over a Superdex 75 HiLoad column. The monitorization of the protein within the fractions was performed by 280 nm absorbance and selected fractions were analyzed in 15% polyacrylamide gels to confirm the purity of the protein. Once the protein was pure, the concentration was determined by UV-absorbance at 280 nm using the extinction coefficient calculated from the amino acid composition ($13200 \text{ M}^{-1} \text{ cm}^{-1}$). The secondary structure of the protein was verified by Circular Dichroism (CD).

3. Bioconjugation of hIL-15HIS in IONP micelles

The limiting molecule was considered the carboxylic groups of the PEG-COOH phospholipid. Hence, to the suspension of IONPm (stock PEG-COOH = 0.179 μmol), EDC and NHS in 1:100:50 (COOH:EDC:NHS) molar ratio were added in a total volume of 500 μL and incubated under stirring during 2h at 37°C in a thermomixer (Thermo Fisher Scientific). After reagent excess purification in a NAP-5 prepacked column (GE Healthcare Life Science) Nitrilotriacetic acid-Lys (NTA-Lys) (Merck) molecule in 1:21 (COOH:NTA) molar ratio was added in total volume of 500 μL , and incubated under stirring ON at 37°C. Once the covalent binding was formed (IONP-NTA), NAP5 column was again used to eliminate reagent excess and to change the reaction media from PBS to H₂O in this case. Then, IONP-NTA was incubated with Ni₂SO₄ at 1:20 (COOH: Ni₂SO₄) molar ratio in 1 ml as reaction volume during 2h at RT at 20 rpm. After Ni₂SO₄ excess was eliminated, hIL-15HIS (which contains His-tag sequence) was added in a 1:1 (COOH:hIL-15HIS) molar ratio and in a total volume of 500 μL during 1h at RT to induce the coordination binding of the protein with the NTA molecule. A final gel filtration purification step to eliminate the not bound protein to the IONPs was carried out through 6cLB column.

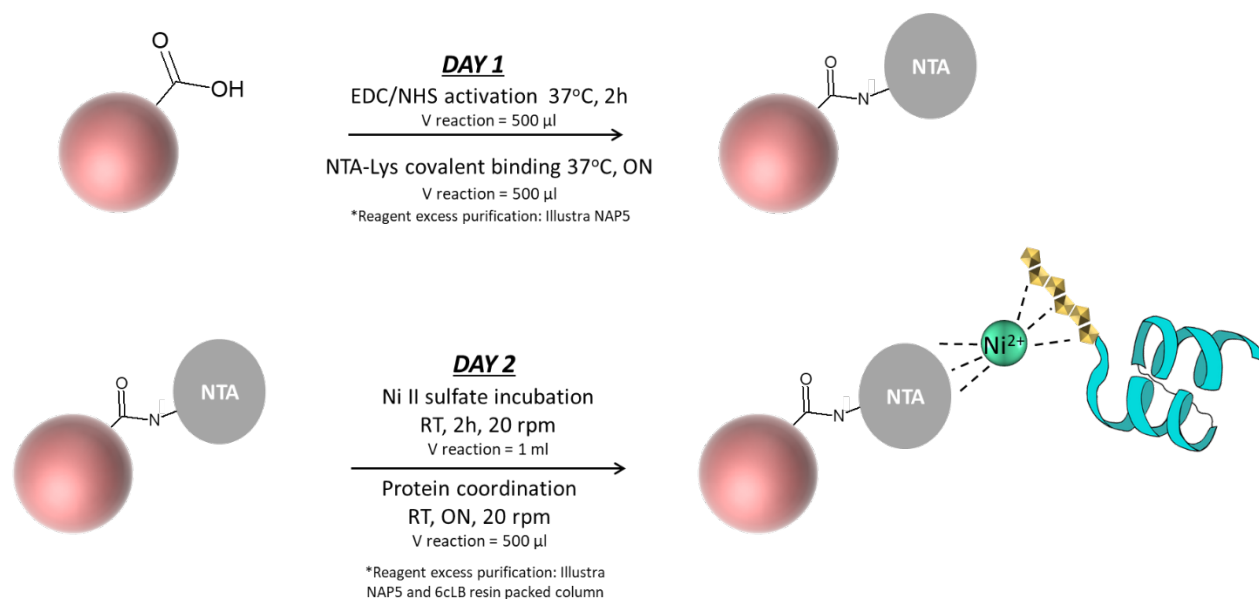


Figure ES2 Conjugation strategy reaction scheme. NTA-Lys molecule binds to the carboxylic group of phospholipid covalently and the protein bind to the NTA molecule by coordination between NTA-Ni²⁺-hIL-15HIS.

4. Cell culture

- **Blood samples management.** Blood samples are from adult healthy donors and were collected through the Basque Biobank for Research (<http://www.biobancovasco.org>). The Basque Biobank complies with the quality management, traceability and biosecurity established in the Spanish Law 14/2007 of Biomedical Research and in the Royal Decree 1716/2011. All subjects wrote and signed the informed consent in accordance with the Declaration of Helsinki. The protocol was approved by the Basque Ethics Committee for Clinical Research (PI+INC-BIOEF 2014-02 14-27 and PI2014079).
- **Peripheral blood mononuclear cells (PBMCs) isolation.** PBMCs were isolated from buffy coats by ficoll (GE Healthcare) density centrifugation. For the experiments, both fresh and frozen PBMCs were used. For cell stimulation and culture, PBMCs were cultured in a cell incubator (37°C, 5% CO₂ and 95% O₂ atmosphere with 95% of relative humidity) in RPMI medium (Gibco) supplemented with 10% human AB serum (Invitrogen), 1% GlutaMax (ThermoFisher Scientific) and 1% penicillin/streptavidin (ThermoFisher Scientific). This supplemented medium was called complete RPMI medium or cRPMI.
- **PBMCs proliferation assay.** For proliferation assay 4x10⁶ cells/ml were stained with 0.5 μM CFSE before the preactivation phase following the manufacturer protocol. Then, PBMCs were plated in a 48-well plate at 1x10⁶ cells/ml in the presence of IL-12, IL-18 and hIL-15HIS or IONP@hIL15HIS (10, 50 and 63,10 ng/ml respectively) for 16-18h. After the pre-stimulation phase, cells were washed and cultured in the cell incubator in cRPMI during 4 days in the presence of IL-2 (2-20 U/ml) for their expansion. Then, cells were collected and stained for flow cytometer acquisition and analysis. This assay was also used to determine the proliferation of PBMCs incubated with bare IONPm (5 and 10 μm/ml of Fe) and IL-2 (1000 U/ml) during 4 days. In this case the pre-stimulation phase was not considered.
- **Cell activation markers and polyfunctionality at day 0 and day 4.** To study activation and polyfunctionality of PBMCs at day 0, cells in cRPMI were plated in a 48-well plate at 1x10⁶ cells/ml in the presence of IL-12, IL-18 and hIL-15HIS or IONP@hIL15HIS cytokines (10, 50 and 63.10 ng/ml respectively) for 16-18h in the incubator. After this incubation period, cells were collected and

stained for acquisition in a flow cytometer. To study cells at day 4, after the pre-activation phase, cells were washed and resuspended in cRPMI with IL-2 or IL-15 to induce cell expansion. This phase lasted for 4 days. Then, cells were collected and stained for flow cytometer acquisition and analysis.

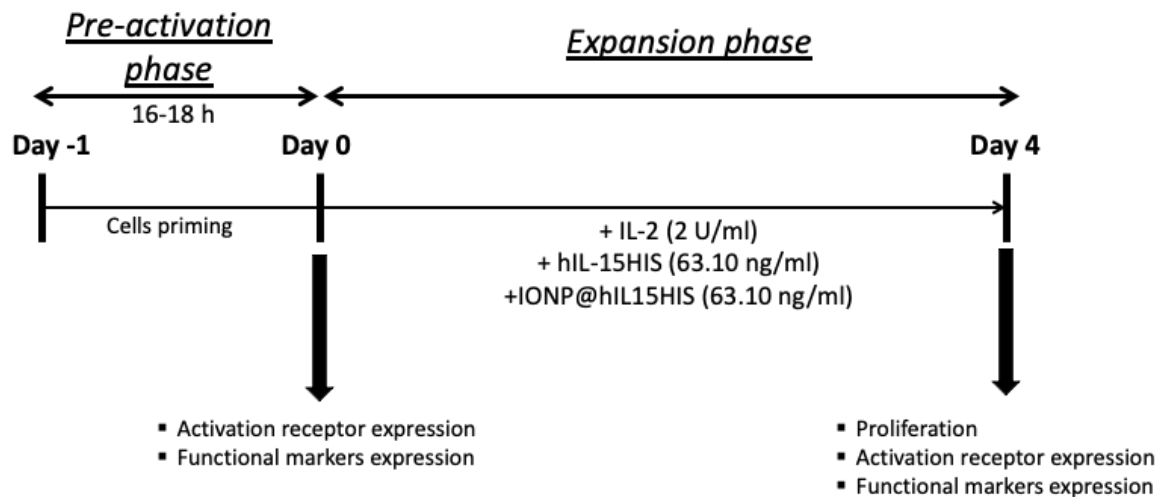


Figure ES3. Scheme of cell culture protocol and the studied parameters. PBMCs were isolated from healthy donors buffy coats and primed during 16-18h (pre-activation phase) to analyze activation and functional markers (day 0). Cells were washed after pre-activation phase and expanded for 4 days with IL-2, hIL-15HIS or IONP@hIL15HIS. At day 4, activation, functional markers and proliferation were determined.

- Cell staining for flow cytometry studies.** Cell viability was determined by staining cells for 30 min on ice and protected from light with LIVE/DEAD™ reagent (Invitrogen) following manufacturer protocol to exclude dead cells in the analysis. After the incubation cells were washed with 2 ml of PBS. For proliferation assays, 4×10^6 PBMCs/ml were labeled with 0.5 μ M CFSE before pre-stimulation phase following a published protocol by the Immunopathology Group in Biocruces Bizkaia Health Research Institute⁵¹¹. Extracellular staining of cell membrane markers was performed by incubating cells for 30 min on ice in the dark with the respective fluorochrome-conjugated mouse anti-human antibodies (see panels in Table ES4). Cells were then washed with PBS containing 2.5% Bovine Serum Albumin (BSA) (Sigma-Aldrich), hereafter PBS-BSA. Next, for the intracellular staining, cells were fixed and permeabilized with BD Cytofix/Cytoperm™ (BD Biosciences) or with paraformaldehyde (4%) and washed with 1X Perm/Wash buffer (BD Biosciences). After the permeabilization step, the respective fluorochrome-conjugated mouse

anti-human antibodies were added for intracellular markers labelling (see panels in Table ES4). After the staining steps, cells were washed twice with PBS and resuspended in PBS followed by the acquisition in the flow cytometer. For the functional assays, after pre-stimulation or expansion phase, fluorochrome conjugated anti-CD107a mAb was added to the culture and incubated at 37° C. After 1h, Golgi Stop and Golgi Plug (brefeldin A and monensin, respectively) protein transport inhibitors were added and incubated 6h at 37° C in the cell incubator.

Table ES1. Flow cytometry panels for multiparametric cell analysis *in vitro*. Automatic compensation with antibody-conjugated beads was performed before cell acquisition.

A) FACS CANTO II. Panel for testing hIL-15HIS activity.

<i>Laser (excitation)</i>	<i>Filters</i>	<i>Fluorochrome</i>	<i>Ab specificity (clone)</i>	<i>Brand</i>	<i>Used volume</i>
Violet (405 nm)	450/50				
	510/50 502LP				
Blue (488 nm)	530/30 502LP	FITC	CFSE	Invitrogen	
	585/40 556LP				
	670LP 655LP	PerCP-Cy5.5	CD3 (SK7)	BioLegend	3 µL
	780/60 735LP				
Red (633 nm)	655/730	APC	CD56 (MEM-188)	BioLegend	3 µL
	750LP				

B) MACSQuant X. Functional markers panel.

<i>Laser (excitation)</i>	<i>Filters</i>	<i>Fluorochrome</i>	<i>Ab specificity (clone)</i>	<i>Brand</i>	<i>Volume</i>
Violet (405 nm)	450/50	BV421	IFN-γ (B27)	BD Biosciences	5 µL
	525/50	BV510	CD3 (UCHT1)	BD Biosciences	3 µL
Blue (488 nm)	525/50	FITC	MIP-1β (D21-1351)	BD Biosciences	20 µL
	585/40	PE	CD107a (REA792)	Miltenyi	2 µL
	655-730				
	750LP	PE-Vio770	CD56 (REA196)	Miltenyi	2 µL
Red (635 nm)	655/730	APC	TNF-α (Mab11)	BioLegend	3 µL
	750LP	Near-IR (NIR) stain	Live/dead fixable NIR	Invitrogen	1 µL

C) MACSQuant X. Activation markers panel.

<i>Laser (excitation)</i>	<i>Filters</i>	<i>Fluorochrome</i>	<i>Ab specificity (clone)</i>	<i>Brand</i>	<i>Volume</i>
Violet (405 nm)	450/50	BV421	CD62L (DREG-56)	BD Biosciences	5 µL
	525/50	BV510	CD3 (UCHT1)	BD Biosciences	3 µL
Blue (488 nm)	525/50				
	585/40	PE	CD25 (M-A251)	BD Biosciences	20 µL
	655-730	PE-Vio615	CD69 (REA824)	Miltenyi	2 µL
	750LP	PE-Vio770	CD56 (REA196)	Miltenyi	2 µL
Red (635 nm)	655/730	APC	CD184 (CXCR4) (12G5)	BD Biosciences	20 µL
	750LP	Near-IR (NIR) stain	Live/dead fixable NIR	Invitrogen	1 µL

D) Fortessa X-20. Activation and effector markers panel.

<i>Laser (excitation)</i>	<i>Filters</i>	<i>Fluorochrome</i>	<i>Ab specificity (clone)</i>	<i>Brand</i>	<i>Volume</i>
Violet (405 nm)	450/50	BV421	CD62L (DREG-56)	BD Biosciences	5 µL
	525/50	BV510	CD3 (UCHT1) CD14 (MφP9)	BD Biosciences	3 µL
	610/20	BV605	CD16 (3G8)	BD Biosciences	4 µL
	670/30				
	710/50	BV711	Perforin (dG9)	BioLegend	3 µL
	780/60				
Blue (488 nm)	530/30	FITC	CFSE	Invitrogen	
	575/25 (575/26)	PE	CD25 (M-A251)	BD Biosciences	20 µL
	610/20	PE-Vio615	CD69 (REA824)	Miltenyi	2 µL
	710/50 (695/40)				
	780/60	PE-Vio770	CD56 (REA196)	Miltenyi	2 µL
Red (635 nm)	670/30	APC	CD184 (CXCR4) (12G5)	BD Biosciences	20 µL
	730/45				
	780/60	Near-IR (NIR) stain	Live/dead fixable NIR	Invitrogen	1 µL

5. In vivo experiments

- **IONP@hIL15HIS primed cells biodistribution (adoptive cell transfer therapy, ACTT).** NOD *scid* gamma mice (6-8 weeks old from The Jackson Laboratory) were intravenously injected with *in vitro* IONP@hIL15HIS primed human PBMCs for 14-16h (3.5 x 10⁶ cells/mouse). Following ACT, mice were intraperitoneally injected with IL-2 (2.5 x 10⁶ IU/kg) every two days (QOD). At day 6,

mice were euthanized by carbon dioxide inhalation and spleen, lymph nodes and blood samples were collected for further analysis by flow cytometry (Table ES5 A).

- **Antitumor effect of IONP@hIL15HIS.** C57BL/6 mice (6–8 weeks old) were subcutaneously injected into the right part of the back with 2.5×10^5 B16-F10 cells diluted in a mixture of Matrigel® and PBS (Matrigel®-to-cells ratio 1:1). On day 6, 13 and 20 after tumor reached 300 mm^3 , blood was extracted for flow cytometric analyses (Table ES5 B). On day 7, 14 and 21 after tumor reached 300 mm^3 , mice were treated with IL-15 formulations (hIL-15HIS or IONP@hIL15HIS) ($50 \mu\text{g}/\text{mouse}$ of IL-15) and vehicle (PBS and IONPm) (the corresponding Fe concentration as in IONP@hIL15HIS condition). Tumor growth was monitored with a digital caliper and volumes calculated by using the formula $(\text{length} \times (\text{width}^2))/2$. Initially, 6 mice per group were used for experiment, but a significant number of them displayed ulcers and only data from mice without ulcers were considered for the final results. Mice were euthanized if they reached the humane endpoint which includes tumor size bigger than 1500 mm^3 , sudden weight loss or tumor ulceration.

Table ES2. Flow cytometry panels for multiparametric cell analysis *in vivo*.

A) FACS Canto II. NOD *scid* gamma mice: Human PBMCs biodistribution panel.

<i>Laser (excitation)</i>	<i>Filters</i>	<i>Fluorochrome</i>	<i>Ab specificity (clone)</i>	<i>Brand</i>	<i>Volume</i>
Violet (405 nm)	450/50	BV421	CD62L (DREG-56)	BD Biosciences	3 μL
	510/50 502LP	BV510	mCD45 (30-F11)	BD Biosciences	2 μL
Blue (488 nm)	530/30 502LP	FITC	hCD45 (HI30)	BD Biosciences	10 μL
	585/40 556LP	PE	CD25 (M-A251)	BD Biosciences	10 μL
	670LP 655LP				
	780/60 735LP	PE-Cy7	CD3 (SK7)	BD Biosciences	5 μL
Red (633 nm)	655/730	APC	CD184 (CXCR4) (12G5)	BD Biosciences	10 μL
	750LP	APC-Vio770	CD56 (REA196)	Miltenyi	2 μL

B) FACS Canto II. C57BL/6 mice: blood NK and T cells panel.

<i>Laser (excitation)</i>	<i>Filters</i>	<i>Fluorochrome</i>	<i>Ab specificity (clone)</i>	<i>Brand</i>	<i>Volume</i>
Violet (405 nm)	450/50	BV421	CD69 (H1.2F3)	BD Biosciences	2.5 µL
	510/50 502LP	BV510	CD4 (RM4-5)	BD Biosciences	2.5 µL
Blue (488 nm)	530/30 502LP	FITC	CD8 (53-6.7)	BD Biosciences	2.5 µL
	585/40 556LP	PE	NK1.1 (PK136)	BD Biosciences	2.5 µL
	670LP 655LP	PerCP-Cy5.5	CD62L (MEL-14)	BD Biosciences	2.5 µL
	780/60 735LP	PE-Cy7	CD3 (145-2C11)	BD Biosciences	2.5 µL
Red (633 nm)	655/730	APC	CD25 (PC61)	BD Biosciences	2.5 µL
	750LP	APC-Cy7	CD44 (IM7)	BD Biosciences	2.5 µL

6. Instrumentation

- Gel electrophoresis.** Sodium dodecyl sulfate polyacrylamide gel electrophoresis (SDS-PAGE) was performed using 15% acrylamide gels on dual-gel vertical electrophoresis systems (kuroGEL Verti 1010 provided by VWR, 700-0166) and with low protein marker (nzytech, MB21401) for protein size fast characterization and for protein purity degree evaluation. PAGE (Invitrogen) was performed occasionally to check the absence of dimerization of protein using a mix of known weight proteins as molecular weight marker. SDS-PAGE and PAGE runs were done at 150 V for 1h and 30 minutes and 200 V for 30 minutes respectively. All gels were stained with Coomassie blue.
- Size exclusion chromatography.** Gel filtration chromatography was performed in an AKTA prime plus Fast Protein Liquid Chromatography (FPLC) equipment from GE Healthcare. The protein samples were injected into a Superdex 75 HL 16/600 size exclusion chromatography column (GE Healthcare) and run at 1 ml/min in PBS with 0.5 M Urea at 4°C. The purified samples were dialyzed in PBS and then collected and stored frozen at -20°C.
- Circular dichroism (CD) measurements.** CD spectra of the proteins was measured in a Jasco J-815 CD Spectrometer in PBS buffer acquired in a 0.1 cm path length quartz cuvette. All CD spectra were recorded from 260 to 190 nm range and the protein concentration was always around 20

µM. Measurement parameters were the following: data pitch = 0.1 nm, speed = 50 nm/min, sensibility = 20 or 200 mdeg, Digital Integration Time (D.I.T.) = 4-8 sec.

- **UV/Vis spectrometer (Nanodrop, plate reader, Jasco).** UV/Vis absorption spectra of protein samples were recorded on a NanoDrop One^c (Thermo Scientific), Synergy H1 microplate reader (Biotek) and on a V-630Bio Spectrophotometer (JASCO analytical instruments). The first one was generally used to calculate the protein concentration from the absorbance at 280 nm. Microplate reader and Jasco provided the spectra from 800 nm to 190 nm to check the conjugation of the protein in the nanoparticle surface by observing the scattering of the NP around 500 nm and the absorption peak of protein at 280 nm simultaneously.
- **Maldi-TOF/TOF mass spectroscopy.** The protein samples were analyzed using MALDI-TOF/TOF MS UltrafleXtreme III (Bruker) mass spectrometer. Used matrix was 4-hydroxy-3-5-dimethoxycinnamic acid 10 mg/ml dissolved in a 70% acetonitrile and 0.1% tri-fluoroacetic acid (TFA) solution. Then sample was mixed with matrix in a sample:matrix ratio of 1:1 (v/v) and 1 µL of the mix was deposited on the sample plate (Hudson Surface Technology, PL-PC-000050-P). Acquisition method was linear between 5-20 kDa and data was the result of 10000 shots media. Protein samples were originally in PBS but for MALDI-TOF/TOF characterization proteins were transferred to water solution.
- **Ultrapformance liquid chromatography-tandem mass spectrometer (UP-LC MS).** Chromatographic separation was performed in an Acquity UPLC system using a reverse phase BEH C18 column (100 x 2.1 mm, 1.7 µm) from Waters (Mildford, MA, USA). The samples were eluted using a flow rate of 300 µLmin⁻¹ and using as mobile phase 0.1% formic acid in water (A) and ACN (B). The gradient method was as follows: 0-0.5 min at 99% A, 1-4 min to 1% A, 4-26 min at 1% A, 26-26.2 min to 99% A, 26.2-30 min at 99% A. The column temperature was set at 30°C and the injection volume was 5 µL.

The mass spectrometry detection was carried out using an instrument equipped with an electrospray ionization source and a time-of-flight analyzer mass spectrometer (ESI-ToF-MS) LCT Premier XE from Waters (Mildford, MA, USA), working in positive / W mode. The MS acquisition range was between 100-4000 m/z. The capillary and cone voltages were set at 1500V and 100V respectively. For other parameters, desolvation gas temperature was 350°C and source

temperature was 100°C. The desolvation and cone gas were set at 600 Lh⁻¹ and 30 Lh⁻¹ respectively. Masslynx v4.1 software was used to analyze all the chromatograms and spectra (Waters, Milford, MA, USA). All these measurements were carried out by the Mass spectrometry platform from CIC biomaGUNE.

- **DLS.** Particle Dynamy light scattering of IONP micelles and biofunctionalized NPs (IONP@hIL15HIS) was measured with a NanoSizer (Malvern Nano-AS, UK) with 173° scattering angle at 25°C. In all measurements the samples were measured 3 times and the average size was used for plotting data.

Zeta potential measurements were performed with the same equipment at 25° also and with cell drive voltage of 20 V using Smoluchowski model.

All data was monitored with the ZetaSizer Software v7.11 (Malvern) and was exported. Graph representation was done with GraphPad Prism 9.

- **ICP-MS.** For the Fe concentration quantification, Fe containing samples were digested with HNO₃ (70%, Fisher Scientific) over 72h and then diluted in water until 1% HNO₃. The studies were performed on ICP-MS iCAP-Q (Thermo) by Mass Spectrometry platform on CIC biomaGUNE.
- **Transmission electron microscopy (TEM).** TEM images of hIONP and IONP micelles were gotten from JEOL JEM 2011 electron microscope operating at 200 kV and recorded using Kodak SO-163 at CIC biomaGUNE. The samples were prepared by drop deposition of IONP into a copper specimen grid coated with a holey carbon film and allowing to dry at RT. For the image acquisition of the micelles the protocol was the same.
- **Minispec.** Relaxation time of IONP micelles suspended on PBS were measured at 37°C on Bruker Minispec mq60 instrument operating at 1.47 T. The values of T₁ and T₂ were measured for each sample at different Fe concentration, from 0.1 mM to 0.00625 mM, using inversion recovery for T₁ measurement and CPMP method for T₂. r₁ and r₂ values were calculated from the linear fitting of 1/relaxation time (s⁻¹) versus the iron concentration ([Fe] mM).
- **MRI images.** IONP micelles suspension was introduced on a thin-walled NMR tubes and then, the tubes were introduced in a falcon to immobilize them to perform the MRI imaging measurement. All experiments were performed on a 7-T Bruker Biospec 70/30 USR MRI system (Bruker Biospin GmbH, Ettlingen, Germany), interfaced to an AVANCE III console. The BGA12 imaging gradient (maximum gradient strength 400 mT/m) and a 40 mm diameter quadrature volume resonator

were used. For T_2 maps imaging of the phantoms the following parameters were adopted: Bruker's MSME (Multi slice Spin echo) sequence was used. The Echo Time (TE) values were varied in 50 steps ranging from 8 ms to 400 ms and Repetition Time (TR) 10000 ms. For T_1 maps imaging of the phantoms the following parameters were adopted: Spin echo saturation recovery using a variable repetition time Bruker's RAREVTR method. Images were acquired at 16 different TR values 45, 100, 150, 220, 300, 360, 450, 550, 700, 900, 1200, 1800, 3000, 4500, 7000, 10000 ms), TE 7ms, RARE factor 1. All data were acquired with 2 averages, 256 x 256 points, a Field of View of 2.5 cm x 2.5 cm and 3 slices with a slice thickness of 2.0 mm. The images were fitted into Levenberg-Margardt method to calculate T_1 and T_2 values using Bruker's Paravision 6.0.1 software.

- **Flow cytometer.** Three flow cytometers were used during this thesis. FACS Canto II (BD Biosciences) (located at CIC biomaGUNE) for *ex vivo* samples acquisition and LSRFortessa X-20 (BD Biosciences) and MACSQuant[®] X (Miltenyi) in all *in vitro* studies (located at Biocruces Bizkaia Health Research Institute) (Table ES6). The three cytometers have an excitation source with three lasers: violet (405 nm), blue (488 nm), and red (633-640 nm). Scattered light and fluorescence signals from the samples are directed by collection optics through spectral filters to the detectors (Fig. ES7). The difference between the three cytometers is the powder of the lasers and the number of detectors, which is higher in the LSRFortessa X-20, and the optics configuration. The flow cytometers from BD Biosciences (FACS Canto II and LSRFortessa X-20) configuration is based on separated geometric shaped compartments for each laser (violet, blue and red) where side scatter (SSC) and fluorescence signals are reflected or absorbed through bandpass (BP), longpass (LP) and dichroic filters (Fig. ES7 A,B). The MACSQuant X optics configuration is based on the same idea where SSC and fluorescence signal is reflected or absorbed but, in this case, the signal flow through channels and the signal from different lasers is separated during the path. It is very important to calibrate the flow cytometers. The calibration ensures that results measured on different days are comparable. This calibration is daily performed with the Cytometer Setup and Tracking (CST) beads. Other calibrations are performed by the platform manager monthly or once a year.

Data acquired in the flow cytometers were analyzed with different softwares: FlowLogic v7.3, for data acquired in MACSQuant X, and FlowJo v7.6.3 and FlowJo v10.7.2, for data acquired in FACS Canto II and LSRFortessa X-20. For the representation and the statistical analysis of the data GraphPad Prism 9 and SPICE 6 were used.

Table ES3 Flow cytometer configurations. The settings of the three flow cytometers used in this thesis are summarized in this table. PMT is the detector of the fluorescence signal which is V1-2, B1-4, and R1-2 for MACSQuant X and listed with alphabetic letters in FACS Canto II and LSRFortessa X-20. Laser properties are highlighted in the respective color (violet, blue or red). When parameters are similar but slightly different, numbers are detailed and separated by “//” in the following order: MACSQuantX//FACS Canto II//LSRFortessa X-20. *PMT: photomultiplier tube. LP: longpass filter.*

PMT	Laser	Filter	Dichroic filter	Cytometers		
				MACSQuant X	FACS Canto II	LSRFortessa X-20
FSC	488 nm	488/10		●	●	●
SSC	488 nm	488/10		●	●	●
A	405 nm	780/60	750LP			●
B	405 nm	710/50	685LP			●
C	405 nm	670/30	635LP			●
D	405 nm	610/20	600LP			●
V1//B//F	405 nm	450/50		●	●	●
V2//A//E	405 nm	525/50//510/50//525/50	502LP//505LP	●	●	●
B4//A	488 nm	750LP//780/60	735//750	●	●	●
B3//B	488 nm	655-730//670LP//695/40	655//685	●	●	●
C	488 nm	610/20	600LP			●
B2//D	488 nm	585/40//585/42//575/26	556LP//550LP	●	●	●
B1//E	488 nm	525/50//530/30	502LP//505LP	●	●	●
R2//A	633//640 nm	750LP //780/60	735LP//750LP	●	●	●
B	640 nm	730/45	690LP			●
R1//C	638//633//640 nm	655-730//660/20//670/30	665LP	●	●	●

FACS Canto II and LSRFortessa X-20 optics configuration

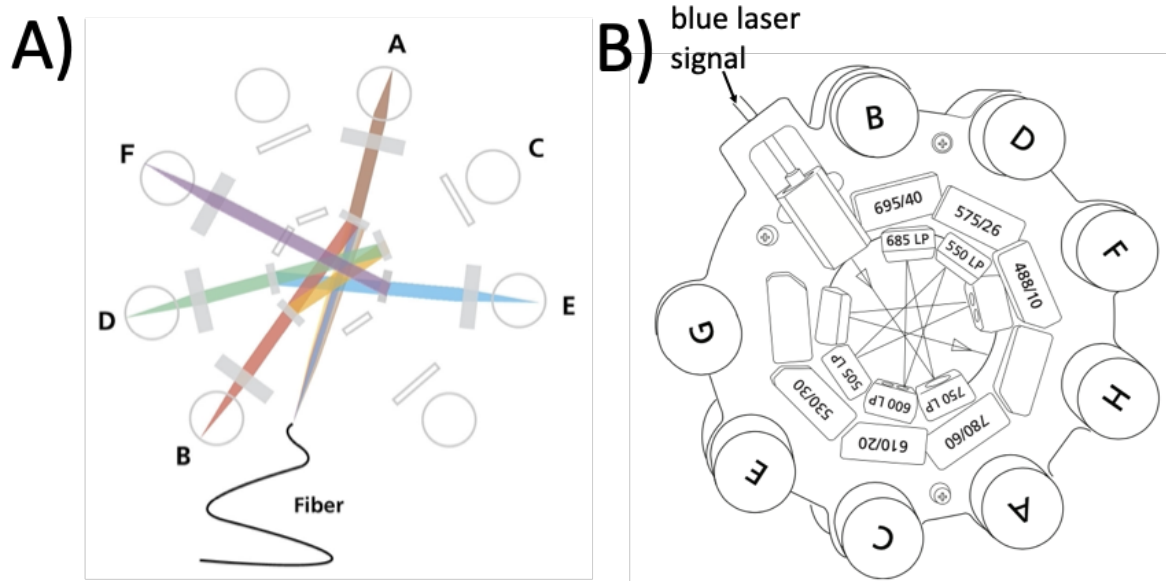


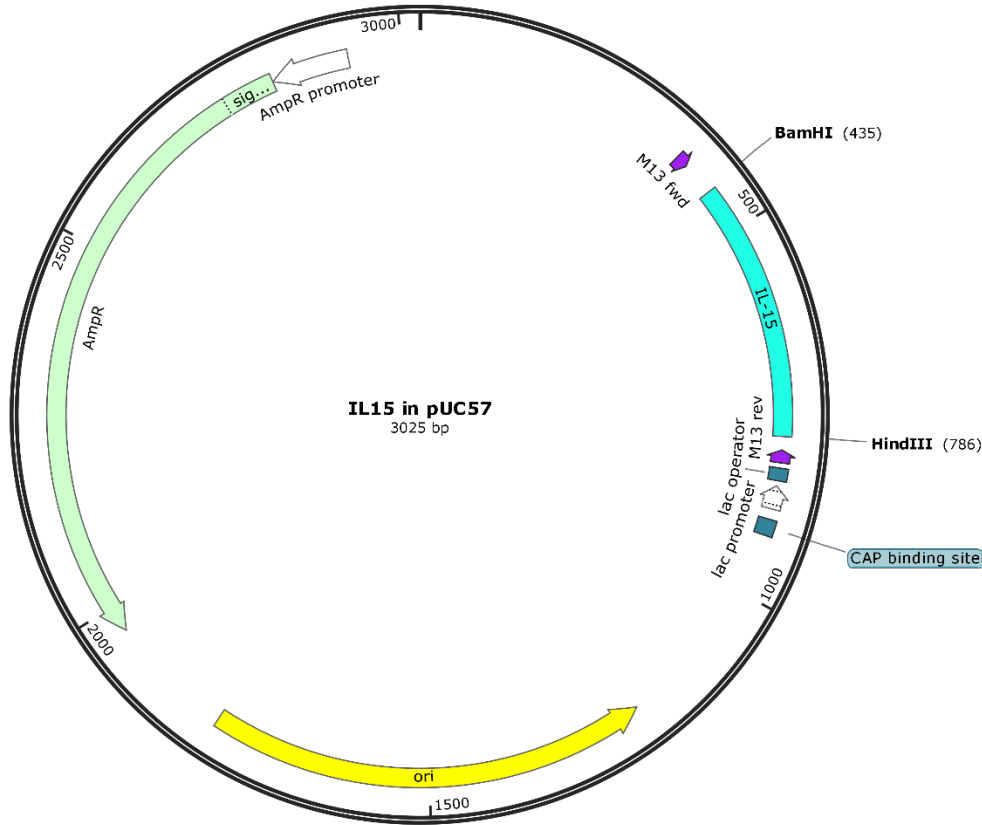
Figure ES4. Flow cytometers optics configuration. FACS Canto II and LSRFortessa X-20 are configured as separated compartments (one for each laser) with different photomultiplier tubes (PMT). (A) When light arrives to the corresponding compartment, a LP filter transmits the highest wavelength to the first PMT (PMT called A). The signal arrives to the first PMT because LP permits the signal to pass and, at the same time, the LP reflects lower wavelengths to the next PMT (PMT called B). This process is repeated until the signal is totally absorbed in the last PMT and did not reflect to another filter (scheme from the FACS Canto II user manual provided by BD Biosciences, p.22). (B) As a real example, 5 color blue laser configuration in a LSRFortessa X-20 cytometer is shown (scheme from LSRFortessa X-20 user manual provided by BD Biosciences, p.148). *PMT: photomultiplier tube. LP: longpass filter.*

Appendixes

Appendixes

Appendix I

Created with SnapGene®



```

1 TCGCGCGTTT CGGTGATGAC GGTGAAAACC TCTGACACAT GCAGCTCCCG GAGACGGTCA
61 CAGCTTGCTCT GTAAGCGGAT GCCGGGAGCA GACAAGCCCG TCAGGGCGCG TCAGCGGGTG
121 TTGGCGGGTG TCGGGGCTGG CTTAACTATG CGGCATCAGA GCAGATTGTA CTGAGAGTGC
181 ACCATATGCG GTGTGAAATA CCGCACAGAT CCGTAAGGAG AAAATACCGC ATCAGGCGCC
241 ATTCGCCATT CAGGCTGCGC AACTGTTGGG AAGGGCGATC GGTGCGGGCC TCTTCGCTAT
301 TACGCCAGCT GCGGAAAAGG GGATGTGCTG CAAGGCGATT AAGTTGGGTA ACGCCAGGGT
361 TTTCCCAGTC ACGACGTTGT AAAACGACGG CCAGTGAATT CGAGCTCGGT ACCTCGCGAA
421 TGCATCTAGA TATCGGATCC AACTGGGTGA ATGTTATTAG TGATCTGAAA AAGATTGAGG
481 ATCTGATTCA GAGCATGCAT ATTGATGCAA CCCTGTATAC CGAAAGTGAT GTTCATCCGA
541 GCTGTAAAGT GACCGCCATG AAATGCTTTC TGCTGGAAC TGCAGGTTATT AGTCTGAAA
601 GTGGTGACGC CAGCATTCAT GATACCGTGG AAAATCTGAT TATTCTGGCC AATAATAGTC
661 TGAGCAGCAA TGGCAATGTT ACCGAAAGTG GCTGTAAAGA ATGCGAAGAA CTGGAAAAGA
721 AAAATATTAA GGAGTTCCTG CAGAGTTTGT TGCATATTGT GCAGATGTTT ATTAACACCA
781 GCTAAAAGCT TGGCGTAATC ATGGTCATAG CTGTTTCCTG TGTGAAATTG TTATCCGCTC
841 ACAATTCCAC ACAACATACG AGCCGGAAGC ATAAAGTGTA AAGCCTGGGG TGCCTAATGA
901 GTGAGCTAAC TCACATTAAT TGC GTTGCGC TCACTGCCCG CTTTCCAGTC GGGAAACCTG
961 TCGTGCCAGC TGCATTAATG AATCGGCCAA CGCGCGGGGA GAGGCGGTTT GCGTATTGGG
1021 CGCTCTTCCG CTTCTCGCT CACTGACTCG CTGCGCTCGG TCGTTCGGCT GCGGCGAGCG
1081 GTATCAGCTC ACTCAAAGGC GGTAATACGG TTATCCACAG AATCAGGGGA TAACGCAGGA
1141 AAGAACATGT GAGCAAAAGG CCAGCAAAAG GCCAGGAACC GTAAAAAGGC CGCGTTGCTG
1201 GCGTTTTTCC ATAGGCTCCG CCCCCTGAC GAGCATCACA AAAATCGACG CTC AAGTCAG
1261 AGGTGGCGAA ACCCGACAGG ACTATAAGA TACCAGGCGT TTCCCCTGG AAGCTCCCTC
1321 GTGCGCTCTC CTGTTCCGAC CCTGCCGCTT ACCGGATACC TGTCGGCCTT TCTCCCTTCG
    
```

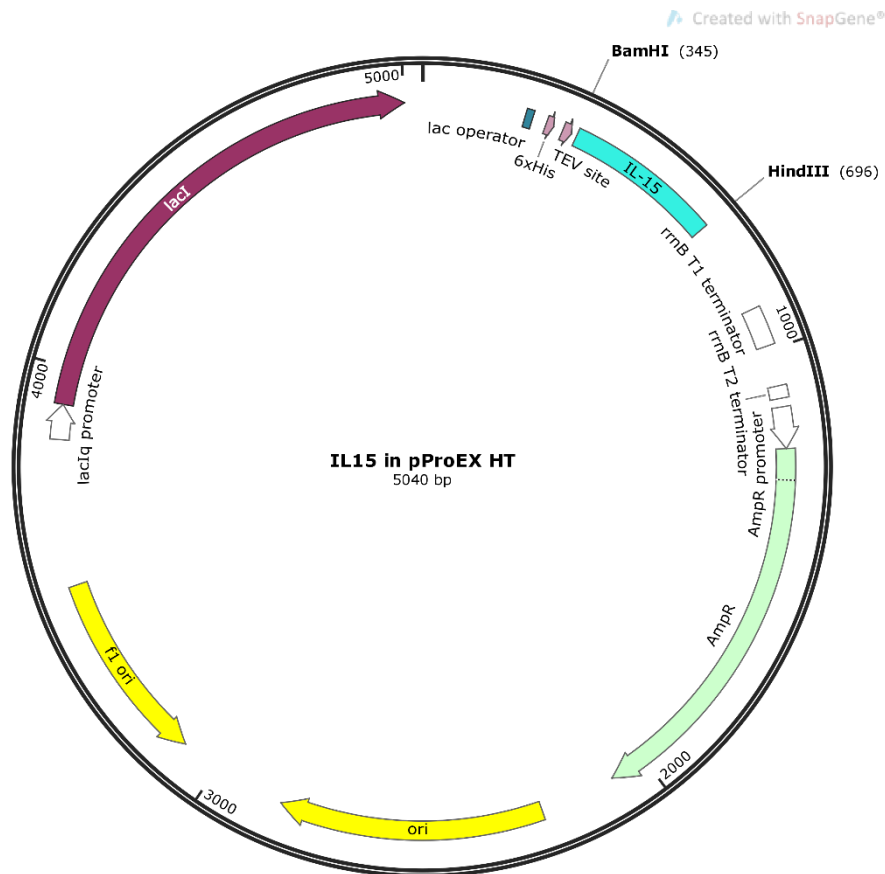


```

1381 GGAAGCGTGG CGCTTTCTCA TAGCTCACGC TGTAGGTATC TCAGTTCGGT GTAGGTCGTT
1441 CGCTCCAAGC TGGGCTGTGT GCACGAACCC CCCGTTTCAGC CCGACCGCTG CGCCTTATCC
1501 GGTAACCTATC GTCTTGAGTC CAACCCGGTA AGACACGACT TATCGCCACT GGCAGCAGCC
1561 ACTGGTAACA GGATTAGCAG AGCGAGGTAT GTAGGCGGTG CTACAGAGTT CTTGAAGTGG
1621 TGGCCTAACT ACGGCTACAC TAGAAGAACA GTATTTGGTA TCTGCGCTCT GCTGAAGCCA
1681 GTTACCTTCG GAAAAAGAGT TGGTAGCTCT TGATCCGGCA AACAAACCAC CGCTGGTAGC
1741 GGTGGTTTTT TTGTTTGCAA GCAGCAGATT ACGCGCAGAA AAAAAGGATC TCAAGAAGAT
1801 CCTTTGATCT TTTCTACGGG GTCTGACGCT CAGTGGAACG AAAACTCACG TTAAGGGATT
1861 TTGGTCATGA GATTATCAAA AAGGATCTTC ACCTAGATCC TTTTAAATTA AAAATGAAGT
1921 TTTAAATCAA TCTAAAGTAT ATATGAGTAA ACTTGGTCTG ACAGTTACCA ATGCTTAATC
1981 AGTAGGGCAC CTATCTCAGC GATCTGTCTA TTTTCGTTTCA CCATAGTTGC TGAATCCCTC
2041 GTCGTGTAGA TAACTACGAT ACGGGAGGGC TTACCATCTG GCCCCAGTGC TGCAATGATA
2101 CCGCGAGATC CACGCTCACC GGCTCCAGAT TTATCAGCAA TAAACCAGCC AGCCGGAAGG
2161 GCCGAGCGCA GAAGTGGTCC TGCAACTTTA TCCGCCTCCA TCCAGTCTAT TAATTGTTGC
2221 CGGGAAGCTA GAGTAAGTAG TTCGCCAGTT AATAGTTTGC GCAACGTTGT TGCCATTGCT
2281 ACAGGCATCG TGGTGTACAG CTCGTCGTTT GGTATGGCTT CATTCAGCTC CGGTTCCCAA
2341 CGATCAAGGC GAGTTACATG ATCCCCCATG TTGTGCAAAA AAGCGGTTAG CTCCTTCGGT
2401 CCTCCGATCG TTGTCAGAAG TAAGTTGGCC GCAGTGTAT CACTCATGGT TATGGCAGCA
2461 CTGCATAATT CTCTTACTGT CATGCCATCC GTAAGATGCT TTTCTGTGAC TGGTGTGAGTAC
2521 TCAACCAAGT CATTCTGAGA ATAGTGTATG CGGCGACCGA GTTGCTCTTG CCCGGCGTCA
2581 ATACGGGATA ATACCGCGCC ACATAGCAGA ACTTTAAAAG TGCTCATCAT TGGAAAACGT
2641 TCTTCGGGGC GAAAACTCTC AAGGATCTTA CCGCTGTTGA GATCCAGTTC GATGTAACCC
2701 ACTCGTGCAC CCAACTGATC TTCAGCATCT TTTACTTTCA CCAGCGTTTC TGGGTGAGCA
2761 AAAACAGGAA GGCAAAATGC CGCAAAAAAG GGAATAAGGG CGACACGGAA ATGTTGAATA
2821 CTCATACTCT TCCTTTTTCA ATATTATTGA AGCATTATC AGGGTTATTG TCTCATGAGC
2881 GGATACATAT TTGAATGTAT TTAGAAAAAT AAACAAATAG GGGTTCGCG CACATTTCCC
2941 CGAAAAGTGC CACCTGACGT CTAAGAAACC ATTATTATCA TGACATTAAC CTATAAAAAAT
3001 AGGCGTATCA CGAGGCCCTT TCGTC

```

Figure AI.1. IL-15 in pUC57 vector map and sequence. The vector map showed the different elements of the vector: the gene encoding the resistance to ampicillin (AmpR) and its promoter, origin of replication (ori), lac operon promoter and the IL-15 gene. The restriction sites (BamHI and HindIII) used for the cloning are also shown. In the sequence appear in bold characteres the open reading frame (ORF) of IL-15 gene and IL-15 gene sequence is highlighted in green.



```

1  GTTTGACAGC TTATCATCGA CTGCACGGTG CACCAATGCT TCTGGCGTCA
51  GGCAGCCATC GGAAGCTGTG GTATGGCTGT GCAGGTCGTA AATCACTGCA
101 TAATTCGTGT CGCTCAAGGC GCACTCCCGT TCTGGATAAT GTTTTTTGCG
151 CCGACATCAT AACGGTTCTG GCAAATATTC TGAAATGAGC TGTGACAAT
201 TAATCATCCG GTCCGTATAA TCTGTGGAAT TGTGAGCGGA TAACAATTTT
251 ACACAGGAAA CAGACCATGT CGTACTAC GATT
301 ACGATATCCC AACGACCGAA AACCTGTATT TTCAGGGCGC CATGGGATCC
351 AACTGGGTGA ATGTTATTAG TGATCTGAAA AAGATTGAGG ATCTGATTCA
401 GAGCATGCAT ATTGATGCAA CCCTGTATAC CGAAAGTGAT GTTCATCCGA
451 GCTGTAAAGT GACCGCCATG AAATGCTTTC TGCTGGAAct GCAGGTTATT
501 AGTCTGAAA GTGGTGACGC CAGCATTGAT GATACCGTGG AAAATCTGAT
551 TATTCTGGCC AATAATAGTC TGAGCAGCAA TGGCAATGTT ACCGAAAGTG
601 GCTGTAAAGA ATGCGAAGAA CTGGAAAAGA AAAATATTAA GGAGTTCCTG
651 CAGAGTTTTG TGCATATTGT GCAGATGTTT ATTAACACCA GCTAAAAGCT
701 TGGCTGTTTT GCGGATGAG AGAAGATTTT CAGCCTGATA CAGATTAAAT
751 CAGAACGCAG AAGCGGTCTG ATAAAACAGA ATTTGCCTGG CGGCAGTAGC
801 GCGGTGGTCC CACCTGACCC CATGCCGAAC TCAGAAGTGA AACGCCGTAG
851 CGCCGATGGT AGTGTGGGGT CTCCCCATGC GAGAGTAGGG AACTGCCAGG
901 CATCAAATAA AACGAAAGGC TCAGTCGAAA GACTGGGCCT TTCGTTTTAT
951 CTGTTGTTTG TCGGTGAACG CTCTCCTGAG TAGGACAAAT CCGCCGGGAG
1001 CGGATTTGAA CGTTGCGAAG CAACGGCCCC GAGGGTGCGG GCGCAGACGC
1051 CCGCCATAAA CTGCCAGGCA TCAAATTAAG CAGAAGGCCA TCCTGACGGA
1101 TGGCCTTTTT GCGTTTCTAC AAATCTTTT TGTTTATTTT TCTAAATACA
1151 TTCAAATATG TATCCGCTCA TGAGACAATA ACCCTGATAA ATGCTTCAAT
1201 AATATTGAAA AAGGAAGAGT ATGAGTATTC AACATTTCG TGTCGCCCTT
1251 ATTCCCTTTT TTGCGGCATT TTGCCTTCCT GTTTTTGCTC ACCCAGAAAC
1301 GCTGGTGAAA GTAAAAGATG CTGAAGATCA GTTGGGTGCA CGAGTGGGTT
1351 ACATCGAACT GGATCTCAAC AGCGGTAAGA TCCTTGAGAG TTTTCGCCCC
1401 GAAGAACGTT TTCCAATGAT GAGCACTTTT AAAGTTCTGC TATGTGGCGC
    
```

1451 GGTATTATCC CGTGTGACG CCGGGCAAGA GCAACTCGGT CGCCGCATAC
1501 ACTATTCTCA GAATGACTTG GTTGAGTACT CACCAGTCAC AGAAAAGCAT
1551 CTTACGGATG GCATGACAGT AAGAGAATTA TGCAGTGCTG CCATAACCAT
1601 GAGTGATAAC ACTGCGGCCA ACTTACTTCT GACAACGATC GGAGGACCGA
1651 AGGAGCTAAC CGCTTTTTTTG CACAACATGG GGGATCATGT AACTCGCCTT
1701 GATCGTTGGG AACCGGAGCT GAATGAAGCC ATACCAAACG ACGAGCGTGA
1751 CACCACGATG CCTACAGCAA TGGCAACAAC GTTGCGCAAA CTATTAACTG
1801 GCGAACTACT TACTCTAGCT TCCCGGCAAC AATTAATAGA CTGGATGGAG
1851 GCGGATAAAG TTGCAGGACC ACTTCTGCGC TCGGCCCTTC CGGCTGGCTG
1901 GTTTATTGCT GATAAATCTG GAGCCGGTGA GCGTGGGTCT CGCGGTATCA
1951 TTGCAGCACT GGGGCCAGAT GGTAAAGCCCT CCCGTATCGT AGTTATCTAC
2001 ACGACGGGGA GTCAGGCAAC TATGGATGAA CGAAATAGAC AGATCGTGA
2051 GATAGGTGCC TCACTGATTA AGCATTGGTA ACTGTCAGAC CAAGTTTACT
2101 CATATATACT TTAGATTGAT TTAAAACCTC ATTTTTTAATT TAAAAGGATC
2151 TAGGTGAAGA TCCTTTTTTGA TAATCTCATG ACCAAAAATCC CTTAACGTGA
2201 GTTTTCGTTT CACTGAGCGT CAGACCCCGT AGAAAAGATC AAAGGATCTT
2251 CTTGAGATCC TTTTTTCTG CGCGTAATCT GCTGCTTGCA AACAAAAAAA
2301 CCACCGCTAC CAGCGGTGGT TTGTTTGCCG GATCAAGAGC TACCAACTCT
2351 TTTTCCGAAG GTAACCTGGT TCAGCAGAGC GCAGATACCA AATACTGTCC
2401 TTCTAGTGTA GCCGTAGTTA GGCCACCACT TCAAGAACTC TGTAGCACC
2451 CCTACATACC TCGCTCTGCT AATCCTGTTA CCAGTGGCTG CTGCCAGTGG
2501 CGATAAGTCG TGTCTTACCG GGTGACTC AAGACGATAG TTACCGGATA
2551 AGGCGCAGCG GTCGGGCTGA ACGGGGGGTT CGTGCACACA GCCCAGCTTG
2601 GAGCGAACGA CCTACACCGA ACTGAGATAC CTACAGCGTG AGCTATGAGA
2651 AAGCGCCACG CTTCCCGAAG GGAGAAAGGC GGACAGGTAT CCGGTAAGCG
2701 GCAGGGTCGG AACAGGAGAG CGCACGAGGG AGCTTCCAGG GGGAAACGCC
2751 TGGTATCTTT ATAGTCCTGT CGGGTTTCGC CACCTCTGAC TTGAGCGTGC
2801 ATTTTGTGTA TGCTCGTCAG GGGGGCGGAG CCTATGGAAA AACGCCAGCA
2851 ACGCGCCCTT TTTACGGTTC CTGGCCTTTT GCTGGCCTTT TGCTCACATG
2901 TTCTTTCCTG CGTTATCCCC TGATTCTGTG GATAACCGTA TTACCOCCTT
2951 TGAGTGAGCT GATAACCGCTC GCCGCAGCCG AACGACCGAG CGCAGCGAGT
3001 CAGTGAGCGA GGAAGCGGAA GAGCGCCTGA TCGGGTATTT TCTCCTTACG
3051 CATCTGTGCG GTATTTTACA CCGCATAATT TTGTTAAAAAT TCGCGTTAAA
3101 TTTTTGTTAA ATCAGCTCAT TTTTTAACCA ATAGGCCGAA ATCGGCAAAA
3151 TCCCTTATAA ATCAAAAGAA TAGACCGAGA TAGGGTTGAG TGTGTGTTCCA
3201 GTTTGGAACA AGAGTCCACT ATTAAGAAGC GTGGACTCCA ACGTCAAAGG
3251 GCGAAAAACC GTCTATCAGG GCGATGGCCC ACTACGTGAA CCATCACCTT
3301 AATCAAGTTT TTTGGGGTCG AGGTGCCGTA AAGCACTAAA TCGGAACCTT
3351 AAAGGGAGCC CCCGATTTAG AGCTTGACGG GGAAAGCCGG CGAACGTGGC
3401 GAGAAAGGAA GGAAGAAAG CGAAAGGAGC GGGCGCTAGG GCGCTGGCAA
3451 GTGTAGCGGT CACGCTGCGC GTAACCACCA CACCCGCCGC GCTTAATGCG
3501 CCGCTACAGG GCGCGTCCCA TTCGCCATTC AGGCTGCTAT GGTGCACTCT
3551 CAGTACAATC TGCTCTGATG CCGCATAGTT AAGCCAGTAC CAGTACGTA
3601 GCGATATCGG AGTGTATACA CTCCGCTATC GCTACGTGAC TGGGTCAATGG
3651 CTGCGCCCCG ACACCCGCCA ACACCCGCTG ACGCGCCCTG ACGGGCTTGT
3701 CTGCTCCCGG CATCCGCTTA CAGACAAGCT GTGACCGTCT CCGGGAGCTG
3751 CATGTGTCAG AGGTTTTCAC CGTCATCACC GAAACGCGCG AGGCAGCAGA
3801 TCAATTGCGC CGCGAAGGCG AAGCGGCATG CATTTACGTT GACACCATCG
3851 AATGGTGCAA AACCTTTCGC GGTATGGCAT GATAGCGCCC GGAAGAGAGT
3901 CAATTCAGGG TGGTGAATGT GAAACCAGTA ACGTTATACG ATGTGCGAGA
3951 GTATGCCGGT GTCTCTTATC AGACCGTTTC CCGCGTGGTG AACCAGGCCA
4001 GCCACGTTTT TGCGAAAACG CGGGAAAAAAG TGGAAGCGGC GATGGCGGAG
4051 CTGAATTACA TTCCCAACCG CGTGGCACA CAACTGGCGG GCAAACAGTC
4101 GTTGCTGATT GCGGTTGCCA CCTCCAGTCT GGCCCTGCAC GCGCCGTCG
4151 AAATTGTCGC GCGGATTTAA TCTCGCGCCG ATCAACTGGG TGCCAGCGTG
4201 GTGGTGTGCGA TGGTAGAACG AAGCGGCGTC GAAGCCTGTA AAGCGCGGT
4251 GCACAATCTT CTCGCGCAAC GCGTCAGTGG GCTGATCATT AACTATCCGC
4301 TGGATGACCA GGATGCCATT GCTGTGGAAG CTGCCTGCAC TAATGTTCCG
4351 GCGTTATTTT TTGATGTCTC TGACCAGACA CCCATCAACA GTATTATTTT
4401 CTCCCATGAA GACGGTACGC GACTGGGCGT GGAGCATCTG GTCGCATTTG
4451 GTCACCAGCA AATCGCGCTG TTAGCGGGCC CATTAAAGTT TGTCTCGGCG

```

4501 CGTCTGCGTC TGGCTGGCTG GCATAAATAT CTCACTCGCA ATCAAATTCA
4551 GCCGATAGCG GAACGGGAAG GCGACTGGAG TGCCATGTCC GGTTTTCAAC
4601 AAACCATGCA AATGCTGAAT GAGGGCATCG TTCCCCTGC GATGCTGGTT
4651 GCCAACGATC AGATGGCGCT GGGCGCAATG CGCGCCATTA CCGAGTCCGG
4701 GCTGCGCGTT GGTGCGGATA TCTCGGTAGT GGGATACGAC GATACCGAAG
4751 ACAGCTCATG TTATATCCCG CCGTTAACCA CCATCAAACA GGATTTTCGC
4801 CTGCTGGGGC AAACCAGCGT GGACCGCTTG CTGCAACTCT CTCAGGGCCA
4851 GGCGGTGAAG GGCAATCAGC TGTTGCCCGT CTCACTGGTG AAAAGAAAAA
4901 CCACCCTGGC ACCCAATACG CAAACCGCCT CTCCCCGCGC GTTGGCCGAT
4951 TCATTAATGC AGCTGGCACG ACAGGTTTCC CGACTGGAAA GCGGGCAGTG
5001 AGCGCAACGC AATTAATGTG AGTTAGCGCG AATTGATCTG

```

Figure Al.2. IL-15 in pProEX-HT vector map and sequence. The vector map showed the different elements of the vector: the gene encoding the resistance to ampicilin (AmpR) and its promoter, origin or replication (ori), lac operon promoter and the IL-15 gene in frame of his-tag and TEV cleavage site. The restriction sites used (BamHI and HindIII) for the cloning are also shown. In the sequence is showed in bold and underlined the open reading frame (ORF) with the his-tag highlighted in pink and IL-15 gene in green.

A)
 Cat cac cat cac cat cac gat tac gat atc cca acg acc gaa aac ctg tat ttt cag ggc
 gcc atg gga tcc aac tgg gtg aat gtt att agt gat ctg aaa aag att gag gat ctg att
 cag agc atg cat att gat gca acc ctg tat acc gaa agt gat gtt cat ccg agc tgt aaa
 gtg acc gcc atg aaa tgc ttt ctg ctg gaa ctg cag gtt att agt ctg gaa agt ggt gac
 gcc agc att cat gat acc gtg gaa aat ctg att att ctg gcc aat aat agt ctg agc agc
 aat ggc aat gtt acc gaa agt ggc tgt aaa gaa tgc gaa gaa ctg gaa aag aaa aat
 att aag gag ttc ctg cag agt ttt gtg cat att gtg cag atg ttt att aac acc agc taa

B)
 HHHHHH DYDIPTTENLYFQGA **Met** GS **NWVNVISDLKKIED**
LIQS **Met** **HIDATLYTESDVHP** **SCKVTA** **Met** **KCFLLELQVISLE**
SGDASI **HDTVENLIILANNSLSS** **NGNV** **TESGCKECELEKK**
NIKEFLQSFVHIVQ **Met** **FINTS** **Stop**

Figure Al.3. Sequences of his-tagged IL-15. DNA sequence composed by ORF of IL-15 gene start with the his-tag sequence (A). His-tagged hIL-15HIS protein sequence of from before showed ORF is represented and his-tag sequence is showed with green characters and IL-15 in blue (B).

References

1. Sung H, Ferlay J, Siegel RL, et al. Global Cancer Statistics 2020: GLOBOCAN Estimates of Incidence and Mortality Worldwide for 36 Cancers in 185 Countries. *CA Cancer J Clin.* 2021;71(3):209-249. doi:10.3322/caac.21660
2. Sung H, Ferlay J, Siegel RL, et al. Global Cancer Statistics 2020: GLOBOCAN Estimates of Incidence and Mortality Worldwide for 36 Cancers in 185 Countries. *CA Cancer J Clin.* 2021;71(3):209-249. doi:10.3322/caac.21660
3. Qiu Z, Li H, Zhang Z, et al. A Pharmacogenomic Landscape in Human Liver Cancers. *Cancer Cell.* 2019;36(2):179-193.e11. doi:10.1016/j.ccell.2019.07.001
4. Lim ZF, Ma PC. Emerging insights of tumor heterogeneity and drug resistance mechanisms in lung cancer targeted therapy. *J Hematol Oncol J Hematol Oncol.* 2019;12(1):1-18. doi:10.1186/s13045-019-0818-2
5. Parikh AR, Leshchiner I, Elagina L, et al. Liquid versus tissue biopsy for detecting acquired resistance and tumor heterogeneity in gastrointestinal cancers. *Nat Med.* 2019;25(9):1415-1421. doi:10.1038/s41591-019-0561-9
6. Martín-Lorenzo A, Gonzalez-Herrero I, Rodríguez-Hernández G, García-Ramírez I, Vicente-Dueñas C, Sánchez-García I. Early epigenetic cancer decisions. *Biol Chem.* 2014;395(11):1315-1320. doi:10.1515/hsz-2014-0185
7. Poljsak B, Kovac V, Dahmane R, Levec T, Starc A. Cancer Etiology: A Metabolic Disease Originating from Life's Major Evolutionary Transition? *Oxid Med Cell Longev.* 2019;2019. doi:10.1155/2019/7831952
8. Hanahan D, Weinberg RA. Hallmarks of cancer: The next generation. *Cell.* 2011;144(5):646-674. doi:10.1016/j.cell.2011.02.013
9. Hillen T, Enderling H, Hahnfeldt P. The Tumor Growth Paradox and Immune System-Mediated Selection for Cancer Stem Cells. *Bull Math Biol.* 2013;75(1):161-184. doi:10.1007/s11538-012-9798-x
10. Schirmacher V. Complete remission of cancer in late-stage disease by radiation and transfer of allogeneic MHC-matched immune T cells: lessons from GvL studies in animals. *Cancer Immunol Immunother.* 2014;63(6):535-543. doi:10.1007/s00262-014-1530-2
11. Hirayama AV, Gauthier J, Hay KA, et al. High rate of durable complete remission in follicular lymphoma after CD19 CAR-T cell immunotherapy. 2019;134(7):5. doi:10.1182/blood.2019000905
12. Ferro K, Peuß R, Yang W, Rosenstiel P, Schulenburg H, Kurtz J. Experimental evolution of immunological specificity. *Proc Natl Acad Sci.* 2019;116(41):20598-20604. doi:10.1073/pnas.1904828116
13. Natoli G, Ostuni R. Adaptation and memory in immune responses. *Nat Immunol.*

2019;20(7):783-792. doi:10.1038/s41590-019-0399-9

14. de Visser KE, Eichten A, Coussens LM. Paradoxical roles of the immune system during cancer development. *Nat Rev Cancer*. 2006;6(1):24-37. doi:10.1038/nrc1782
15. Chen DS, Mellman I. Oncology meets immunology: The cancer-immunity cycle. *Immunity*. 2013;39(1):1-10. doi:10.1016/j.immuni.2013.07.012
16. Wculek SK, Cueto FJ, Mujal AM, Melero I, Krummel MF, Sancho D. Dendritic cells in cancer immunology and immunotherapy. *Nat Rev Immunol*. 2020;20(1):7-24. doi:10.1038/s41577-019-0210-z
17. van der Leun AM, Thommen DS, Schumacher TN. CD8+ T cell states in human cancer: insights from single-cell analysis. *Nat Rev Cancer*. 2020;20(4):218-232. doi:10.1038/s41568-019-0235-4
18. Shimasaki N, Jain A, Campana D. NK cells for cancer immunotherapy. *Nat Rev Drug Discov*. 2020;19(3):200-218. doi:10.1038/s41573-019-0052-1
19. Li C, Xu X, Wei S, Jiang P, Xue L, Wang J. Tumor-associated macrophages: potential therapeutic strategies and future prospects in cancer. *J Immunother Cancer*. 2021;9(1):e001341. doi:10.1136/jitc-2020-001341
20. Herberman RB, Nunn ME, Holden HT, Lavrin DH. Natural cytotoxic reactivity of mouse lymphoid cells against syngeneic and allogeneic tumors. II. Characterization of effector cells. *Int J Cancer*. Published online 1975. doi:10.1002/ijc.2910160205
21. Kiessling R, Klein E, Pross H, Wigzell H. „Natural” killer cells in the mouse. II. Cytotoxic cells with specificity for mouse Moloney leukemia cells. Characteristics of the killer cell. *Eur J Immunol*. Published online 1975. doi:10.1002/eji.1830050209
22. Vivier E, Artis D, Colonna M, et al. Innate Lymphoid Cells: 10 Years On. *Cell*. 2018;174(5):1054-1066. doi:10.1016/j.cell.2018.07.017
23. Freud AG, Mundy-Bosse BL, Yu J, Caligiuri MA. The Broad Spectrum of Human Natural Killer Cell Diversity. *Immunity*. 2017;47(5):820-833. doi:10.1016/j.immuni.2017.10.008
24. Caligiuri MA. Human natural killer cells. *Blood*. Published online 2008. doi:10.1182/blood-2007-09-077438
25. Vivier E, Tomasello E, Baratin M, Walzer T, Ugolini S. Functions of natural killer cells. *Nat Immunol*. Published online 2008. doi:10.1038/ni1582
26. Sun JC, Lanier LL. NK cell development, homeostasis and function: parallels with CD8+ T cells. *Nat Rev Immunol*. 2011;11(10):645-657. doi:10.1038/nri3044
27. Hernandez C, Huebener P, Schwabe RF. Damage-associated molecular patterns in cancer: a double-edged sword. *Oncogene*. 2016;35(46):5931-5941. doi:10.1038/onc.2016.104
28. Screpanti V, Wallin RPA, Grandien A, Ljunggren HG. Impact of FASL-induced apoptosis in the

- elimination of tumor cells by NK cells. *Mol Immunol*. Published online 2005. doi:10.1016/j.molimm.2004.07.033
29. Cretney E, Takeda K, Yagita H, Glaccum M, Peschon JJ, Smyth MJ. Increased Susceptibility to Tumor Initiation and Metastasis in TNF-Related Apoptosis-Inducing Ligand-Deficient Mice. *J Immunol*. Published online 2002. doi:10.4049/jimmunol.168.3.1356
 30. Brandstadter JD, Yang Y. Natural killer cell responses to viral infection. *J Innate Immun*. Published online 2011. doi:10.1159/000324176
 31. Jost S, Altfeld M. Control of human viral infections by natural killer cells. *Annu Rev Immunol*. Published online 2013. doi:10.1146/annurev-immunol-032712-100001
 32. Cerwenka A, Lanier LL. Natural killer cell memory in infection, inflammation and cancer. *Nat Rev Immunol*. 2016;16(2):112-123. doi:10.1038/nri.2015.9
 33. Moretta A. Natural killer cells and dendritic cells: Rendezvous in abused tissues. *Nat Rev Immunol*. Published online 2002. doi:10.1038/nri956
 34. Lucas M, Schachterle W, Oberle K, Aichele P, Diefenbach A. Dendritic Cells Prime Natural Killer Cells by trans-Presenting Interleukin 15. *Immunity*. Published online 2007. doi:10.1016/j.immuni.2007.03.006
 35. Waggoner SN, Cornberg M, Selin LK, Welsh RM. Natural killer cells act as rheostats modulating antiviral T cells. *Nature*. Published online 2012. doi:10.1038/nature10624
 36. Terrén I, Mikelez I, Odriozola I, et al. Implication of Interleukin-12/15/18 and Ruxolitinib in the Phenotype, Proliferation, and Polyfunctionality of Human Cytokine-Preactivated Natural Killer Cells. *Front Immunol*. 2018;9:737. doi:10.3389/fimmu.2018.00737
 37. Vitallé J, Terrén I, Orrantia A, et al. CD300a inhibits CD16-mediated NK cell effector functions in HIV-1-infected patients. *Cell Mol Immunol*. Published online 2019. doi:10.1038/s41423-019-0275-4
 38. Martín-Fontecha A, Thomsen LL, Brett S, et al. Induced recruitment of NK cells to lymph nodes provides IFN- γ for TH1 priming. *Nat Immunol*. Published online 2004. doi:10.1038/ni1138
 39. Van Kaer L, Postoak JL, Wang C, Yang G, Wu L. Innate, innate-like and adaptive lymphocytes in the pathogenesis of MS and EAE. *Cell Mol Immunol*. Published online 2019. doi:10.1038/s41423-019-0221-5
 40. Münz C. Natural killer cells and autoimmunity. In: *Natural Killer Cells*. ; 2010. doi:10.1016/B978-0-12-370454-2.00034-X
 41. Moffett-King A. Natural killer cells and pregnancy. *Nat Rev Immunol*. Published online 2002. doi:10.1038/nri886
 42. Vivier E, Tomasello E, Baratin M, Walzer T, Ugolini S. Functions of natural killer cells. *Nat Immunol*. 2008;9(5):503-510. doi:10.1038/ni1582

43. Martinet L, Smyth MJ. Balancing natural killer cell activation through paired receptors. *Nat Rev Immunol*. 2015;15(4):243-254. doi:10.1038/nri3799
44. Lin SJ, Kuo ML, Hsiao HS, Lee PT, Chen JY, Huang JL. Activating and inhibitory receptors on natural killer cells in patients with systemic lupus erythematosus-regulation with interleukin-15. *PLoS ONE*. 2017;12(10):1-20. doi:10.1371/journal.pone.0186223
45. Kim N, Lee HH, Lee HJ, Choi WS, Lee J, Kim HS. Natural killer cells as a promising therapeutic target for cancer immunotherapy. *Arch Pharm Res*. 2019;42:591-606. doi:10.1007/s12272-019-01143-y
46. Lanier LL. NK cell recognition. *Annu Rev Immunol*. Published online 2005. doi:10.1146/annurev.immunol.23.021704.115526
47. Pegram HJ, Andrews DM, Smyth MJ, Darcy PK, Kershaw MH. Activating and inhibitory receptors of natural killer cells. *Immunol Cell Biol*. 2011;89(2):216-224. doi:10.1038/icb.2010.78
48. Freud AG, Mundy-Bosse BL, Yu J, Caligiuri MA. The Broad Spectrum of Human Natural Killer Cell Diversity. *Immunity*. Published online 2017. doi:10.1016/j.immuni.2017.10.008
49. Long EO, Sik Kim H, Liu D, Peterson ME, Rajagopalan S. Controlling natural killer cell responses: Integration of signals for activation and inhibition. *Annu Rev Immunol*. Published online 2013. doi:10.1146/annurev-immunol-020711-075005
50. Vivier E, Raulet DH, Moretta A, et al. Innate or Adaptive Immunity? The Example of Natural Killer Cells. *Science*. 2011;331(6013):44-49. doi:10.1126/science.1198687
51. González S, López-Soto A, Suarez-Alvarez B, López-Vázquez A, López-Larrea C. NKG2D ligands: key targets of the immune response. *Trends Immunol*. Published online 2008. doi:10.1016/j.it.2008.04.007
52. Smith HRC, Heusel JW, Mehta IK, et al. Recognition of a virus-encoded ligand by a natural killer cell activation receptor. *Proc Natl Acad Sci U S A*. Published online 2002. doi:10.1073/pnas.092258599
53. Brandt CS, Baratin M, Yi EC, et al. The B7 family member B7-H6 is a tumor cell ligand for the activating natural killer cell receptor NKp30 in humans. *J Exp Med*. Published online 2009. doi:10.1084/jem.20090681
54. Chester C, Fritsch K, Kohrt HE. Natural killer cell immunomodulation: Targeting activating, inhibitory, and co-stimulatory receptor signaling for cancer immunotherapy. *Front Immunol*. 2015;6(601):1-9. doi:10.3389/fimmu.2015.00601
55. Guo M, Sun C, Qian Y, et al. Proliferation of Highly Cytotoxic Human Natural Killer Cells by OX40L Armed NK-92 With Secretory Neoleukin-2/15 for Cancer Immunotherapy. *Front Oncol*. 2021;11:1162. doi:10.3389/fonc.2021.632540
56. Carlsten M, Järås M. Natural Killer Cells in Myeloid Malignancies: Immune Surveillance, NK Cell Dysfunction, and Pharmacological Opportunities to Bolster the Endogenous NK Cells. *Front*

Immunol. 2019;10(October):1-18. doi:10.3389/fimmu.2019.02357

57. Childs RW, Carlsten M. Therapeutic approaches to enhance natural killer cell cytotoxicity against cancer: the force awakens. *Nat Rev Drug Discov.* 2015;14(7):487-498. doi:10.1038/nrd4506
58. Myers JA, Miller JS. Exploring the NK cell platform for cancer immunotherapy. *Nat Rev Clin Oncol.* Published online 2020. doi:10.1038/s41571-020-0426-7
59. Shimasaki N, Jain A, Campana D. NK cells for cancer immunotherapy. *Nat Rev Drug Discov.* Published online 2020. doi:10.1038/s41573-019-0052-1
60. Liu E, Marin D, Banerjee P, et al. Use of CAR-Transduced Natural Killer Cells in CD19-Positive Lymphoid Tumors. *N Engl J Med.* Published online 2020. doi:10.1056/nejmoa1910607
61. Daher M, Rezvani K. The evolution of NK cell immunotherapy for hematologic malignancies: A historical and contemporary perspective. *Semin Hematol.* Published online 2020. doi:10.1053/j.seminhematol.2020.11.005
62. Terrén I, Orrantia A, Vitallé J, Astarloa-Pando G, Zenarruzabeitia O, Borrego F. Modulating NK cell metabolism for cancer immunotherapy. *Semin Hematol.* 2020;57(4):213-224. doi:10.1053/j.seminhematol.2020.10.003
63. Terrén I, Orrantia A, Mikelez-Alonso I, Vitallé J, Zenarruzabeitia O, Borrego F. NK cell-based immunotherapy in renal cell carcinoma. *Cancers.* Published online 2020. doi:10.3390/cancers12020316
64. Gang M, Wong P, Berrien-Elliott MM, Fehniger TA. Memory-like natural killer cells for cancer immunotherapy. *Semin Hematol.* 2020;57(4):185-193. doi:10.1053/j.seminhematol.2020.11.003
65. Gao F, Ye Y, Gao Y, Huang H, Zhao Y. Influence of KIR and NK Cell Reconstitution in the Outcomes of Hematopoietic Stem Cell Transplantation. *Front Immunol.* Published online 2020. doi:10.3389/fimmu.2020.02022
66. Ruggeri L, Capanni M, Urbani E, et al. Effectiveness of donor natural killer cell alloreactivity in mismatched hematopoietic transplants. *Science.* Published online 2002. doi:10.1126/science.1068440
67. Miller JS, Soignier Y, Panoskaltsis-Mortari A, et al. Successful adoptive transfer and in vivo expansion of human haploidentical NK cells in patients with cancer. *Blood.* Published online 2005. doi:10.1182/blood-2004-07-2974
68. Rosenberg SA. IL-2: The First Effective Immunotherapy for Human Cancer. *J Immunol.* Published online 2014. doi:10.4049/jimmunol.1490019
69. Rosenberg SA, Lotze MT, Muul LM, et al. Observations on the Systemic Administration of Autologous Lymphokine-Activated Killer Cells and Recombinant Interleukin-2 to Patients with Metastatic Cancer. *N Engl J Med.* Published online 1985. doi:10.1056/nejm198512053132327
70. Curti A, Ruggeri L, D'Addio A, et al. Successful transfer of alloreactive haploidentical KIR

ligand-mismatched natural killer cells after infusion in elderly high risk acute myeloid leukemia patients. *Blood*. Published online 2011. doi:10.1182/blood-2011-01-329508

71. Romee R, Rosario M, Berrien-Elliott MM, et al. Cytokine-induced memory-like natural killer cells exhibit enhanced responses against myeloid leukemia. *Sci Transl Med*. 2016;8(357):357ra123. doi:10.1126/scitranslmed.aaf2341
72. Ito S, Bollard CM, Carlsten M, et al. Ultra-low dose interleukin-2 promotes immune-modulating function of regulatory t cells and natural killer cells in healthy volunteers. In: *Molecular Therapy*. ; 2014. doi:10.1038/mt.2014.50
73. Abbas AK, Trotta E, Simeonov DR, Marson A, Bluestone JA. Revisiting IL-2: Biology and therapeutic prospects. *Sci Immunol*. Published online 2018. doi:10.1126/sciimmunol.aat1482
74. Becknell B, Caligiuri MA. Interleukin-2, interleukin-15, and their roles in human natural killer cells. *Adv Immunol*. Published online 2005. doi:10.1016/S0065-2776(04)86006-1
75. Conlon KC, Lugli E, Welles HC, et al. Redistribution, hyperproliferation, activation of natural killer cells and CD8 T cells, and cytokine production during first-in-human clinical trial of recombinant human interleukin-15 in patients with cancer. *J Clin Oncol*. Published online 2015. doi:10.1200/JCO.2014.57.3329
76. Rosario M, Liu B, Kong L, et al. The IL-15-Based ALT-803 Complex Enhances FcγRIIIa-Triggered NK Cell Responses and in Vivo Clearance of B Cell Lymphomas. *Clin Cancer Res*. Published online 2016. doi:10.1158/1078-0432.CCR-15-1419
77. Sanchez-Correa B, Valhondo I, Hassouneh F, et al. DNAM-1 and the TIGIT/PVRIG/TACTILE axis: Novel immune checkpoints for natural killer cell-based cancer immunotherapy. *Cancers*. Published online 2019. doi:10.3390/cancers11060877
78. Borrego F, Kabat J, Kim DK, et al. Structure and function of major histocompatibility complex (MHC) class I specific receptors expressed on human natural killer (NK) cells. *Mol Immunol*. Published online 2002. doi:10.1016/S0161-5890(01)00107-9
79. Sun H, Sun C. The rise of nk cell checkpoints as promising therapeutic targets in cancer immunotherapy. *Front Immunol*. Published online 2019. doi:10.3389/fimmu.2019.02354
80. Benson DM, Bakan CE, Zhang S, et al. IPH2101, a novel anti-inhibitory KIR antibody, and lenalidomide combine to enhance the natural killer cell versus multiple myeloma effect. *Blood*. Published online 2011. doi:10.1182/blood-2011-06-360255
81. Carlsten M, Korde N, Kotecha R, et al. Checkpoint inhibition of KIR2D with the monoclonal antibody IPH2101 induces contraction and hyporesponsiveness of NK cells in patients with myeloma. *Clin Cancer Res*. Published online 2016. doi:10.1158/1078-0432.CCR-16-1108
82. Bagot M, Porcu P, Marie-Cardine A, et al. IPH4102, a first-in-class anti-KIR3DL2 monoclonal antibody, in patients with relapsed or refractory cutaneous T-cell lymphoma: an international, first-in-human, open-label, phase 1 trial. *Lancet Oncol*. Published online 2019. doi:10.1016/S1470-2045(19)30320-1

83. André P, Denis C, Soulas C, et al. Anti-NKG2A mAb Is a Checkpoint Inhibitor that Promotes Anti-tumor Immunity by Unleashing Both T and NK Cells. *Cell*. Published online 2018. doi:10.1016/j.cell.2018.10.014
84. Kamiya T, Seow SV, Wong D, Robinson M, Campana D. Blocking expression of inhibitory receptor NKG2A overcomes tumor resistance to NK cells. *J Clin Invest*. Published online 2019. doi:10.1172/JCI123955
85. Zhang Q, Bi J, Zheng X, et al. Blockade of the checkpoint receptor TIGIT prevents NK cell exhaustion and elicits potent anti-tumor immunity. *Nat Immunol*. Published online 2018. doi:10.1038/s41590-018-0132-0
86. Keir ME, Butte MJ, Freeman GJ, Sharpe AH. PD-1 and its ligands in tolerance and immunity. *Annu Rev Immunol*. Published online 2008. doi:10.1146/annurev.immunol.26.021607.090331
87. Hsu J, Hodgins JJ, Marathe M, et al. Contribution of NK cells to immunotherapy mediated by PD-1/PD-L1 blockade. *J Clin Invest*. Published online 2018. doi:10.1172/JCI99317
88. Benson DM, Bakan CE, Mishra A, et al. The PD-1/PD-L1 axis modulates the natural killer cell versus multiple myeloma effect: A therapeutic target for CT-011, a novel monoclonal anti-PD-1 antibody. *Blood*. Published online 2010. doi:10.1182/blood-2010-02-271874
89. Jiang XR, Song A, Bergelson S, et al. Advances in the assessment and control of the effector functions of therapeutic antibodies. *Nat Rev Drug Discov*. Published online 2011. doi:10.1038/nrd3365
90. Zhou Q, Gil-Krzewska A, Peruzzi G, Borrego F. Matrix metalloproteinases inhibition promotes the polyfunctionality of human natural killer cells in therapeutic antibody-based anti-tumour immunotherapy. *Clin Exp Immunol*. Published online 2013. doi:10.1111/cei.12095
91. Pander J, Gelderblom H, Antonini NF, et al. Correlation of FCGR3A and EGFR germline polymorphisms with the efficacy of cetuximab in KRAS wild-type metastatic colorectal cancer. *Eur J Cancer*. Published online 2010. doi:10.1016/j.ejca.2010.03.017
92. Weng WK, Levy R. Two immunoglobulin G fragment C receptor polymorphisms independently predict response to rituximab in patients with follicular lymphoma. *J Clin Oncol*. Published online 2003. doi:10.1200/JCO.2003.05.013
93. Butler LA, Tam CS, Seymour JF. Dancing partners at the ball: Rational selection of next generation anti-CD20 antibodies for combination therapy of chronic lymphocytic leukemia in the novel agents era. *Blood Rev*. Published online 2017. doi:10.1016/j.blre.2017.05.002
94. Pereira NA, Chan KF, Lin PC, Song Z. The “less-is-more” in therapeutic antibodies: Afucosylated anti-cancer antibodies with enhanced antibody-dependent cellular cytotoxicity. *mAbs*. Published online 2018. doi:10.1080/19420862.2018.1466767
95. Falconer DJ, Subedi GP, Marcella AM, Barb AW. Antibody Fucosylation Lowers the FcγRIIIa/CD16a Affinity by Limiting the Conformations Sampled by the N162-Glycan. *ACS Chem Biol*.

Published online 2018. doi:10.1021/acscchembio.8b00342

96. Gleason MK, Verneris MR, Todhunter DA, et al. Bispecific and trispecific killer cell engagers directly activate human NK cells through CD16 signaling and induce cytotoxicity and cytokine production. *Mol Cancer Ther*. Published online 2012. doi:10.1158/1535-7163.MCT-12-0692
97. Gauthier L, Morel A, Anceriz N, et al. Multifunctional Natural Killer Cell Engagers Targeting NKp46 Trigger Protective Tumor Immunity. *Cell*. Published online 2019. doi:10.1016/j.cell.2019.04.041
98. Shi J, Tricot G, Szmania S, et al. Infusion of haplo-identical killer immunoglobulin-like receptor ligand mismatched NK cells for relapsed myeloma in the setting of autologous stem cell transplantation. *Br J Haematol*. Published online 2008. doi:10.1111/j.1365-2141.2008.07340.x
99. Pérez-Martínez A, Fernández L, Valentín J, et al. A phase I/II trial of interleukin-15-stimulated natural killer cell infusion after haplo-identical stem cell transplantation for pediatric refractory solid tumors. *Cytotherapy*. Published online 2015. doi:10.1016/j.jcyt.2015.07.011
100. Cooper MA, Elliott JM, Keyel PA, Yang L, Carrero JA, Yokoyama WM. Cytokine-induced memory-like natural killer cells. *Proc Natl Acad Sci*. 2009;106(6):1915-1919. doi:10.1073/pnas.0813192106
101. Romee R, Schneider SE, Leong JW, et al. Cytokine activation induces human memory-like NK cells. *Blood*. Published online 2012. doi:10.1182/blood-2012-04-419283
102. Simhadri VR, Dimitrova M, Mariano JL, et al. A human anti-M2 antibody mediates antibody-dependent cell-mediated cytotoxicity (ADCC) and cytokine secretion by resting and cytokine-preactivated natural killer (NK) cells. *PLoS ONE*. Published online 2015. doi:10.1371/journal.pone.0124677
103. Garg TK, Szmania SM, Khan JA, et al. Highly activated and expanded natural killer cells for multiple myeloma immunotherapy. *Haematologica*. Published online 2012. doi:10.3324/haematol.2011.056747
104. Lapteva N, Durett AG, Sun J, et al. Large-scale ex vivo expansion and characterization of natural killer cells for clinical applications. *Cytotherapy*. Published online 2012. doi:10.3109/14653249.2012.700767
105. Carlsten M, Childs RW. Genetic manipulation of NK cells for cancer immunotherapy: Techniques and clinical implications. *Front Immunol*. Published online 2015. doi:10.3389/fimmu.2015.00266
106. Mehta RS, Rezvani K. Chimeric Antigen Receptor Expressing Natural Killer Cells for the Immunotherapy of Cancer. *Front Immunol*. 2018;9:283. doi:10.3389/fimmu.2018.00283
107. Daher M, Rezvani K. Outlook for New CAR-Based Therapies with a Focus on CAR NK Cells: What Lies Beyond CAR-Engineered T Cells in the Race against Cancer. *Cancer Discov*. Published online 2021. doi:10.1158/2159-8290.cd-20-0556

108. Caruso S, De Angelis B, Carlomagno S, et al. NK cells as adoptive cellular therapy for hematological malignancies: Advantages and hurdles. *Semin Hematol*. Published online 2020. doi:10.1053/j.seminhematol.2020.10.004
109. Daher M, Basar R, Gokdemir E, et al. Targeting a cytokine checkpoint enhances the fitness of armored cord blood CAR-NK cells. *Blood*. Published online 2020. doi:10.1182/blood.2020007748
110. Gang M, Marin ND, Wong P, et al. CAR-modified memory-like NK cells exhibit potent responses to NK-resistant lymphomas. *Blood*. 2020;136(20):2308-2318. doi:10.1182/blood.2020006619
111. Zhang C, Oberoi P, Oelsner S, et al. Chimeric Antigen Receptor-Engineered NK-92 Cells: An Off-the-Shelf Cellular Therapeutic for Targeted Elimination of Cancer Cells and Induction of Protective Antitumor Immunity. *Front Immunol*. 2017;8:533. doi:10.3389/fimmu.2017.00533
112. Neely HR, Mazo IB, Gerlach C, Von Andrian UH. Is there natural killer cell memory and can it be harnessed by vaccination?: Natural killer cells in vaccination. *Cold Spring Harb Perspect Biol*. Published online 2018. doi:10.1101/cshperspect.a029488
113. Sun JC, Lanier LL. Is there natural killer cell memory and can it be harnessed by vaccination?: NK cell memory and immunization strategies against infectious diseases and cancer. *Cold Spring Harb Perspect Biol*. Published online 2018. doi:10.1101/cshperspect.a029538
114. Fehniger TA, Cooper MA. Harnessing NK Cell Memory for Cancer Immunotherapy. *Trends Immunol*. 2016;37(12):877-888. doi:10.1016/j.it.2016.09.005
115. Brillantes M, Beaulieu AM. Memory and Memory-Like NK Cell Responses to Microbial Pathogens. *Front Cell Infect Microbiol*. Published online 2020. doi:10.3389/fcimb.2020.00102
116. Min-Oo G, Kamimura Y, Hendricks DW, Nabekura T, Lanier LL. Natural killer cells: Walking three paths down memory lane. *Trends Immunol*. Published online 2013. doi:10.1016/j.it.2013.02.005
117. Netea MG, Domínguez-Andrés J, Barreiro LB, et al. Defining trained immunity and its role in health and disease. *Nat Rev Immunol*. Published online 2020. doi:10.1038/s41577-020-0285-6
118. Berrien-Elliott MM, Cashen AF, Cubitt CC, et al. Multidimensional Analyses of Donor Memory-Like NK Cells Reveal New Associations with Response after Adoptive Immunotherapy for Leukemia. *Cancer Discov*. 2020;10(12):1854-1871. doi:10.1158/2159-8290.CD-20-0312
119. Cooper MA, Colonna M, Yokoyama WM. Hidden talents of natural killers: NK cells in innate and adaptive immunity. *EMBO Rep*. 2009;10(10):1103-1110. doi:10.1038/embor.2009.203
120. Leong JW, Chase JM, Romee R, et al. Preactivation with IL-12, IL-15, and IL-18 induces cd25 and a functional high-affinity il-2 receptor on human cytokine-induced memory-like natural killer cells. *Biol Blood Marrow Transplant*. Published online 2014. doi:10.1016/j.bbmt.2014.01.006
121. Simhadri VR, Mariano JL, Zenarruzabeitia O, et al. Intact IL-12 signaling is necessary for the

generation of human natural killer cells with enhanced effector function after restimulation. *J Allergy Clin Immunol*. 2014;134(5):1190-3.e1. doi:10.1016/j.jaci.2014.06.006

122. Hüber CM, Doisne JM, Colucci F. IL-12/15/18-preactivated NK cells suppress GvHD in a mouse model of mismatched hematopoietic cell transplantation. *Eur J Immunol*. Published online 2015. doi:10.1002/eji.201445200

123. Wagner JA, Berrien-Elliott MM, Rosario M, et al. Cytokine-Induced Memory-Like Differentiation Enhances Unlicensed Natural Killer Cell Antileukemia and FcγRIIIa-Triggered Responses. *Biol Blood Marrow Transplant*. Published online 2017. doi:10.1016/j.bbmt.2016.11.018

124. Rasid O, Chevalier C, Camarasa TMN, Fitting C, Cavaillon JM, Hamon MA. H3K4me1 Supports Memory-like NK Cells Induced by Systemic Inflammation. *Cell Rep*. Published online 2019. doi:10.1016/j.celrep.2019.11.043

125. Ni J, Miller M, Stojanovic A, Garbi N, Cerwenka A. Sustained effector function of IL-12/15/18-preactivated NK cells against established tumors. *J Exp Med*. 2012;209(13):2351-2365. doi:10.1084/jem.20120944

126. Ni J, Hölsken O, Miller M, et al. Adoptively transferred natural killer cells maintain long-term antitumor activity by epigenetic imprinting and CD4+ T cell help. *Oncoimmunology*. 2016;5(9):e1219009. doi:10.1080/2162402X.2016.1219009

127. Song Y, Hu B, Liu Y, et al. IL-12/IL-18-preactivated donor NK cells enhance GVL effects and mitigate GvHD after allogeneic hematopoietic stem cell transplantation. *Eur J Immunol*. Published online 2018. doi:10.1002/eji.201747177

128. Boieri M, Ulvmoen A, Sudworth A, et al. IL-12, IL-15, and IL-18 pre-activated NK cells target resistant T cell acute lymphoblastic leukemia and delay leukemia development in vivo. *Oncoimmunology*. Published online 2017. doi:10.1080/2162402X.2016.1274478

129. Zhuang L, Fulton RJ, Rettman P, et al. Activity of IL-12/15/18 primed natural killer cells against hepatocellular carcinoma. *Hepatol Int*. Published online 2019. doi:10.1007/s12072-018-9909-3

130. Uppendahl LD, Felices M, Bendzick L, et al. Cytokine-induced memory-like natural killer cells have enhanced function, proliferation, and in vivo expansion against ovarian cancer cells. *Gynecol Oncol*. Published online 2019. doi:10.1016/j.ygyno.2019.01.006

131. O'Leary JG, Goodarzi M, Drayton DL, von Andrian UH. T cell- and B cell-independent adaptive immunity mediated by natural killer cells. *Nat Immunol*. 2006;7(5):507-516. doi:10.1038/ni1332

132. S P, HS G, BZ W, et al. Critical role for the chemokine receptor CXCR6 in NK cell-mediated antigen-specific memory of haptens and viruses. *Nat Immunol*. 2010;11(12). doi:10.1038/Ni.1953

133. Gumá M, Angulo A, Vilches C, Gómez-Lozano N, Malats N, López-Botet M. Imprint of human cytomegalovirus infection on the NK cell receptor repertoire. *Blood*. 2004;104(12):3664-3671. doi:10.1182/blood-2004-05-2058

134. Gumá M, Budt M, Sáez A, et al. Expansion of CD94/NKG2C+ NK cells in response to human cytomegalovirus-infected fibroblasts. *Blood*. Published online 2006. doi:10.1182/blood-2005-09-3682
135. Lopez-Vergès S, Milush JM, Schwartz BS, et al. Expansion of a unique CD57 +NKG2C hi natural killer cell subset during acute human cytomegalovirus infection. *Proc Natl Acad Sci U S A*. Published online 2011. doi:10.1073/pnas.1110900108
136. Rölle A, Pollmann J, Ewen EM, et al. IL-12-producing monocytes and HLA-E control HCMV-driven NKG2C+ NK cell expansion. *J Clin Invest*. Published online 2014. doi:10.1172/JCI77440
137. Hammer Q, Rückert T, Borst EM, et al. Peptide-specific recognition of human cytomegalovirus strains controls adaptive natural killer cells article. *Nat Immunol*. Published online 2018. doi:10.1038/s41590-018-0082-6
138. Rölle A, Brodin P. Immune Adaptation to Environmental Influence: The Case of NK Cells and HCMV. *Trends Immunol*. Published online 2016. doi:10.1016/j.it.2016.01.005
139. Cichocki F, Taras E, Chiuppesi F, et al. Adaptive NK cell reconstitution is associated with better clinical outcomes. *JCI Insight*. Published online 2019. doi:10.1172/jci.insight.125553
140. Kim KH, Yu HT, Hwang I, et al. Phenotypic and Functional Analysis of Human NK Cell Subpopulations According to the Expression of FcεRγ and NKG2C. *Front Immunol*. Published online 2019. doi:10.3389/fimmu.2019.02865
141. Liu W, Scott JM, Langguth E, Chang H, Park PH, Kim S. FcRγ Gene Editing Reprograms Conventional NK Cells to Display Key Features of Adaptive Human NK Cells. *iScience*. Published online 2020. doi:10.1016/j.isci.2020.101709
142. Gumá M, Cabrera C, Erkizia I, et al. Human cytomegalovirus infection is associated with increased proportions of NK cells that express the CD94/NKG2C receptor in aviremic HIV-1-positive patients. *J Infect Dis*. Published online 2006. doi:10.1086/504719
143. Björkström NK, Lindgren T, Stoltz M, et al. Rapid expansion and long-term persistence of elevated NK cell numbers in humans infected with hantavirus. *J Exp Med*. Published online 2011. doi:10.1084/jem.20100762
144. Petitdemange C, Becquart P, Wauquier N, et al. Unconventional repertoire profile is imprinted during acute chikungunya infection for natural killer cells polarization toward cytotoxicity. *PLoS Pathog*. Published online 2011. doi:10.1371/journal.ppat.1002268
145. Maucourant C, Filipovic I, Ponzetta A, et al. Natural killer cell immunotypes related to COVID-19 disease severity. *Sci Immunol*. Published online 2020. doi:10.1126/SCIIMMUNOL.ABD6832
146. Zenarruzabeitia O, Astarloa-Pando G, Terrén I, et al. T Cell Activation, Highly Armed Cytotoxic Cells and a Shift in Monocytes CD300 Receptors Expression Is Characteristic of Patients With Severe COVID-19. *Front Immunol*. 2021;12:655934. doi:10.3389/fimmu.2021.655934

147. Nikzad R, Angelo LS, Aviles-Padilla K, et al. Human natural killer cells mediate adaptive immunity to viral antigens. *Sci Immunol*. Published online 2019. doi:10.1126/sciimmunol.aat8116
148. Stary V, Pandey RV, Strobl J, et al. A discrete subset of epigenetically primed human NK cells mediates antigen-specific immune responses. *Sci Immunol*. Published online 2020. doi:10.1126/sciimmunol.aba6232
149. Sun JC, Beilke JN, Lanier LL. Adaptive immune features of natural killer cells. *Nature*. 2009;457(7229):557-561. doi:10.1038/nature07665
150. Brown MG, Dokun AO, Heusel JW, et al. Vital Involvement of a Natural Killer Cell Activation Receptor in Resistance to Viral Infection. *Science*. 2001;292(5518):934-937. doi:10.1126/science.1060042
151. Grassmann S, Pachmayr LO, Leube J, et al. Distinct Surface Expression of Activating Receptor Ly49H Drives Differential Expansion of NK Cell Clones upon Murine Cytomegalovirus Infection. *Immunity*. 2019;50(6):1391-1400.e4. doi:10.1016/j.immuni.2019.04.015
152. Adams NM, Geary CD, Santosa EK, et al. Cytomegalovirus Infection Drives Avidity Selection of Natural Killer Cells. *Immunity*. 2019;50(6):1381-1390.e5. doi:10.1016/j.immuni.2019.04.009
153. Sun JC, Madera S, Bezman NA, Beilke JN, Kaplan MH, Lanier LL. Proinflammatory cytokine signaling required for the generation of natural killer cell memory. *J Exp Med*. 2012;209(5):947-954. doi:10.1084/jem.20111760
154. Madera S, Sun JC. Cutting Edge: Stage-Specific Requirement of IL-18 for Antiviral NK Cell Expansion. *J Immunol*. 2015;194(4):1408-1412. doi:10.4049/jimmunol.1402001
155. Mikelez-Alonso I, Magadán S, González-Fernández Á, Borrego F. Natural killer (NK) cell-based immunotherapies and the many faces of NK cell memory: A look into how nanoparticles enhance NK cell activity. *Adv Drug Deliv Rev*. 2021;176:113860. doi:10.1016/j.addr.2021.113860
156. Bennett IL, Beeson PB. STUDIES ON THE PATHOGENESIS OF FEVER ii. Characterization of fever-producing substances from polymorphonuclear leukocytes and from the fluid of sterile exudates. *J Exp Med*. 1953;(1):493-508. doi:10.1084/jem.98.5.493
157. Stenken JA, Poschenrieder AJ. Bioanalytical chemistry of cytokines – A review. *Anal Chim Acta*. 2015;853:95-115. doi:10.1016/j.aca.2014.10.009
158. Lunney JK. Cytokines orchestrating the immune response. *OIE Rev Sci Tech*. 1998;17(1):84-94. doi:10.20506/rst.17.1.1094
159. Vogel DYS, Glim JE, Stavenuiter AWD, et al. Human macrophage polarization in vitro: Maturation and activation methods compared. *Immunobiology*. 2014;219(9):695-703. doi:10.1016/j.imbio.2014.05.002
160. Wu MF, Lin CA, Yuan TH, et al. The M1/M2 spectrum and plasticity of malignant pleural effusion-macrophage in advanced lung cancer. *Cancer Immunol Immunother*. 2021;70:1435-1450. doi:10.1007/s00262-020-02781-8

161. Genin M, Clement F, Fattaccioli A, Raes M, Michiels C. M1 and M2 macrophages derived from THP-1 cells differentially modulate the response of cancer cells to etoposide. *BMC Cancer*. 2015;15(1):1-14. doi:10.1186/s12885-015-1546-9
162. Chen Y, Zhang S, Wang Q, Zhang X. Tumor-recruited M2 macrophages promote gastric and breast cancer metastasis via M2 macrophage-secreted CHI3L1 protein. *J Hematol Oncol/J Hematol Oncol*. 2017;10(36):1-13. doi:10.1186/s13045-017-0408-0
163. Zhang Q, Wang H, Mao C, et al. Fatty acid oxidation contributes to IL-1 β secretion in M2 macrophages and promotes macrophage-mediated tumor cell migration. *Mol Immunol*. 2018;94(December 2017):27-35. doi:10.1016/j.molimm.2017.12.011
164. Lee SH, Kim JW, Lee HW, et al. Interferon regulatory factor-1 (IRF-1) is a mediator for interferon- γ induced attenuation of telomerase activity and human telomerase reverse transcriptase (hTERT) expression. *Oncogene*. 2003;22(3):381-391. doi:10.1038/sj.onc.1206133
165. Guinn ZP, Petro TM. IFN- γ synergism with poly I:C reduces growth of murine and human cancer cells with simultaneous changes in cell cycle and immune checkpoint proteins. *Cancer Lett*. 2018;438:1-9. doi:10.1016/j.canlet.2018.09.003
166. Burke JD, Young HA. IFN- γ : A cytokine at the right time, is in the right place. *Semin Immunol*. 2019;43(May):101280. doi:10.1016/j.smim.2019.05.002
167. Ding G, Shen T, Yan C, Zhang M, Wu Z, Cao L. IFN- γ down-regulates the PD-1 expression and assist nivolumab in PD-1-blockade effect on CD8+ T-lymphocytes in pancreatic cancer. *BMC Cancer*. 2019;19(1):1-11. doi:10.1186/s12885-019-6145-8
168. Yin H, Jiang Z, Wang S, Zhang P. IFN- γ restores the impaired function of RNase L and induces mitochondria-mediated apoptosis in lung cancer. *Cell Death Dis*. 2019;10(9). doi:10.1038/s41419-019-1902-9
169. Reichert TE, Nagashima S, Kashii Y, et al. Interleukin-2 expression in human carcinoma cell lines and its role in cell cycle progression. *Oncogene*. 2000;19(4):514-525. doi:10.1038/sj.onc.1203391
170. Jen EY, Poindexter NJ, Farnsworth ES, Grimm EA. IL-2 regulates the expression of the tumor suppressor IL-24 in melanoma cells. *Melanoma Res*. 2012;22(1):19-29. doi:10.1097/CMR.0b013e32834d2506
171. Balemans LTM, Steerenberg PA, Koppenhagen FJ, et al. PEG-IL-2 therapy of advanced cancer in the guinea pig. Impact of the primary tumor and beneficial effect of cyclophosphamide. *Int J Cancer*. 1994;58(6):871-876. doi:10.1002/ijc.2910580621
172. Levin AM, Bates DL, Ring AM, et al. Exploiting a natural conformational switch to engineer an interleukin-2 "superkine." *Nature*. 2012;484(7395):529-533. doi:10.1038/nature10975
173. Tietze JK, Wilkins DEC, Sckisel GD, et al. Delineation of antigen-specific and antigen-nonspecific CD8+ memory T-cell responses after cytokine-based cancer immunotherapy. *Blood*.

2012;119(13):3073-3083. doi:10.1182/blood-2011-07-369736

174. Carmentate T, Pacios A, Enamorado M, et al. Human IL-2 Mutein with Higher Antitumor Efficacy Than Wild Type IL-2. *J Immunol*. 2013;190(12):6230-6238. doi:10.4049/jimmunol.1201895
175. Sun Z, Ren Z, Yang K, et al. A next-generation tumor-targeting IL-2 preferentially promotes tumor-infiltrating CD8+ T-cell response and effective tumor control. *Nat Commun*. 2019;10(1). doi:10.1038/s41467-019-11782-w
176. Deng L, Fan J, Guo M, Huang B. Oncolytic and immunologic cancer therapy with GM-CSF-armed vaccinia virus of Tian Tan strain Guang9. *Cancer Lett*. 2016;372(2):251-257. doi:10.1016/j.canlet.2016.01.025
177. Etxeberria I, Bolaños E, Quetglas JI, et al. Intratumor Adoptive Transfer of IL-12 mRNA Transiently Engineered Antitumor CD8+ T Cells. *Cancer Cell*. 2019;36(6):613-629. doi:10.1016/j.ccell.2019.10.006
178. Conlon KC, Miljkovic MD, Waldmann TA. Cytokines in the Treatment of Cancer. *J Interferon Cytokine Res*. 2019;39(1):6-21. doi:10.1089/jir.2018.0019
179. Qiu Y, He X, Li Z, Jiang Y, Jia Y. Efficacy of early combination of local radiotherapy and GM-CSF for advanced non-small cell lung cancer treated with icotinib. *Ir J Med Sci*. 2020;189(3):791-797. doi:10.1007/s11845-019-02137-x
180. Berraondo P, Sanmamed MF, Ochoa MC, et al. Cytokines in clinical cancer immunotherapy. *Br J Cancer*. 2019;120(1):6-15. doi:10.1038/s41416-018-0328-y
181. Fehniger TA, Shah MH, Turner MJ, et al. Differential cytokine and chemokine gene expression by human NK cells following activation with IL-18 or IL-15 in combination with IL-12: implications for the innate immune response. *J Immunol Baltim Md 1950*. 1999;162(8):4511-4520.
182. Michelle Longmire, Peter L. Choyke, M.D., and Hisataka Kobayashi, M.D. PhD. Clearance Properties of Nano-sized Particles and Molecules as Imaging Agents: Consideration and Caveats. *Nanomedicine Lond*. 2008;3(5):703-717. doi:10.2217/17435889.3.5.703.
183. Votavova P, Tomala J, Subr V, et al. Novel IL-2-poly(HPMA)nanoconjugate based immunotherapy. *J Biomed Nanotechnol*. 2015;11(9):1662-1673. doi:10.1166/jbn.2015.2114
184. Saha AK, Zhen MYS, Erogbogbo F, Ramasubramanian AK. Design Considerations and Assays for Hemocompatibility of FDA-Approved Nanoparticles. *Semin Thromb Hemost*. 2020;46(5):637-652. doi:10.1055/s-0039-1688491
185. Liu X, Gao X, Zheng S, et al. Modified nanoparticle mediated IL-12 immunogene therapy for colon cancer. *Nanomedicine Nanotechnol Biol Med*. 2017;13(6):1993-2004. doi:10.1016/j.nano.2017.04.006
186. Prijic S, Prosen L, Cemazar M, et al. Surface modified magnetic nanoparticles for immunogene therapy of murine mammary adenocarcinoma. *Biomaterials*. 2012;33(17):4379-4391. doi:10.1016/j.biomaterials.2012.02.061

187. Hu Q, Shang L, Wang M, et al. Co-Delivery of Paclitaxel and Interleukin-12 Regulating Tumor Microenvironment for Cancer Immunochemotherapy. *Adv Healthc Mater.* 2020;9(10):1901858. doi:10.1002/adhm.201901858
188. Huang KW, Hsu FF, Qiu JT, et al. Highly efficient and tumor-selective nanoparticles for dual-targeted immunogene therapy against cancer. *Sci Adv.* 2020;6(3). doi:10.1126/sciadv.aax5032
189. Ultimo A, De La Torre C, Giménez C, et al. Nanoparticle-cell-nanoparticle communication by stigmergy to enhance poly(I:C) induced apoptosis in cancer cells. *Chem Commun.* 2020;56(53):7273-7276. doi:10.1039/d0cc02795b
190. Tan L, Han S, Ding S, et al. Chitosan nanoparticle-based delivery of fused NKG2D-IL-21 gene suppresses colon cancer growth in mice. *Int J Nanomedicine.* 2017;12:3095-3107. doi:10.2147/IJN.S128032
191. Lv Q, He C, Quan F, Yu S, Chen X. DOX/IL-2/IFN- γ co-loaded thermo-sensitive polypeptide hydrogel for efficient melanoma treatment. *Bioact Mater.* 2018;3(1):118-128. doi:10.1016/j.bioactmat.2017.08.003
192. Barberio AE, Smith SG, Correa S, et al. Cancer Cell Coating Nanoparticles for Optimal Tumor-Specific Cytokine Delivery. *ACS Nano.* 2020;14(9):11238-11253. doi:10.1021/acsnano.0c03109
193. Wu T, Qiao Q, Qin X, Zhang D, Zhang Z. Immunostimulatory cytokine and doxorubicin co-loaded nanovesicles for cancer immunochemotherapy. *Nanomedicine Nanotechnol Biol Med.* 2019;18:66-77. doi:10.1016/j.nano.2019.02.008
194. Jiang D, Gao T, Liang S, et al. Lymph Node Delivery Strategy Enables the Activation of Cytotoxic T Lymphocytes and Natural Killer Cells to Augment Cancer Immunotherapy. *ACS Appl Mater Interfaces.* 2021;13(19):22213-22224. doi:10.1021/acsmi.1c03709
195. Waldmann TA. The shared and contrasting roles of IL2 and IL15 in the life and death of normal and neoplastic lymphocytes: Implications for cancer therapy. *Cancer Immunol Res.* 2015;3(3):219-227. doi:10.1158/2326-6066.CIR-15-0009
196. Carson WE, Giri JG, Lindemann MJ, et al. Interleukin (IL) 15 is a novel cytokine that activates human natural killer cells via components of the IL-2 receptor. *J Exp Med.* 1994;180(4):1395-1403. doi:10.1084/jem.180.4.1395
197. Chirifu M, Hayashi C, Nakamura T, et al. Crystal structure of the IL-15-IL-15R α complex, a cytokine-receptor unit presented in trans. *Nat Immunol.* 2007;8(9):1001-1007. doi:10.1038/ni1492
198. Ring AM, Lin JX, Feng D, et al. Mechanistic and structural insight into the functional dichotomy between IL-2 and IL-15. *Nat Immunol.* 2012;13(12):1187-1195. doi:10.1038/ni.2449
199. Hong E, Usiskin IM, Bergamaschi C, et al. Configuration-dependent presentation of multivalent IL-15: IL-15R α enhances the antigen-specific T cell response and anti-tumor immunity. *J Biol Chem.* 2016;291(17):8931-8950. doi:10.1074/jbc.M115.695304

200. Kobayashi H, Dubois S, Sato N, et al. Role of trans-cellular IL-15 presentation in the activation of NK cell-mediated killing, which leads to enhanced tumor immunosurveillance. *Blood*. 2005;105(2):721-727. doi:10.1182/blood-2003-12-4187
201. Cornish GH, Sinclair L V., Cantrell DA. Differential regulation of T-cell growth by IL-2 and IL-15. *Blood*. 2006;108(2):600-608. doi:10.1182/blood-2005-12-4827
202. Yang Y, Lundqvist A. Immunomodulatory Effects of IL-2 and IL-15; Implications for Cancer Immunotherapy. *Cancers*. 2020;12:3586. doi:10.3390/cancers12123586
203. Rausch A, Heßmann M, Hölscher A, et al. Interleukin-15 mediates protection against experimental tuberculosis: A role for NKG2D-dependent effector mechanisms of CD8+ T cells. *Eur J Immunol*. 2006;36(5):1156-1167. doi:10.1002/eji.200535290
204. Gillgrass A, Gill N, Babian A, Ashkar AA. The Absence or Overexpression of IL-15 Drastically Alters Breast Cancer Metastasis via Effects on NK Cells, CD4 T Cells, and Macrophages. *J Immunol*. 2014;193(12):6184-6191. doi:10.4049/jimmunol.1303175
205. Zhang M, Wen B, Anton OM, et al. IL-15 enhanced antibody-dependent cellular cytotoxicity mediated by NK cells and macrophages. *Proc Natl Acad Sci U S A*. 2018;115(46):E10915-E10924. doi:10.1073/pnas.1811615115
206. Aehnlich P, Carnaz Simões AM, Skadborg SK, Holmen Olofsson G, thor Straten P. Expansion With IL-15 Increases Cytotoxicity of V γ 9V δ 2 T Cells and Is Associated With Higher Levels of Cytotoxic Molecules and T-bet. *Front Immunol*. 2020;11. doi:10.3389/fimmu.2020.01868
207. Rautela J, Huntington ND. IL-15 signaling in NK cell cancer immunotherapy. *Curr Opin Immunol*. 2017;44:1-6. doi:10.1016/j.coi.2016.10.004
208. Wrangle JM, Velcheti V, Patel MR, et al. ALT-803, an IL-15 superagonist, in combination with nivolumab in patients with metastatic non-small cell lung cancer: a non-randomised, open-label, phase 1b trial. *Lancet Oncol*. 2018;19(5):694-704. doi:10.1016/S1470-2045(18)30148-7
209. Hu Q, Ye X, Qu X, et al. Discovery of a novel IL-15 based protein with improved developability and efficacy for cancer immunotherapy. *Sci Rep*. 2018;8(1):1-11. doi:10.1038/s41598-018-25987-4
210. Van der Meer JMR, Maas RJA, Guldevall K, et al. IL-15 superagonist N-803 improves IFN γ production and killing of leukemia and ovarian cancer cells by CD34+ progenitor-derived NK cells. *Cancer Immunol Immunother*. 2021;70(5):1305-1321. doi:10.1007/s00262-020-02749-8
211. Zhang D, Baldwin P, Leal AS, Carapellucci S, Sridhar S, Liby KT. A nano-liposome formulation of the PARP inhibitor Talazoparib enhances treatment efficacy and modulates immune cell populations in mammary tumors of BRCA-deficient mice. *Theranostics*. 2019;9(21):6224-6238. doi:10.7150/thno.36281
212. Roma-Rodrigues C, Pombo I, Raposo L, Pedrosa P, Fernandes AR, Baptista P V. Nanotheranostics Targeting the Tumor Microenvironment. *Front Bioeng Biotechnol*. 2019;7(August):1-18. doi:10.3389/fbioe.2019.00197

213. Li SD, Huang L. Pharmacokinetics and Biodistribution of Nanoparticles. *Mol Pharm*. 2008;5(4):496-504. doi:10.1021/mp800049w
214. Couzin-Frankel J. Cancer immunotherapy. *Science*. 2013;342(6165):1432-1433. doi:10.1080/10408360902937809
215. Khang D, Lee YK, Choi EJ, Webster TJ, Kim SH. Effect of the protein corona on nanoparticles for modulating cytotoxicity and immunotoxicity. *Int J Nanomedicine*. Published online December 2014:97. doi:10.2147/IJN.S72998
216. Corbo C, Molinaro R, Parodi A, Furman NET, Salvatore F, Tasciotti E. The impact of nanoparticle protein corona on cytotoxicity, immunotoxicity and target drug delivery. *Nanomed*. 2016;11(1):81-100. doi:10.2217/nnm.15.188
217. Barbalinardo M, Bertacchini J, Bergamini L, et al. Surface properties modulate protein corona formation and determine cellular uptake and cytotoxicity of silver nanoparticles. *Nanoscale*. 2021;13(33):14119-14129. doi:10.1039/D0NR08259G
218. Mikelez-alonso I, Aires A, Cortajarena AL. Cancer nano-immunotherapy from the injection to the target: The role of protein corona. *Int J Mol Sci*. 2020;21(2). doi:10.3390/ijms21020519
219. Zanganeh S, Hutter G, Spitler R, et al. Iron oxide nanoparticles inhibit tumour growth by inducing pro-inflammatory macrophage polarization in tumour tissues. *Nat Nanotechnol*. 2016;11(11):986-994. doi:10.1038/nnano.2016.168.Iron
220. Lizotte PH, Wen AM, Sheen MR, et al. In situ vaccination with cowpea mosaic virus nanoparticles suppresses metastatic cancer. *Nat Nanotechnol*. 2016;11(3):295-303. doi:10.1038/nnano.2015.292
221. Duval KEA, Wagner RJ, Beiss V, Fiering SN, Steinmetz NF, Hoopes PJ. Cowpea Mosaic Virus Nanoparticle Enhancement of Hypofractionated Radiation in a B16 Murine Melanoma Model. *Front Oncol*. 2020;10:594614. doi:10.3389/fonc.2020.594614
222. Kranz LM, Diken M, Haas H, et al. Systemic RNA delivery to dendritic cells exploits antiviral defence for cancer immunotherapy. *Nature*. 2016;534(7607):396-401. doi:10.1038/nature18300
223. Beg MS, Brenner AJ, Sachdev J, et al. Phase I study of MRX34, a liposomal miR-34a mimic, administered twice weekly in patients with advanced solid tumors. *Invest New Drugs*. 2017;35(2):180-188. doi:10.1007/s10637-016-0407-y
224. Martín M, Chacón JI, Antón A, et al. Neoadjuvant Therapy with Weekly Nanoparticle Albumin-Bound Paclitaxel for Luminal Early Breast Cancer Patients: Results from the NABRAX Study (GEICAM/2011-02), a Multicenter, Non-Randomized, Phase II Trial, with a Companion Biomarker Analysis. *The Oncologist*. 2017;22(11):1301-1308. doi:10.1634/theoncologist.2017-0052
225. Li Y, Zeng J, Huang M, et al. A phase 2 study of nanoparticle albumin-bound paclitaxel plus nedaplatin for patients with advanced, recurrent, or metastatic cervical carcinoma. *Cancer*. 2017;123(3):420-425. doi:10.1002/cncr.30328

226. Chen Q, Wang C, Zhang X, et al. In situ sprayed bioresponsive immunotherapeutic gel for post-surgical cancer treatment. *Nat Nanotechnol.* 2019;14(1):89-97. doi:10.1038/s41565-018-0319-4
227. Higano CS, Armstrong AJ, Sartor AO, et al. Real-world outcomes of sipuleucel-T treatment in PROCEED, a prospective registry of men with metastatic castration-resistant prostate cancer. *Cancer.* Published online 2019:1-9. doi:10.1002/cncr.32445
228. Dufner V, Sayehli CM, Chatterjee M, et al. Long-term outcome of patients with relapsed/refractory B-cell non-Hodgkin lymphoma treated with blinatumomab. *Blood Adv.* 2019;3(16):2491-2498. doi:10.1182/bloodadvances.2019000025
229. Zhang Y, Fang Z, Li R, Huang X, Liu Q. Design of Outer Membrane Vesicles as Cancer Vaccines: A New Toolkit for Cancer Therapy. *Cancers.* 2019;11(9):1314. doi:10.3390/cancers11091314
230. Kaufman HL, Shalhout SZ, Iodice G. Talimogene Laherparepvec: Moving From First-In-Class to Best-In-Class. *Front Mol Biosci.* 2022;9:834841. doi:10.3389/fmolb.2022.834841
231. Von Hoff DD, Mita MM, Ramanathan RK, et al. Phase I study of PSMA-targeted docetaxel-containing nanoparticle BIND-014 in patients with advanced solid tumors. *Clin Cancer Res.* 2016;22(13):3157-3163. doi:10.1158/1078-0432.CCR-15-2548
232. Autio KA, Dreicer R, Anderson J, et al. Safety and Efficacy of BIND-014, a Docetaxel Nanoparticle Targeting Prostate-Specific Membrane Antigen for Patients with Metastatic Castration-Resistant Prostate Cancer: A Phase 2 Clinical Trial. *JAMA Oncol.* 2018;4(10):1344-1351. doi:10.1001/jamaoncol.2018.2168
233. Barenholz Y. Doxil® - The first FDA-approved nano-drug: Lessons learned. *J Controlled Release.* 2012;160(2):117-134. doi:10.1016/j.jconrel.2012.03.020
234. Zhang J, Chen Y, Li X, Liang X, Luo X. The influence of different long-circulating materials on the pharmacokinetics of liposomal vincristine sulfate. *Int J Nanomedicine.* 2016;11:4187-4197. doi:10.2147/IJN.S109547
235. Wang Z, Zheng Q, Zhang H, et al. Ontak-like human IL-2 fusion toxin. *J Immunol Methods.* 2017;448:51-58. doi:10.1016/j.jim.2017.05.008
236. Cousin S, Seneschal J, Italiano A. Toxicity profiles of immunotherapy. *Pharmacol Ther.* Published online 2018. doi:10.1016/j.pharmthera.2017.07.005
237. Saikia J, Yazdimamaghani M, Hadipour Moghaddam SP, Ghandehari H. Differential Protein Adsorption and Cellular Uptake of Silica Nanoparticles Based on Size and Porosity. *ACS Appl Mater Interfaces.* 2016;8(50):34820-34832. doi:10.1021/acsami.6b09950
238. Glancy D, Zhang Y, Wu JLY, Ouyang B, Ohta S, Chan WCW. Characterizing the protein corona of sub-10 nm nanoparticles. *J Controlled Release.* 2019;304(January):102-110. doi:10.1016/j.jconrel.2019.04.023
239. Franqui LS, De Farias MA, Portugal R V., et al. Interaction of graphene oxide with cell culture

- medium: Evaluating the fetal bovine serum protein corona formation towards in vitro nanotoxicity assessment and nanobiointeractions. *Mater Sci Eng C*. 2019;100(September 2018):363-377. doi:10.1016/j.msec.2019.02.066
240. Hühn D, Kantner K, Geidel C, et al. Polymer-coated nanoparticles interacting with proteins and cells: Focusing on the sign of the net charge. *ACS Nano*. 2013;7(4):3253-3263. doi:10.1021/nn3059295
241. Lai W, Wang Q, Li L, Hu Z, Chen J, Fang Q. Interaction of gold and silver nanoparticles with human plasma: Analysis of protein corona reveals specific binding patterns. *Colloids Surf B Biointerfaces*. 2017;152:317-325. doi:10.1016/j.colsurfb.2017.01.037
242. Giulimondi F, Digiacomio L, Pozzi D, et al. Interplay of protein corona and immune cells controls blood residency of liposomes. *Nat Commun*. 2019;10(1):3686. doi:10.1038/s41467-019-11642-7
243. Partikel K, Korte R, Stein NC, et al. Effect of nanoparticle size and PEGylation on the protein corona of PLGA nanoparticles. *Eur J Pharm Biopharm*. 2019;141(February):70-80. doi:10.1016/j.ejpb.2019.05.006
244. Aires A, Cabrera D, Alonso-Pardo LC, Cortajarena AL, Teran FJ. Elucidation of the physicochemical properties ruling the colloidal stability of iron oxide nanoparticles under physiological conditions. *ChemNanoMat*. 2017;3(3):183-189. doi:10.1002/cnma.201600333
245. Ekdahl KN, Fromell K, Mohlin C, Teramura Y, Nilsson B. A human whole-blood model to study the activation of innate immunity system triggered by nanoparticles as a demonstrator for toxicity. *Sci Technol Adv Mater*. 2019;20(1):688-698. doi:10.1080/14686996.2019.1625721
246. Zhou H, Fan Z, Li PY, et al. Dense and Dynamic Polyethylene Glycol Shells Cloak Nanoparticles from Uptake by Liver Endothelial Cells for Long Blood Circulation. *ACS Nano*. 2018;12(10):10130-10141. doi:10.1021/acsnano.8b04947
247. Kokkinopoulou M, Simon J, Landfester K, Mailänder V, Lieberwirth I. Visualization of the protein corona: Towards a biomolecular understanding of nanoparticle-cell-interactions. *Nanoscale*. 2017;9(25):8858-8870. doi:10.1039/c7nr02977b
248. Martinez-Moro M, Di Silvio D, Moya SE. Fluorescence correlation spectroscopy as a tool for the study of the intracellular dynamics and biological fate of protein corona. *Biophys Chem*. 2019;253(July):106218. doi:10.1016/j.bpc.2019.106218
249. Carrillo-Carrion C, Carril M, Parak WJ. Techniques for the experimental investigation of the protein corona. *Curr Opin Biotechnol*. 2017;46(Figure 1):106-113. doi:10.1016/j.copbio.2017.02.009
250. Carril M, Padro D, Del Pino P, Carrillo-Carrion C, Gallego M, Parak WJ. In situ detection of the protein corona in complex environments. *Nat Commun*. 2017;8(1). doi:10.1038/s41467-017-01826-4
251. Bousquet Y, Swart PJ, Schmitt-Colin N, et al. Molecular Mechanisms of the Adsorption of a Model Protein (Human Serum Albumin) on Poly(Methylidene Malonate 2.1.2) Nanoparticles.pdf.

Pharm Res. 1999;16(1):141-147.

252. Lindman S, Lynch I, Thulin E, Nilsson H, Dawson KA, Linse S. Systematic investigation of the thermodynamics of HSA adsorption to N-iso-propylacrylamide/N-tert-butylacrylamide copolymer nanoparticles. Effects of particle size and hydrophobicity. *Nano Lett.* 2007;7(4):914-920. doi:10.1021/nl062743+
253. Baier G, Costa C, Zeller A, et al. BSA Adsorption on Differently Charged Polystyrene Nanoparticles using Isothermal Titration Calorimetry and the Influence on Cellular Uptake. *Macromol Biosci.* 2011;11(5):628-638. doi:10.1002/mabi.201000395
254. Milani S, Baldelli Bombelli F, Pitek AS, Dawson KA, Rädler J. Reversible versus irreversible binding of transferrin to polystyrene nanoparticles: Soft and hard corona. *ACS Nano.* 2012;6(3):2532-2541. doi:10.1021/nn204951s
255. Jiang X, Weise S, Hafner M, et al. Quantitative analysis of the protein corona on FePt nanoparticles formed by transferrin binding. *J R Soc Interface.* 2010;7(SUPPL. 1). doi:10.1098/rsif.2009.0272.focus
256. Partikel K, Korte R, Mulac D, Humpf HU, Langer K. Serum type and concentration both affect the protein-corona composition of PLGA nanoparticles. *Beilstein J Nanotechnol.* 2019;10:1002-1015. doi:10.3762/BJNANO.10.101
257. Gossmann R, Fahrländer E, Hummel M, Mulac D, Brockmeyer J, Langer K. Comparative examination of adsorption of serum proteins on HSA- and PLGA-based nanoparticles using SDS-PAGE and LC-MS. *Eur J Pharm Biopharm.* 2015;93(March):80-87. doi:10.1016/j.ejpb.2015.03.021
258. Kah JCY, Wong KY, Neoh KG, et al. Critical parameters in the pegylation of gold nanoshells for biomedical applications: An in vitro macrophage study. *J Drug Target.* 2009;17(3):181-193. doi:10.1080/10611860802582442
259. Barbero F, Russo L, Vitali M, et al. Formation of the Protein Corona: The Interface between Nanoparticles and the Immune System. *Semin Immunol.* 2017;34(September):52-60. doi:10.1016/j.smim.2017.10.001
260. Shanehsazzadeh S, Gruettner C, Lahooti A, et al. Monoclonal antibody conjugated magnetic nanoparticles could target MUC-1-positive cells in vitro but not in vivo. *Contrast Media Mol Imaging.* 2015;10(3):225-236. doi:10.1002/cmimi.1627
261. Varnamkhasti BS, Hosseinzadeh H, Azhdarzadeh M, et al. Protein corona hampers targeting potential of MUC1 aptamer functionalized SN-38 core-shell nanoparticles. *Int J Pharm.* 2015;494(1):430-444. doi:10.1016/j.ijpharm.2015.08.060
262. Bargheer D, Nielsen J, Gébel G, et al. The fate of a designed protein corona on nanoparticles in vitro and in vivo. *Beilstein J Nanotechnol.* 2015;6(1):36-46. doi:10.3762/bjnano.6.5
263. Monteiro-Riviere NA, Riviere JE, Choi K. Biocorona formation on gold nanoparticles modulates human proximal tubule kidney cell uptake, cytotoxicity and gene expression. *Toxicol In Vitro.* 2017;42(April):150-160. doi:10.1016/j.tiv.2017.04.020

264. PrabhuDas MR, Baldwin CL, Bollyky PL, et al. A Consensus Definitive Classification of Scavenger Receptors and Their Roles in Health and Disease. *J Immunol*. 2017;198(10):3775-3789. doi:10.4049/jimmunol.1700373
265. Fleischer CC, Payne CK. Nanoparticle-cell interactions: Molecular structure of the protein corona and cellular outcomes. *Acc Chem Res*. 2014;47(8):2651-2659. doi:10.1021/ar500190q
266. Fleischer CC, Payne CK. Secondary structure of corona proteins determines the cell surface receptors used by nanoparticles. *J Phys Chem B*. 2014;118(49):14017-14026. doi:10.1021/jp502624n
267. Mortimer GM, Butcher NJ, Musumeci AW, Deng ZJ, Martin DJ, Minchin RF. Cryptic epitopes of albumin determine mononuclear phagocyte system clearance of nanomaterials. *ACS Nano*. 2014;8(4):3357-3366. doi:10.1021/nn405830g
268. Lartigue L, Wilhelm C, Servais J, et al. Nanomagnetic sensing of blood plasma protein interactions with iron oxide nanoparticles: Impact on macrophage uptake. *ACS Nano*. 2012;6(3):2665-2678. doi:10.1021/nn300060u
269. Dai Q, Guo J, Yan Y, Ang CS, Bertleff-Zieschang N, Caruso F. Cell-Conditioned Protein Coronas on Engineered Particles Influence Immune Responses. *Biomacromolecules*. 2017;18(2):431-439. doi:10.1021/acs.biomac.6b01545
270. Escamilla-Rivera V, Uribe-Ramírez M, González-Pozos S, Lozano O, Lucas S, De Vizcaya-Ruiz A. Protein corona acts as a protective shield against Fe₃O₄-PEG inflammation and ROS-induced toxicity in human macrophages. *Toxicol Lett*. 2016;240(1):172-184. doi:10.1016/j.toxlet.2015.10.018
271. Zhu Y, Jiang P, Luo B, Lan F, He J, Wu Y. Dynamic protein corona influences immune-modulating osteogenesis in magnetic nanoparticle (MNP)-infiltrated bone regeneration scaffolds *in vivo*. *Nanoscale*. 2019;11(14):6817-6827. doi:10.1039/C8NR08614A
272. Deng ZJ, Liang M, Monteiro M, Toth I, Minchin RF. Nanoparticle-induced unfolding of fibrinogen promotes Mac-1 receptor activation and inflammation. *Nat Nanotechnol*. 2011;6(1):39-44. doi:10.1038/nnano.2010.250
273. Visalakshan RM, MacGregor MN, Sasidharan S, et al. Biomaterial Surface Hydrophobicity-Mediated Serum Protein Adsorption and Immune Responses. *ACS Appl Mater Interfaces*. Published online 2019. doi:10.1021/acsami.9b09900
274. Wang G, Griffin JI, Inturi S, et al. In vitro and in vivo differences in murine third complement component (C3) opsonization and macrophage/leukocyte responses to antibody-functionalized iron oxide nanoworms. *Front Immunol*. 2017;8(FEB):1-9. doi:10.3389/fimmu.2017.00151
275. Chen F, Wang G, Griffin JI, et al. Complement proteins bind to nanoparticle protein corona and undergo dynamic exchange in vivo. *Nat Nanotechnol*. 2017;12(4):387-393. doi:10.1038/nnano.2016.269
276. Bertrand N, Grenier P, Mahmoudi M, et al. Mechanistic understanding of in vivo protein corona formation on polymeric nanoparticles and impact on pharmacokinetics. *Nat Commun*.

2017;8(1). doi:10.1038/s41467-017-00600-w

277. Jackson MA, Werfel TA, Curvino EJ, et al. Zwitterionic Nanocarrier Surface Chemistry Improves siRNA Tumor Delivery and Silencing Activity Relative to Polyethylene Glycol. *ACS Nano*. 2017;11(6):5680-5696. doi:10.1021/acsnano.7b01110

278. Wu YQ, Qu H, Sfyroera G, et al. Protection of Nonsel surfaces from Complement Attack by Factor H-Binding Peptides: Implications for Therapeutic Medicine. *J Immunol*. 2011;186(7):4269-4277. doi:10.4049/jimmunol.1003802

279. Gao M, Liang C, Song X, et al. Erythrocyte-membrane-enveloped perfluorocarbon as nanoscale artificial red blood cells to relieve tumor hypoxia and enhance cancer radiotherapy. *Adv Mater*. 2017;29(35):1-7. doi:10.1002/adma.201701429

280. Li PY, Fan Z, Cheng H. Cell Membrane Bioconjugation and Membrane-Derived Nanomaterials for Immunotherapy. *Bioconjug Chem*. 2018;29(3):624-634. doi:10.1021/acs.bioconjchem.7b00669

281. Fang RH, Kroll A V., Gao W, Zhang L. Cell Membrane Coating Nanotechnology. *Adv Mater*. 2018;30(23):1-34. doi:10.1002/adma.201706759

282. Fan Z, Li PY, Deng J, Bady SC, Cheng H. Cell membrane coating for reducing nanoparticle-induced inflammatory responses to scaffold constructs. *Nano Res*. 2018;11(10):5573-5583. doi:10.1007/s12274-018-2084-y

283. Figueiredo Borgognoni C, Kim JH, Zucolotto V, Fuchs H, Riehemann K. Human macrophage responses to metal-oxide nanoparticles: a review. *Artif Cells Nanomedicine Biotechnol*. 2018;46(sup2):694-703. doi:10.1080/21691401.2018.1468767

284. Cheng N, Watkins-Schulz R, Junkins RD, et al. A nanoparticle-incorporated STING activator enhances antitumor immunity in PD-L1-insensitive models of triple-negative breast cancer. *JCI Insight*. 2018;3(22). doi:10.1172/jci.insight.120638

285. Alhallak K, Sun J, Wasden K, et al. Nanoparticle T-cell engagers as a modular platform for cancer immunotherapy. *Leukemia*. 2021;35(8):2346-2357. doi:10.1038/s41375-021-01127-2

286. Mi Y, Smith CC, Yang F, et al. A Dual Immunotherapy Nanoparticle Improves T-Cell Activation and Cancer Immunotherapy. *Adv Mater*. 2018;30(25):1-9. doi:10.1002/adma.201706098

287. Fan M, Han Y, Gao S, et al. Ultrasmall gold nanoparticles in cancer diagnosis and therapy. *Theranostics*. 2020;10(11):4944-4957. doi:10.7150/thno.42471

288. Fernandes DA, Fernandes DD, Malik A, et al. Multifunctional nanoparticles as theranostic agents for therapy and imaging of breast cancer. *J Photochem Photobiol B*. 2021;218:112110. doi:10.1016/j.jphotobiol.2020.112110

289. Huang Y, He N, Wang Y, et al. Self-assembly of nanoparticles by human serum albumin and photosensitizer for targeted near-infrared emission fluorescence imaging and effective phototherapy of cancer. *J Mater Chem B*. 2019;7(7):1149-1159. doi:10.1039/C8TB03054E

290. Chen Q, Xu L, Liang C, Wang C, Peng R, Liu Z. Photothermal therapy with immune-adjuvant

nanoparticles together with checkpoint blockade for effective cancer immunotherapy. *Nat Commun.* 2016;7:1-13. doi:10.1038/ncomms13193

291. Crous A, Abrahamse H. Effective gold nanoparticle-antibody-mediated drug delivery for photodynamic therapy of lung cancer stem cells. *Int J Mol Sci.* 2020;21(11). doi:10.3390/ijms21113742
292. El-Hussein A, Mfouo-Tynga I, Abdel-Harith M, Abrahamse H. Comparative study between the photodynamic ability of gold and silver nanoparticles in mediating cell death in breast and lung cancer cell lines. *J Photochem Photobiol B.* 2015;153:67-75. doi:10.1016/j.jphotobiol.2015.08.028
293. Kucharczyk K, Kaczmarek K, Jozefczak A, Slachcinski M, Mackiewicz A, Dams-Kozłowska H. Hyperthermia treatment of cancer cells by the application of targeted silk/iron oxide composite spheres. *Mater Sci Eng C.* 2021;120:111654. doi:10.1016/j.msec.2020.111654
294. Phung CD, Tran TH, Kim JO. Engineered nanoparticles to enhance natural killer cell activity towards onco-immunotherapy: a review. *Arch Pharm Res.* Published online 2020. doi:10.1007/s12272-020-01218-1
295. Savitsky K, Yu X. Combined strategies for tumor immunotherapy with nanoparticles. *Clin Transl Oncol.* Published online 2019. doi:10.1007/s12094-019-02081-3
296. Sabel MS, Arora A, Su G, et al. Generation of a tumor-specific systemic response after intratumoral injection of IL-12 and IL-18-loaded polylactic acid microspheres. *J Immunother.* 2007;30(8):808-816. doi:10.1097/CJI.0b013e318156e6a7
297. Liu X, Li Y, Sun X, et al. Powerful anti-colon cancer effect of modified nanoparticle-mediated IL-15 immunogene therapy through activation of the host immune system. *Theranostics.* 2018;8(13):3490-3503. doi:10.7150/thno.24157
298. Zhu L, Kalimuthu S, Oh JM, et al. Enhancement of antitumor potency of extracellular vesicles derived from natural killer cells by IL-15 priming. *Biomaterials.* 2019;190-191:38-50. doi:10.1016/j.biomaterials.2018.10.034
299. Shoaie-Hassani A, Hamidieh AA, Behfar M, Mohseni R, Mortazavi-Tabatabaei SA, Asgharzadeh S. NK Cell-derived Exosomes from NK Cells Previously Exposed to Neuroblastoma Cells Augment the Antitumor Activity of Cytokine-Activated NK Cells. *J Immunother.* 2017;40(7):265-276. doi:10.1097/CJI.000000000000179
300. Viaud S, Terme M, Flament C, et al. Dendritic cell-derived exosomes promote natural killer cell activation and proliferation: A role for NKG2D ligands and IL-15R α . *PLoS ONE.* 2009;4(3). doi:10.1371/journal.pone.0004942
301. Damo M, Wilson DS, Simeoni E, Hubbell JA. TLR-3 stimulation improves anti-tumor immunity elicited by dendritic cell exosome-based vaccines in a murine model of melanoma. *Sci Rep.* 2015;5(December):1-15. doi:10.1038/srep17622
302. Oyer JL, Igarashi RY, Kulikowski AR, et al. Generation of highly cytotoxic natural killer cells for

- treatment of acute myelogenous leukemia using a feeder-free, particle-based approach. *Biol Blood Marrow Transplant*. 2015;21(4):632-639. doi:10.1016/j.bbmt.2014.12.037
303. Oyer JL, Pandey V, Igarashi RY, et al. Natural killer cells stimulated with PM21 particles expand and biodistribute in vivo: Clinical implications for cancer treatment. *Cytotherapy*. 2016;18(5):653-663. doi:10.1016/j.jcyt.2016.02.006
304. Siegler EL, Kim YJ, Chen X, et al. Combination Cancer Therapy Using Chimeric Antigen Receptor-Engineered Natural Killer Cells as Drug Carriers. *Mol Ther*. 2017;25(12):2607-2619. doi:10.1016/j.ymthe.2017.08.010
305. Zhang Y, Li N, Suh H, Irvine DJ. Nanoparticle anchoring targets immune agonists to tumors enabling anti-cancer immunity without systemic toxicity. *Nat Commun*. 2018;9(1). doi:10.1038/s41467-017-02251-3
306. Loftus C, Saeed M, Davis DM, et al. Activation of Human Natural Killer Cells by Graphene Oxide-Templated Antibody Nanoclusters. Published online 2018. doi:10.1021/acs.nanolett.8b01089
307. Kang T, Huang Y, Zhu Q, et al. Necroptotic cancer cells-mimicry nanovaccine boosts anti-tumor immunity with tailored immune-stimulatory modality. *Biomaterials*. 2018;164:80-97. doi:10.1016/j.biomaterials.2018.02.033
308. Jang ES, Shin JH, Ren G, et al. The manipulation of natural killer cells to target tumor sites using magnetic nanoparticles. *Biomaterials*. 2012;33(22):5584-5592. doi:10.1016/j.biomaterials.2012.04.041
309. Wu L, Zhang F, Wei Z, et al. Magnetic delivery of Fe₃O₄@polydopamine nanoparticle-loaded natural killer cells suggest a promising anticancer treatment. *Biomater Sci*. 2018;6(10):2714-2725. doi:10.1039/c8bm00588e
310. Kim SY, Noh YW, Kang TH, et al. Synthetic vaccine nanoparticles target to lymph node triggering enhanced innate and adaptive antitumor immunity. *Biomaterials*. 2017;130:56-66. doi:10.1016/j.biomaterials.2017.03.034
311. Atukorale PU, Raghunathan SP, Raguveer V, et al. Nanoparticle encapsulation of synergistic immune agonists enables systemic codelivery to tumor sites and IFN β -driven antitumor immunity. *Cancer Res*. 2019;79(20):5394-5406. doi:10.1158/0008-5472.CAN-19-0381
312. Jiao P, Otto M, Geng Q, et al. Enhancing both CT imaging and natural killer cell-mediated cancer cell killing by a GD2-targeting nanoconstruct. *J Mater Chem B*. 2016;4(3):513-520. doi:10.1039/c5tb02243f
313. Xu M, Wen Y, Liu Y, et al. Hollow mesoporous ruthenium nanoparticles conjugated bispecific antibody for targeted anti-colorectal cancer response of combination therapy. *Nanoscale*. 2019;11(19):9661-9678. doi:10.1039/c9nr01904a
314. Au KM, Par SI, Wa AZ. Trispecific natural killer cell nanoengagers for targeted chemoimmunotherapy. *Sci Adv*. 2020;6(27):1-16. doi:10.1126/sciadv.aba8564

315. Astorga-Gamaza A, Vitali M, Borrajo ML, et al. Antibody cooperative adsorption onto AuNPs and its exploitation to force natural killer cells to kill HIV-infected T cells. *Nano Today*. 2021;36:101056. doi:10.1016/j.nantod.2020.101056
316. Matosevic S. Viral and nonviral engineering of natural killer cells as emerging adoptive cancer immunotherapies. *J Immunol Res*. Published online 2018. doi:10.1155/2018/4054815
317. Oyer JL, Igarashi RY, Kulikowski AR, et al. Generation of highly cytotoxic natural killer cells for treatment of acute myelogenous leukemia using a feeder-free, particle-based approach. *Biol Blood Marrow Transplant*. Published online 2015. doi:10.1016/j.bbmt.2014.12.037
318. Oyer JL, Pandey V, Igarashi RY, et al. Natural killer cells stimulated with PM21 particles expand and biodistribute in vivo: Clinical implications for cancer treatment. *Cytotherapy*. Published online 2016. doi:10.1016/j.jcyt.2016.02.006
319. Loftus C, Saeed M, Davis DM, Dunlop IE. Activation of Human Natural Killer Cells by Graphene Oxide-Templated Antibody Nanoclusters. *Nano Lett*. Published online 2018. doi:10.1021/acs.nanolett.8b01089
320. Jang ES, Shin JH, Ren G, et al. The manipulation of natural killer cells to target tumor sites using magnetic nanoparticles. *Biomaterials*. Published online 2012. doi:10.1016/j.biomaterials.2012.04.041
321. Wu L, Zhang F, Wei Z, et al. Magnetic delivery of Fe₃O₄@polydopamine nanoparticle-loaded natural killer cells suggest a promising anticancer treatment. *Biomater Sci*. Published online 2018. doi:10.1039/c8bm00588e
322. Tan L, Han S, Ding S, et al. Chitosan nanoparticle-based delivery of fused NKG2D-IL-21 gene suppresses colon cancer growth in mice. *Int J Nanomedicine*. Published online 2017. doi:10.2147/IJN.S128032
323. Atukorale PU, Raghunathan SP, Raguveer V, et al. Nanoparticle encapsulation of synergistic immune agonists enables systemic codelivery to tumor sites and IFN β -driven antitumor immunity. *Cancer Res*. Published online 2019. doi:10.1158/0008-5472.CAN-19-0381
324. Siegler EL, Kim YJ, Chen X, et al. Combination Cancer Therapy Using Chimeric Antigen Receptor-Engineered Natural Killer Cells as Drug Carriers. *Mol Ther*. Published online 2017. doi:10.1016/j.ymthe.2017.08.010
325. Kim SY, Noh YW, Kang TH, et al. Synthetic vaccine nanoparticles target to lymph node triggering enhanced innate and adaptive antitumor immunity. *Biomaterials*. Published online 2017. doi:10.1016/j.biomaterials.2017.03.034
326. Kim H, Khanna V, Kucaba TA, et al. TLR7/8 Agonist-Loaded Nanoparticles Augment NK Cell-Mediated Antibody-Based Cancer Immunotherapy. *Mol Pharm*. Published online 2020. doi:10.1021/acs.molpharmaceut.0c00271
327. Kang T, Huang Y, Zhu Q, et al. Necroptotic cancer cells-mimicry nanovaccine boosts anti-

- tumor immunity with tailored immune-stimulatory modality. *Biomaterials*. Published online 2018. doi:10.1016/j.biomaterials.2018.02.033
328. Viaud S, Terme M, Flament C, et al. Dendritic cell-derived exosomes promote natural killer cell activation and proliferation: A role for NKG2D ligands and IL-15R α . *PLoS ONE*. Published online 2009. doi:10.1371/journal.pone.0004942
329. Damo M, Wilson DS, Simeoni E, Hubbell JA. TLR-3 stimulation improves anti-tumor immunity elicited by dendritic cell exosome-based vaccines in a murine model of melanoma. *Sci Rep*. Published online 2015. doi:10.1038/srep17622
330. Liu X, Li Y, Sun X, et al. Powerful anti-colon cancer effect of modified nanoparticle-mediated IL-15 immunogene therapy through activation of the host immune system. *Theranostics*. Published online 2018. doi:10.7150/thno.24157
331. Sabel MS, Arora A, Su G, et al. Generation of a tumor-specific systemic response after intratumoral injection of IL-12 and IL-18-loaded polylactic acid microspheres. *J Immunother*. Published online 2007. doi:10.1097/CJI.0b013e318156e6a7
332. Jiao P, Otto M, Geng Q, et al. Enhancing both CT imaging and natural killer cell-mediated cancer cell killing by a GD2-targeting nanoconstruct. *J Mater Chem B*. Published online 2016. doi:10.1039/c5tb02243f
333. Schmohl JU, Felices M, Taras E, Miller JS, Vallera DA. Enhanced ADCC and NK cell activation of an anticarcinoma bispecific antibody by genetic insertion of a modified IL-15 cross-linker. *Mol Ther*. Published online 2016. doi:10.1038/mt.2016.88
334. Wu J, Fu J, Zhang M, Liu D. AFM13: A first-in-class tetravalent bispecific anti-CD30/CD16A antibody for NK cell-mediated immunotherapy. *J Hematol Oncol J Hematol Oncol*. Published online 2015. doi:10.1186/s13045-015-0188-3
335. Xu M, Wen Y, Liu Y, et al. Hollow mesoporous ruthenium nanoparticles conjugated bispecific antibody for targeted anti-colorectal cancer response of combination therapy. *Nanoscale*. Published online 2019. doi:10.1039/c9nr01904a
336. Au KM, Par SI, Wa AZ. Trispecific natural killer cell nanoengagers for targeted chemoimmunotherapy. *Sci Adv*. Published online 2020. doi:10.1126/sciadv.aba8564
337. Astorga-Gamaza A, Vitali M, Borrajo ML, et al. Antibody cooperative adsorption onto AuNPs and its exploitation to force natural killer cells to kill HIV-infected T cells. *Nano Today*. Published online 2021. doi:10.1016/j.nantod.2020.101056
338. Shen M, Ren X. New insights into the biological impacts of immune cell-derived exosomes within the tumor environment. *Cancer Lett*. Published online 2018. doi:10.1016/j.canlet.2018.05.040
339. Li Q, Wang H, Peng H, Huyan T, Cacalano NA. Exosomes: Versatile nano mediators of immune regulation. *Cancers*. Published online 2019. doi:10.3390/cancers11101557
340. Fais S. NK cell-released exosomes Natural nanobullets against tumors. *Oncol Immunology*.

Published online 2013. doi:10.4161/onco.22337

341. Pitchaimani A, Nguyen TDT, Aryal S. Natural killer cell membrane infused biomimetic liposomes for targeted tumor therapy. *Biomaterials*. Published online 2018. doi:10.1016/j.biomaterials.2018.01.018
342. Zhu L, Kalimuthu S, Gangadaran P, et al. Exosomes derived from natural killer cells exert therapeutic effect in melanoma. *Theranostics*. Published online 2017. doi:10.7150/thno.18752
343. Zhu L, Kalimuthu S, Oh JM, et al. Enhancement of antitumor potency of extracellular vesicles derived from natural killer cells by IL-15 priming. *Biomaterials*. Published online 2019. doi:10.1016/j.biomaterials.2018.10.034
344. Shoaee-Hassani A, Hamidieh AA, Behfar M, Mohseni R, Mortazavi-Tabatabaei SA, Asgharzadeh S. NK Cell-derived Exosomes from NK Cells Previously Exposed to Neuroblastoma Cells Augment the Antitumor Activity of Cytokine-Activated NK Cells. *J Immunother*. Published online 2017. doi:10.1097/CJI.0000000000000179
345. Kang YT, Niu Z, Hadlock T, et al. On-Chip Biogenesis of Circulating NK Cell-Derived Exosomes in Non-Small Cell Lung Cancer Exhibits Antitumoral Activity. *Adv Sci*. Published online 2021. doi:10.1002/advs.202003747
346. Heinhuis KM, Ros W, Kok M, Steeghs N, Beijnen JH, Schellens JHM. Enhancing antitumor response by combining immune checkpoint inhibitors with chemotherapy in solid tumors. *Ann Oncol*. 2019;30(2):219-235. doi:10.1093/annonc/mdy551
347. Depil S, Duchateau P, Grupp SA, Mufti G, Poirot L. 'Off-the-shelf' allogeneic CAR T cells: development and challenges. *Nat Rev Drug Discov*. 2020;19(3):185-199. doi:10.1038/s41573-019-0051-2
348. Syn NL, Teng MWL, Mok TSK, Soo RA. De-novo and acquired resistance to immune checkpoint targeting. *Lancet Oncol*. 2017;18(12):e731-e741. doi:10.1016/S1470-2045(17)30607-1
349. Cheng N, Watkins-Schulz R, Junkins RD, et al. A nanoparticle-incorporated STING activator enhances antitumor immunity in PD-L1-insensitive models of triple-negative breast cancer. *JCI Insight*. 2018;3(22):e120638. doi:10.1172/jci.insight.120638
350. Yazdanpanah P, Alavianmehr A, Ghaderi A, et al. PD-L1 expression in tumor lesions and soluble PD-L1 serum levels in patients with breast cancer: TNBC versus TPBC. *Breast Dis*. 2021;40(1):43-50. doi:10.3233/BD-201049
351. Tian T, Shi X, Cheng L, et al. Graphene-based nanocomposite as an effective, multifunctional, and recyclable antibacterial agent. *ACS Appl Mater Interfaces*. 2014;6(11):8542-8548. doi:10.1021/am5022914
352. Cao D, Jin X, Gan L, Wang T, Chen Z. Removal of phosphate using iron oxide nanoparticles synthesized by eucalyptus leaf extract in the presence of CTAB surfactant. *Chemosphere*. 2016;159:23-31. doi:10.1016/j.chemosphere.2016.05.080

353. Zou P, Tyner K, Raw A, Lee S. Physicochemical Characterization of Iron Carbohydrate Colloid Drug Products. *AAPS J.* 2017;19(5):1359-1376. doi:10.1208/s12248-017-0126-0
354. Xiao YD, Paudel R, Liu J, Ma C, Zhang ZS, Zhou SK. MRI contrast agents: Classification and application (Review). *Int J Mol Med.* 2016;38(5):1319-1326. doi:10.3892/ijmm.2016.2744
355. Amiri M, Salavati-Niasari M, Akbari A. Magnetic nanocarriers: Evolution of spinel ferrites for medical applications. *Adv Colloid Interface Sci.* 2019;265:29-44. doi:10.1016/j.cis.2019.01.003
356. Colombo M, Carregal-Romero S, Casula MF, et al. Biological applications of magnetic nanoparticles. *Chem Soc Rev.* 2012;41(11):4306-4334. doi:10.1039/c2cs15337h
357. Reimer P, Balzer T. Ferucarbotran (Resovist): A new clinically approved RES-specific contrast agent for contrast-enhanced MRI of the liver: Properties, clinical development, and applications. *Eur Radiol.* 2003;13(6):1266-1276. doi:10.1007/s00330-002-1721-7
358. Hsu JC, Naha PC, Lau KC, et al. An all-in-one nanoparticle (AION) contrast agent for breast cancer screening with DEM-CT-MRI-NIRF imaging. *Nanoscale.* 2018;10(36):17236-17248. doi:10.1039/c8nr03741h
359. Zhang J, Ring HL, Hurley KR, et al. Quantification and Biodistribution of Iron Oxide Nanoparticles in the primary Clearance Organs of Mice using T1 Contrast for Heating. *Magn Reson Med.* 2017;78(2):702-712. doi:10.1002/mrm.26394
360. Zhou Z, Bai R, Wang Z, et al. An Albumin-Binding T1-T2 Dual-Modal MRI Contrast Agents for Improved Sensitivity and Accuracy in Tumor Imaging. *Bioconjug Chem.* 2019;30(6):1821-1829. doi:10.1021/acs.bioconjchem.9b00349
361. Cui Y, Zhang M, Zeng F, Jin H, Xu Q, Huang Y. Dual-Targeting Magnetic PLGA Nanoparticles for Codelivery of Paclitaxel and Curcumin for Brain Tumor Therapy. *ACS Appl Mater Interfaces.* 2016;8(47):32159-32169. doi:10.1021/acsami.6b10175
362. Li X, Wang Y, Shi L, et al. Magnetic targeting enhances the cutaneous wound healing effects of human mesenchymal stem cell-derived iron oxide exosomes. *J Nanobiotechnology.* 2020;18(1):1-14. doi:10.1186/s12951-020-00670-x
363. Chen J, Huang N, Ma B, et al. Guidance of stem cells to a target destination in vivo by magnetic nanoparticles in a magnetic field. *ACS Appl Mater Interfaces.* 2013;5(13):5976-5985. doi:10.1021/am400249n
364. Yun WS, Choi JS, Ju HM, et al. Enhanced homing technique of mesenchymal stem cells using iron oxide nanoparticles by magnetic attraction in olfactory-injured mouse models. *Int J Mol Sci.* 2018;19(5). doi:10.3390/ijms19051376
365. Hickey JW, Isser AY, Vicente FP, Warner SB, Mao HQ, Schneck JP. Efficient magnetic enrichment of antigen-specific T cells by engineering particle properties. *Biomaterials.* 2018;187:105-116. doi:10.1016/j.biomaterials.2018.09.029
366. Xia B, Huang L, Zhu L, et al. Manipulation of Schwann cell migration across the astrocyte

boundary by polysialyltransferase-loaded superparamagnetic nanoparticles under magnetic field. *Int J Nanomedicine*. 2016;11:6727-6741. doi:10.2147/IJN.S122358

367. Eyvazzadeh N, Shakeri-Zadeh A, Fekrazad R, Amini E, Ghaznavi H, Kamran Kamrava S. Gold-coated magnetic nanoparticle as a nanotheranostic agent for magnetic resonance imaging and photothermal therapy of cancer. *Lasers Med Sci*. 2017;32(7):1469-1477. doi:10.1007/s10103-017-2267-x

368. Ravichandran M, Velumani S, Ramirez JT, Vera A, Leija L. Biofunctionalized MnFe₂O₄@Au core-shell nanoparticles for pH-responsive drug delivery and hyperthermal agent for cancer therapy. *Artif Cells Nanomedicine Biotechnol*. 2018;46(sup3):S993-S1003. doi:10.1080/21691401.2018.1523182

369. Xiang JJ, Tang JQ, Zhu SG, et al. IONP-PLL: A novel non-viral vector for efficient gene delivery. *J Gene Med*. 2003;5(9):803-817. doi:10.1002/jgm.419

370. Shi J, Yu X, Wang L, et al. PEGylated fullerene/iron oxide nanocomposites for photodynamic therapy, targeted drug delivery and MR imaging. *Biomaterials*. 2013;34(37):9666-9677. doi:10.1016/j.biomaterials.2013.08.049

371. Martínez-Banderas AI, Aires A, Quintanilla M, et al. Iron-Based Core-Shell Nanowires for Combinatorial Drug Delivery and Photothermal and Magnetic Therapy. *ACS Appl Mater Interfaces*. 2019;11(47):43976-43988. doi:10.1021/acsami.9b17512

372. Turetschek K, Preda A, Floyd E, et al. MRI monitoring of tumor response to a novel VEGF tyrosine kinase inhibitor in an experimental breast cancer model. *Acad Radiol*. 2002;9(SUPPL. 2):519-520. doi:10.1016/S1076-6332(03)80281-7

373. Jahnke A, Hirschberger J, Fischer C, et al. Intra-tumoral gene delivery of fclL-2, fclFN- γ and fclGM-CSF using magnetofection as a neoadjuvant treatment option for feline fibrosarcomas: A phase-I study. *J Vet Med Ser Physiol Pathol Clin Med*. 2007;54(10):599-606. doi:10.1111/j.1439-0442.2007.01002.x

374. Aoki T, Saito M, Koseki H, et al. Macrophage Imaging of Cerebral Aneurysms with Ferumoxytol: an Exploratory Study in an Animal Model and in Patients. *J Stroke Cerebrovasc Dis*. 2017;26(10):2055-2064. doi:10.1016/j.jstrokecerebrovasdis.2016.10.026

375. Shore D, Pailloux SL, Zhang J, et al. Electrodeposited Fe and Fe-Au nanowires as MRI contrast agents. *Chem Commun*. 2016;52(85):12634-12637. doi:10.1039/c6cc06991f

376. Cha R, Li J, Liu Y, Zhang Y, Xie Q, Zhang M. Fe₃O₄ nanoparticles modified by CD-containing star polymer for MRI and drug delivery. *Colloids Surf B Biointerfaces*. 2017;158:213-221. doi:10.1016/j.colsurfb.2017.06.049

377. Groult H, García-álvarez I, Romero-Ramírez L, et al. Micellar iron oxide nanoparticles coated with anti-tumor glycosides. *Nanomaterials*. 2018;8(8):1-14. doi:10.3390/nano8080567

378. Abenojar EC, Wickramasinghe S, Bas-Concepcion J, Samia ACS. Structural effects on the

- magnetic hyperthermia properties of iron oxide nanoparticles. *Prog Nat Sci Mater Int*. 2016;26(5):440-448. doi:10.1016/j.pnsc.2016.09.004
379. Cellai F, Munnia A, Viti J, et al. Magnetic hyperthermia and oxidative damage to dna of human hepatocarcinoma cells. *Int J Mol Sci*. 2017;18(5):1-15. doi:10.3390/ijms18050939
380. Aljarrah K, Mhaidat NM, Al-Akhras MAH, et al. Magnetic nanoparticles sensitize MCF-7 breast cancer cells to doxorubicin-induced apoptosis. *World J Surg Oncol*. 2012;10:2-6. doi:10.1186/1477-7819-10-62
381. Moise S, Byrne JM, El Haj AJ, Telling ND. The potential of magnetic hyperthermia for triggering the differentiation of cancer cells. *Nanoscale*. 2018;10(44):20519-20525. doi:10.1039/c8nr05946b
382. Kumeria T, Maher S, Wang Y, et al. Naturally Derived Iron Oxide Nanowires from Bacteria for Magnetically Triggered Drug Release and Cancer Hyperthermia in 2D and 3D Culture Environments: Bacteria Biofilm to Potent Cancer Therapeutic. *Biomacromolecules*. 2016;17(8):2726-2736. doi:10.1021/acs.biomac.6b00786
383. Li M, Bu W, Ren J, et al. Enhanced synergism of thermo-chemotherapy for liver cancer with magnetothermally responsive nanocarriers. *Theranostics*. 2018;8(3):693-709. doi:10.7150/thno.21297
384. Johannsen M, Gneveckow U, Taymoorian K, et al. Morbidity and quality of life during thermotherapy using magnetic nanoparticles in locally recurrent prostate cancer: Results of a prospective phase I trial. *Int J Hyperthermia*. 2007;23(3):315-323. doi:10.1080/02656730601175479
385. Johannsen M, Gneveckow U, Thiesen B, et al. Thermotherapy of Prostate Cancer Using Magnetic Nanoparticles: Feasibility, Imaging, and Three-Dimensional Temperature Distribution. *Eur Urol*. 2007;52(6):1653-1662. doi:10.1016/j.eururo.2006.11.023
386. Maier-Hauff K, Ulrich F, Nestler D, et al. Efficacy and safety of intratumoral thermotherapy using magnetic iron-oxide nanoparticles combined with external beam radiotherapy on patients with recurrent glioblastoma multiforme. *J Neurooncol*. 2011;103(2):317-324. doi:10.1007/s11060-010-0389-0
387. Jaiswal MK, Pradhan L, Vasavada S, et al. Magneto-thermally responsive hydrogels for bladder cancer treatment: Therapeutic efficacy and in vivo biodistribution. *Colloids Surf B Biointerfaces*. 2015;136:625-633. doi:10.1016/j.colsurfb.2015.09.058
388. Qiao G, Wang X, Zhou X, et al. Immune correlates of clinical benefit in a phase I study of hyperthermia with adoptive T cell immunotherapy in patients with solid tumors. *Int J Hyperthermia*. 2019;36(sup1):74-82. doi:10.1080/02656736.2019.1647350
389. Zhu M, Yang Z, Yu H, et al. The efficacy and safety of low-frequency rotating static magnetic field therapy combined with chemotherapy on advanced lung cancer patients: a randomized, double-blinded, controlled clinical trial. *Int J Radiat Biol*. 2020;96(7):943-950. doi:10.1080/09553002.2020.1748737

390. Johannsen M, Gneveckow U, Eckelt L, et al. Clinical hyperthermia of prostate cancer using magnetic nanoparticles: Presentation of a new interstitial technique. *Int J Hyperthermia*. 2005;21(7):637-647. doi:10.1080/02656730500158360
391. Farzin A, Hassan S, Emadi R, Etesami SA, Ai J. Comparative evaluation of magnetic hyperthermia performance and biocompatibility of magnetite and novel Fe-doped hardystonite nanoparticles for potential bone cancer therapy. *Mater Sci Eng C*. 2019;98(January):930-938. doi:10.1016/j.msec.2019.01.038
392. Kesse X, Adam A, Begin-Colin S, et al. Elaboration of Superparamagnetic and Bioactive Multicore-Shell Nanoparticles (γ -Fe₂O₃@SiO₂-CaO): A Promising Material for Bone Cancer Treatment. *ACS Appl Mater Interfaces*. 2020;12(42):47820-47830. doi:10.1021/acsami.0c12769
393. Manshadi MKD, Saadat M, Mohammadi M, et al. Delivery of magnetic micro/nanoparticles and magnetic-based drug/cargo into arterial flow for targeted therapy. *Drug Deliv*. 2018;25(1):1963-1973. doi:10.1080/10717544.2018.1497106
394. Haimov-Talmoud E, Harel Y, Schori H, et al. Magnetic Targeting of mTHPC to Improve the Selectivity and Efficiency of Photodynamic Therapy. *ACS Appl Mater Interfaces*. 2019;11(49):45368-45380. doi:10.1021/acsami.9b14060
395. Hickey JW, Isser AY, Vicente FP, Warner SB, Mao H quan, Schneck JP. Biomaterials Efficient magnetic enrichment of antigen-specific T cells by engineering particle properties. 2018;187(September):105-116. doi:10.1016/j.biomaterials.2018.09.029
396. Jin H, Qian Y, Dai Y, et al. Magnetic enrichment of dendritic cell vaccine in lymph node with fluorescent-magnetic nanoparticles enhanced cancer immunotherapy. *Theranostics*. 2016;6(11):2000-2014. doi:10.7150/thno.15102
397. Fadel TR, Sharp FA, Vudattu N, et al. A carbon nanotube-polymer composite for T-cell therapy. *Nat Nanotechnol*. 2014;9(8):639-647. doi:10.1038/nnano.2014.154
398. Foy SP, Manthe RL, Foy ST, Dimitrijevic S, Krishnamurthy N, Labhasetwar V. Optical Imaging and Magnetic Field Targeting of Magnetic Nanoparticles in Tumors. *ACS Nano*. 2010;4(9):5217-5224. doi:10.1021/nn101427t
399. Qi H, Liu C, Long L, et al. Blood Exosomes Endowed with Magnetic and Targeting Properties for Cancer Therapy. *ACS Nano*. 2016;10(3):3323-3333. doi:10.1021/acs.nano.5b06939
400. Zanganeh S, Hutter G, Spitler R, et al. Iron oxide nanoparticles inhibit tumour growth by inducing pro-inflammatory macrophage polarization in tumour tissues. *Nat Nanotechnol*. 2016;11(11):986-994. doi:10.1038/nnano.2016.168
401. Ruiz-de-Angulo A, Bilbao-Asensio M, Cronin J, et al. Chemically Programmed Vaccines: Iron Catalysis in Nanoparticles Enhances Combination Immunotherapy and Immunotherapy-Promoted Tumor Ferroptosis. *iScience*. 2020;23(9). doi:10.1016/j.isci.2020.101499
402. Bouras A, Kaluzova M, Hadjipanayis CG. Radiosensitivity enhancement of radioresistant

- glioblastoma by epidermal growth factor receptor antibody-conjugated iron- oxide nanoparticles. *J Neurooncology*. 2015;1(124):13-22. doi:110.1007/s11060-015-1807-0
403. Kaluzova M, Bouras A, Machaidze R, Hadjipanayis CG. Targeted therapy of glioblastoma stem-like cells and tumor non-stem cells using cetuximab-conjugated iron-oxide nanoparticles. *Oncotarget*. 2015;6(11):8788-8806. doi:10.18632/oncotarget.3554
404. Pramanik N, Ranganathan S, Rao S, et al. A Composite of Hyaluronic Acid-Modified Graphene Oxide and Iron Oxide Nanoparticles for Targeted Drug Delivery and Magnetothermal Therapy. *ACS Omega*. 2019;4(5):9284-9293. doi:10.1021/acsomega.9b00870
405. Feng ZQ, Yan K, Li J, et al. Magnetic Janus particles as a multifunctional drug delivery system for paclitaxel in efficient cancer treatment. *Mater Sci Eng C*. 2019;104(June):110001. doi:10.1016/j.msec.2019.110001
406. Kanamala M, Wilson WR, Yang M, Palmer BD, Wu Z. Mechanisms and biomaterials in pH-responsive tumour targeted drug delivery: A review. *Biomaterials*. 2016;85:152-167. doi:10.1016/j.biomaterials.2016.01.061
407. Thong QX, Biabanikhankahdani R, Ho KL, Alitheen NB, Tan WS. Thermally-responsive Virus-like Particle for Targeted Delivery of Cancer Drug. *Sci Rep*. 2019;9(1):1-14. doi:10.1038/s41598-019-40388-x
408. Choi Y, Kim J, Yu S, Hong S. PH-and temperature-responsive radially porous silica nanoparticles with high-capacity drug loading for controlled drug delivery. *Nanotechnology*. 2020;31(33). doi:10.1088/1361-6528/ab9043
409. Jun YW, Huh YM, Choi JS, et al. Nanoscale Size Effect of Magnetic Nanocrystals and Their Utilization for Cancer Diagnosis via Magnetic Resonance Imaging. *J Am Chem Soc*. 2005;127(16):5732-5733. doi:10.1021/ja0422155
410. Guardia P, Labarta A, Batlle X. Tuning the size, the shape, and the magnetic properties of iron oxide nanoparticles. *J Phys Chem C*. 2011;115(2):390-396. doi:10.1021/jp1084982
411. K. LaMer V, H. Dinegar R. Theory, Production and Mechanism of Formation of Monodispersed Hydrosols. *Am Chem Soc*. 1950;72:4847-4854. doi:10.1021/ja01167a001
412. Thanh NTK, Maclean N, Mahiddine S. Mechanisms of nucleation and growth of nanoparticles in solution. *Chem Rev*. 2014;114(15):7610-7630. doi:10.1021/cr400544s
413. de Oliveira PN, Moussa A, Milhau N, et al. *In situ* synthesis of Fe₃O₄ nanoparticles coated by chito-oligosaccharides: physico-chemical characterizations and cytotoxicity evaluation for biomedical applications. *Nanotechnology*. 2020;31(17):175602. doi:10.1088/1361-6528/ab68f9
414. Nassireslami E, Ajdarzade M. Gold coated superparamagnetic iron oxide nanoparticles as effective nanoparticles to eradicate breast cancer cells via photothermal therapy. *Adv Pharm Bull*. 2018;8(2):201-209. doi:10.15171/apb.2018.024
415. Li J, Wang S, Shi X, Shen M. Aqueous-phase synthesis of iron oxide nanoparticles and

- composites for cancer diagnosis and therapy. *Adv Colloid Interface Sci.* 2017;249:374-385. doi:10.1016/j.cis.2017.02.009
416. Lee E, Park AH, Park HU, Kwon YU. Facile sonochemical synthesis of amorphous NiFe-(oxy)hydroxide nanoparticles as superior electrocatalysts for oxygen evolution reaction. *Ultrason Sonochem.* 2018;40(July 2017):552-557. doi:10.1016/j.ultsonch.2017.07.048
417. Bronstein LM, Atkinson JE, Malyutin AG, et al. Nanoparticles by decomposition of long chain iron carboxylates: From spheres to stars and cubes. *Langmuir.* 2011;27(6):3044-3050. doi:10.1021/la104686d
418. Bronstein LM, Huang X, Retrum J, et al. Influence of iron oleate complex structure on iron oxide nanoparticle formation. *Chem Mater.* 2007;19(15):3624-3632. doi:10.1021/cm062948j
419. Muzzio M, Li J, Yin Z, Delahunty IM, Xie J, Sun S. Monodisperse nanoparticles for catalysis and nanomedicine. *Nanoscale.* 2019;11(41):18946-18967. doi:10.1039/c9nr06080d
420. Imlimthan S, Correia A, Figueiredo P, et al. Systematic in vitro biocompatibility studies of multimodal cellulose nanocrystal and lignin nanoparticles. *J Biomed Mater Res - Part A.* 2020;108(3):770-783. doi:10.1002/jbm.a.36856
421. Abdul Rasool BK, Khalifa AZ, Abu-Gharbieh E, Khan R. Employment of alginate floating in situ gel for controlled delivery of celecoxib: Solubilization and formulation studies. *BioMed Res Int.* 2020;2020. doi:10.1155/2020/1879125
422. Russo Krauss I, Picariello A, Vitiello G, et al. Interaction with Human Serum Proteins Reveals Biocompatibility of Phosphocholine-Functionalized SPIONs and Formation of Albumin-Decorated Nanoparticles. *Langmuir.* 2020;36(30):8777-8791. doi:10.1021/acs.langmuir.0c01083
423. Navarro-Palomares E, González-Saiz P, Renero-Lecuna C, et al. Dye-doped biodegradable nanoparticle SiO₂ coating on zinc- and iron-oxide nanoparticles to improve biocompatibility and for: In vivo imaging studies. *Nanoscale.* 2020;12(10):6164-6175. doi:10.1039/c9nr08743e
424. Palade P, Comanescu C, Kuncser A, et al. Mesoporous cobalt ferrite nanosystems obtained by surfactant-assisted hydrothermal method: Tuning morpho-structural and magnetic properties via pH-variation. *Nanomaterials.* 2020;10(3):1-18. doi:10.3390/nano10030476
425. Sun Z, Yathindranath V, Worden M, et al. Characterization of cellular uptake and toxicity of aminosilane-coated iron oxide nanoparticles with different charges in central nervous system-relevant cell culture models. *Int J Nanomedicine.* 2013;8:961-970. doi:10.2147/IJN.S39048
426. Zan X, Li Q, Pan Y, et al. Versatile Ligand-Exchange Method for the Synthesis of Water-Soluble Monodisperse AuAg Nanoclusters for Cancer Therapy. *ACS Appl Nano Mater.* 2018;1(12):6773-6781. doi:10.1021/acsnm.8b01559
427. Lojk J, Prpar Mihevc S, Bregar VB, Pavlin M, Rogelj B. The Effect of Different Types of Nanoparticles on FUS and TDP-43 Solubility and Subcellular Localization. *Neurotox Res.* 2017;32(3):325-339. doi:10.1007/s12640-017-9734-9

428. Moros M, Pelaz B, López-Larrubia P, García-Martin ML, Grazú V, De La Fuente JM. Engineering biofunctional magnetic nanoparticles for biotechnological applications. *Nanoscale*. 2010;2(9):1746-1755. doi:10.1039/c0nr00104j
429. Penon O, Marín MJ, Russell DA, Pérez-García L. Water soluble, multifunctional antibody-porphyrin gold nanoparticles for targeted photodynamic therapy. *J Colloid Interface Sci*. 2017;496:100-110. doi:10.1016/j.jcis.2017.02.006
430. Mustafa S, Devi VK, Pai RS. Effect of PEG and water-soluble chitosan coating on moxifloxacin-loaded PLGA long-circulating nanoparticles. *Drug Deliv Transl Res*. 2017;7(1):27-36. doi:10.1007/s13346-016-0326-7
431. Zhang Y, Liu AT, Cornejo YR, van Haute D, Berlin JM. A Systematic comparison of in vitro cell uptake and in vivo biodistribution for three classes of gold nanoparticles with saturated PEG coatings. *PLoS ONE*. 2020;15(7):1-16. doi:10.1371/journal.pone.0234916
432. Ogawa M, Uchino R, Kawai A, Kosugi M, Magata Y. PEG modification on ¹¹¹In-labeled phosphatidyl serine liposomes for imaging of atherosclerotic plaques. *Nucl Med Biol*. 2015;42(3):299-304. doi:10.1016/j.nucmedbio.2014.12.004
433. Shen L, Tenzer S, Storck W, et al. Protein corona-mediated targeting of nanocarriers to B cells allows redirection of allergic immune responses. *J Allergy Clin Immunol*. 2018;142(5):1558-1570. doi:10.1016/j.jaci.2017.08.049
434. Mikelez-alonso I, Aires A, Cortajarena AL. Cancer nano-immunotherapy from the injection to the target: The role of protein corona. *Int J Mol Sci*. 2020;21(2). doi:10.3390/ijms21020519
435. Yang X, Gondikas AP, Marinakos SM, et al. Mechanism of Silver Nanoparticle Toxicity Is Dependent on Dissolved Silver and Surface Coating in *Caenorhabditis elegans*. *Environ Sci Technol*. 2012;46(2):1119-1127. doi:10.1021/es202417t
436. Berti L, Woldeyesus T, Li Y, Lam KS. Maximization of loading and stability of ssDNA: Iron oxide nanoparticle complexes formed through electrostatic interaction. *Langmuir*. 2010;26(23):18293-18299. doi:10.1021/la103237e
437. Wu R, Jiang LP, Zhu JJ, Liu J. Effects of Small Molecules on DNA Adsorption by Gold Nanoparticles and a Case Study of Tris(2-carboxyethyl)phosphine (TCEP). *Langmuir*. 2019;35:13461-13468. doi:10.1021/acs.langmuir.9b02652
438. Chen Q, Zheng J, Yang Q, Dang Z, Zhang L. Insights into the Glyphosate Adsorption Behavior and Mechanism by a MnFe₂O₄@Cellulose-Activated Carbon Magnetic Hybrid. *ACS Appl Mater Interfaces*. 2019;11(17):15478-15488. doi:10.1021/acsami.8b22386
439. Yang L, Mao H, Andrew Wang Y, et al. Single chain epidermal growth factor receptor antibody conjugated nanoparticles for in vivo tumor targeting and imaging. *Small*. 2009;5(2):235-243. doi:10.1002/smll.200800714
440. Lin EW, Boehnke N, Maynard HD. Protein-Polymer Conjugation via Ligand Affinity and Photoactivation of Glutathione S-Transferase. *Bioconjug Chem*. 2014;25(10):1902-1909.

doi:10.1021/bc500380r

441. Oh E, Susumu K, Blanco-Canosa JB, Medintz IL, Dawson PE, Mattoussi H. Preparation of stable maleimide-functionalized Au nanoparticles and their use in counting surface ligands. *Small*. 2010;6(12):1273-1278. doi:10.1002/smll.201000279
442. Jeong S, Park JY, Cha MG, et al. Highly robust and optimized conjugation of antibodies to nanoparticles using quantitatively validated protocols. *Nanoscale*. 2017;9(7):2548-2555. doi:10.1039/c6nr04683e
443. Choi JS, Jang WS, Park JS. Comparison of adsorption and conjugation of Herceptin on poly(lactic-co-glycolic acid) nanoparticles – Effect on cell internalization in breast cancer cells. *Mater Sci Eng C*. 2018;92(July):496-507. doi:10.1016/j.msec.2018.06.059
444. Hennig R, Pollinger K, Vesper A, Breunig M, Goepferich A. Nanoparticle multivalency counterbalances the ligand affinity loss upon PEGylation. *J Controlled Release*. 2014;194:20-27. doi:10.1016/j.jconrel.2014.07.062
445. Sun S, Zeng H, Robinson DB, et al. Monodisperse MFe_2O_4 (M = Fe, Co, Mn) Nanoparticles. *J Am Chem Soc*. 2004;126(1):273-279. doi:10.1021/ja0380852
446. Gomez Blanco N, Jauregui-Osoro M, Coboleda-Siles M, et al. Iron oxide-filled micelles as ligands for fac-[M(CO)₃]⁺ (M = (99m)Tc, Re). *Chem Commun Camb Engl*. 2012;48(35):4211-4213. doi:10.1039/c2cc31045g
447. Avasthi A, Caro C, Pozo-Torres E, Leal MP, García-Martín ML. *Magnetic Nanoparticles as MRI Contrast Agents*. Vol 378. Springer International Publishing; 2020. doi:10.1007/s41061-020-00302-w
448. Alipour A, Soran-Erdem Z, Utkur M, et al. A new class of cubic SPIONs as a dual-mode T1 and T2 contrast agent for MRI. *Magn Reson Imaging*. 2018;49:16-24. doi:10.1016/j.mri.2017.09.013
449. Fernández-Barahona I, Gutiérrez L, Veintemillas-Verdaguer S, et al. Cu-Doped Extremely Small Iron Oxide Nanoparticles with Large Longitudinal Relaxivity: One-Pot Synthesis and in Vivo Targeted Molecular Imaging. *ACS Omega*. 2019;4(2):2719-2727. doi:10.1021/acsomega.8b03004
450. Fernández-Barahona I, Muñoz-Hernando M, Ruiz-Cabello J, Herranz F, Pellico J. Iron oxide nanoparticles: An alternative for positive contrast in magnetic resonance imaging. *Inorganics*. 2020;8(4):1-22. doi:10.3390/inorganics8040028
451. Pernia Leal M, Rivera-Fernández S, Franco JM, Pozo D, De La Fuente JM, García-Martín ML. Long-circulating PEGylated manganese ferrite nanoparticles for MRI-based molecular imaging. *Nanoscale*. 2015;7(5):2050-2059. doi:10.1039/c4nr05781c
452. Wang YXJ, Hussain SM, Krestin GP. Superparamagnetic iron oxide contrast agents: Physicochemical characteristics and applications in MR imaging. *Eur Radiol*. 2001;11(11):2319-2331. doi:10.1007/s003300100908
453. Maccioni F, Bruni A, Viscido A, et al. MR imaging in patients with Crohn disease: Value of T2-

versus T1-weighted gadolinium-enhanced MR sequences with use of an oral superparamagnetic contrast agent. *Radiology*. 2006;238(2):517-530. doi:10.1148/radiol.2381040244

454. Naqvi S, Samim M, Abdin MZ, et al. Concentration-dependent toxicity of iron oxide nanoparticles mediated by increased oxidative stress. *Int J Nanomedicine*. 2010;5(1):983-989. doi:10.2147/IJN.S13244
455. Coccini T, De Simone U, Roccio M, et al. In vitro toxicity screening of magnetite nanoparticles by applying mesenchymal stem cells derived from human umbilical cord lining. *J Appl Toxicol*. 2019;39(9):1320-1336. doi:10.1002/jat.3819
456. Montenegro JM, Grazu V, Sukhanova A, et al. Controlled antibody/(bio-) conjugation of inorganic nanoparticles for targeted delivery. *Adv Drug Deliv Rev*. 2013;65(5):677-688. doi:10.1016/j.addr.2012.12.003
457. Huaman MA, Fiske CT, Jones TF, et al. A Comparison of Nanoparticle-Antibody Conjugation Strategy in Sandwich Immunoassay. *J Immunoassay Immunochem*. 2017;38(4):355-377. doi:10.1080/15321819.2016.1269338.A
458. Pabst TM, Thai J, Hunter AK. Evaluation of recent Protein A stationary phase innovations for capture of biotherapeutics. *J Chromatogr A*. 2018;1554:45-60. doi:10.1016/j.chroma.2018.03.060
459. Kim S, Sung D, Chang JH. Highly efficient antibody purification with controlled orientation of protein A on magnetic nanoparticles. *MedChemComm*. 2018;9(1):108-112. doi:10.1039/c7md00468k
460. Seyedinkhorasani M, Cohan RA, Fardood ST, Roohvand F, Norouzian D, Keramati M. Affinity based nano-magnetic particles for purification of recombinant proteins in form of inclusion body. *Iran Biomed J*. 2020;24(3):192-200. doi:10.29252/ibj.24.3.192
461. Kulsharova G, Dimov N, Marques MPC, Szita N, Baganz F. Simplified immobilisation method for histidine-tagged enzymes in poly(methyl methacrylate) microfluidic devices. *New Biotechnol*. 2018;47(December 2017):31-38. doi:10.1016/j.nbt.2017.12.004
462. Ward A, Anderson M, Craggs RI, et al. E. coli expression and purification of human and cynomolgus IL-15. *Protein Expr Purif*. 2009;68(1):42-48. doi:10.1016/j.pep.2009.05.004
463. Lorenzen I, Dingley AJ, Jacques Y, Grötzinger J. The structure of the interleukin-15 α receptor and its implications for ligand binding. *J Biol Chem*. 2006;281(10):6642-6647. doi:10.1074/jbc.M513118200
464. Gupta M, Caniard A, Touceda-Varela Á, Campopiano DJ, Mareque-Rivas JC. Nitrilotriacetic acid-derivatized quantum dots for simple purification and site-selective fluorescent labeling of active proteins in a single step. *Bioconjug Chem*. 2008;19(10):1964-1967. doi:10.1021/bc800273j
465. Townson JL, Lin YS, Agola JO, et al. Re-examining the size/charge paradigm: Differing in vivo characteristics of size- and charge-matched mesoporous silica nanoparticles. *J Am Chem Soc*. 2013;135(43):16030-16033. doi:10.1021/ja4082414
466. Belanova AA, Gavalas N, Makarenko YM, Belousova MM, Soldatov A V., Zolotukhin P V.

Physicochemical Properties of Magnetic Nanoparticles: Implications for Biomedical Applications in Vitro and in Vivo. *Oncol Res Treat.* 2018;41(3):139-143. doi:10.1159/000485020

467. Barbero F, Russo L, Vitali M, et al. Formation of the Protein Corona: The Interface between Nanoparticles and the Immune System. *Semin Immunol.* 2017;34(September):52-60. doi:10.1016/j.smim.2017.10.001

468. Champion JA, Pustulka SM, Ling K, Pish SL. Protein nanoparticle charge and hydrophobicity govern protein corona and macrophage uptake. *ACS Appl Mater Interfaces.* 2020;12(43):48284-48295. doi:10.1021/acscami.0c12341

469. Su J, Olvera De La Cruz M, Guo H. Solubility and transport of cationic and anionic patterned nanoparticles. *Phys Rev E - Stat Nonlinear Soft Matter Phys.* 2012;85(1):1-5. doi:10.1103/PhysRevE.85.011504

470. Chirifu M, Hayashi C, Nakamura T, et al. Crystal structure of the IL-15-IL-15R α complex, a cytokine-receptor unit presented in trans. *Nat Immunol.* 2007;8(9):1001-1007. doi:10.1038/ni1492

471. Zhang S, Zhao J, Bai X, Handley M, Shan F. Biological effects of IL-15 on immune cells and its potential for the treatment of cancer. *Int Immunopharmacol.* 2021;91:107318. doi:10.1016/j.intimp.2020.107318

472. Steel JC, Waldmann TA, Morris JC. Interleukin-15 biology and its therapeutic implications in cancer. *Trends Pharmacol Sci.* 2012;33(1):35-41. doi:10.1016/j.tips.2011.09.004

473. Wuest TY, Willette-Brown J, Durum SK, Hurwitz AA. The influence of IL-2 family cytokines on activation and function of naturally occurring regulatory T cells. *J Leukoc Biol.* 2008;84(4):973-980. doi:10.1189/jlb.1107778

474. Ohue Y, Nishikawa H. Regulatory T (Treg) cells in cancer: Can Treg cells be a new therapeutic target? *Cancer Sci.* 2019;110(7):2080-2089. doi:10.1111/cas.14069

475. Kinter AL, Godbout EJ, McNally JP, et al. The Common gamma-Chain Cytokines IL-2, IL-7, IL-15, and IL-21 Induce the Expression of Programmed Death-1 and Its Ligands. *J Immunol.*:9. doi:10.4049/jimmunol.181.10.6738

476. Tallerico R, Cristiani CM, Staaf E, et al. IL-15, TIM-3 and NK cells subsets predict responsiveness to anti-CTLA-4 treatment in melanoma patients. *Oncol Immunology.* 2017;6(2):e1261242. doi:10.1080/2162402X.2016.1261242

477. Waldmann TA, Dubois S, Miljkovic MD, Conlon KC. IL-15 in the Combination Immunotherapy of Cancer. *Front Immunol.* 2020;11:868. doi:10.3389/fimmu.2020.00868

478. Knudson KM, Hicks KC, Alter S, Schlom J, Gameiro SR. Mechanisms involved in IL-15 superagonist enhancement of anti-PD-L1 therapy. *J Immunother Cancer.* 2019;7(1):82. doi:10.1186/s40425-019-0551-y

479. Juliá EP, Mordoh J, Levy EM. Cetuximab and IL-15 Promote NK and Dendritic Cell Activation

- In Vitro in Triple Negative Breast Cancer. *Cells*. 2020;9(7):1573. doi:10.3390/cells9071573
480. Wrangle JM, Velcheti V, Patel MR, et al. ALT-803, an IL-15 superagonist, in combination with nivolumab in patients with metastatic non-small cell lung cancer: a non-randomised, open-label, phase 1b trial. *Lancet Oncol*. 2018;19(5):694-704. doi:10.1016/S1470-2045(18)30148-7
481. Shapiro RM, Nikiforow S, Rambaldi B, et al. Cytokine-Induced Memory-like NK Cells Exhibit Massive Expansion and Long-Term Persistence after Infusion Post-Haploidentical Stem Cell Transplantation: A Report of the First Three Cases in a Phase I Trial. *Blood*. 2020;136(Supplement 1):8-9. doi:10.1182/blood-2020-133933
482. Qian X, Wang X, Jin H. Cell Transfer Therapy for Cancer: Past, Present, and Future. *J Immunol Res*.:10. doi:https://doi.org/10.1155/2014/525913
483. Rosenberg SA, Restifo NP. Adoptive cell transfer as personalized immunotherapy for human cancer. *CANCER Immunol Immunother*.:8. doi:10.1126/science.aaa4967
484. Miller JS, Soignier Y, Panoskaltsis-Mortari A, et al. Successful adoptive transfer and in vivo expansion of human haploidentical NK cells in patients with cancer. *Blood*. 2005;105(8):3051-3057. doi:10.1182/blood-2004-07-2974
485. Shi J, Tricot G, Rosen N, et al. Infusion of haplo-identical killer immunoglobulin-like receptor ligand mismatched NK cells for relapsed myeloma in the setting of autologous stem cell transplantation. *Br J Haematol*. Published online 2008:13. doi:10.1111/j.1365-2141.2008.07340.x
486. Pérez-Martínez A, Fernández L, Valentín J, et al. A phase I/II trial of interleukin-15–stimulated natural killer cell infusion after haplo-identical stem cell transplantation for pediatric refractory solid tumors. *Cytotherapy*. 2015;17(11):1594-1603. doi:10.1016/j.jcyt.2015.07.011
487. Gang M, Wong P, Berrien-Elliott MM, Fehniger TA. Memory-like natural killer cells for cancer immunotherapy. *Semin Hematol*. 2020;57(4):185-193. doi:10.1053/j.seminhematol.2020.11.003
488. Romee R, Rosario M, Berrien-Elliott MM, et al. Cytokine-induced memory-like natural killer cells exhibit enhanced responses against myeloid leukemia. *Sci Transl Med*. 2016;8(357). doi:10.1126/scitranslmed.aaf2341
489. Terrén I, Mikelez I, Odriozola I, et al. Implication of interleukin-12/15/18 and ruxolitinib in the phenotype, proliferation, and polyfunctionality of human cytokine-preactivated natural killer cells. *Front Immunol*. 2018;9:737. doi:10.3389/fimmu.2018.00737
490. Romee R, Schneider SE, Leong JW, et al. Cytokine activation induces human memory-like NK cells. *Blood*. 2012;120(24):4751-4760. doi:10.1182/blood-2012-04-419283
491. Simhadri VR, Dimitrova M, Mariano JL, et al. A Human Anti-M2 Antibody Mediates Antibody-Dependent Cell-Mediated Cytotoxicity (ADCC) and Cytokine Secretion by Resting and Cytokine-Preactivated Natural Killer (NK) Cells. *PLOS ONE*. Published online 2015:13. doi:10.1371/journal.pone.0124677
492. Cooper MA, Elliott JM, Keyel PA, Yang L, Carrero JA, Yokoyama WM. Cytokine-induced

- memory-like natural killer cells. *Proc Natl Acad Sci*. 2009;106(6):1915-1919.
doi:10.1073/pnas.0813192106
493. Childs RW, Carlsten M. Therapeutic approaches to enhance natural killer cell cytotoxicity against cancer: the force awakens. *DRUG Discov*. Published online 2015:12. doi:10.1038/nrd4506
494. Myers JA, Miller JS. Exploring the NK cell platform for cancer immunotherapy. *Nat Rev Clin Oncol*. 2021;18(2):85-100. doi:10.1038/s41571-020-0426-7
495. Garg TK, Szmania SM, Khan JA, et al. Highly activated and expanded natural killer cells for multiple myeloma immunotherapy. *Haematologica*. 2012;97(9):1348-1356.
doi:10.3324/haematol.2011.056747
496. Lapteva N, Durett AG, Sun J, et al. Large-scale ex vivo expansion and characterization of natural killer cells for clinical applications. *Cytotherapy*. 2012;14(9):1131-1143.
doi:10.3109/14653249.2012.700767
497. Patidar M, Yadav N, Dalai SK. Development of Stable Chimeric IL-15 for Trans-Presentation by the Antigen Presenting Cells. *Front Immunol*. 2021;12:14.
doi:doi.org/10.3389/fimmu.2021.646159
498. Robinson TO, Hegde SM, Chang A, et al. NKTR-255 is a polymer-conjugated IL-15 with unique mechanisms of action on T and natural killer cells. *J Clin Invest*.:15. doi:doi.org/10.1172/JCI144365.
499. Han K ping, Zhu X, Liu B, et al. IL-15:IL-15 receptor alpha superagonist complex: High-level co-expression in recombinant mammalian cells, purification and characterization. *Cytokine*. 2011;56(3):804-810. doi:10.1016/j.cyto.2011.09.028
500. Xu W, Jones M, Liu B, et al. Efficacy and Mechanism-of-Action of a Novel Superagonist Interleukin-15: Interleukin-15 Receptor α Su/Fc Fusion Complex in Syngeneic Murine Models of Multiple Myeloma. *Cancer Res*. 2013;73(10):3075-3086. doi:10.1158/0008-5472.CAN-12-2357
501. Silva AL, Peres C, Connot J, et al. Nanoparticle impact on innate immune cell pattern-recognition receptors and inflammasomes activation. *Semin Immunol*. 2017;34:3-24.
doi:10.1016/j.smim.2017.09.003
502. Ruiz-de-Angulo A, Bilbao-Asensio M, Cronin J, et al. Chemically Programmed Vaccines: Iron Catalysis in Nanoparticles Enhances Combination Immunotherapy and Immunotherapy-Promoted Tumor Ferroptosis. *iScience*. 2020;23(9):101499. doi:10.1016/j.isci.2020.101499
503. Tarantola M, Schneider D, Sunnick E, et al. Cytotoxicity of Metal and Semiconductor Micromotility. *ACS Nano*. 2009;3(1):213-222. doi:10.1021/nn800721j
504. Kim Y, Kong SD, Chen LH, Pisanic TR, Jin S, Shubayev VI. In vivo nanoneurotoxicity screening using oxidative stress and neuroinflammation paradigms. *Nanomedicine Nanotechnol Biol Med*. 2013;9(7):1057-1066. doi:10.1016/j.nano.2013.05.002
505. Sharma G, Kodali V, Gaffrey M, et al. Iron oxide nanoparticle agglomeration influences dose

- rates and modulates oxidative stress-mediated dose-response profiles in vitro. *Nanotoxicology*. 2014;8(6):663-675. doi:10.3109/17435390.2013.822115
506. Erofeev A, Gorelkin P, Garanina A, et al. Novel method for rapid toxicity screening of magnetic nanoparticles. *Sci Rep*. 2018;8(1):1-11. doi:10.1038/s41598-018-25852-4
507. Demir E, Qin T, Li Y, et al. Cytotoxicity and genotoxicity of cadmium oxide nanoparticles evaluated using in vitro assays. *Mutat Res - Genet Toxicol Environ Mutagen*. 2020;850-851. doi:10.1016/j.mrgentox.2020.503149
508. Gaharwar US, Meena R, Rajamani P. Iron oxide nanoparticles induced cytotoxicity, oxidative stress and DNA damage in lymphocytes. *J Appl Toxicol*. 2017;37(10):1232-1244. doi:10.1002/jat.3485
509. Aires A, Cabrera D, Alonso-Pardo LC, Cortajarena AL, Teran FJ. Elucidation of the physicochemical properties ruling the colloidal stability of iron oxide nanoparticles under physiological conditions. *ChemNanoMat*. 2016;3(3):183-189. doi:10.1002/cnma.201600333
510. Li X, Wang L, She L, et al. Immunotoxicity assessment of ordered mesoporous carbon nanoparticles modified with PVP/PEG. *Colloids Surf B Biointerfaces*. 2018;171(April):485-493. doi:10.1016/j.colsurfb.2018.07.072
511. Terrén I, Orrantia A, Vitallé J, Zenarruzabeitia O, Borrego F. CFSE dilution to study human T and NK cell proliferation in vitro. In: *Methods in Enzymology*. Vol 631. Elsevier; 2020:239-255. doi:10.1016/bs.mie.2019.05.020
512. Wang X, Rickert M, Garcia KC. Structural biology: Structure of the quaternary complex of Interleukin-2 with its α , β and γ c receptors. *Science*. 2005;310:1159-1163. doi:10.1126/science.1117893
513. Borrego, Robertson, Ritz, Peña, Solana. CD69 is a stimulatory receptor for natural killer cell and its cytotoxic effect is blocked by CD94 inhibitory receptor. *Immunology*. 1999;97(1):159-165. doi:10.1046/j.1365-2567.1999.00738.x
514. Ding L, Chen T, Wang XJ, Zhou L, Shi AC, Ning Q. CD69+NK cells contribute to the murine hepatitis virus strain 3-induced murine hepatitis. *J Huazhong Univ Sci Technol - Med Sci*. 2013;33(4):505-510. doi:10.1007/s11596-013-1150-7
515. Ghafourian M, Karami N, Khodadadi A, Nikbakhat R. Increase of CD69, CD161 and CD94 on NK cells in women with recurrent spontaneous abortion and in vitro fertilization failure. *Iran J Immunol*. 2014;11(2):84-96.
516. Nervi B, Link DC, DiPersio JF. Cytokines and hematopoietic stem cell mobilization. *J Cell Biochem*. 2006;99(3):690-705. doi:10.1002/jcb.21043
517. Alter G, Malenfant JM, Altfeld M. CD107a as a functional marker for the identification of natural killer cell activity. *J Immunol Methods*. 2004;294(1-2):15-22. doi:10.1016/j.jim.2004.08.008
518. Aktas E, Kucuksezer UC, Bilgic S, Erten G, Deniz G. Relationship between CD107a expression and cytotoxic activity. *Cell Immunol*. 2009;254(2):149-154. doi:10.1016/j.cellimm.2008.08.007

519. Bradley LM, Dalton DK, Croft M. A direct role for IFN-gamma in regulation of Th1 cell development. *J Immunol*. 1996;157(4):1350-1358.
520. Rankin EB, Yu D, Jiang J, et al. An essential role of Th1 responses and interferon gamma in infection-mediated suppression of neoplastic growth. *Cancer Biol Ther*. 2003;2(6):687-693. doi:10.4161/cbt.2.6.557
521. Vitale M, Della Chiesa M, Carlomagno S, et al. NK-dependent DC maturation is mediated by TNF α and IFN γ released upon engagement of the Nkp30 triggering receptor. *Blood*. 2005;106(2):566-571. doi:10.1182/blood-2004-10-4035
522. Dorner BG, Scheffold A, Rolph MS, et al. MIP-1 α , MIP-1 β , RANTES, and ATAC/lymphotactin function together with IFN- γ as type 1 cytokines. *Proc Natl Acad Sci U S A*. 2002;99(9):6181-6186. doi:10.1073/pnas.092141999
523. Sabry M, Zubiak A, Hood SP, et al. Tumor- And cytokine-primed human natural killer cells exhibit distinct phenotypic and transcriptional signatures. *PLoS ONE*. 2019;14(6):1-20. doi:10.1371/journal.pone.0218674
524. Johnston B, Kim CH, Soler D, Emoto M, Butcher EC. Differential Chemokine Responses and Homing Patterns of Murine TCR $\alpha\beta$ NKT Cell Subsets. *J Immunol*. 2003;171(6):2960-2969. doi:10.4049/jimmunol.171.6.2960
525. Roederer M, Nozzi JL, Nason MC. SPICE: Exploration and analysis of post-cytometric complex multivariate datasets. *Cytometry A*. 2011;79 A(2):167-174. doi:10.1002/cyto.a.21015
526. Cao X, Cai SF, Fehniger TA, et al. Granzyme B and Perforin Are Important for Regulatory T Cell-Mediated Suppression of Tumor Clearance. *Immunity*. 2007;27:635-646. doi:10.1016/j.immuni.2007.08.014
527. Li Y, Orange JS. Degranulation enhances presynaptic membrane packing, which protects NK cells from perforin-mediated autolysis. *PLOS Biol*. 2021;19(8):e3001328. doi:10.1371/journal.pbio.3001328
528. Rodella L, Zamai L, Rezzani R, et al. Interleukin 2 and interleukin 15 differentially predispose natural killer cells to apoptosis mediated by endothelial and tumour cells: Apoptosis in IL2- and IL15-stimulated NK Cells. *Br J Haematol*. 2001;115(2):442-450. doi:10.1046/j.1365-2141.2001.03055.x
529. Yamasaki S, Maeda M, Ohshima K, Kikuchi M, Otsuka T, Harada M. Growth and apoptosis of human natural killer cell neoplasms: role of interleukin-2/15 signaling. *Leuk Res*. 2004;28(10):1023-1031. doi:10.1016/j.leukres.2004.02.006
530. Perdreau H, Mortier E, Bouchaud G, et al. Different dynamics of IL-15R activation following IL-15 cis- or trans-presentation. *Eur Cytokine Netw*. 2010;21:297-307. doi:10.1684/ecn.2010.0207
531. Levy E, Reger R, Segerberg F, et al. Enhanced Bone Marrow Homing of Natural Killer Cells Following mRNA Transfection With Gain-of-Function Variant CXCR4R334X. *Front Immunol*. 2019;10:13. doi:10.3389/fimmu.2019.01262

532. Tomescu C, Chehimi J, Maino VC, Montaner LJ. Retention of viability, cytotoxicity, and response to IL-2, IL-15, or IFN- α by human NK cells after CD107a degranulation. *J Leukoc Biol.* 2009;85(5):871-876. doi:10.1189/jlb.1008635
533. Rasid O, Chevalier C, Camarasa TMN, Fitting C, Cavaillon JM, Hamon MA. H3K4me1 Supports Memory-like NK Cells Induced by Systemic Inflammation. *Cell Rep.* 2019;29:3933-3945. doi:10.1016/j.celrep.2019.11.043
534. Nikzad R, Angelo LS, Aviles-Padilla K, et al. Human natural killer cells mediate adaptive immunity to viral antigens. *Sci Immunol.* 2019;4:1-13. doi:10.1126/sciimmunol.aat8116
535. Placek K, Schultze JL, Netea MG. Immune memory characteristics of innate lymphoid cells. *Curr Opin Infect Dis.* 2019;32:196-203. doi:10.1097/QCO.0000000000000540
536. Netea MG, Domínguez-Andrés J, Barreiro LB, et al. Defining trained immunity and its role in health and disease. *Nat Rev Immunol.* 2020;20(6):375-388. doi:10.1038/s41577-020-0285-6
537. Tanzi M, Consonni M, Falco M, et al. Cytokine-induced memory-like nk cells with high reactivity against acute leukemia blasts and solid tumor cells suitable for adoptive immunotherapy approaches. *Cancers.* 2021;13:1-19. doi:10.3390/cancers13071577
538. Terrén I, Orrantia A, Mosteiro A, Vitallé J, Zenarruzabeitia O, Borrego F. Metabolic changes of Interleukin-12/15/18-stimulated human NK cells. *Sci Rep.* 2021;11:1-15. doi:10.1038/s41598-021-85960-6
539. Pal M, Schwab L, Yermakova A, et al. Tumor-priming converts NK cells to memory-like NK cells. *Oncol Immunology.* 2017;6:1-13. doi:10.1080/2162402X.2017.1317411
540. Leong JW, Chase JM, Romee R, et al. Preactivation with IL-12, IL-15, and IL-18 induces cd25 and a functional high-affinity il-2 receptor on human cytokine-induced memory-like natural killer cells. *Biol Blood Marrow Transplant.* 2014;20(4):463-473. doi:10.1016/j.bbmt.2014.01.006
541. Uppendahl LD, Felices M, Bendzick L, et al. Cytokine-induced memory-like natural killer cells have enhanced function, proliferation, and in vivo expansion against ovarian cancer cells. *Gynecol Oncol.* 2019;153:149-157. doi:10.1016/j.ygyno.2019.01.006
542. Widowati W, Jasaputra DK, Sumitro SB, et al. Effect of interleukins (IL-2, il-15, il-18) on receptors activation and cytotoxic activity of natural killer cells in breast cancer cell. *Afr Health Sci.* 2020;20(2):822-832. doi:10.4314/ahs.v20i2.36
543. Berrien-Elliott MM, Cashen AF, Cubitt CC, et al. Multidimensional analyses of donor memory-like NK cells reveal new associations with response after adoptive immunotherapy for leukemia. *Cancer Discov.* 2020;10(12):1854-1872. doi:10.1158/2159-8290.CD-20-0312
544. Drost J, Clevers H. Organoids in cancer research. *Nat Rev Cancer.* 2018;18(7):407-418. doi:10.1038/s41568-018-0007-6
545. Xia T, Du W, Chen X, Zhang Y. Organoid models of the tumor microenvironment and their applications. *J Cell Mol Med.* 2021;25(13):5829-5841. doi:10.1111/jcmm.16578

546. Wilson DR, Sen R, Sunshine JC, Pardoll DM, Green JJ, Kim YJ. Biodegradable STING agonist nanoparticles for enhanced cancer immunotherapy. *Nanomedicine Nanotechnol Biol Med*. 2018;14(2):237-246. doi:10.1016/j.nano.2017.10.013
547. Rodell CB, Arlauckas SP, Cuccarese MF, et al. TLR7/8-agonist-loaded nanoparticles promote the polarization of tumour-associated macrophages to enhance cancer immunotherapy. *Nat Biomed Eng*. 2018;2(8):578-588. doi:10.1038/s41551-018-0236-8
548. Rao L, Zhao SK, Wen C, et al. Activating Macrophage-Mediated Cancer Immunotherapy by Genetically Edited Nanoparticles. *Adv Mater*. 2020;32(47):1-9. doi:10.1002/adma.202004853
549. Liu Y, Qiao L, Zhang S, et al. Dual pH-responsive multifunctional nanoparticles for targeted treatment of breast cancer by combining immunotherapy and chemotherapy. *Acta Biomater*. 2018;66:310-324. doi:10.1016/j.actbio.2017.11.010
550. Kang M, Hong J, Jung M, et al. T-Cell-Mimicking Nanoparticles for Cancer Immunotherapy. *Adv Mater*. 2020;32(39):1-10. doi:10.1002/adma.202003368
551. Fang RH, Hu CMJ, Luk BT, et al. Cancer cell membrane-coated nanoparticles for anticancer vaccination and drug delivery. *Nano Lett*. 2014;14(4):2181-2188. doi:10.1021/nl500618u
552. Zhao P, Wang M, Chen M, et al. Programming cell pyroptosis with biomimetic nanoparticles for solid tumor immunotherapy. *Biomaterials*. 2020;254:120142. doi:10.1016/j.biomaterials.2020.120142
553. Longmire M, Choyke PL, Kobayashi H. Clearance properties of nano-sized particles and molecules as imaging agents: considerations and caveats. *Nanomed*. 2008;3(5):703-717. doi:10.2217/17435889.3.5.703
554. Ernsting MJ, Murakami M, Roy A, Li SD. Factors controlling the pharmacokinetics, biodistribution and intratumoral penetration of nanoparticles. *J Controlled Release*. 2013;172(3):782-794. doi:10.1016/j.jconrel.2013.09.013
555. Ruiz-de-Angulo A, Zabaleta A, Gómez-Vallejo V, Llop J, Mareque-Rivas JC. Microdosed Lipid-Coated ⁶⁷Ga-Magnetite Enhances Antigen-Specific Immunity by Image Tracked Delivery of Antigen and CpG to Lymph Nodes. *ACS Nano*. 2016;10(1):1602-1618. doi:10.1021/acsnano.5b07253
556. Ruiz-de-Angulo A, Bilbao-Asensio M, Cronin J, et al. Chemically Programmed Vaccines: Iron Catalysis in Nanoparticles Enhances Combination Immunotherapy and Immunotherapy-Promoted Tumor Ferroptosis. *iScience*. 2020;23(9):101499. doi:10.1016/j.isci.2020.101499
557. Leong JW, Chase JM, Romee R, et al. Preactivation with IL-12, IL-15, and IL-18 induces cd25 and a functional high-affinity il-2 receptor on human cytokine-induced memory-like natural killer cells. *Biol Blood Marrow Transplant*. 2014;20:463-473. doi:10.1016/j.bbmt.2014.01.006
558. Rhode PR, Egan JO, Xu W, et al. Comparison of the superagonist complex, ALT-803, to IL15 as cancer immunotherapeutics in animal models. *Cancer Immunol Res*. 2016;4(1):49-60. doi:10.1158/2326-6066.CIR-15-0093-T

559. Romee R, Rosario M, Berrien-Elliott MM, et al. Cytokine-induced memory-like natural killer cells exhibit enhanced responses against myeloid leukemia. *Sci Transl Med*. 2016;8(357). doi:10.1126/scitranslmed.aaf2341
560. Hu Q, Ye X, Qu X, et al. Discovery of a novel IL-15 based protein with improved developability and efficacy for cancer immunotherapy. *Sci Rep*. 2018;8:7675. doi:10.1038/s41598-018-25987-4
561. Stoklasek TA, Schluns KS, Lefrançois L. Combined IL-15/IL-15R α Immunotherapy Maximizes IL-15 Activity In Vivo. *J Immunol*. 2006;177(9):6072-6080. doi:10.4049/jimmunol.177.9.6072
562. Eisenman J, Ahdieh M, Beers C, et al. INTERLEUKIN-15 INTERACTIONS WITH INTERLEUKIN-15 RECEPTOR COMPLEXES: CHARACTERIZATION AND SPECIES SPECIFICITY. *Cytokine*. 2002;20(3):121-129. doi:10.1006/cyto.2002.1989
563. Goedhart M, Gessel S, van der Voort R, et al. CXCR4, but not CXCR3, drives CD8 + T-cell entry into and migration through the murine bone marrow. *Eur J Immunol*. 2019;49(4):576-589. doi:10.1002/eji.201747438
564. Chen L, Li Y, Chen W, et al. Enhanced recruitment and hematopoietic reconstitution of bone marrow-derived mesenchymal stem cells in bone marrow failure by the SDF-1/CXCR4. *J Tissue Eng Regen Med*. 2020;14(9):1250-1260. doi:10.1002/term.3096
565. Poli A, Michel T, Thérésine M, Andrès E, Hentges F, Zimmer J. CD56^{bright} natural killer (NK) cells: an important NK cell subset. *Immunology*. 2009;126(4):458-465. doi:10.1111/j.1365-2567.2008.03027.x
566. Li XC, Demirci G, Ferrari-Lacraz S, et al. IL-15 and IL-2: A matter of life and death for T cells in vivo. *Nat Med*. 2001;7(1):114-118. doi:10.1038/83253
567. Vahedi F, Nham T, Poznanski SM, et al. Ex Vivo Expanded Human NK Cells Survive and Proliferate in Humanized Mice with Autologous Human Immune Cells. *Sci Rep*. 2017;7(1):1-6. doi:10.1038/s41598-017-12223-8
568. Huntington ND, Alves NL, Legrand N, et al. IL-15 transpresentation promotes both human T-cell reconstitution and T-cell-dependent antibody responses in vivo. *Proc Natl Acad Sci U S A*. 2011;108(15):6217-6222. doi:10.1073/pnas.1019167108
569. Guo Y, Luan L, Rabacal W, et al. IL-15 Superagonist-Mediated Immunotoxicity: Role of NK Cells and IFN- γ . *J Immunol*. 2015;195(5):2353-2364. doi:10.4049/jimmunol.1500300
570. Cooley S, He F, Bachanova V, et al. First-in-human trial of rhIL-15 and haploidentical natural killer cell therapy for advanced acute myeloid leukemia. *Blood Adv*. 2019;3(13):1970-1980. doi:10.1182/bloodadvances.2018028332
571. Chertova E, Bergamaschi C, Chertov O, et al. Characterization and favorable in vivo properties of heterodimeric soluble IL-15•IL-15R α cytokine compared to IL-15 monomer. *J Biol Chem*. 2013;288(25):18093-18103. doi:10.1074/jbc.M113.461756
572. Galkina E, Florey O, Zarbock A, et al. T lymphocyte rolling and recruitment into peripheral

lymph nodes is regulated by a saturable density of L-selectin (CD62L). *Eur J Immunol.* 2007;37(5):1243-1253. doi:10.1002/eji.200636481

573. Bergamaschi C, Pandit H, Nagy BA, et al. Heterodimeric IL-15 delays tumor growth and promotes intratumoral CTL and dendritic cell accumulation by a cytokine network involving XCL1, IFN- γ , CXCL9 and CXCL10. *J Immunother Cancer.* 2020;8(1):1-14. doi:10.1136/jitc-2020-000599

574. Guo J, Liang Y, Xue D, et al. Tumor-conditional IL-15 pro-cytokine reactivates anti-tumor immunity with limited toxicity. *Cell Res.* 2021;31(11):1190-1198. doi:10.1038/s41422-021-00543-4

575. Berger A, Colpitts SJ, Seabrook MSS, et al. Interleukin-15 in cancer immunotherapy: IL-15 receptor complex versus soluble IL-15 in a cancer cell-delivered murine leukemia model. *J Immunother Cancer.* 2019;7(1):1-13. doi:10.1186/s40425-019-0777-8

576. Thi VA Do, Jeon HM, Park SM, Lee H, Kim YS. Cell-based IL-15:IL-15 α secreting vaccine as an effective therapy for CT26 colon cancer in mice. *Mol Cells.* 2019;42(12):869-883. doi:10.14348/molcells.2019.0188

577. Vallera DA, Ferrone S, Kodala B, et al. NK-cell-mediated targeting of various solid tumors using a B7-H3 tri-specific killer engager in vitro and in vivo. *Cancers.* 2020;12(9):1-18. doi:10.3390/cancers12092659

578. Lei S, Zhang X, Men K, et al. Efficient Colorectal Cancer Gene Therapy with IL-15 mRNA Nanoformulation. *Mol Pharm.* 2020;17(9):3378-3391. doi:10.1021/acs.molpharmaceut.0c00451

579. Cui F, Qu D, Sun R, Zhang M, Nan K. NK cell-produced IFN- γ regulates cell growth and apoptosis of colorectal cancer by regulating IL-15. *Exp Ther Med.* 2020;19(2):1400-1406. doi:10.3892/etm.2019.8343

580. Ochoa MC, Fioravanti J, Rodriguez I, et al. Antitumor immunotherapeutic and toxic properties of an HDL-conjugated chimeric IL-15 fusion protein. *Cancer Res.* 2013;73(1):139-149. doi:10.1158/0008-5472.CAN-12-2660

581. Santana Carrero RM, Beceren-Braun F, Rivas SC, et al. IL-15 is a component of the inflammatory milieu in the tumor microenvironment promoting antitumor responses. *Proc Natl Acad Sci U S A.* 2019;116(2):599-608. doi:10.1073/pnas.1814642116

582. Morris JC, Ramlogan-Steel CA, Yu P, et al. Vaccination with tumor cells expressing IL-15 and IL-15R inhibits murine breast and prostate cancer. *Gene Ther.* 2014;21(4):393-401. doi:10.1038/gt.2014.10

583. Sakellariou C, Elhage O, Papaevangelou E, et al. Prostate cancer cells enhance interleukin-15-mediated expansion of NK cells. *BJU Int.* 2020;125(1):89-102. doi:10.1111/bju.14893

584. Ishimitsu R, Nishimura H, Yajima T, Watase T, Kawachi H, Yoshikai Y. Overexpression of IL-15 In Vivo Enhances Tc1 Response, Which Inhibits Allergic Inflammation in a Murine Model of Asthma. *J Immunol.* 2001;166(3):1991-2001. doi:10.4049/jimmunol.166.3.1991

585. Rückert R, Brandt K, Braun A, et al. Blocking IL-15 Prevents the Induction of Allergen-Specific T Cells and Allergic Inflammation In Vivo. *J Immunol*. 2005;174(9):5507-5515. doi:10.4049/jimmunol.174.9.5507
586. Knudson KM, Hicks KC, Ozawa Y, Schlom J, Gameiro SR. Functional and mechanistic advantage of the use of a bifunctional anti-PD-L1/IL-15 superagonist. *J Immunother Cancer*. 2020;8(1):1-15. doi:10.1136/jitc-2019-000493
587. Chu Y, Nayyar G, Jiang S, et al. Combinatorial immunotherapy of N-803 (IL-15 superagonist) and dinutuximab with ex vivo expanded natural killer cells significantly enhances in vitro cytotoxicity against GD2+ pediatric solid tumors and in vivo survival of xenografted immunodeficient NSG m. *J Immunother Cancer*. 2021;9(7):1-13. doi:10.1136/jitc-2020-002267
588. Fassan M, Cavallin F, Guzzardo V, et al. PD-L1 expression, CD8+ and CD4+ lymphocyte rate are predictive of pathological complete response after neoadjuvant chemoradiotherapy for squamous cell cancer of the thoracic esophagus. *Cancer Med*. 2019;8(13):6036-6048. doi:10.1002/cam4.2359
589. Waki K, Kawano K, Tsuda N, Komatsu N, Yamada A. CD4/CD8 ratio is a prognostic factor in IgG nonresponders among peptide vaccine-treated ovarian cancer patients. *Cancer Sci*. 2020;111(4):1124-1131. doi:10.1111/cas.14349
590. Ma Y, Li J, Wang H, et al. Combination of PD-1 Inhibitor and OX40 Agonist Induces Tumor Rejection and Immune Memory in Mouse Models of Pancreatic Cancer. *Gastroenterology*. 2020;159(1):306-319. doi:10.1053/j.gastro.2020.03.018
591. Clausen J, Vergeiner B, Enk M, Petzer AL, Gastl G, Gunsilius E. Functional significance of the activation-associated receptors CD25 and CD69 on human NK-cells and NK-like T-cells. *Immunobiology*. 2003;207(2):85-93. doi:10.1078/0171-2985-00219
592. Berard M, Tough DF, Rg B. Qualitative differences between naïve and memory T cells. Published online 2002:12.
593. Kaech SM, Wherry EJ, Ahmed R. Effector and memory T-cell differentiation: Implications for vaccine development. *Nat Rev Immunol*. 2002;2(4):251-262. doi:10.1038/nri778
594. Golubovskaya V, Wu L. Different subsets of T cells, memory, effector functions, and CAR-T immunotherapy. *Cancers*. 2016;8(3). doi:10.3390/cancers8030036
595. Klebanoff CA, Finkelstein SE, Surman DR, et al. IL-15 enhances the in vivo antitumor activity of tumor-reactive CD8 + T Cells. *Proc Natl Acad Sci U S A*. 2004;101(7):1969-1974. doi:10.1073/pnas.0307298101
596. Dijkstra KK, Cattaneo CM, Weeber F, et al. Generation of Tumor-Reactive T Cells by Co-culture of Peripheral Blood Lymphocytes and Tumor Organoids. *Cell*. 2018;174(6):1586-1598. doi:10.1016/j.cell.2018.07.009
597. Pagès F, Berger A, Camus M, et al. Effector Memory T Cells, Early Metastasis, and Survival in Colorectal Cancer. *N Engl J Med*. 2005;353(25):2654-2666. doi:10.1056/nejmoa051424

598. Enomoto K, Sho M, Wakatsuki K, et al. Prognostic importance of tumour-infiltrating memory T cells in oesophageal squamous cell carcinoma. *Clin Exp Immunol*. 2012;168(2):186-191. doi:10.1111/j.1365-2249.2012.04565.x
599. Bonaventura P, Shekarian T, Alcazer V, et al. Cold tumors: A therapeutic challenge for immunotherapy. *Front Immunol*. 2019;10:1-10. doi:10.3389/fimmu.2019.00168
600. Zuo S, Wei M, Wang S, Dong J, Wei J. Pan-Cancer Analysis of Immune Cell Infiltration Identifies a Prognostic Immune-Cell Characteristic Score (ICCS) in Lung Adenocarcinoma. *Front Immunol*. 2020;11:1-13. doi:10.3389/fimmu.2020.01218
601. Hotta K, Sho M, Fujimoto K, et al. Prognostic significance of CD45RO+ memory T cells in renal cell carcinoma. *Br J Cancer*. 2011;105(8):1191-1196. doi:10.1038/bjc.2011.368
602. Böttcher JP, Bonavita E, Chakravarty P, et al. NK Cells Stimulate Recruitment of cDC1 into the Tumor Microenvironment Promoting Cancer Immune Control. *Cell*. 2018;172(5):1022-1037.e14. doi:10.1016/j.cell.2018.01.004
603. Li B, Cui Y, Nambiar DK, Sunwoo JB, Li R. The immune subtypes and landscape of squamous cell carcinoma. *Clin Cancer Res*. Published online March 4, 2019:clincanres.4085.2018. doi:10.1158/1078-0432.CCR-18-4085
604. Melaiu O, Lucarini V, Cifaldi L, Fruci D. Influence of the Tumor Microenvironment on NK Cell Function in Solid Tumors. *Front Immunol*. 2020;10:3038. doi:10.3389/fimmu.2019.03038

Acknowledgement

I would like to express my gratitude to my supervisors Aitziber L. Cortajarena and Francisco Borrego Rabasco for guiding me through this enriching experience. I would also like to thank Juan C. Mareque-Rivas for giving me the opportunity of working at CIC biomaGUNE at the beginning of my career in the laboratory.

I am very grateful to have developed this thesis in a center such as CIC biomaGUNE and Biocruces, excellent spaces for learning and scientific development. In fact, they have professionals without whom this thesis would not have been possible.

Finally, I would like to comment that I have been very lucky in all the groups I have belonged to (Theranostic Nanomedicine, Biomolecular Nanotechnology and Immunopathology group), since you have paved the way.



Curriculum Vitae

Idoia Mikelez Alonso

ORCID ID: 0000-0002-9304-1658

imikelez.alonso@gmail.com

Academic formation

Master degree on Molecular Biology and Biomedicine on Euskal Herriko Unibertsitatea (EHU)-Universidad del País Vasco (UPV), 2015-2016

Postgraduate course of Innovation in cancer on Universidad Nacional de Educación a Distancia (UNED), 2014-2015

Biochemistry degree on Universidad de Navarra (UNAV), 2009-2013

Publications

Idoia Mikelez-Alonso, Susana Magadán, África González-Fernández & Francisco Borrego. Natural killer (NK) cell-based immunotherapies and the many faces of NK cell memory: A look into how nanoparticles enhance NK cell activity. *Advanced Drug Delivery Reviews*, **2021**, 176, 113860. <https://doi.org/10.1016/j.addr.2021.113860> [Impact factor: 15.47]

Susana Magadán, **Idoia Mikelez-Alonso**, Francisco Borrego & África González-Fernández. Nanoparticles and trained immunity: Glimpse into the future. *Advanced Drug Delivery Reviews*, **2021**, 175, 113821. <https://doi.org/10.1016/j.addr.2021.05.031> [Impact factor: 15.47]

Jaione Auzmendi-Iriarte, Ander Saenz-Antoñanzas, **Idoia Mikelez-Alonso**, Estefania Carrasco-Garcia, Maitena Tellaetxe-Abete, Charles H. Lawrie, Nicolás Sampron, Aitziber L. Cortajarena & Ander Matheu. Characterization of a new small-molecule inhibitor of HDAC6 in glioblastoma. *Cell death & Disease*, **2020**, 11 (417). <https://doi.org/10.1038/s41419-020-2586-x> [Impact factor: 8.469]

Idoia Mikelez-Alonso, Antonio Aires & Aitziber L. Cortajarena. Cancer Nano-Immunotherapy from the Injection to the Target: The Role of Protein Corona. *International Journal and Molecular Science*, **2020**, 21(2), 519. <https://doi.org/10.3390/ijms21020519> [Impact factor: 5.923]

Iñigo Terrén, Ane Orrantia, **Idoia Mikelez-Alonso**, Joana Vitallé, Olatz Zenarruzabeitia & Francisco Borrego. NK Cell-Based Immunotherapy in Renal Cell Carcinoma. *Cancers*, **2020**, 12(2), 316. <https://doi.org/10.3390/cancers12020316> [Impact factor: 6.639]

Iñigo Terrén, **Idoia Mikelez**, Irati Odriozola, Andrea Gredilla, Javier González, Ane Orrantia, Joana Vitallé, Olatz Zenarruzabeitia & Francisco Borrego. Implication of Interleukin-12/15/18 and Ruxolitinib in the Phenotype, Proliferation, and Polyfunctionality of Human Cytokine-Preactivated Natural Killer Cells. *Frontiers in Immunology*, **2018**, 9. <https://doi.org/10.3389/fimmu.2018.00737> [Impact Factor: 7.561]

Conferences

Poster presentation

Mikelez-Alonso, I.; Ruiz-de-Angulo, A.; Borrego, F.; Mareque-Rivas, J.C. Exploitation of Immune Cell Iron Oxide Nanoparticle Interaction for Cancer Immunotherapy. *International Conference on Nanomedicine and Nanobiotechnology (ICONAN)*, **2017**. Barcelona, Spain.

Mikelez-Alonso, I.; Mareque-Rivas, J.C.; Borrego, F.; Cortajarena, A. L. IL15 vehiculized Iron Oxide nanoparticles as a tool to enhanceNK cell mediated-activity. *NanoBio&Med*, **2018**. Barcelona, Spain.

Mikelez-Alonso, I.; Borrego, F.; Cortajarena, A.L. Enhanced NK cell activity by IL15 functionalized Iron Oxide nanoparticles. *NanoMed Europe Conference*, **2019**. Braga, Portugal.

Oral presentation

Mikelez-Alonso, I.; Borrego, F.; Cortajarena, A.L. Enhanced NK cell activity by IL-15 functionalized Iron Oxide Nano-particles. *Annual Workshop of Young Researchers of CICbiomaGUNE*, **2019**. San Sebastian, Spain.

Mikelez-Alonso, I.; Uribe, K. B.; Borrego, F.; Cortajarena, A.L. NK cell and T cell stimulation with IONP@hIL15HIS: enhanced targeting and tumor cell killing. *Annual Workshop of Young Researchers of CICbiomaGUNE*, **2020**. San Sebastian, Spain. [price to best oral presentation]

Scientific formation

Magnetism in biomedicine, an introduction. BCmaterials, **2017**. Leioa, Spain. [16 h]

Discover wide-ranging approaches and opportunities in Multicolor flow cytometry. *BD Horizon tour*, **2017**. San Sebastian, Spain. [5 h]

Inmunología, inmunopatología e inmunoterapia. *Summer course from Euskal Herriko Unibertsitatea (EHU)-Universidad del País Vasco (UPV)*, **2017**. Bilbao, Spain. [30 h]

Outreach projects participation

<u>Project</u>	<u>Organizer</u>	<u>Year/Period</u>
Participate as mentor in InspiraSTEAM project	Deusto University	2017
Participate in activities of La Salle Beasain school visit to CICbiomaGUNE	CIC biomaGUNE	2018
Participate as investigator mentor in Elhuyar Zientzia Azoka project	Elhuyar Ezagutuz Aldatzea	2018
Presentation of a outreach project in Euskal Esperientzia	DIPC, CFM	2018

Zientzia Zabalkuntzan (EEZZ)

congress

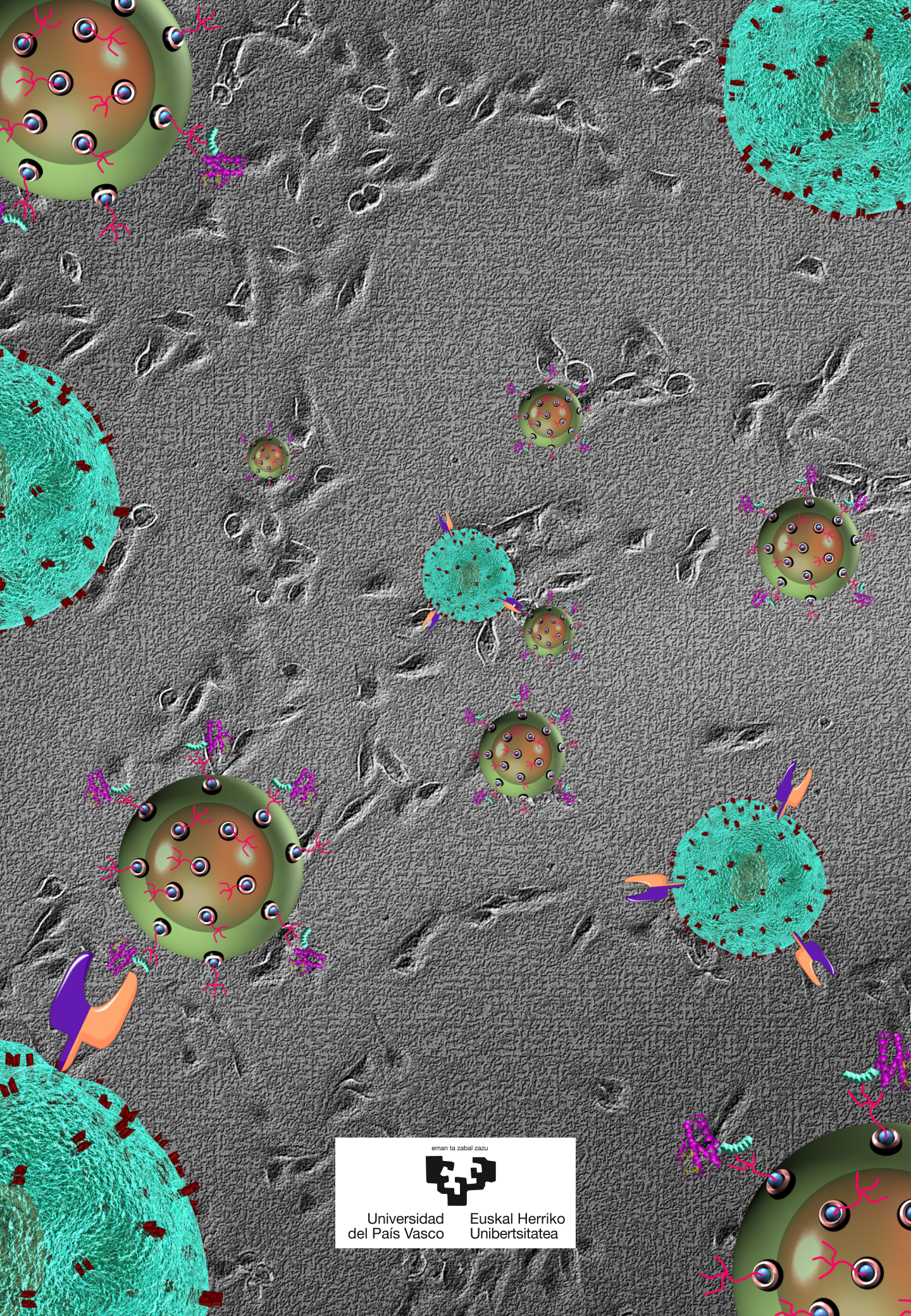
Responsible of funding in Pint of Science in Donostia	Pint Of Science Donostia	2018 and 2019 editions
--	--------------------------	------------------------

Participate in Women in Science (WinS) activities	CIC biomaGUNE	2018 and 2019
--	---------------	---------------

Zientzia eta Teknología emakumeen ikuspegitik	Parke	2021
---	-------	------

Visiting school in the vocation week (La Salle Zarautz)	CIC biomaGUNE	2021
--	---------------	------

Language adaptation (from Spanish to Basque) of educational school material about nanomedicine	NANOMED SPAIN	2022
---	---------------	------



eman ta zabal zazu



Universidad
del País Vasco

Euskal Herriko
Unibertsitatea